190

2
t

Bulletin of the Fisheries Research Board of Canada

HYDRODYNAMICS AND ENERGETICS OF FISH PROPULSION

P. W. WEBB

Historical Resumé

6th Century B.C. First reference to propulsive function of the tail.

1680 G. A. Borelli compared movements of the caudal fin to an oar.

1873 J. B. Pettigrew observed shape of the propulsive wave.

1895 E. J. Marey used cinephotography to study locomotory kinematics of swimming fish.

1912 S. F. Houssay attempted to measure thrust and drag of fish.

1926 C. M. Breder summarized and classified types of propulsive movements in fish.

1933 Sir James Gray showed how propulsive movements generate thrust, and defined kinematic conditions required.

1936 Sir James Gray used hydrodynamic theory of drag for rigid bodies of revolution to calculate drag of a swimming dolphin, and compared this with the then best known values for mammalian muscle power output. Insufficient power output was available to overcome the theoretically expected hydrodynamic drag — Gray's Paradox.

1938, 1939 A. V. Hill used direct calorimetry to determine power characteristics for contracting vertebrate muscle.

1952 Sir Geoffrey Taylor used hydrofoil theory to formulate a quantitative hydrodynamic model for fish propulsion.

1961 R. Bainbridge used hydrodynamic theory for drag of rigid bodies of revolution as a model for the swimming drag of fish and cetaceans; drag was compared with the latest values for muscle power output. Gray's Paradox not supported for most fish or cetaceans. M. F. M. Osborne used the same hydrodynamic theory, and compared drag of migrating salmon with power expended, as determined by indirect calorimetry. Insufficient power was available to overcome hydrodynamic drag.

HYDRODYNAMICS

AND ENERGETICS

OF FISH PROPULSION

Hydrodynamics

and Energetics

of Fish Propulsion

PAUL W. WEBB
Department of the Environment
Fisheries and Marine Service
Pacific Biological Station
Nanaimo, B.C.

Frontispiece: Edward Mitchell, Department of the Environment,
Fisheries and Marine Service, Arctic Biological Station,
Ste. Anne de Bellevue, Que.

Contents

Contents — Continued

Contents — Continued

Contents — Concluded

Abstract

WEBB, P. W. 1974. Hydrodynamics and energetics of fish propulsion. Bull. Fish. Res. Board Can. 190: 159 p.

The object of this monograph is to span the gap between biological and physical science approaches to fish propulsion problems. An attempt is made to summarize and collate the two principal disciplinary approaches as a basis for dialogue and ongoing research.

Principles of hydrodynamics are discussed, oriented to biologists. Following a discussion of kinematics and swimming performance, the hydrodynamic principles are applied in discussing the fundamental problem of drag and thrust. The traditionally employed rigid-body analogy (theoretical drag calculation for equivalent rigid bodies or dead-drag measurements on fish with the body stretched straight) is not considered a valid assumption from which swimming thrust (= drag) power may be computed. Movements made by most fish during swimming are likely to severely distort flow. As a result, the flow around a swimming fish is not likely to be mechanically equivalent to that assumed by the rigid-body analogy.

Alternative methods of calculating thrust power from hydrodynamic models based on the movements of swimming fish are discussed. Reaction models developed by Lighthill are considered most appropriate for biological application at present, although no current model is complete. It is likely that a complete model would be too complex for biological application. Problematic measurement or mathematical formulation areas could be incorporated in coefficient form in a semiempirical model. Coefficients could be based on key kinematic parameter modes. Such a semiempirical model is considered a viable alternative to a complete model, and would be particularly suitable for application to field situations in calculating propulsion energy expenditure. Development of both basic models and a semiempirical model is contingent upon further comparative research on propulsion kinematics.

A variety of mechanisms to reduce the drag of swimming fish has been proposed in the literature. Only a few are likely to operate. These include special body shapes in fish that swim with the bulk of the body held fairly straight, distributed dynamic damping in *Desmodema*, distributed viscous damping possibly in cetaceans, induction and maintenance of turbulent boundary-layer flow to avoid premature separation, vortex sheets filling fin gaps, and vortex interaction among schooling fish. Mucus may be a universal drag-reducing mechanism among fish.

Principles of biological energy metabolism are discussed oriented to nonbiologists. Biological energetics and mechanics are integrated in a discussion of propulsion efficiency. The use of hydromechanical models is supported providing reasonably complete data are available. Efficiency studies emphasize biological areas requiring additional research. These include characteristics, energetics, and division of labor between various muscle systems, contributions of aerobic and anaerobic metabolism to total energy expenditure at all activity levels, and energy distribution to propulsion system components.

Discussion is largely restricted to caudal fin and body propulsion at relatively low activity levels. Few data are available for other propulsion modes. A preliminary model is constructed to describe mechanical energy expenditure during acceleration. This suggests that highest final swimming speeds are reached in the shortest time with lowest energy expenditure at highest acceleration rates.

Résumé

WEBB, P. W. 1974. Hydrodynamics and energetics of fish propulsion. Bull. Fish. Res. Board Can. 190 : 159 p.

L'objectif de cette monographie est de combler le vide entre les disciplines biologique et physique dans l'étude des problèmes de propulsion chez les poissons. L'auteur tente de résumer et d'assembler les méthodes d'attaque des deux principales disciplines en vue de fournir une base au dialogue et à la recherche en cours.

Il discute, à l'intention des biologistes, des principes de l'hydrodynamique. Après une analyse de la cinématique et de la performance de la nage, le problème de la résistance et de la poussée est examiné à la lumière des principes hydrodynamiques. L'analogie traditionnelle du corps rigide (calcul de la résistance théorique pour des corps rigides équivalents, ou mesures de résistance statique sur un poisson dont le corps est étiré et droit) n'est pas considérée comme hypothèse valide pour le calcul de la force de poussée natatoire (= résistance). Les mouvements exécutés par la majorité des poissons pendant la nage sont de nature à déformer fortement l'écoulement. Comme résultat, il est peu probable que l'écoulement autour d'un poisson qui nage équivaille mécaniquement à celui que laisse supposer l'analogie du corps rigide.

L'auteur examine des variantes pour le calcul de la force de poussée à partir des modèles fondés sur les mouvements de poissons qui nagent. Les modèles à réaction mis au point par Lighthill semblent, pour le moment, les plus appropriés à une application biologique. L'auteur admet qu'aucun des modèles courants n'est complet. De plus, il est probable qu'un modèle complet soit trop compliqué pour application biologique. Des mesures problématiques ou des formules mathématiques pourraient être incorporées, sous forme de coefficients, dans un modèle semi-empirique. Des coefficients pourraient être établis à partir de paramètres cinématiques de modèles clefs. Un modèle semi-empirique de cette nature est considéré comme alternative viable d'un modèle complet, et qui pourrait être appliqué particulièrement bien à des situations sur le terrain pour le calcul de la dépense d'énergie de propulsion. Le développement, tant des modèles de base que des modèles semi-empiriques, dépend de recherches comparatives plus poussées sur la cinématique de propulsion.

On a suggéré dans la littérature une variété de mécanismes ayant pour fonction de réduire la résistance chez les poissons qui nagent. Quelques-uns seulement sont considérés comme fonctionnels. Parmi ceux-ci, on compte les formes corporelles spéciales de poissons qui nagent avec le plus gros de leur corps maintenu assez droit, l'amortissement dynamique réparti de *Desmodema*, l'amortissement visqueux réparti possiblement des cétacés, l'induction et le maintien d'un écoulement turbulent aux surfaces de discontinuité afin d'éviter une séparation prématurée, les lames tourbillonnaires remplissant les vides et l'interaction tourbillonnaire entre les poissons d'un banc. Il se peut que le mucus soit un mécanisme universel de réduction de la résistance chez les poissons.

L'auteur discute, à l'intention des non-biologistes, les principes du métabolisme énergétique biologique. Ils intègrent l'énergétique et la mécanique biologiques dans une discussion de l'efficacité de propulsion. Il est en faveur de l'usage de modèles hydromécaniques, pourvu qu'on ait des données raisonnablement complètes. Les études d'efficacité font ressortir les domaines biologiques qui requièrent des recherches supplémentaires. Ceux-ci comprennent les caractéristiques, l'énergétique et la division du travail parmi les divers groupes de muscles, les contributions du métabolisme aérobie et anaérobie à la dépense totale d'énergie à tous les niveaux d'activité, et la distribution de l'énergie aux divers composants du système de propulsion.

La discussion se limite en grande partie à la propulsion de la nageoire caudale et du corps à de bas niveaux d'activité. Il existe peu de données sur la propulsion des nageoires. L'auteur construit un modèle préliminaire décrivant la dépense d'énergie mécanique pendant l'accélération. Il en ressort que les plus grandes vitesses de nage finales seraient atteintes dans le plus bref délai avec la plus faible dépense d'énergie lors des taux maximums d'accélération.

Preface

Animals moving in air or water have long occupied a special place to both casual or systematic students of locomotion. Compared to terrestrial locomotion, the mechanics of animals moving in the fluids water and air are problematic and have a fascinating if somewhat turbulent history. This is epitomized by such paradoxes as "the bumblebee that cannot fly" or "the dolphin that cannot swim!" The future of fish locomotion studies, to which this work restricts itself, promises to be equally fascinating and certainly more exciting as a rapid evolution of new ideas and techniques follows recently renewed interest in all facets of the subject.

We cannot move ahead without thoroughly evaluating past studies (particularly the complexities of paradoxical and conflicting biological literature on energetics) because the basic fish propulsion questions remain remarkably unchanged. These concern swimming mechanics — questions of how a fish swims and, especially for the biologist, how much energy is expended. These questions lead to a central problem, typical of any multidisciplinary subject as complex as fish locomotion, and this is the common communications gap between disciplines and the extensive amount of time required to obtain an initial working familiarity with each other's language and concepts. Biological scientists have additional problems, potentiated by such a communications gap, for they seek to evaluate the significance and practical utility of mechanical solutions with a view to applying these in "real world" situations.

When I joined Dr Roly Brett's physiology team at Nanaimo, B.C., it was inevitable that our mutual interests in locomotory bioenergetics should lead to discussions of fish propulsion problems and how we might contribute to the solution. As a result, Dr Brett encouraged me to try to put together a synthesis of various bioenergetic aspects of fish locomotion. Primary objectives were to span as far as possible the existing communications gap between "interested parties" and to review the bioenergetics problem, emphasizing the contribution and significant potential for biologists of research by physical scientists in this area. This I have attempted to do to the best of my ability.

Introduction

Fish locomotion has always excited man's interest — a fisherman wondering at the remarkable speeds fish can attain, or a scientist making detailed field or laboratory studies. This book is concerned with the latter. Earlier scientific studies have been summarized by Hora (1935) and Gray (1968), and include accounts of important technical and conceptual research developments that have contributed to the evolution of understanding fish locomotion problems. Rigorous scientific study has been confined largely to the last 50 years. Generally two main approaches have been followed — one by biologists and a second by applied mathematicians, theoretical physicists, and hydrodynamic engineers. Exchanges of ideas between the two groups have been relatively few, but when the gap has been bridged, great advances have been made, almost of quantal nature. Sir James Gray has been by far the most important figure in these advances, through his own work and influence on his colleagues.

The best known and most significant of Gray's contributions is the so-called "Gray's Paradox," a result of the first attempt to evaluate swimming energetics. Gray (1936b) applied theoretical hydrodynamics to a swimming dolphin in an attempt to predict the drag of the animal when swimming. The calculated power required to overcome drag was compared with the best estimates for mammalian muscle power output. Results suggested that insufficient muscle power was available to overcome drag for the calculated flow conditions.

The influence of this bridge between biology and hydrodynamics on subsequent studies of fish locomotion can hardly be overestimated. "Gray's Paradox" stimulated much research into drag-reducing mechanisms. Perhaps of greater influence, especially for energetic studies, was the assumption that drag of a swimming fish or cetacean could be equated to that of an equivalent rigid body or model, and easily calculated as Gray had shown. The ready adoption of this assumption by many biologists and engineers possibly stemmed from an earlier observation by Sir George Cayley (about 1809; see Gibbs-Smith 1962): that many fish and cetaceans had streamline bodies comparable to man-made vehicles designed to have a low drag. As a result of this assumed rigid-body analogy for calculating drag of a swimming fish, there has been something of a seesaw controversy of refutation or support of "Gray's Paradox." One addition by biologists to the increasing complexity of the picture was the measurement of drag of actual fish, but unfortunately such measurements only served to add to the growing confusion. Nevertheless, such discrepancies and controversy have not prevented the adoption of the rigid-body analogy in recent biological literature to calculate the "apparent" swimming drag for conditions as diverse as swimming energetics of goldfish (Smit et al. 1971) and models of fish productivity (Weatherley 1972). The ready adoption of the rigid-body analogy in subjects of undoubted biological importance has been without critical examination of the basic assumptions involved, or for that matter, their validity.

Whereas biologists principally pursued paths suggested by "Gray's Paradox," physical scientists concentrated on the formulation of mathematical models, based on measurements of actual movements made by swimming fish. Again an important influence on the development of such models was that of Gray, as is clear from accorded acknowledgments (Taylor 1952; Lighthill 1972). Early models such as those of Taylor (1952) and Lighthill (1960) contained potential for numerical solution for the drag of a swimming fish, and a possible alternative to the rigid-body analogy. However, this latter potential was neglected by biologists until recently.

There has been a recent "bloom" of new and modified models (see Table 7). At the same time biologists have begun to question the validity of the traditionally employed rigid-body analogy. This state of arrival (probably focussed by Lighthill's (1969) review) provided an excellent opportunity for biologists to experimentally research new models with a view to providing more realistic solutions to the question of energy requirements of swimming fish.

Such research opportunities, however, depend on the availability of a "treadmill" for fish. Scientists working on the energetics of terrestrial

5

animals early developed treadmills and ergometers to measure both mechanical power expended and metabolic power required at different activity levels. Before 1960, no adequate equivalent was available for aquatic animals, and biological studies rested principally on indirect data. Water treadmills, or water tunnel respirometers, were developed by Blazka et al. (1960) and Marr (1959) (see Brett 1963, 1964), that permitted accurate measurement of metabolic energy expenditure for a range of precisely controlled swimming speeds. At the same time, by "fixing" the fish relative to the observer, accurate measurement of the complex deformations of the body of swimming fish could be made. The latter data are of course vital in formulating and improving mathematical models. The development of treadmills for fish was followed by another "bloom" of biological studies, mainly on swimming performance and metabolic rates.

Full development of the technological "treadmill breakthrough" requires a new, more permanent collaboration between biological and physical scientists. The historical temporary bridges (for such was their nature) can no longer suffice. Lighthill (1972) eloquently put the case for the necessity of amalgamating the two approaches on a more permanent basis — both in the laboratory for experiment and in the armchair for elaboration.

At present, amalgamation of the two approaches is hindered by a discipline and expertise gap. A major purpose of this work is to assist in bridging the gap. Failure to do so, and concomitant failure to exchange ideas, can only be detrimental to the developing understanding of fish locomotion for both biological and physical scientists.

This work is divided into two principal sections. The first introduces elementary hydrodynamic concepts for biologists. Following a review of swimming performance of fish and cetacea and their swimming kinematics, hydrodynamic principles are applied in discussing the question of drag of swimming fish, the rigid-body analogy, drag-reducing mechanisms, and finally the application of models to calculate swimming power requirements. The second part reviews physiological and bioenergetic concepts relevant to propulsion studies for nonbiologists, leading to a discussion of propulsion efficiency.

Chapters on hydrodynamics for biologists and bioenergetics for nonbiologists are included to provide a working familiarity with pertinent aspects of the two approaches to propulsion studies. It is important to realize that such a treatment of both subjects is simplified, of necessity sometimes oversimplified, and is no substitute for consulting original texts.

Finally, some comment should be made concerning the emphasis on body and caudal fin propulsion. This is inevitable because most research has been done within the sphere of these relatively simple locomotor patterns. It is hoped that a synthesis of biological and physical science expertise can provide the same insight into other locomotor patterns.

PART I

Chapter 1 — Hydrodynamics

Introduction

One major difficulty faced by biologists who begin studies on propulsive energetics of fish and cetaceans is an inadequate understanding of hydrodynamics. In general, the principles of metabolism for the components of the propulsive system are readily available. There is an increasing literature on the overall metabolic rate of small- and intermediate-size fish, particularly at sustained swimming speeds (Fry 1971). When an attempt is made to relate these physiological data to swimming performance to draw up an energetics balance sheet, some estimate of the hydrodynamic resistance to motion (drag) must be made. In many cases insufficient knowledge of hydrodynamics has resulted in the acceptance of standards and values for drag which have produced conflicting and often energetically impossible results.

It is the purpose of this chapter to outline principles of hydrodynamics that are relevant to fish propulsion problems. The outline is intended first, to provide a basis for the interpretation of fish propulsive mechanics (discussed in the following chapters), and second, to indicate those areas of hydrodynamics of particular importance to a further understanding of the complex phenomena. In addition to discussing the hydrodynamic principles relevant to fish propulsion studies, many equations are included for the practical application of these principles. These show more clearly than any text the various parameters of practical importance.

This chapter is based mainly on a few standard texts. It is convenient to list them here rather than repeat them continually; Prandtl and Tietjens (1934a, b), von Mises (1945), Schlichting (1968), and a useful introductory text by Shapiro (1961). Other references are given in the text.

Some Physical Properties of Water

The physical properties of water pertinent to hydrodynamics are mass (M), density (ρ), viscosity (μ), and kinematic viscosity (ν, or μ/ρ). These properties are affected by salinity and, all but mass, by temperature. Effects of pressure may be neglected because of the incompressible nature of water, even at pressures encountered deep in the sea.

Density

Variations with temperature in the density of water for various salinities are shown in Fig. 1, after Hobbs (1952). Density of pure water is only slightly affected by temperature. With increasing salinity the dependence of density on temperature increases, so that the density maximum of fresh water at 4 C is obscured.
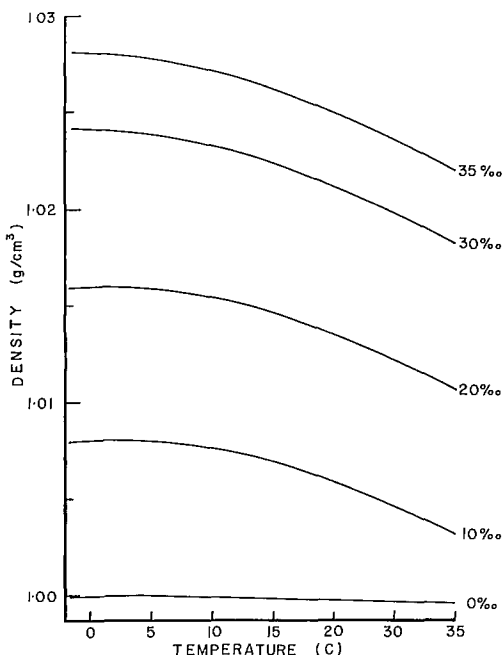
FIG. 1. Relation between density (g/cm³) and temperature (C) for water of various salinities ‰. (Data from Hobbs 1952)

Viscosity

The viscosity of a fluid is the index of its resistance to deformation, which occurs whenever there is relative motion between different points in the fluid. The concept of viscosity and its

mathematical expression can most readily be described with reference to the "Couette" flow pattern in Fig. 2. This is a special flow pattern which occurs in a fluid confined between two parallel flat plates (ab and cd), separated by a distance, h, and moving at a velocity, U, relative to each other. Experiment shows there is no slip between the fluid and surfaces of the plates. Thus, if cd is stationary, and ab moves with the velocity U in the direction + x, the velocity of the fluid is similarly zero at cd and U at ab. Velocity of the fluid at different points can be indicated by vector arrows showing the direction and magnitude of velocity at each point. When the vector arrows are drawn for a line normal to the surface of the plates, pq, and the arrow heads are joined, a line showing the velocity profile in the fluid is obtained. In Couette flow the velocity profile is linear and there is a uniform velocity gradient, U/h, between the two plates. The velocity gradient is a measure of distortion of the fluid resulting from the relative motion between ab and cd.

Because the fluid resists distortion, a force, F_ν, must be applied to ab in the direction + x to maintain the motion at velocity U. In his pioneer studies on viscosity, Sir Isaac Newton found that the magnitude of F_ν was dependent on the surface area of the plates and on distortion of the fluid. Thus for plates of unit surface area

$$F_\nu \; \alpha \; U/h \tag{1}$$

The coefficient of proportionality is the viscosity, μ, defined as the resistance of a fluid per unit velocity gradient per unit of the surface area wetted by the fluid.

Thus
$$F_\nu = \frac{\mu U}{h} \text{ per unit area} \tag{2}$$

and
$$\mu = \frac{F_\nu \, h}{S_w \, U} \tag{3}$$

when S_w is the wetted surface area.

Values for μ at various temperatures and salinities are depicted in Fig. 3. μ is only slightly affected by salinity but is highly dependent on temperature.

The unit of viscosity in the cgs system is the poise which has the dimensions

$$\text{Mass} \times \text{Length}^{-1} \times \text{Time}^{-1}$$

from Equation 3.
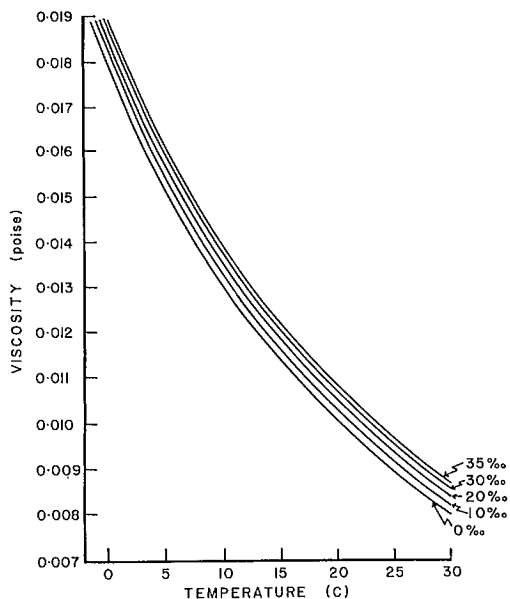
FIG. 3. Relation between viscosity (poise) and temperature (C) for water of various salinities ‰. (Data from Sverdrup et al. 1963)

FIG. 2. The Couette flow pattern for a fluid with viscosity confined between two flat parallel plates moving relative to each other at a velocity, U. Arrows represent velocity vectors, showing magnitude and direction of velocities u_1, u_2, etc., in the fluid at points y_1, y_2, etc., along the section of flow. The line joining heads of the velocity vectors gives velocity profile between p and q. (Redrawn from Boundary-layer Theory by H. Schlichting; © McGraw-Hill Book Co. 1968; used by permission.)

Methods of Describing Flow

Fluids are considered to be made up of numerous individual "pieces" of fluid, called fluid particles. Each fluid particle is an arbitrarily defined piece of fluid that is large in relation to the fluid molecules, but small in comparison with the volume of fluid being considered. Fluid particles can be marked in real fluids by means of dyes, small bubbles, or other very small particles.

The motion of each fluid particle in a moving fluid can be described by a vector arrow as with the Couette flow pattern. The velocity profile then describes the velocity distribution for a given cross section of the flow, and the velocity distribution throughout the whole fluid is called the velocity field.

Vector arrows that describe the motion of fluid particles within the velocity field can be joined together to construct a map showing the directions of fluid velocity throughout that field. The contours of such a map are called streamlines. When the streamlines in a flow pattern become compressed, the flow is similarly compressed and there is an increase in velocity along those streamlines. Similarly, when streamlines become more widely spaced, a decrease in velocity is indicated.

Under steady conditions the path of a fluid particle will coincide with a streamline. Such stable flow is termed laminar, so-called because the fluid can be thought of as made up of strips or laminae of fluid. In laminar flow the motion of a fluid particle can be described by a single velocity vector directed along the streamline (Fig 4A). When flow conditions are unstable, flow is called turbulent. In unsteady flow, forces act on fluid particles in directions other than those along streamlines. A fluid particle moves in the direction of the resultant of forces acting on it at any instant, and its subsequent path may or may not coincide with a streamline (Fig. 4B). Streamlines in turbulent flow represent the mean direction

Fig. 4. Diagram illustrating the axes along which velocity of a fluid particle may be resolved in laminar and turbulent flow. Solid lines represent streamlines: A) laminar flow; velocity of the fluid particle may be resolved into a single velocity vector orientated along the streamline; B) turbulent flow; velocity of the fluid particle may be resolved into components along x, y, and z axes.

of the fluid, but not the motion of any identified fluid particle. When there is a change in conditions of flow from laminar to turbulent the intermediate region is called the transition zone.

Pressure and Velocity

An important principle in hydrodynamics is the relation between the pressure in a fluid and its velocity, known as Bernoulli's theorem. For constant flow along a streamline, this shows that

$$\tfrac{1}{2}\rho U^2 + \rho gh + P = \text{constant} \quad (4)$$

when

U = the velocity along a streamline, cm/s

g = acceleration due to gravity, cm/s^2

h = depth of the streamline, cm

P = reference pressure, dyn/cm^2

$\tfrac{1}{2}\rho U^2$ is the dynamic pressure of the motion of the fluid, and ρgh is the static pressure of the mass of fluid above the streamline.

The constant, often called the Bernoulli constant, varies from streamline to streamline, depending on the value of h at a given value of U. For streamlines at the same depth, the total pressure of the fluid is inversely proportional to U^2.

Hydromechanics, Hydraulics, and the Boundary-Layer Concept

In the most common fluids, water and air, viscosity can often be neglected because viscous forces are small compared to inertial forces. In some cases motion of the fluid can be described in terms of inertial forces acting on fluid particles. The inertial force acting on a fluid particle at any instant is given by Bernoulli's theorem, and the particle's subsequent motion can be predicted from Newton's Laws of Motion. This forms the basis of hydromechanics, the science describing flow in inviscid (frictionless) or perfect fluids; hydromechanics predicts the potential flow in a fluid in the absence of viscosity.

Hydromechanical theory does not predict flow correctly in all cases because it neglects viscosity. For example, the theory leads to the conclusion that a streamlined body, like that of a gliding fish moving at uniform velocity, has zero drag. This is obviously not the case and the discrepancy is called d'Alembert's Paradox. Discrepancies of this nature gave rise historically to a separate synthetic science, hydraulics, based on empirical observation.

The solution to such discrepancies was proposed by Prandtl in 1904. He suggested that the flow around bodies could be divided into two regions (Fig. 5). The first region is that immediately adjacent to a body surface where the velocity in the fluid varies from that of the surface (to which it sticks) to the velocity of the free stream. In this region there is a steep velocity gradient, and the fluid is subject to extensive distortion. Viscous forces are large and, in comparison, inertial forces negligible. This region of flow is called the boundary layer. Beyond the boundary layer is the second region of outer flow in which the velocity distribution is fairly uniform. Viscous forces are nonexistent or negligible, and the fluid motion is largely defined by inertial forces. This important division of the flow into two regions, with an emphasis on the behavior of the first, is called the boundary-layer concept.

Prandtl subsequently showed that boundary-layer flow could be laminar, turbulent, or transitional, in the same way as the potential flow outside the boundary layer (Fig. 5). It is possible to predict the conditions under which each type of flow could be expected, based on the relative magnitude of viscous and inertial forces (Reynolds Number).

It was also found that conditions in the two regions of flow could markedly affect each other. Conditions in the outer flow can cause the boundary layer to detach or separate from the surface of a body and produce trailing vortices and an increased wake. This phenomenon of separation markedly affects the outer flow, and has an important effect on drag.

PRESSURE   GRADIENTS

adverse   favorable

OUTER
FLOW

LAMINAR
TRANSITIONAL
TURBULENT

BOUNDARY   LAYER

LAMINAR

TRANSITIONAL
(PARTLY LAMINAR,
PARTLY TURBULENT)

ATTACHED

TURBULENT

Some causes of Transition and
Turbulence
1) poor body shape.
2) adverse pressure gradient.
3) turbulence in outer flow.
4) surface roughness.
5) large size and/or speed.

SEPARATED

Separation is encouraged
by adverse pressure
gradients.

FIG. 5. Diagram illustrating the two regions of flow proposed by Prandtl to explain various flow phenomena. Diagram illustrates principal flow conditions in each region. Further explanation is given in the text.

Laws of Similitude

Types of forces that affect the flow around bodies moving in fluids must be considered; how they can be related to size, velocity, and characteristics of the fluids to predict flow conditions, particularly in the boundary layer. This is done by application of Reynolds and Froudes Laws of Similitude.

The Laws of Similitude interrelate the three main forces acting on bodies that move in fluids. These forces are inertial, viscous, and gravitational. The first two are significant when a body is well-submerged (the usual condition for fish) or in an enclosed system like a water tunnel. Inertial and gravitational forces are of greatest importance when a body moves at or close to the surface of the fluid, and surface waves are formed. This applies to fish in shallow water and surface-swimming cetaceans. The Laws of Similitude predict the type of flow conditions around a body, and are used in defining the necessary conditions for a mechanically similar flow to occur around objects of differing sizes moving at different speeds or in different fluids. This is the basis of model building for testing performance of new designs for ships and airplanes.

Reynolds Law

Reynolds Law considers the forces acting on a submerged body, that is, inertial and viscous forces. These forces are expressed as a nondimensional number, the Reynolds Number, R, when

$$R = \frac{\text{Inertial force}}{\text{Viscous force}} \qquad (5)$$

To derive R, and illustrate its meaning, consider a body, length, L, moving through a fluid at a uniform velocity, U. The total inertial force acting on the body is the sum of the rates of change in momentum of the fluid affected by the body. If this force is F_i, then

$$F_i \propto Mu/t \qquad (6)$$

when

t = time over which changes in U to u occur.

M = mass of fluid affected by the body, which will be proportional to density of the fluid, and the cube of L. Then, M may be assumed

$$M = \rho L^3 \qquad (7)$$

u is the velocity of the fluid resulting from the influence of the body. Usually, changes from U to u may be assumed to be negligible in comparison with U.

The time, t, over which velocity changes occur is then given by

$$t = L/U \qquad (8)$$

Then from Equation 6, 7, and 8

$$F_i \propto \rho L^2 U^2 \qquad (9)$$

The magnitude of the viscous force depends on the viscosity of the fluid, the surface area of the body (proportional to L^2) and the velocity gradient in the vicinity of the body surface (U/L) from Equation 3. If the viscous force is F_v, then its magnitude is given by

$$F_v \propto \mu LU \qquad (10)$$

Inserting values for F_i and F_v from Equation 9 and 10 into Equation 5

$$R_L = \frac{\rho LU}{\mu} \qquad (11)$$

As densities and viscosity of water have fixed values for a given temperature, they are often expressed as kinematic viscosity, $v = \mu/\rho$ and thus,

$$R_L = \frac{LU}{v} \qquad (12)$$

R can be calculated for any characteristic linear dimension of a body, although L is most commonly used. A subscript (as used in Equation 11 and 12) will be used to denote the characteristic dimension on which R is based.

It will be realized from the calculation of R that it is an order of magnitude estimate, rather than an accurate measurement of the ratio of inertial and viscous forces. Nevertheless, the estimate of R is good and is commonly used with great efficacy throughout practical hydrodynamics.

Under stable conditions, flow in the boundary layer on a flat plate or rigid streamlined body will be laminar for values of R_L less than 5×10^5, and turbulent when R_L is greater than 5×10^6 (von Mises 1945). Between these values, flow will tend to be partly laminar, partly turbulent. The transitional flow itself is characterized by patches of laminar and turbulent flow. The value of R_L at which transition occurs is called the critical Reynolds Number, $R_{L\ crit}$, and is variable in practice. It may be lower than the value given here, as flow is often unsteady outside the boundary layer. In some cases, the outer flow can be made stable, in which case $R_{L\ crit}$ will be higher. The latter conditions do not occur naturally.

13

As well as predicting boundary-layer flow conditions, Reynolds Law predicts the required conditions for a mechanically similar flow to occur around geometrically similar bodies. Mechanical similarity of flow is achieved when the ratio of inertial to viscous forces is the same around each object for geometrically similar points in the velocity field. This condition is realized when R is the same for each object.

For example, Harris (1936) performed experiments on a model dogfish in a wind tunnel to determine the influence of fins on the stability of the fish. For this he required the flow around the fish in water and the model in the wind tunnel to be mechanically similar. The kinematic viscosity of air is about 13 times that of water. The dogfish was estimated to swim at about 3 mph. Velocity of the air in the wind tunnel was set at about 40 mph for the experiments. Similarly, fish of different sizes must swim at different speeds for the flow to be mechanically similar. A downstream migrant salmon, approximately 10 cm long, swims at about 4 body lengths/s or 40cm/s, and R_L is approximately 4×10^4. An upstream migrant, say 40 cm long, will have a mechanically similar flow pattern to that about the smaller fish at a speed of only 0.4 body lengths/s or 10 cm/s.

Within the animal kingdom, R_L ranges from about 10^{-5} for a spermatozoan (Gray 1955) to 3×10^8 for a blue whale (Gawn 1948). From Reynolds Law, the dominant forces acting on the spermatozoan are viscous, and inertial forces can be ignored. In the case of the blue whale, the dominant forces are inertial. The viscous forces cannot be ignored, as they are significant in the boundary layer. The range of R_L which includes aquatic vertebrates is much smaller than this, ranging from below about 10^3 for small fish larvae, to that for the blue whale. This range is illustrated in Fig. 6, which shows how R_L varies with U, with isopleths for L. Most observations on fish have been made in the narrow R_L range between 3×10^4 to 10^6, and will be considered in greater detail than other areas. Highest values for R_L are found among mammals, particularly whales. This is mainly because they reach the greatest lengths, not because they reach greater swimming speeds. When lengths are similar between fish and mammals, as with some scombrids, dolphins, and porpoises, maximum swimming speeds are also similar, and so is R_L.

Froudes Law

Froudes Law considers the forces acting on the surface of a body moving at or close to a fluid/fluid (fluid/gas) interface. When a body moves close to such an interface, surface waves are created which are subject to gravitational forces. The energy required to form these waves greatly exceeds the energy associated with viscous forces. The most important forces acting on the body are inertial and gravitational. The ratio between these forces is expressed, like R, as a nondimensional number, the Froude Number, F, when

$$F = \frac{\text{Inertial force}}{\text{Gravitational force}} \qquad (13)$$

The inertial force was derived in Equation 9. The gravitational force, F_g, is the product of the mass affected by the body (Equation 7) and the acceleration due to gravity, g,

$$F_g = \rho L^3 g \qquad (14)$$

Therefore, by substituting for F and F_g from Equation 9 and 14 into Equation 13

$$F_L = U^2/L g \qquad (15)$$

when the subscript again shows the characteristic dimension for which F is calculated.

It can be seen from Equation 15 that a small geometrically similar model must move at a higher velocity than its larger counterpart for flow to be mechanically similar and F_L the same. This is opposite to the conditions for R_L to be the same, and it is difficult to apply Reynolds and Froudes laws simultaneously to the same object. In test situations, mechanical similarity of flow for both laws can be obtained by using two fluids of different kinematic viscosity, providing they are in certain ratios to L or U. If the lengths of two geometrically similar models are L and L_i, and their velocities U and U_i, respectively, in fluids with kinematic viscosities of v and v_i, then mechanical similarity of flow is obtained when

$$\frac{L\ U}{v} = \frac{L_i\ U_i}{v_i} \quad \text{Reynolds Law}$$

and

$$\frac{U^2}{L\ g} = \frac{U_i^2}{L_i\ g} \quad \text{Froudes Law}$$

Therefore, v/v_i must be in the ratios

$$\frac{v}{v_i} = \left[\frac{L}{L_i}\right]^{0.66} \text{ or } \left[\frac{U}{U_i}\right]^3 \qquad (16)$$

Hertel (1966) measured the increase in drag with reference to the frictional drag a dolphin-shaped body would experience swimming near

14
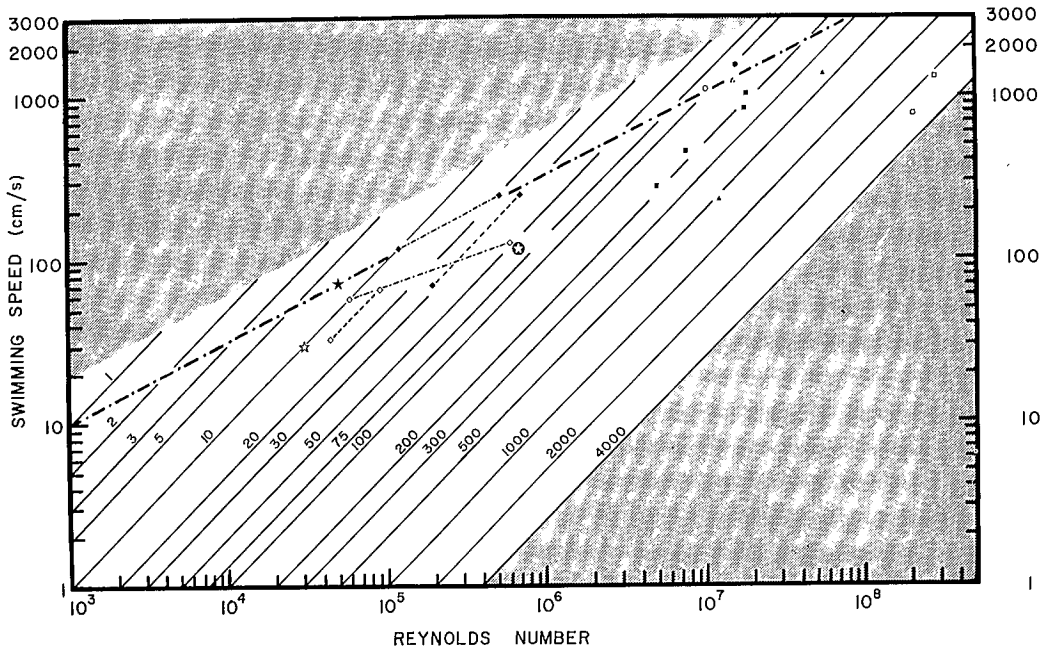
FIG. 6. Relation between Reynolds Number, R_L, and swimming speed, U, for fish of various lengths (diagonal isopleths). Length, L (cm), is shown above the relevant diagonal. Kinematic viscosity was assumed to be 10^{-2}. Heavy chain dotted line relates values of R_L and L for U of 10 body lengths/s. Shaded portions cover areas of R_L and U outside the range commonly observed among aquatic vertebrates. Other points have been calculated from swimming speeds given in the literature. ◆——·—·—◆ *Leuciscus leuciscus*, sprint speeds maintained for 1 s for fish of various lengths (Bainbridge 1960); ■ — — — ■ *Salmo irideus*, sprint speeds from 20 to 1 s for a 28 cm fish (Bainbridge 1960); ◇—·—·—◇ *Oncorhynchus nerka*, sustained speeds maintained for 60 min for fish of various lengths (from Brett 1965a); □ — — — □ *Oncorhynchus nerka*, sustained speeds maintained for more than 300 min to about 6 min for fish approximately 13.5 cm in length (Brett 1967a); ★ *Clupea harengus*, sprint (Blaxter and Dickson 1959); ☆ *Pholis gunnellus*, sprint (Blaxter and Dickson 1959); ✪ *Anguilla vulgaris*, sprint (Blaxter and Dickson 1959); ○ *Thunnus albacares*, sprint (Walters and Fierstine 1964); ● *Acanthocybium solanderi*, sprint (Walters and Fierstine 1964); △ *Sphyraena barracuda*, sprint (Gero 1952); ■ Dolphin species, various speeds from sustained to maximum sprints (Gray 1936b; Johannesen and Harder 1960; Norris and Prescott 1961); ▲ *Globiocephala scammoni*, schooling speed and 15 s sprint (Norris and Prescott 1961); □ *Balaenoptera commenseri*, speeds maintained for 120 and 10 min (Gawn 1948).

the surface of the water (Fig. 7). Hertel found that Reynolds Law became applicable to such a body when it was submerged to a depth equal to 3 times its maximum body depth.

The Boundary Layer

The boundary layer is the region of flow around a body where the fluid velocity increases from that of the body to that of the undisturbed fluid of the outer flow (the free stream velocity). Velocity in the boundary layer reaches a velocity only slightly different from that of the free stream at a short distance from the surface. The boundary layer is, therefore, assumed to be of finite dimensions.

Boundary-layer thickness

For present purposes the thickness of the boundary layer can be defined in two ways: the velocity thickness, δ, defined as the distance from the surface to which the boundary layer is attached to the position where the velocity of the fluid differs by 1% from the free stream velocity (Fig. 8); the displacement thickness, δ*, represents the distance from the surface by which the streamlines of the outer flow are displaced by the boundary layer. δ* is shown in Fig. 8 by the

15
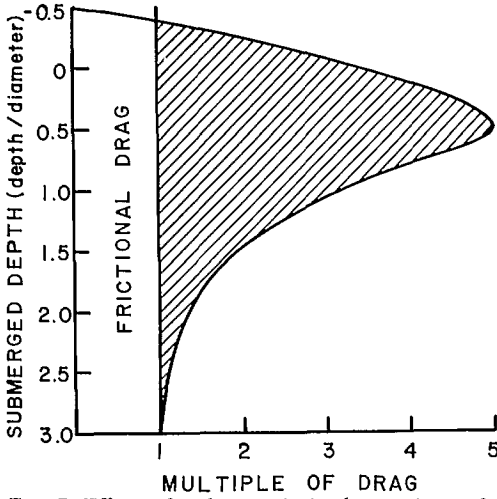
FIG. 7. Effect of submerged depth on drag of a dolphin-shaped body. Increase in drag of the body shown by shaded area as a multiple of frictional drag experienced in the absence of free surface. Submerged depth shown as a multiple of depth of the body. (Redrawn from *Structure, Form and Movement* by H. Hertel © 1966; reprinted by permission of Van Nostrand Reinhold Co.)
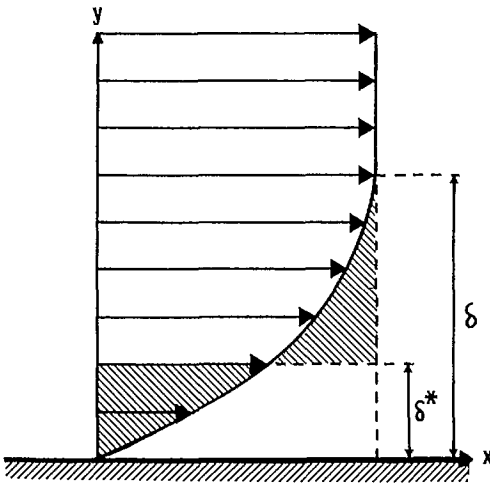
FIG. 8. Velocity distribution in a boundary layer attached to a flat plate showing velocity vectors (horizontal arrows) and the flow profile. Velocity thickness, δ, and displacement thickness, δ^*, are also shown. Further explanation is given in text. Note the y-axis is greatly exaggerated for clarity. (Redrawn from *Applied Hydro- and Aeromechanics* by L. Prandtl and O. G. Tietjens (1934b); © Dover Publications Inc.; used with permission.)

horizontal line. At this point, the sum of the differences between velocities in the boundary layer and those of the free stream above the line are equal to the sum of velocities in the boundary layer below the line. That is, the shaded areas are equal. The displacement thickness of the boundary layer is used to calculate the mean flow around a body, and is related to the velocity thickness by

$$\delta^* \simeq \delta/3 \qquad (17)$$

The thickness of the boundary layer depends on the amount of fluid influenced by a surface. This will be dependent on the viscosity of the fluid and the time for which the viscous forces act. Thus, the boundary layer increases in thickness with distance from the leading edge (the front) of a body as progressively more fluid in the free stream is affected.

Velocity thickness of the boundary layer was calculated by Blasius in 1908. δ was found to be related to R_L, and if the distance from the leading edge is represented by x, then

$$\frac{\delta_{lam}}{x} \simeq 5.0 \, R_L^{-\frac{1}{2}} \qquad (18)$$

and

$$\frac{\delta_{turb}}{x} \simeq 0.37 \, R_L^{-\frac{1}{5}} \qquad (19)$$

when the subscripts *lam* and *turb* represent laminar and turbulent boundary-layer flow conditions, respectively.

A turbulent boundary layer at a given value of R_L, tends to be thicker than a laminar one, because of the unsteady flow in the former. A laminar boundary layer can only extend its influence normal to a surface to which it is attached by frictional forces and the transfer of negligible amounts of momentum between laminae by molecular diffusion. However, in a turbulent boundary layer, fluid particles with velocity components normal to the surface transfer considerable amounts of momentum through the boundary layer. This tends to slow down fluid further into the free stream by exchange of low momentum fluid particles with those of the free stream which have a higher momentum. As a result, the influence of a turbulent boundary layer is more extensive.

Transition

The boundary layer on a flat plate, at zero angle of incidence to a stable laminar flow, is initially laminar. At some point downstream from the leading edge the boundary-layer flow becomes turbulent. The change in flow (transition)

16

is the result of small random disturbances in the boundary layer which tend to disrupt the flow. Near the leading edge, where the boundary layer is relatively thin, viscous forces are large and tend to damp out disturbances. When the boundary layer is thin, only large disturbances cause transition.

As the boundary layer increases in thickness with distance from the leading edge, the magnitude of the velocity gradient in the boundary layer and viscous forces becomes smaller. In addition, inertial forces become important relative to the viscous forces. A point is eventually reached when the viscous damping forces are too small to damp out a disturbance, that is amplified instead by inertial forces. The point at which disturbances are undamped is the point of instability. Transition is not immediate. Amplitude of the disturbance is increased as it travels downstream until the boundary layer flow becomes turbulent at the point of transition. In the transitional area between these two points there are irregular areas of laminar and turbulent flow, and some disturbances may still be damped out, even after partial amplification.

Transition occurs at a point when the ratio between inertial forces and viscous forces obtains a critical value for amplification rather than damping. Therefore, the transition point can be related to R, occurring at R_{crit}, which takes values between 5×10^5 and 5×10^6 for R_L.

The ratio of the inertial to viscous forces depends on the thickness of the boundary layer, as shown in Equation 18 and 19 when the thickness was related to R_L. Therefore, there will also be critical thickness, δ_{crit}, at which transition occurs, related to $R_{L\ crit}$ by Equation 18. Thus

$$\delta_{crit} = 5.0 \left[R_{L\ crit} \right]^{-\frac{1}{2}} \qquad (20)$$

Transition in the boundary layer is encouraged by any extra disturbances in the outer flow, roughness on the surface to which it is attached, or by pressure gradients in the opposite direction to the mean flow. These factors cause transition at values of R_L lower than $R_{L\ crit}$, and if they are of sufficient magnitude, points of instability and transition can coincide, often close to the leading edge.

Causes of transition and separation

TURBULENCE IN OUTER FLOW

A common source of external disturbance is turbulence in the free stream. This results in local velocity fluctuations in the neighborhood of the boundary layer that are associated with local pressure changes or inertial forces. Turbulence in the free stream can be thought of as increasing local R, that sometimes exceeds R_{crit} when transition is encouraged.

A measure of the disturbance caused by the free stream is given by the intensity of turbulence, I. I relates the mean square velocity fluctuations, $\overline{u^2}$, $\overline{v^2}$, and $\overline{w^2}$ of the fluid in the x, y, and z planes respectively, to the mean free stream velocity, U, along the $\pm x$ axis. The root mean square velocity of the fluid is thus

$$\sqrt{\tfrac{1}{3} (\overline{u^2} + \overline{v^2} + \overline{w^2})}$$

and I is given by

$$I = \frac{\sqrt{\tfrac{1}{3} (\overline{u^2} + \overline{v^2} + \overline{w^2})}}{U} \qquad (21)$$

In many test situations, for example the fish water tunnel respirometers described by Brett (1964) and Bell and Terhune (1970), a turbulent flow is induced by grids and has a regular structure where the velocity fluctuations in the three axes are equal. Such a flow is called isotropic and $\overline{u^2} = \overline{v^2} = \overline{w^2}$.

Then

$$I = \frac{\sqrt{\overline{u^2}}}{U} \qquad (22)$$

When I obtains values between 0.02 and 0.03, points of instability and transition coincide. Above this critical range, disturbances will be immediately amplified, leading to full turbulence of the whole boundary layer covering a body. In such cases a laminar portion of the boundary layer is never considered to have existed.

It is probable that most fish swim in water where I exceeds the critical range. This will certainly be the case for freshwater fish swimming in turbulent streams or rivers (including weirs, dam outlets, and fish ladders) and for fish swimming in shoals, where fish swim in the wake of others. Exceptions are probably fish that swim in the open ocean singly or in loose, slow shoals.

SURFACE ROUGHNESS

Surface roughness is only important in encouraging transition if the roughness elements penetrate through the boundary layer to disturb the outer flow. Otherwise, disturbances are small, and are damped out by the viscous forces in the boundary layer and a laminar regime is maintained. There is a certain critical height, k_{crit}, for

a roughness element that will lead to full, immediate transition.

The value of k_{crit} depends on the type of roughness element. There are two types relevant to fish propulsion, a single roughness element like a tripping wire, and a distributed roughness, typical of the skin of elasmobranchs (Bone and Howarth 1966).

For each type of roughness, k_{crit} can be related with U and v to a constant in an expression similar to that for R. For the single roughness element complete transition will be caused when

$$\frac{U \, k_{crit}}{v} \geq 900 \tag{23}$$

For distributed roughness elements

$$\frac{U \, k_{crit}}{v} \geq 120 \tag{24}$$

When roughness is present among fishes, it is designed to cause premature transition, and is usually required to be effective at low speeds. For example, Ovchinnikov (1966) described denticles on the rostrum of the sailfish, *Histiophorus americanus*, which he considered designed to create turbulent boundary-layer flow. Height of the denticles was about 0.035 cm and v was about 0.01. The denticles would be fully effective in causing transition at a swimming speed of 34 cm/s, about 0.2 body lengths/s for the sailfish considered.

PRESSURE GRADIENTS

Pressure in the outer flow is impressed onto the boundary layer. When there is a pressure gradient increasing in the direction of mean flow, the pressure forces assist boundary-layer flow. Such a pressure gradient is called favorable, and discourages transition.

The converse gradient is unfavorable or adverse, as it has a retarding effect on the boundary-layer flow. Unfavorable gradients tend to encourage transition, and can also cause the boundary layer to separate from the surface to which it is attached. This is shown in Fig. 9, which illustrates the velocity profile in a boundary layer at four points in a pressure gradient increasing along the $+ x$ axis. Under the influence of retarding frictional forces in the boundary layer and the unfavorable pressure gradient, velocity of fluid particles becomes progressively lower. Particles close to the surface slow down faster than those further from the surface and closer to the higher velocity of the free stream. At some point (S in Fig. 9) velocity of the fluid at the surface
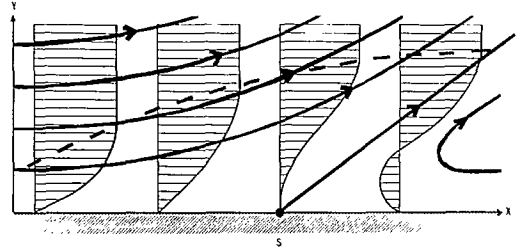
FIG. 9. Diagram illustrating flow in a boundary layer near point of separation, S. Horizontal lines represent velocity vectors, and curved line bounding them, velocity profiles. Dotted line represents velocity thickness of the boundary layer, and solid curved lines, streamlines. The y-axis is exaggerated for clarity. Redrawn from *Applied Hydro- and Aeromechanics* by L. Prandtl and O. C. Tietjens (1934b); © Dover Publications Inc.; used with permission of Dover Publications Inc.)

becomes zero. Then the only forces acting on it are pressure forces, which are acting on the fluid to accelerate it in the opposite direction to that of the remainder of the boundary layer and the free stream. Thus, fluid downstream of S tends to move toward the leading edge of a body. This back flow (relative to the mean flow) causes the boundary layer to separate from the surface, the point of separation being at S. The separated boundary-layer flow penetrates into the outer-flow region, leaving a "stagnant" (low velocity) flow area between the original boundary layer and the surface. This fluid forms an extensive wake into which large quantities of energy are dissipated. This energy appears as a pressure drag (see below).

Separation can occur with a laminar or turbulent boundary layer. However, more uniform distribution of energy throughout a turbulent boundary layer and its higher energy content make it more stable. As a result, separation may be delayed with a turbulent boundary layer.

Flow and Origin of Drag

So far only the flow in the boundary-layer region has been described. The behavior of the outer-flow region, resulting from interactions between this region and the boundary layer, can only be understood in light of the behavior of the boundary layer, particularly in pressure gradients. In the flow pattern around any profile or solid body the velocity field becomes distorted in the region of the body. This distortion in the flow produces streamwise (i.e. in the direction of flow), favorable, and adverse pressure gradients. If there

is a difference in the two gradients and the flow remains distorted downstream of the body, there is a pressure difference between leading and trailing edges which is a drag force. The magnitude of this pressure drag force depends on the magnitude of the adverse pressure gradient, for if it causes the boundary layer to separate, flow is markedly distorted downstream, and pressure drag correspondingly higher.

The pressure drag component is only one source of drag; the other is a viscous drag force arising in the boundary layer. The latter will depend on the wetted surface area of the body and boundary-layer flow conditions. The viscous resistance tends to have a maximum possible magnitude when flow conditions within the boundary layer are turbulent. In contrast the pressure drag component may be variable and several orders of magnitude higher.

To show the interaction between the two regions of flow, flow conditions will be considered first for a circular profile, when adverse pressure gradients are high, and then for a streamline body when they are low. In addition, pressure forces involved in the flow will be discussed by considering first in each case, the potential flow pattern that could be obtained in a perfect (inviscid) fluid.

Flow around circular profile

The potential flow pattern around a circular object is depicted in Fig. 10A. Streamlines are deflected around the body, resulting in distortion to the flow. Continuity of the flow is realized by an increase in velocity from the leading edge of the body, a, to the point of maximum thickness, b, and an equal decrease in velocity from b to the trailing edge of c. Point a is often called the stagnation point, as a fluid particle at this point would be stationary relative to the body. The point of maximum thickness is called the shoulder.

Bernoulli's theorem predicts that changes in fluid velocity in the neighborhood of the body will be associated with changes in pressure. Pressure increases from a maximum at a to a minimum at b, followed by an equal decrease in pressure from b to c. There are equal pressure gradients between these points, but the gradient between a and b is favorable to flow and vice versa between b and c.

In a perfect fluid pressure gradients are equal and opposite and there is no net disturbance to flow. The drag is, therefore, zero as viscosity is assumed absent. It can readily be seen how studies in hydrodynamics and hydraulics could lead to problems like d'Alembert's paradox.
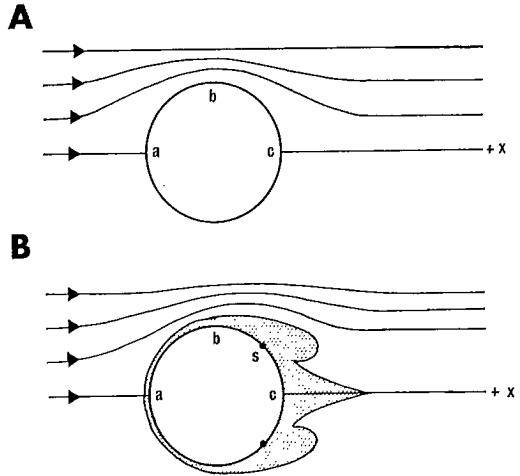
FIG. 10. Flow pattern about a circular profile. A) potential flow pattern for flow in an inviscid fluid; B) flow pattern in a fluid with viscosity. Dotted areas represent the boundary layer which will be turbulent beyond b. The point of separation is S.

Figure 10B illustrates the flow pattern around a circular profile for a real fluid with viscosity. In this case a boundary layer is formed which experiences the pressure gradients described above. On the upstream side of the circular profile the gradient is favorable and assists flow in the boundary layer. On the downstream side, the gradient is unfavorable and steep and the boundary layer separates. The separated flow of boundary-layer fluid severely distorts the flow so it is no longer symmetrical upstream and downstream. An extensive wake is formed.

Velocity in the center of the wake is lower than in the free stream, whereas immediately outside the wake, velocity is higher. Consequently, the net downstream pressure exceeds the net upstream pressure, the pressure difference being the pressure drag force. As this drag force originates because of the shape of the object, it is often called form (pressure) drag.

If the viscous drag is represented by D_f, and the pressure drag by D_p, then the total drag, D_T, is the sum

$$D_{T_c} = D_{f_c} + D_{p_c} \qquad (25)$$

when the subscript, c, denotes a circular cross section.

At R_d (based on cylinder diameter) greater than 300, the wake downstream of a circular body is not disorganized as would be found, for example, downstream of a flat plate normal to the incident flow. Instead, the wake forms an

19
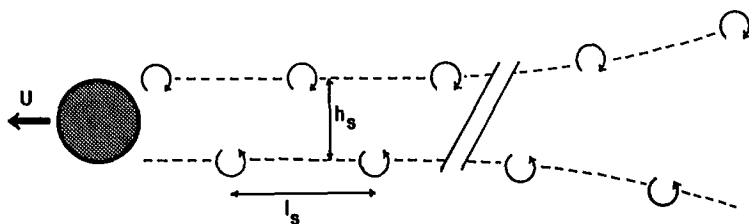
FIG. 11. A Karman vortex street forming the wake downstream from a circular profile. h_s is the row interval and l_s the vortex interval. Figure shows part of the stable portion of Karman Street and beginning of its expansion downstream prior to extinction. (Modified after Prandtl and Tietjens 1934b; Hertel 1966)

organized Karman vortex street named after von Karman who first described the phenomenon (Fig. 11). The vortex street consists of a double row of vortices, each row rotating in the opposite direction relative to the other. The vortices are shed alternately from each side of the body so that the rows are staggered. Structure of the street can be described in terms of the distance between the two rows, the row interval, h_s, and the distance between the vortices in any row, the vortex interval, l_s. The value of l_s tends to remain fairly constant as the vortex street moves downstream, so the two parameters describing the vortex street structure are often expressed as the ratio h_s/l_s. Immediately behind a circular object this ratio is about 0.10–0.15. After the wake has moved a distance equal to about 15 times the diameter of the object, h_s/l_s increases to a value of about 0.28 and remains at this value for a long time. A long distance downstream, h_s/l_s finally increases to about 0.4 as the street begins to break down and mingle with the remainder of the flow.

The frequency of vortex formation, f_v, depends on the characteristic diameter of the object, d, and the incident velocity of the fluid, U

$$f_v = U\,\omega_s/d \qquad (26)$$

ω_s is the Strouhal Number or reduced frequency. This is often shown as a function of R, based on d as R_d, as shown in Fig. 12. In the

medium range of R_d, which is most commonly encountered among fish, ω_s takes a fairly constant value of 0.2.

Vortex streets are commonly formed downstream of swimming fish (Fig. 13), and arise from similar strong pressure gradients around the trailing edge of the caudal fin. However, there is a fundamental difference between such vortex streets and a Karman vortex street. Caudal fin trailing-edge vortices are actively generated and are associated with thrust (Rosen 1959; Hertel 1966; Lighthill 1969).
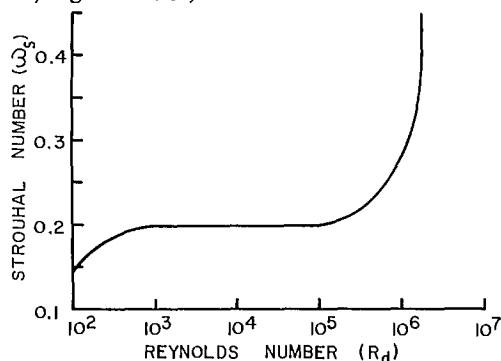
FIG. 12. Relation between Strouhal Number, ω_s, and Reynolds Number, R_a for a circular profile of diameter, d. (Redrawn from *Structure, Form and Movement* by H. Hertel © 1966; reprinted by permission of Van Nostrand Reinhold Co.)

FIG. 13. Photographs of the vortex pattern downstream from a swimming fish (*Brachydanio albolindeatus*). Vortices were detected at some distance from the fish by a thin layer of milk at the bottom of a shallow tank. Photographs were taken at 100 frames/s. Scale is in inches. (From Rosen 1959; used with permission of U.S. Ordnance Test Station, China Lake, Calif.)

Streamline profile

The concept of streamlining was first formulated by Sir George Cayley in 1809 as a result of his observations of the body of trout and later a dolphin (Gibbs-Smith 1962). Ideally, a streamlined body is designed to have zero pressure drag in a real fluid. In practice this is not possible and a streamline body is defined as a body with least resistance.

The importance of the design of a body on flow and drag can be illustrated by the potential flow pattern in Fig. 14A. The flow pattern is in fact the same as that around a circular profile as there is no net distortion of flow, and drag would be zero. However, it differs from that flow in the magnitude of the pressure gradients. The pressure difference between the shoulder at *b*, and the trailing edge of the profile, *c*, occurs over the extended rear portion. The unfavorable pressure gradient over the rear is smaller than that on the downstream face of a circular object.

The importance of the smaller pressure gradient can be seen when the flow pattern is considered for a real fluid with viscosity (Fig. 14B). Because of the smaller gradient, separation of the
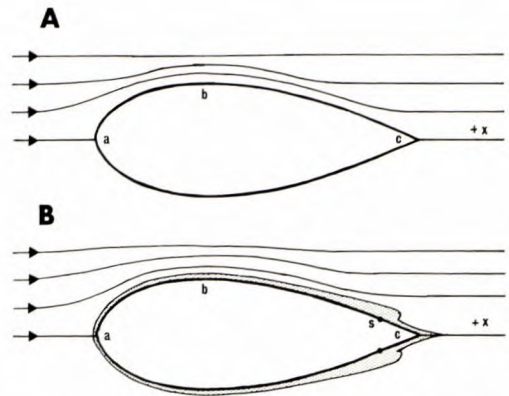
FIG. 14. Flow pattern around a streamline profile. A) potential flow around a streamline profile; B) flow pattern for a real fluid with viscosity. Dotted area represents the boundary layer which will be turbulent at least from point of separation, S.

boundary layer is delayed and, in fact, occurs close to, or at, the trailing edge. The wake behind a streamlined body is consequently small, and so is the net disturbance to the flow. Therefore, pressure drag is also small.

As with the circular object discussed above, the total drag is given by

$$D_{T_b} = D_{f_b} + D_{p_b} \qquad (27)$$

when the subscript represents drag components for a streamline profile.

For a circular object of the same shoulder diameter as a streamline object the wetted surface area will be lower. Therefore, for the same boundary-layer flow conditions

$$D_{f_c} < D_{f_b}$$

However, reduction in the pressure drag component results in a larger difference in form drag

$$D_{p_c} > > D_{p_b}$$

As a result

$$D_{T_b} < < D_{T_c}$$

Streamline bodies are usually characterized by the fineness ratio FR given by

$$FR = \frac{\text{Length of body, L}}{\text{Maximum diameter of the body, } d} \qquad (28)$$

The value of FR which gives the least resistance depends on requirements for the body. For airplane fuselages and bodies of fish it is the value that gives minimum drag for maximum

21

body volume. This requirement is obtained for FR of 4.5. In practice FR can vary between about 3 and 7 and result in only about a 10% change in drag from the optimum value.

Values of D_{f_b} and D_{p_b} will depend on conditions of flow and the precise design of the profile. In the latter case this may be variable, particularly in respect of the position of the shoulder. Special designs can be used which influence not only the magnitude of pressure drag, but also the type of boundary-layer flow over most of the surface. These special designs are discussed in Chapter 4 in relation to drag-reducing mechanisms in fish and cetaceans.

Vortex Sheets in Perfect Fluids

When a wake is formed in a perfect fluid, as behind a flat plate normal to incident flow at velocity U, the velocity in the flow immediately behind the plate is zero. This is the wake velocity U_w. The flow outside the wake still has finite velocity U_o, greater than U because of distortion of streamlines by the plate. Because viscosity is neglected, velocity behind the plate jumps discontinuously from U_w to U_o at the interface between the wake and outer flow. To explain flow in this region a special mathematical concept is used that considers flow conditions in an infinitely thin layer at the interface. This is called a vortex sheet. Discontinuous flow of this nature with its associated vortex sheet can be used to describe more realistically the flow around numerous arbitrary shapes.

The vortex sheet concept is important in fish propulsion problems as it is used in models describing fish locomotion in perfect fluids. As developed in models proposed (e.g., Lighthill 1960, 1969, 1970, 1971; Wu 1971a, b, c, d) describing various fish motions, the concept helps explain much of the variety in body and fin morphology in terms of effects on hydromechanical efficiency (see Chapter 5).

Equations of Drag for Plates and Solid Bodies

Total drag of an object is usually made up of pressure and frictional components as described above. The magnitude of drag components is expressed as drag coefficients which relate the drag to the wetted surface area, S_w, and dynamic pressure, $\frac{1}{2} \rho U^2$. Total drag is expressed as

$$D_T = \frac{1}{2} \rho S_w U^2 C_T \qquad (29)$$

when C_T is a drag coefficient.

In the case of flat plates at zero angle of incidence to flow, the pressure drag component is negligible. For streamline bodies when the drag coefficient contains frictional and pressure drag coefficient components, the latter are often calculated as a fraction of the frictional drag coefficient. It is convenient to consider the frictional drag coefficient first in relation to the boundary layer on a flat plate.

Frictional drag coefficient

Frictional drag arises in the boundary layer. For a flat plate at zero angle of incidence to the flow, Blasius (about 1908) found the frictional drag coefficient, C_f, was related to R_L and to boundary-layer flow conditions. Thus, for a laminar boundary layer

$$C_{f\,lam} = 1.33\,R_L^{-\frac{1}{2}} \qquad (30)$$

and for a turbulent boundary layer

$$C_{f\,turb} = 0.072\,R_L^{-\frac{1}{5}} \qquad (31)$$

In the transitional range of R_L

$$C_{f\,tran} = 0.072\,R_L^{-\frac{1}{5}} - 1700\,R_L^{-1} \qquad (32)$$

These drag coefficients are illustrated as a function of R_L in Fig. 15. The drag coefficient most likely to apply to fish and cetacea is considered under the effect of boundary-layer conditions on total drag.

From Equation 30 and 31 it can be seen that $C_{f\,lam}$ will be less that $C_{f\,turb}$, even though the boundary layer in the latter case is thicker and the velocity gradient would be expected to be lower. In practice the velocity is only lower in a turbulent boundary layer at a short distance from the surface to which it is attached. Immediately adjacent to the surface is a thin sublayer across which the velocity gradient is high, and frictional forces in this region are also high. Energy is also required to maintain the turbulent motion of the fluid particles in the boundary layer.

The two equations show that if the area of a flat plate moving at constant velocity is doubled by doubling its length (providing the velocity is unchanged) drag will be less than double. This is because the boundary layer continues to increase in thickness over the additional length of the plate. Thus, the mean velocity gradient in the
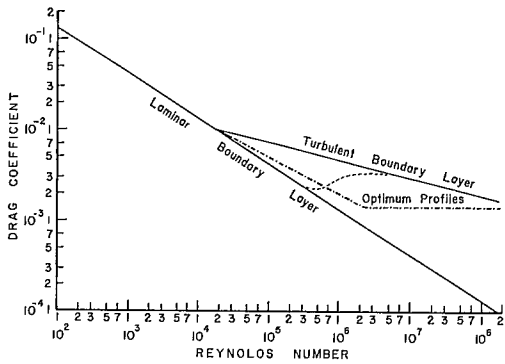
FIG. 15. Relation between drag coefficients for laminar and turbulent boundary-layer flow on an infinite flat plate as a function of Reynolds Number, R_L. Drag coefficients were calculated from Equation 30 and 31. Broken line represents the change in drag coefficient for normal flow at transitional Reynolds Numbers. Chain-dotted line shows minimum drag coefficients for optimum profiles designed to have a minimum drag at each R_L. (Partially based on von Mises (1945) and Hertel (1966))

boundary layer on this section is lower than for the front half. The drag coefficient is also lower and the mean drag coefficient for the whole plate is lower than that for the plate of half its length.

In most experimental situations, such as those using flat plates to test the accuracy of drag balances, the plates are of finite dimensions.

Under these conditions secondary flows occur at the edges of the plate and result in a higher drag than expected (Elder 1960). Elder measured the drag of finite flat plates and related the increase in the drag coefficient to R_L. Results obtained by Elder are shown in Fig. 16.

Pressure drag coefficient

Pressure drag coefficient for flat plates normal to the incident flow is relatively independent of R_L and shape, as drag arises almost entirely from pressure forces. Then C_T is about 1.0–1.3.

For streamline bodies the pressure drag coefficient, C_p, is usually calculated as a fraction of C_f relating the increase in drag due to form to FR. After Hoerner (1958), C_T is then given by

$$C_T = (C_f + C_p)$$
$$= C_f [1 + 1.5 (d/L)^{\frac{3}{2}} + 7 (d/L)^3] \qquad (33)$$

A streamline body usually refers to a body of revolution, that is a body symmetrical about its long axis. Most fish are more or less flattened and are not bodies of revolution. d is generally taken as the mean value of the maximum width and maximum depth for fish and cetaceans. When a fish or cetacean is compared to "an equivalent man-made rigid body" or similar vehicle, this refers to a man-made body of revolution identical with the fish except for the circular rather than elliptical cross section.

FIG. 16. The increment, ΔC_f, applicable to drag coefficient to correct for finite width of a flat plate, shown plotted against Reynolds Number, R_L. (From data in Elder 1960)

23

Boundary-Layer Flow Conditions and Total Drag

Flow conditions in the boundary layer may be laminar, part laminar–part turbulent (transitional), and turbulent, and for each of these conditions it may be attached or separated.

As the size and speed of a body increase (as R_L increases), the boundary layer on a flat plate is first laminar, transitional at $R_{L\ crit}$, and finally turbulent, providing the outer flow is stable and the surface is smooth. The boundary layer on a solid streamline body goes through the same phases and, if it is of small width and depth, the boundary layer will tend to remain attached. However, when width and depth are relatively large, the pressure gradient downstream of the shoulder encourages separation particularly as speed and pressure gradients increase.

Interaction of the boundary-layer flow conditions and drag components are illustrated in Fig. 17 for a streamline body. The lowest drag conditions are obtained only when separation is avoided. Theoretically, only small fish would be expected to avoid separation effects. If it is
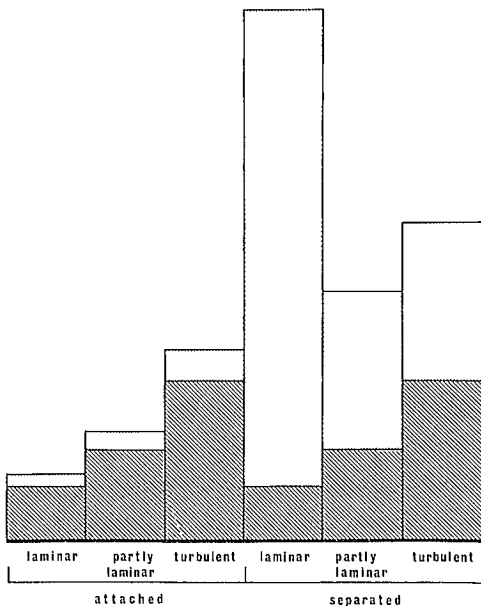
assumed they do avoid separation, it is unlikely they could still achieve the minimum drag conditions found with a laminar boundary layer. This is because the flow in streams, rivers, shoals, etc., is likely to be turbulent. Furthermore, protuberances such as eyes, external flaps on the nares, and fins all behave as large roughness elements leading to turbulence (Allan 1961).

If the external disturbances are not too large, it would still be possible to achieve the transitional flow conditions. It is probable that most fish operate within this range of boundary-layer flow conditions with a laminar boundary layer to the shoulder, and a turbulent boundary layer downstream. Exceptions would be many elasmobranchs with rough skins and possibly larger cetaceans, which are expected to have fully turbulent boundary-layer flow.

It is doubtful if many fish actually achieve attached boundary-layer flow beyond the shoulder (see Chapter 4). As such, they experience a much larger drag component produced by pressure forces. Figure 17 shows that the advantages of the boundary-layer flow conditions are then reversed as total drag with a turbulent boundary layer is much lower than with laminar boundary-layer flow. This is because of greater stability of the turbulent boundary layer and its greater resistance to separation which occurs later. A turbulent boundary layer, at least downstream of the shoulder, may be beneficial to the reduction of total drag.

It is difficult to reduce the frictional component of total drag, although minimal drag can be obtained by specially designed laminar shapes that extend the favorable pressure gradient up to the shoulder over as much of the body as possible. It is more advantageous to reduce the pressure drag component as it is often greater than the frictional component. A great deal of effort has been expended, particularly by the aircraft industry, to find mechanisms to reduce pressure drag. Several successful mechanisms used on aircraft wings and fuselages have been recognized in fish where they probably serve a similar function. These are discussed in detail in Chapter 4.

Periodic and Unsteady Motion

Flow patterns described above are applicable only to bodies moving at uniform velocities. Such behavior is not typical of the bodies of many fish when at least some portions of the body move with periodic or unsteady motions. This behavior markedly affects flow patterns, although it has

FIG. 17. Diagrammatic representation of the relative effect of various boundary-layer flow conditions on the total drag of a streamline body. Shaded areas represent frictional drag, D_f, and dotted areas pressure drag, D_p. (From Webb 1970)

generally been assumed that the motion of water around swimming fish will tend toward steady states.

Periodic motion

Studies of periodic motions of bodies have usually been confined to a simple harmonic motion of small amplitude executed by cylinders or plates. When a cylinder moves in this way, normal to its long axis, flow takes on the form depicted in Fig. 18. The periodic motion of the cylinder imparts a steady secondary flow to the whole fluid. This steady motion occurs at some distance from the cylinder and is the result of viscosity of the fluid, although the magnitude of the secondary flow is independent of viscosity. The stable secondary flow is only set up after some time and results in a flow toward the cylinder along an axis perpendicular to the motion and away from the cylinder along the axis of the periodic motion.

Unsteady motion

The small amplitude periodic motion described above is less like that of body movements of a swimming fish, which are of large amplitude. In addition, fish are propelled forward by their body movements so there would probably be
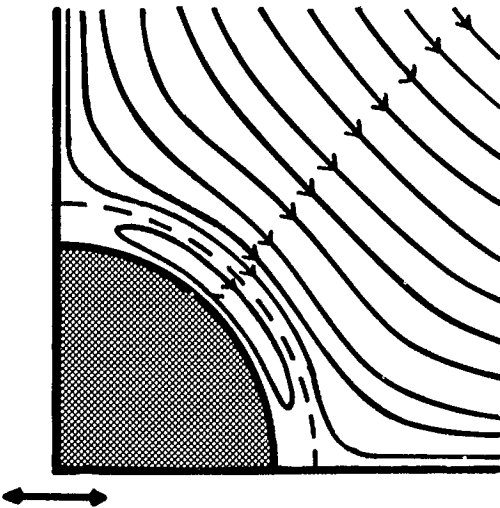
Fig. 18. Diagrammatic illustration of the flow around a circular profile moving with simple harmonic motion in the direction shown by double-headed arrow. Broken line shows limit of the boundary layer, and solid lines the streamlines after steady secondary flow has been established. (Redrawn from *Boundary-layer Theory* by H. Schlichting; © McGraw-Hill Book Co. 1968; used with permission.)

insufficient time to set up steady-state secondary flow. Flow around the body of a fish is probably more similar to that around a body undergoing unsteady motion with periodic stops and starts.

When a cylinder starts to move in a direction normal to its long axis, a boundary layer immediately begins to form, increasing in thickness with time and distance moved. Once the cylinder has ceased to accelerate and begins to move at a uniform velocity, the boundary layer rapidly reaches the thickness expected for the relevant R_d. At the same time as the cylinder accelerates, the boundary layer is progressively affected by pressure gradients on the downstream side of the cylinder. Eventually separation occurs, the separation point depending on time (and acceleration and final velocity) and distance moved. If the distance moved by the cylinder when separation occurs is X_s, then

$$X_s \simeq 0.351 \, R_d \qquad (34)$$

and if t_s is the time to separation, and U the final velocity

$$t_s \simeq 0.351 \, R_d/U \qquad (35)$$

Bodies and fins used in fish and cetacean propulsion are rarely circular, but elliptical. Values for X_s and t_s for elliptical bodies depend on d/w, when w is the width in the direction of motion and d is the depth normal to w (Fig. 19). Values for X_s for various elliptical shapes are shown as a function of d/w in Fig. 19 which also shows some values for d/w found among fish and cetaceans.

In addition to the boundary-layer phenomenon, a body starting from rest affects the fluid to some distance from its surface. The effect of the motion spreads through the fluid at the speed of sound (instantaneously for practical purposes) and a relatively large mass of fluid tends to be accelerated with the body. This fluid mass is called the virtual mass or added mass. For the propulsive portions of the bodies of most fish the virtual mass, m_v, approximates to

$$m_v = \rho \, \pi \, d^2/4 \, g/cm \qquad (36)$$

(Lighthill 1969, 1970).

Similarly, when a body decelerates, the virtual mass will add to the total momentum of the system and must be decelerated with the body. This is particularly important in the case of gliding fish, when a mass of about $0.2 \times$ body mass is generally added to that of the body to calculate the deceleration forces (Gero 1952; Bainbridge 1961).

25
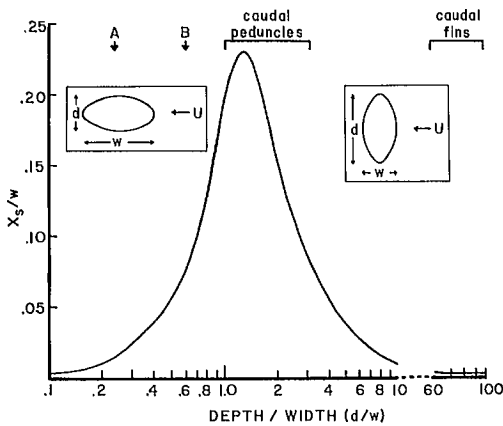
FIG. 19. Relation between distance moved before boundary-layer separation occurs and dimensions of elliptical and circular profiles accelerating from rest. Distance moved before separation (X_s) is shown as the ratio of profile width (w), as X_s/w. Dimensions of the profile are shown as the ratio of depth (d) to width (w), as d/w. Values for d/w for caudal fins and caudal peduncles of fish and cetaceans are shown, and for caudal peduncle of *Balaenoptera borealis* (A) and *Euthynnus affinis* (B). (From data in Hertel (1966) and Magnuson (1970) respectively)

Hydrofoils

Hydrofoil theory has a wide application to the study of fish propulsion, particularly to various aspects of dynamic stability during swimming. The parts of the body which execute propulsive movements have often been compared to hydrofoils to illustrate qualitatively (and sometimes quantitatively) forces acting on the body of a swimming fish. Median and paired fins of many fish behave more obviously as hydrofoils in controlling pitching, rolling, and, to some extent, yawing excursions during swimming, and are important in maneuverability. Similarly pectoral fins of scombrids and elasmobranchs control vertical equilibrium, as do pectoral fins of flying fish.

In all these cases, a surface functions to produce forces perpendicular to the axis of motion and this property will serve as a definition of a hydrofoil. It is, however, usually a requirement that the perpendicular ("lift") forces be produced with a minimum of drag. Most available information is concerned with aerofoils, but such data can be applied to fish by means of laws of similitude. The term hydrofoil will be used throughout this section as being more appropriate for aquatic vertebrates.

Flow pattern and forces

The flow pattern around a flat plate will be considered as the most simple design for a hydrofoil. When a flat plate of finite width moves along its axis at zero angle of incidence to the flow, the flow pattern can be described by a series of parallel lines (Fig. 20A). The only forces experienced by such a plate will be frictional forces as described above. However, when the plate moves at an angle, the angle of attack, α, to the flow, streamlines are deflected above and below the plate (Fig. 20B). Fluid velocity below the plate is lower than above. Bernoulli's theorem predicts this will be associated with a pressure difference, so that the pressure below the plate exceeds that above. The net pressure difference represents a pressure force, P, acting at some angle to the motion of the plate.

This description of hydrofoil principles is highly simplified. A correct description of hydrofoil function requires consideration of a superimposed circulation on the purely translational flow. The simplified description is all that is required here; readers interested in greater detail are referred to the monographs listed in the introduction to this chapter.

The net pressure force, P, can be resolved into two components; a lift force, L, acting normal to the axis of motion, and a drag force, D, acting along that axis and retarding the motion (Fig. 20C).
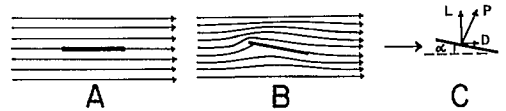
FIG. 20. Flow and forces on a flat plate acting as a hydrofoil: (A) flow around a flat plate at zero angle of attack to the incident flow; (B) flow pattern around a flat plate at a small angle of attack, α, with translational and rotational flow patterns superimposed; (C) forces experienced by hydrofoil in B. Gross pressure force is represented by P, shown resolved into lift, L, and drag, D, components. Boundary layer is not shown. (Redrawn from *Theory of Flight* by R. von Mises (1945); © Dover Publications Inc.; used with permission)

Flow over the two surfaces of the hydrofoil tends to remain streamlined with boundary-layer separation occurring close to the trailing edge only when α is less than a certain critical value, α_{crit}. Above this value separation of the boundary layer occurs close to the leading edge. This has the same effect as early separation on any

26

other body. Flow is greatly distorted and an extensive wake is formed (Fig. 21). There is a great increase in the pressure difference along the axis of motion, with a concomitant decrease in that normal to the axis. Thus, D is greatly increased, and L is reduced. Such a hydrofoil is said to have stalled. At values of α above stall values, the efficiency of a hydrofoil will be reduced, which is undesirable, except when hydrofoils are used as brakes as with paired fins of many fish. Then, the ideal value of α is 90°.
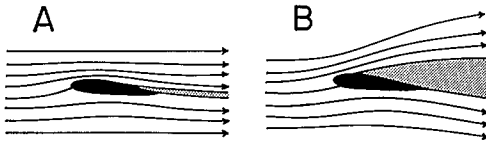
FIG. 21. Flow pattern around a hydrofoil: (A) below $α_{crit}$; and (B) above $α_{crit}$, when hydrofoil is stalled. (Redrawn from *Theory of Flight* by R. von Mises (1945); © Dover Publications Inc.; used with permission)

Geometry

The geometry of aerofoils is extremely variable and much of this variety is seen in fish. Thus, the plan, profile, and angles subtended to the incident flow and with the body can all vary according to the requirements of the particular fish.

Basic plans or planforms are shown in Fig. 22. Each planform can be characterized by a length or chord, C, and a width or span, S, normal to that axis. The ratio, S/C, is the aspect ratio, AR. For arbitrary shapes, as for swept-back and tapered profiles and most fish hydrofoils, AR is calculated from

$$AR = S/C \text{ or } S^2/S_h \text{ or } S_h/C^2 \qquad (37)$$

when S_h is the maximum projected area of the hydrofoil. For paired hydrofoils, S_h is the total maximum projected area for both the hydrofoils, as they usually behave as a single unit.

Fins of fishes, singly or in pairs, are usually tapered and often swept-back. The same is true of caudal fins of fish with a well-defined tail.

The plane of paired hydrofoils may be rotated relative to the normal plane of the fish. The angle subtended between the latter horizontal plane and the hydrofoil is the dihedral angle (Fig. 22D). The pectoral fins of *Euthynnus* are so oriented with a positive dihedral angle (Magnuson 1970).

Various types of planform and dihedral angle are related to the stability of the body to which the hydrofoils are attached. A tapered hydrofoil results in the highest lift forces produced close to the center of mass, reducing the magnitude of rolling forces acting on the body in the event of any asymmetry in the flow. Such planforms have obvious structural advantages as they require less heavy support per unit of lifting area than rectangular hydrofoils of the same area.

Swept-back planforms move the center of lift backward relative to the center of gravity, and affect pitching equilibrium. This is particularly important in fish when the hydrofoils are often
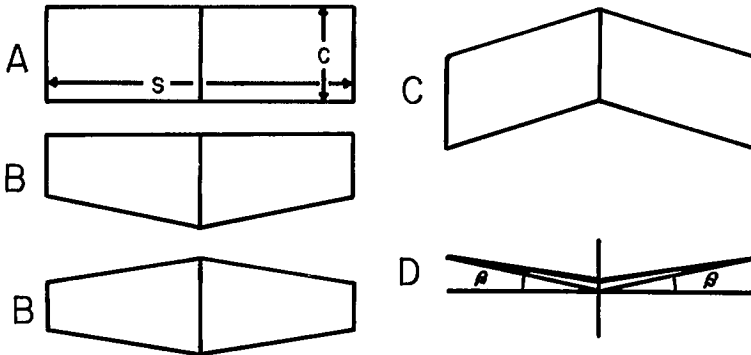
FIG. 22. Basic types of planforms of hydrofoils: (A) rectangular planform showing span, S, and chord, C; (B) tapered planform; (C) sweptback planform; (D) frontal view of a paired hydrofoil showing the dihedral angle, $β$. (Redrawn from *Theory of Flight* by R. von Mises (1945); © Dover Publications Inc.; used with permission)

27

mobile. In fish gliding to a halt, continual variation in the angle of sweepback can often be seen.

The dihedral angle confers stability to yawing, as some component of the pressure force acting on the hydrofoil is oriented laterally. With fixed hydrofoils these forces are balanced, but in fish it is likely that the dihedral angle is varied on either side of the body for fine control during maneuvers.

Variation in hydrofoil profiles in fish is apparently less than for man-made aerofoils (Fig. 23). This is because most fins are more like flat plates, operate at lower Reynolds Numbers, and often do not have to produce maximum lift. As a result, the commonest types of profile are similar to those shown in Fig. 23B, D. The first is a simple flat plate, and the second a cambered plate. A cambered hydrofoil has a profile in which the center line is curved relative to a line joining leading and trailing edges. Maximum displacement of this center line, the camber, is usually expressed as a percentage of the chord, the relative camber. Apparently most fins acting as hydrofoils are cambered as in *Euthynnus* (Magnuson 1970). There are few examples of solid hydrofoils among fish, like those shown in Fig. 23A, C, E. Sections of the pectoral fins of elasmobranchs tend to have some depth (Breder 1926) as do caudal peduncles employed by some scombroid fishes to generate lift (Magnuson 1970). As with relative camber, the maximum thickness, T, characterizing a solid profile, is expressed in relation to the chord length. The ratio, T/C, is called the thickness ratio.

Choice of a particular profile usually depends on the flow conditions under which they operate, as expressed by a Reynolds Number, R_C, based on chord length. For fish, R_C is commonly between 10^2 to 10^5 and the highest lift forces and the highest lift:drag ratio is obtained with flat plates and cambered plates. Above R_C of about 10^5 more conventional solid profiles give better results (Alexander 1968).

Equations for lift and drag

For a given hydrofoil moving with a uniform velocity, U, at an angle of attack, α, the lift, F_L, and drag, F_D, forces are calculated from

$$F_L = \tfrac{1}{2} \rho S_h U^2 C_L \qquad (38)$$

and

$$F_D = \tfrac{1}{2} \rho S_h U^2 C_D \qquad (39)$$

when C_L and C_D are lift and drag coefficients, respectively. They are often expressed as the lift:drag ratio, as C_L/C_D or F_L/F_D. Most hydrofoils are designed for both a maximum C_L and lift:drag ratio at the normal operating velocity.

The magnitude of C_L and C_L/C_D depends on the flow conditions, and R_C (see above) on the angle of attack, planform, and profile.

ANGLE OF ATTACK

Figure 20C shows that the pressure force and F_L and F_D components acting on a hydrofoil will be dependent on α. In practice, C_L tends to be linearly related to sine α to $α_{crit}$ (Fig. 24A). Thus

$$C_L = k \text{ sine } \alpha \qquad (40)$$

when k is a constant for a given hydrofoil.

Above $α_{crit}$, C_L decreases markedly with the disruption in flow over the hydrofoil at the stall.

C_D increases exponentially with $α_{crit}$ (Fig. 24B) usually with a minimum value when α is zero. Above $α_{crit}$, C_D increases markedly as C_L falls.

The relation between the lift:drag ratio (Fig. 24C) and α increases to a maximum value at a relatively small α because, although C_L increases linearly, C_D increases exponentially with α.

For values of α above that giving the maximum C_L/C_D, the lift:drag ratio decreases rapidly, particularly above $α_{crit}$.

ASPECT RATIO

C_L is greatest for a hydrofoil of given area when AR is highest, although in practice, AR values above about 8–10 give little further advantage and are associated with structural problems.
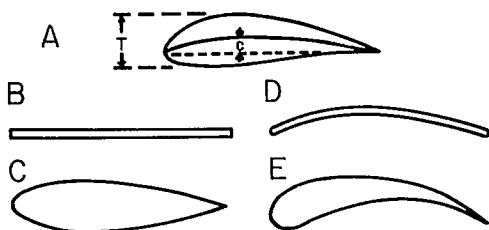
FIG. 23. Basic profiles of hydrofoils: (A) streamlined, cambered profile showing thickness, T, and camber, c; (B) flat plate; (C) conventional, streamlined profile; (D) cambered plate; (E) streamlined, cambered profile. (Based on Alexander 1968; Hoerner 1958; and von Mises 1945)
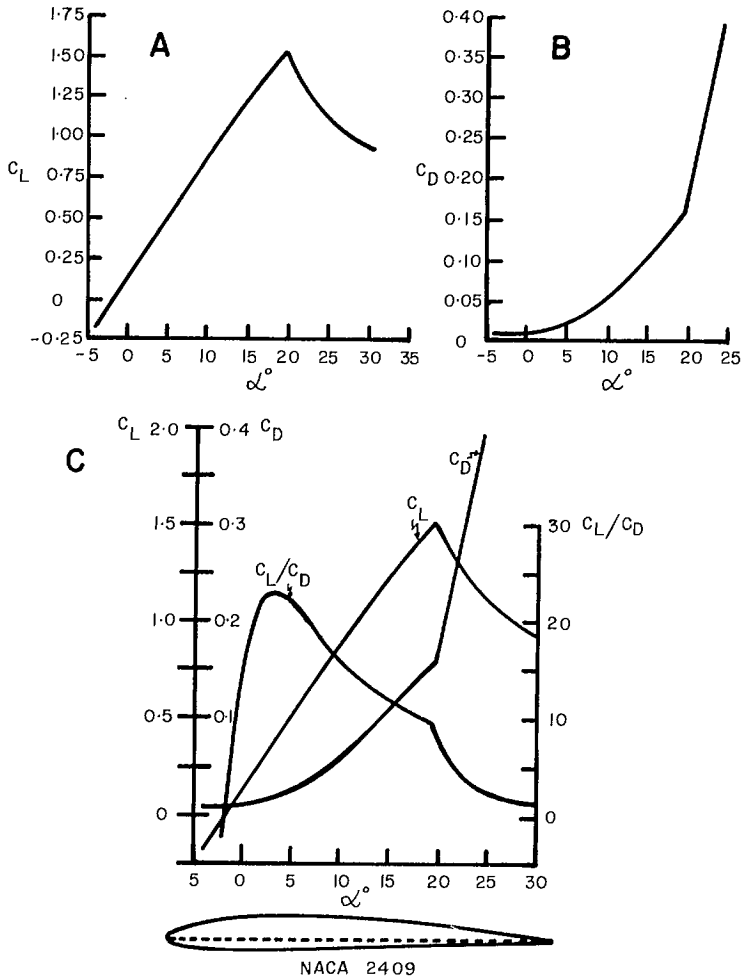
Fig. 24. Relations between C_L, C_D, and lift: drag ratio with α for NACA 2409 profile. (Redrawn from *Theory of Flight* by R. von Mises (1945); © Dover Publications Inc.; used with permission)

In contrast, C_D is inversely related to AR, as one of the important components of C_D is an induced drag component, C_I, dependent on AR. This drag component results from the pressure difference between the two surfaces of the hydrofoil which produces cross flows at the hydrofoil tips. The cross flow causes the formation of longitudinal wing tip vortices, the energy dissipated in these being the induced drag. It follows that the greater the AR the smaller the chord length around which cross flow can occur in relation to the total lifting surface. Not only are C_I and C_D reduced, but a higher mean pressure over the surface is also maintained and C_L is higher. In this respect a tapered planform can be advantageous in concentrating lift forces away from the wing tips.

PROFILE

The magnitude of C_D in particular is affected by any profile differing from a flat plate. This is because a pressure drag component arises in the same way as on a solid body described above. The pressure drag coefficient, C_p, can be approximately related to the thickness ratio (T/C) and to relative camber

$$C_p = C_p' + 0.0056 + 0.01(T/C) \qquad (41)$$
$$+ 0.1(T/C)^2$$

29

C_p' is the pressure component dependent on relative camber: some typical values are in Table 1.

Relative camber %	Pressure drag coefficient (C_p')
0	0.0
2	0.0005
4	0.001
6	0.002

A solid profile will also increase the surface area of the hydrofoil in comparison with a flat plate of the same chord length and AR. However, the magnitudes of C_I and C_p are much greater than those due to frictional drag, which tend to be neglected. As hydrofoil lift and drag equations are usually based on empirical data, the frictional component is included in practice through its calculation from such equations as 39.

Center of lift

Most problems concerning hydrofoils among fish are related to stability and maneuverability. As such, it is necessary to know the point at which the mean lift force acts to calculate moments about the center of mass. The point at which lift acts, often called the hydrodynamic focus or center of lift, can only be found for a given hydrofoil by experiment. Usually the focus lies between 0.25 C (quarter chord point) and 0.33 C from the leading edge.

Note on Propellers

Man-made "screw-type" propellers are obviously not found in fish. However, the general principles of efficient operation of propeller systems are applicable to the fish propeller system, and will be briefly considered.

The principles of propeller operation can be understood in the light of hydrofoil theory. In a screw propeller each section of a propeller blade moves in a circular path, subtending an angle of attack to the incident flow, the angle depending on the angular velocity of the section and the forward speed of the propeller. Movements are associated with thrust, the wake formed downstream of a propeller moving at a velocity, U_w, greater than the free-stream incident velocity, U.

For a screw propeller to generate thrust, there must be a positive angle of attack between the hydrofoil sections of the blade and the incident flow. This is achieved when the local velocity of any section exceeds U, the ratio between the two velocities being expressed as the advance ratio, J. Thus, for a section at the tip of a blade

$$J = U/\omega = U/2 \pi r f \qquad (42)$$

when

ω = angular velocity

r = radius of the propeller disc

f = frequency (revolutions per second).

ω varies along the length of a blade so the angle of attack must similarly vary. This accounts for the "twist" in propeller blades.

For thrust to be generated, J must be less than 1. Otherwise, there would be no relative motion between the water and the blade, and α would be 0.

The same conditions apply to the propulsive portions of bodies of fish. Gray (1933a, b, c) showed there must be relative motion between the water and moving portions of the body. This condition is realized when the forward velocity of the fish, U, is less than the backward velocity of the propulsive wave, V. Thus, the ratio U/V, comparable in many ways to J, must be less than 1. This ratio was called the slip by Kent et al. (1961).

The mechanical efficiency of a screw propeller, η_p, is defined by the ratio between the power supplied to the propeller shaft, E, and the thrust power output, E_T

$$\eta_p = E_T/E \qquad (43)$$

and can be related to J. Similarly, the slip is related to the propeller efficiency of the fish propulsive system, although not as simply (Lighthill 1960, 1969, 1970; Webb 1971b).

As η_p may be related to J, it will also be inversely related to the propeller disc circumference from Equation 42 or, more simply, to the propeller disc diameter. Reasons for the advantage of a large disc diameter are similar to those for high AR. With a large disc diameter, the circumference is small in proportion to the area across which thrust is generated. Thus, the larger the disc the relatively smaller the length around which cross flow and energy losses can occur.

Furthermore, the larger the disc area the smaller the mass of water that must be accelerated for a given thrust force and the smaller the losses in kinetic energy. This is because the thrust generated is proportional to the mass of the fluid, M, and the increase in velocity given to it. That is

$$T_p = M (U_w - U) \qquad (44)$$

The kinetic energy, when T_p = thrust KE, required to accelerate the water to the wake velocity is given by

$$KE = M (U_w^2 - U^2) \qquad (45)$$

High propeller efficiency can be obtained by increasing the mass of water affected, while decreasing the velocity increase it receives (Alexander 1968).

These principles apply equally to the fish propulsive system. The propeller disc area is equivalent to the product of amplitude of the tail beat and height of the trailing edge of the tail. Bainbridge (1963), Hunter and Zweifel (1971), and Webb (1971a) have shown that the amplitude of the tail beat reaches maximum values as swimming speed increases, presumably because efficiency becomes of greater importance as the limit to the supply of metabolic energy is approached. In addition, the amplitude of the tail beat of several scombrids, among them the fastest aquatic vertebrates, is up to 50% greater than in other fish (Fierstine and Walters 1968).

Equation 44 and 45 show that efficiency can be increased by decreasing the absolute values of U_w and U, as well as their relative values. This is apparently achieved by fish which situate the major portions of the propeller system in the slower wake associated with the drag of the body (Hertel 1966).

Flow Through Pipes

The flow of water through pipes and enclosed pipe systems is important to fish propulsion studies for two reasons. First, fish are often forced to swim inside some enclosed pipe system. Second, the flow through the buccal and opercular chambers and the gill sieve is similar to the flow through an enclosed system of pipes. The resistance to the flow through this system contributes to the total drag of a swimming fish.

Flow patterns

As with flow around bodies, flow through a pipe may be laminar, transitional, or turbulent, depending on the ratio of viscous and inertial forces and other flow conditions discussed above. Different conditions can be compared by Reynolds Law, defining a Reynolds Number, R_r, based on the radius of the pipe. The critical value $R_{r\ crit}$ is about 10^3.

The velocity profile of flow through a pipe depends on the type of flow (Fig. 25). With laminar flow, the profile tends to be curved because of dominant frictional forces. With turbulent flow, the flow profile tends to be fairly rectilinear as viscous forces are overridden by the inertial forces associated with the additional motion of fluid particles.

In terms of water tunnel experiments with fish, a laminar flow pattern has an advantage over turbulent flow as it allows normal boundary-layer growth. When flow is turbulent, the intensity of turbulence tends to exceed critical values so that the boundary layer of any body in the flow must also be turbulent. Because of the curved nature of the laminar flow profile, calculation of the mean velocity of a fish within it would be almost impossible. Therefore, a rectilinear profile is desirable, as achieved with microturbulent flow. It was suggested that most fish will swim in a turbulent environment in any case, so the disadvantages of a turbulent flow are undoubtedly of less importance than the advantages.
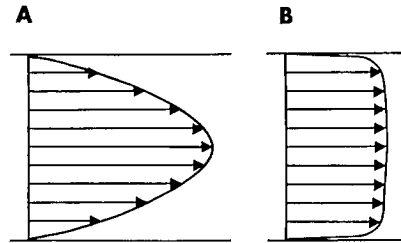
FIG. 25. Velocity profiles for flow of a fluid with viscosity through circular pipes: (A) laminar flow; (B) turbulent flow.

Law of Continuity and Bernoulli's theorem

The Law of Continuity states that flow through all sections of an enclosed pipe system is constant (technically for time-independent flow only). If the cross-sectional area of a pipe is S_x and the velocity of flow, U,

$$\text{Flow} = US_x = \text{Constant} \qquad (46)$$

In an enclosed system when the cross-sectional area varies, the velocity of flow will also vary in inverse proportion to S_x. The importance of the law comes from its coupling with

31

Bernouilli's theorem, which predicts that changes in U will be associated with changes in the net fluid pressure. As a result, the pressure in the fluid increases as S_x increases.

These two principles are important in calculating the pressure drop associated with gill water flow and can be used in conjunction with the equations given below to calculate gill resistance (Brown and Muir 1970).

Pressure drop and resistance to flow

The resistance law for the flow of fluids through pipes is called the Hagen–Poisseuille Law.

For laminar flow, the pressure difference Δp required for a given flow is given by

$$\Delta p = 8 \, \mu \, \ell \, \overline{U} / r^2 + \tfrac{1}{2}, \rho \, \overline{U^2} \qquad (47)$$

$\overline{U}$ = mean velocity of flow
r = radius of pipe
ℓ = length of pipe

The last term in Equation 47 represents the kinetic energy of flow. Equation 47 can be rewritten in terms of R_r.

For laminar flow

$$\Delta p = \frac{16.l}{R} \quad \frac{\rho \, \overline{U^2}}{2} \qquad (48)$$

For turbulent flow

$$\Delta p = \frac{0.133}{\sqrt[4]{R_r}} \quad \frac{\rho \, \overline{U^2} \, \ell}{2 \, r} \qquad (49)$$

The flow through the secondary lamellae gill sieve is likely to be laminar, as the dimensions of gills and water flow all combine to make R_r much less than $R_{r\ crit}$ (Hughes 1966; Hills and Hughes 1970). The equations given above are difficult to apply directly to the gill sieve as this tends to be made up of rectangular rather than round spaces. Hughes (1966) calculated an alternative expression applicable to rectangular tubes

$$\Delta p = \frac{24 \, l \, \mu}{5 \, d^3 \, w \, q} \qquad (50)$$

when

d = depth of pores in the sieve
w = width of pores
q = flow.

Chapter 2 — Kinematics

Classification of Propulsive Movements

Before discussing various hydrodynamic and biological aspects of fish locomotion, it is imperative that body and fin movements of swimming fish be fully understood. Superficial examination of swimming fish suggests that these movements vary markedly in different groups of fish. Long thin fish, like eels or blennies, pass a well-defined propulsive wave back over the body, whereas shorter, thicker fish, like dace or mackerel, appear to swim by moving the caudal fin alone. Other fish, like the electric fish, *Gymnotus*, swim by passing waves along their median fins, while the body remains fairly straight; others may use paired fins while the body remains fairly straight; others may use paired fins as sculls, for example surf perch (Breder 1926; Gray 1968; Webb 1973b).

Breder classified the various movements into different categories, or modes, after Lighthill (1969). Three main categories are distinguished on the basis of body and/or fin movements: fish that use their bodies and caudal fins, fish that use extended median or paired fins, and fish that use shorter median or paired fins. A fourth group of aquatic propulsion mechanisms can be considered for animals using jet propulsion, the common escape system in cephalopods. Breder (1926) considered this could apply to exhalant respiratory flow in fish, but the volumes of water, and their low velocity (Brown and Muir 1970) indicate this would generate negligible thrust. Jet propulsion is not likely to apply to fish.

Fish that use their bodies and/or caudal fins for propulsion

Most studies on fish propulsion have been made on fish that swim by means of body and caudal fin movements. In this category, Breder (1926) originally distinguished three modes, anguilliform, carangiform, and ostraciform (Fig. 26). Classification of swimming movements of fish and cetaceans follows:

Anguilliform mode: whole body thrown into a wave with at least one half-wavelength within the length of the body and usually more than a complete wavelength. Amplitude usually large over whole body length. Body typically long and thin. Named after the eel, *Anguilla*.

Subcarangiform mode: body and caudal fin thrown into a wave, with more than one half-wavelength within the length of the body. Amplitude rapidly increases and is large over posterior-half or third of body length. Body shape fusiform with deep caudal peduncle.

e.g., *Salmo*, *Carassius*, *Leuciscus*, *Gadus*.

Carangiform mode: body and caudal fin usually thrown into wave, with up to one half-wavelength within length of body. Amplitude increasing over posterior third of body length, large at trailing edge. Body shape fusiform with narrow caudal peduncle. Named after *Caranx*.

Carangiform mode with semilunate tail: body movements carangiform. Amplitude increasing over caudal peduncle, large caudal fin. Body shape fusiform with narrow caudal peduncle and large half-moon shaped caudal fin.

e.g. *Lamna*, *Euthynnus*, *Phocoena*, *Balaenoptera*.

Ostraciform mode: body rigid and not thrown into a wave. Propulsion by means of caudal fin oscillation. Body shape variable, but not streamlined. Named after family Ostraciidae, e.g., *Ostracion*.

Fish that use extended median or pectoral fins for propulsion

In all cases the fin(s) used are thrown into a wave formation, similar to the body wave in the anguilliform mode, but of more constant amplitude along the fin length (Fig. 26).

Amiiform mode: use extended dorsal fin. Named after *Amia*.

Gymnotiform mode: use extended ventral fin. Named after *Gymnotus.*

Balistiform mode: use extended dorsal ventral fins. Named after *Balistes.*

Rajiform mode: use extended pectoral fins. Named after *Raja.*

Fish that use shorted median or pectoral fins for propulsion

In all cases fins pass waves along their length.

Tetraodontiform mode: use short dorsal and ventral fins. Named after family Tetraodontidae, e.g., *Lagocephalus.*

Diodontiform mode: use short pectoral fins with short wavelength movement. Named after family Diodontidae, e.g., *Cichlasoma.*

Labriform mode: use pectoral fins with long wavelength movement so fins behave as paddles or sculls. Named after family Labridae, e.g., *Scarus.*

Body modes are distinguished based on the number of half-wavelengths of the propulsive wave contained within the length of the body. Thus, in the anguilliform mode at least one half-wavelength is considered to be involved in propulsion, up to one half-wavelength in the carangiform mode, and less than one half-wavelength in the ostraciform mode (Fig. 26).

ANGUILLIFORM   CARANGIFORM   OSTRACIFORM

AMIIFORM   GYMNOTIFORM

BALISTIFORM   RAJIFORM
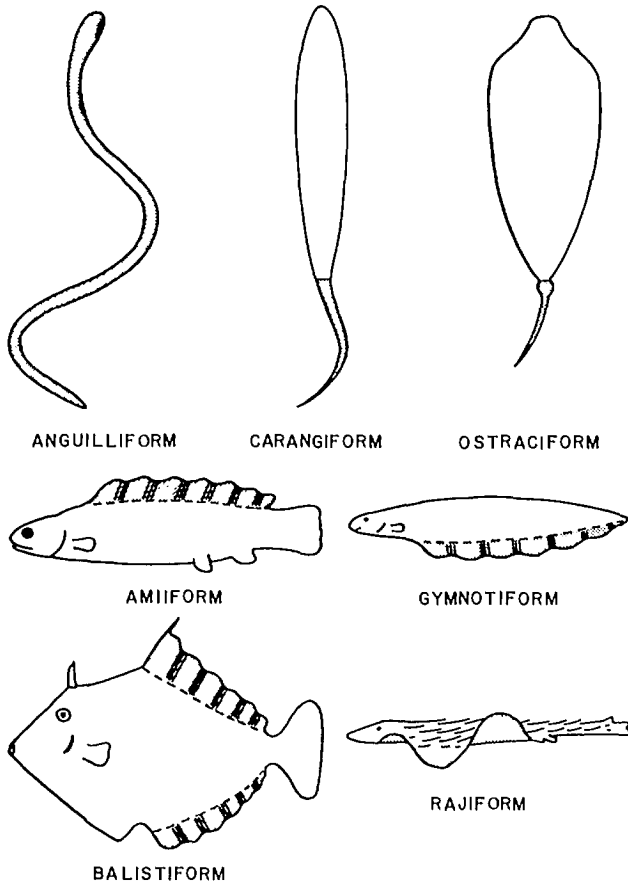
FIG. 26. Some principal types of swimming modes in fish. The portion of body or fins executing lateral movements is shown stippled. (Modified after Breder 1926; Gray 1968)

Gray (1968) suggested that the proportion of the body involved in the propulsive wave, and the number of half-wavelengths was dictated by the flexibility of the body.

Many pelagic fish, originally classed as carangiform by Breder (1926), contain more than one half-wavelength within the length of the body, and sometimes more than a complete wavelength (Bainbridge 1963; Fierstine and Walters 1968; Webb 1971a). These fish swim in the anguilliform mode, by definition, although their body shape is more similar to fish swimming in the carangiform mode. Breder introduced the term subcarangiform to describe this intermediate type, although he originally restricted the term to more rigid fish like heavily scaled holosteans, e.g., *Amiatus.* Fish swimming in the subcarangiform mode according to Breder were those which normally swam by means of an alternative propulsion system (i.e. paired fins) but when using their bodies for swimming, tended towards the carangiform mode. The subcarangiform mode used here will refer to all fish that swim in a manner intermediate between the anguilliform and carangiform modes, whether the movements are primary or secondary means of propulsion. The subcarangiform mode includes such families as Salmonidae and Gadidae.

Breder's (1926) original classification considered average types in a continuous range (i.e. true "modes"), and should not be used too rigorously. The addition of further subdivisions, in the light of more complete data, in no way invalidates the original classification, but rather increases its value.

The two main categories of fish that use median and paired fins, are basically similar. The two groups differ in the length of appendages used, so that the only major difference between them is the freedom with which the axis of movements can be controlled in relation to the body. This freedom is negligible in amiiform, gymnotiform, balistiform, and rajiform modes, but high in tetraodontiform, diodontiform, and labriform modes when fin bases are small (Harris 1937).

It is somewhat misleading to attempt to classify modes involving short-based pectoral fins, as fish exercise a high degree of control over these fins, and movements are consequently complex. In Breder's classification, labriform and diodontiform modes are those normally encountered as the primary locomotory method, whereas other methods usually involving body movements are used in rapid darts, for example

to avoid predators. In addition, paired fin movements are common among fish primarily using body movements for swimming. Paired fins may be used for swimming at very low speeds, but otherwise are usually used in stability control (Breder 1926; Harris 1936, 1937, 1938, 1953).

Body and Caudal Fin Movements

Swimming movements involving the body and caudal fin are the most commonly encountered pattern among fish and cetaceans. Fast swimming fish and cetaceans and those making long migrations swim mainly in this way. Seals and manatees have modified bodies and hind limbs that execute swimming movements of similar fashion. Fish that usually use other alternative methods typically resort to body and caudal fin movements for escape maneuvers and fast turns. Most effort has been expended in studying the kinematics of body and caudal fin propulsion, probably because of its ubiquity among aquatic vertebrates.

Anguilliform, carangiform, and ostraciform modes include an extensive range of morphological forms, correlated within each mode. As such, important trends in morphology can be recognized, and it is useful to summarize them. They will be discussed in greater detail in relation to the body forces generating thrust and swimming efficiency, in Chapter 5 (Fig. 50). First, the correlation between length and thickness (flexibility) with mode has been mentioned. A second trend is the change in distribution of body span (depth) along the length of the fish. In the anguilliform mode, the span is typically fairly constant along the whole length, and is replaced by a discontinuous span associated with several median fins (as in gadoids), which in turn is progressively replaced by reduction in number and size of anterior median fins with emphasis on the caudal fin. The evolution of a discrete enlarged caudal fin is associated with narrow necking (Lighthill 1969). Narrow necking is the progressive decrease in body span towards the caudal peduncle, with a rapid increase in span over the caudal fin, culminating in the narrow streamline caudal peduncle and semilunate tail of scombroid fish and cetaceans.

The trend to decreasing body flexibility is continued into the ostraciform mode, as these fish are often enclosed within rigid protective cases. This, however, interrupts the trend (seen through the anguilliform and carangiform modes) to more streamlined body shapes and narrow necking.

The various body shapes of fish swimming in different modes should be kept in mind during the description of the movements involved.

Anguilliform mode

Body movements and principles of anguilliform locomotion are basic to almost all other swimming modes. Therefore, anguilliform kinematics will be considered first. This has some historic precedence, as observations originally made by Gray (1933a, b, c), particularly on the eel, provided the foundation for most subsequent studies of fish locomotion. The following discussion is based largely on Gray's observations.

BODY MOVEMENTS

As a result of phased muscular contractions on alternate sides of the body, the whole body is thrown laterally into a propulsive wave (Fig. 27A). The propulsive wave has a wavelength, λ_B, with the ratio to length, λ_B/L, much less than 1. When the fish is swimming forward at uniform velocity, U, the propulsive wave passes back over the body at a velocity, V, greater than U. When the fish is decelerating, V may be equal to, or less than, U.

As the propulsive wave passes back over the body, each small portion of the body, called a segment by Gray (1933a, b, c), executes a periodic transverse motion with posterior segments lagging behind immediately anterior segments. Amplitude of the lateral motion increases with distance along the body, reaching a maximum amplitude A_T toward the trailing edge.
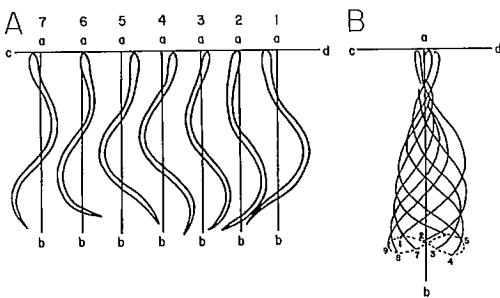
Fig. 27. (A) body shape during a cycle of propulsive movements in anguilliform mode, drawn from tracings from photographs (of *Anguilla vulgaris*) taken at 0.09-s invervals. U = 4 cm/s, V = 6 cm/s. Mean axis of progression is along *ab*; (B) superimposed outline of the leading surfaces in A to show the transverse figure eight of a trailing-edge segment. (Redrawn after Gray (1933a) from *Journal of Experimental Biology* Vol. 10)

The locus of each segment in space, relative to a fixed point in space is a sine curve (Fig. 28) with a wavelength, λ_s less than λ_B. λ_s tends to be constant for all portions of the body, but its amplitude, A, increases with distance from the nose.
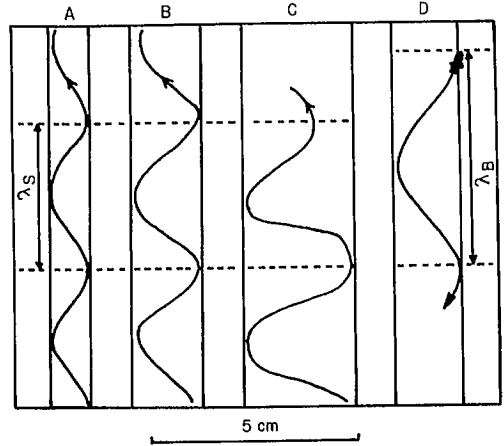
Fig. 28. Sine curves in space traced by segments along the body of *Anguilla* (A) path of the head; (B) midpoint of the body; (C) tip of the tail. The wavelength of the path, λ_s, is less than the body wavelength, λ_B, shown in D. Note increase in amplitude of the lateral movement of segments along the body. (Redrawn from Gray (1933a) from the *Journal of Experimental Biology* Vol. 10)

Following Gray's convention (1933a), the path of each segment in space subtends angles θ_s with the transverse axis of motion, *cd*, in Fig. 27, 28 and following. θ_s varies periodically with the transverse motion of a segment. Mean values of θ_s decrease as the amplitude increases with distance from the nose (Fig. 31).

The locus of a segment in space, relative to a point moving along the axis of progression, *ab*, and at velocity U (that is relative to the fish) is a transverse figure eight. This is most clearly seen for a segment at the trailing edge (Fig. 27B). The transverse figure eight is a result of the propulsive wave passing backward over an inextensible body. Because of the figure eight motion, rather than a simple linear transverse motion, segments do not execute pure simple harmonic motion.

The transverse motion of each segment results in fluctuating transverse velocities and accelerations. The change in transverse velocity, W, and acceleration, *a*, for a hypothetical segment moving symmetrically about *ab* and *cd* can

be related to the position of the segment in space and time (Fig. 29). In space, W is zero at positions of maximum displacement, $\pm A/2$, accelerating to reach its highest value, W_{max}, as the segment crosses the axis of progression. W tends to be fairly constant at W_{max} for about 0.5 A, half the distance covered by the transverse motion. In terms of time, W_{max} represents about 0.2 of the time, t, for a cycle.

For acceleration, changes in a to a_{max} to a occur over about 0.5 A. In terms of time, these changes represent about 0.8 t.

U and W are the components of the motion of a segment most easily measured, but the velocity of a segment relative to the water is the resultant of these. The resultant velocity, W_R, may be calculated from a triangle of velocities, when at some instant

$$W_R \sqrt{W^2 + U^2} \tag{51}$$

The value of θ_s is given by the same triangle as

$$\text{Tan } \theta_s = U/W \tag{52}$$

Theoretically, the value of U for a given segment varies during a cycle of transverse movement because the figure eight motion has velocity components along the axis of motion. However, variations in U will be negligible in comparison with U and W and may be neglected.

For uniform forward motion, changes in a along the axis of motion depend only on the figure eight motion. As with U, variations in a along this axis will be negligible in relation to transverse changes in a, and may be neglected.

The magnitudes of a and W are obviously dependent on A, and will increase with distance from the nose (leading edge).

Superimposed on the transverse motions of each segment is a rotational component, out of
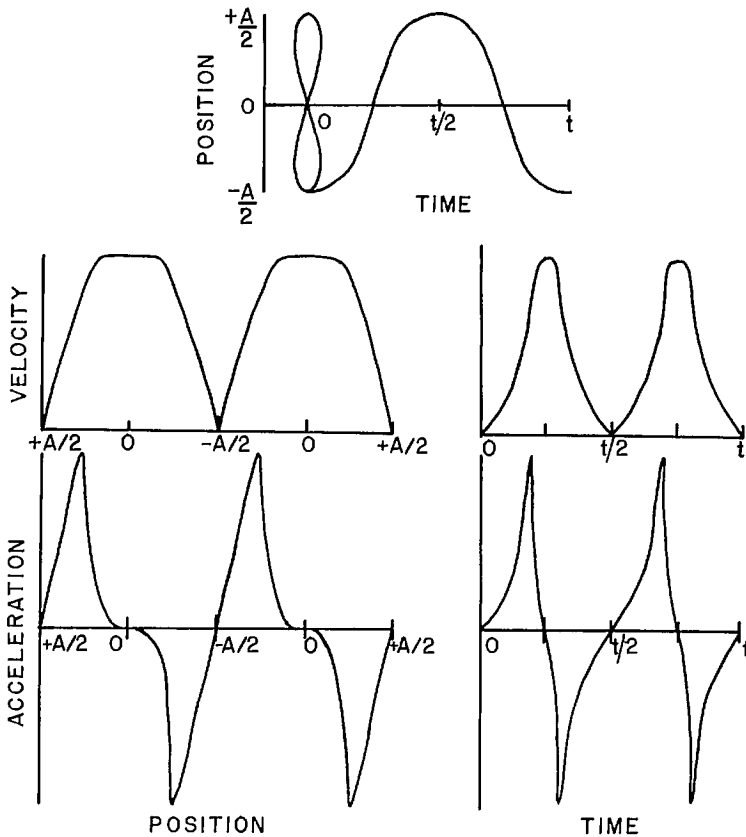
FIG. 29. Relation between the transverse velocity and acceleration of a hypothetical segment in relation to position and time. Motion of the segment in space is between limits of $\pm A/2$, each cycle taking a time, t, as shown at top. Further explanation is given in the text.

phase with the transverse motion by 70–90° (Hertel 1966). Continuing to follow Gray's (1933a) convention for angles, each segment subtends angles θ_B with the transverse axis of motion. This angle varies with position (Fig. 30), approaching 90° at $\pm A/2$, and a minimum value as the segment crosses the axis of progression. The magnitude of θ_B depends on the amplitude of the motion as does θ_s, and is higher for more anterior segments in the same way (Fig. 31).
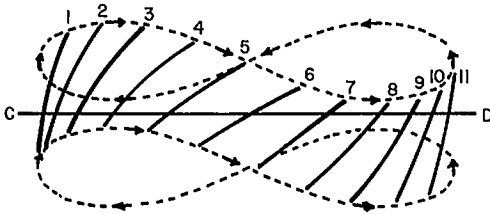
FIG. 30. Diagrammatic representation of the figure eight motion of a segment relative to the fish, with rotational motion superimposed. This is shown by the changing angle subtended by the segment relative to the axis of transverse motion, cd, during half the cycle. Successive positions are numbered. (Redrawn from Gray (1968) with permission of Weidenfeld and Nicolson Ltd.)

The relation between the angles subtended by the path of a segment and the rotational component define the angle at which the incident water with velocity W_R strikes a segment. For uniform forward motion, θ_B is greater than θ_s as λ_B is greater than λ_s. The difference between the two angles is the angle of attack, α, which is then

$$\alpha = \theta_B - \theta_s \qquad (53)$$

The angle, α, is important as it indicates the amount of lateral motion of the body relative to the water. When a segment is compared with a hydrofoil (e.g., Taylor 1952) it can be seen that forward thrust can only be generated when α is positive, although this analogy only strictly applies to steady flow.

RELATIONS BETWEEN BODY MOVEMENTS

Because of the increase in amplitude of the lateral motion of segments with distance along the body, the value of α and W_R will also vary with a segment's position along the body. The interrelations between α and W_R with position can be illustrated for a hypothetical fish swimming in the anguilliform mode. The limits of $\pm A/2$ in relation to the axis of progression can

be shown by two curved lines (Fig. 31A), and, to simplify the discussion, the amplitude at the nose will be assumed zero. Within the limits of the motion of the body, enclosed by the lines showing $\pm A/2$, the figure eight motion of four segments along the body can be shown. Instantaneous values of W, with U constant, can be used with triangles of velocity to calculate instantaneous values of W_R and θ_s, as shown for the instant when each segment crosses the axis of progression in Fig. 31B. The rotational component of motion of the segments can be superimposed on such diagrams with the relevant instantaneous value of θ_B, to obtain α.

From vector diagrams for all positions and values of W throughout a cycle, changes in α and W_R can be shown for each segment (Fig. 31C). α and W_R are inversely related with the position of the segment, so that α is higher for anterior segments, whereas W_R is higher for posterior segments. Gray (1933a) interpreted the effectiveness of the propulsive wave in terms of the change in momentum given to the water after being deflected by a segment through the angle α. The correlations between α and W_R imply a balanced distribution of thrust-per-unit-mass of water affected along the body. Because of the increasing area of influence of the propulsive wave with increasing amplitude, more water will be affected by the propulsive wave travelling down the body associated with progressively increasing velocities, W_R. The propulsive wave can be considered as increasing the total mass and momentum of water in the system, reaching a maximum at the trailing edge. By the use of hydromechanical models, Lighthill (1966, 1970) has shown that the thrust generated by a fish is mainly given by the amount of momentum shed into the wake at the trailing edge.

The hypothetical fish discussed represents the most simple case of symmetrical movements and uniform forward velocity. It can be seen from Fig. 31C that under these conditions α is highest when W_R is highest, that is, when a segment crosses the axis of progression. Nursall (1958b) observed that α may be minimal when W_R is highest. This is presumably the result of active control by the fish over the propulsive wave, probably to smooth out thrust fluctuations in response to instantaneous requirements. A similar interpretation has been made by Bainbridge (1963) to explain the complexities of the behavior of the caudal fin of fish swimming in the subcarangiform mode.

38
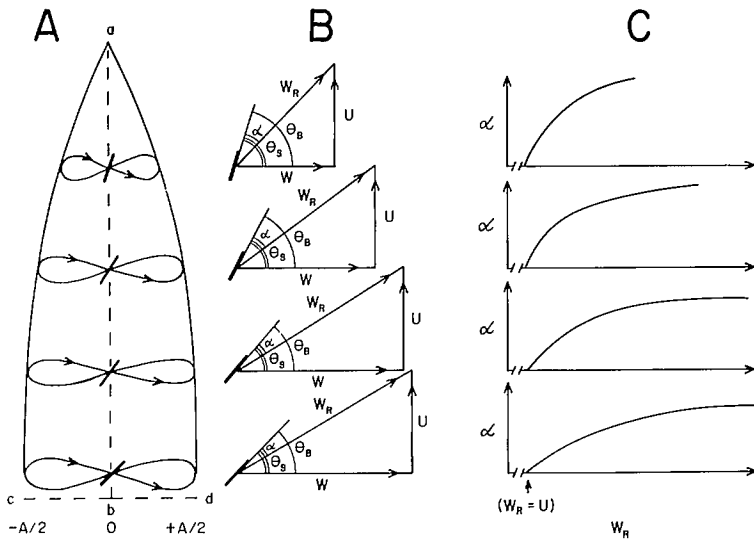
FIG. 31. Relations between the angle of attack, α, subtended between a segment and the incident resultant velocity of the water, W_R, for segments at various positions along the body of a hypothetical fish swimming at velocity U. (A) position of segments along the body for figure eight transverse motion, between the limits ± A/2, increasing with distance of segment from the nose. Angle θ_B subtended between the segment and the axis cd, is illustrated as the segment crosses the axis of progression ab, moving from − A/2 to + A/2; (B) vector diagrams relating the velocities W, U, and W_R with θ_B as the segments cross ab. θ_S is the angle subtended between W_R and cd, and α is given by $\theta_B - \theta_S$; (C) relation between α and W_R calculated from vector diagrams for the motion of segments during a half cycle.

KINEMATIC REQUIREMENTS FOR GENERATION OF THRUST

Kinematic requirements for generation of thrust have been mentioned briefly. Movements of the body must result in lateral motion of a segment relative to the incident water flow, that is, α must be positive. This requires that θ_B and λ_B must exceed θ_S with λ_S, which occurs when V exceeds U. For a given propulsive wave, as U increases toward V, α decreases as the wavelengths of the body and path of a segment approach each other. When U equals V, the path of a segment coincides with the shape of the propulsive wave along the body. Then there is no relative motion between the body and the water, other than tangential motion. In real situations, the tangential motions associated with frictional drag would result in deceleration of the fish until a new equilibrium was reached for a new relation between V and U, when thrust equalled drag.

It is also possible for V to be less than U. Then the propulsive wave will generate negative

thrust, or drag, in the opposite direction to the forward motion of the fish. The propulsive wave could, therefore, be used as an active braking system. As far as it is known, no observations of this form of motion have been made, possibly because it would be more costly energetically than braking by use of paired fins. It should also be noted that many fish can swim backwards (Hertel 1966; Gosline 1971).

Carangiform modes

Carangiform modes include fish with fusiform bodies, swimming in a range from what is technically the anguilliform mode to the specialized carangiform mode with a semilunate tail (see p. 42). According to Lighthill (1969, 1970) and Wu (1971b, c) the hydromechanical theory describing the anguilliform mode is applicable to similar movements, classed as subcarangiform and carangiform modes, up to some stage when thrust is generated exclusively by the caudal fin. This is reached in fish that approach or include

39

the carangiform mode with semilunate tail; a special hydromechanical theory is required to describe this form of locomotion.

Because of the relatively short, thick bodies of fish swimming in carangiform modes, there is a morphological limit to the length of the body wavelength, and the number of wavelengths that can be contained within the body (Webb 1971a). It is convenient to express the wavelength in terms of the length of the body as the specific wavelength:

$$\text{Specific wavelength} = \frac{\text{Length of propulsive wave}}{\text{Length of body}}$$

$$= \lambda_B/L$$

Following Breder's method of classification (1926), the subcarangiform mode like the anguilliform mode has specific wavelengths of less than 1. The carangiform mode and carangiform mode with semilunate tail tend to have specific wavelengths greater than 1 (Fierstine and Walters 1968). This is not always the case. Photographs of a mackerel (Gray 1933a) swimming in the carangiform mode show $\lambda_B/L < 1$, and observations of sockeye salmon swimming in the subcarangiform mode show $\lambda_B/L > 1$ (Webb 1973a).

SUBCARANGIFORM MODE

Body movements of fish swimming in the subcarangiform mode (Fig. 32) are similar to those of the eel. The major difference is the low amplitude of the motion of the anterior portion of the body. Expressing amplitudes in relation to length as specific amplitudes, A/L, they are of the order of 0.04–0.07 at the nose and decrease with distance along the body to a position approximately at the edge of the operculum. From this position specific amplitude increases, at first slowly. Over the posterior third
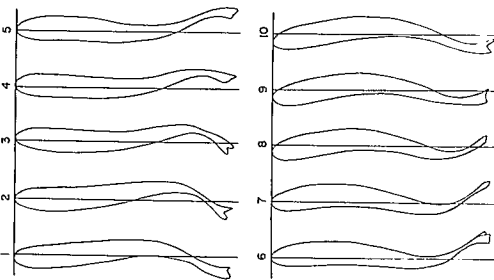
FIG. 32. Body shape during a propulsive cycle for subcarangiform motion, drawn from tracings of *Salmo gairdneri* taken at successive 0.03 s intervals. U = 50 cm/s, V = 80 cm/s. (P. W. Webb unpublished data)

of the body, the specific amplitude increases markedly to reach a maximum value of the order of 0.2 toward the trailing edge (Bainbridge 1958, 1963; Pyatetskiy 1970a, b; Webb 1971a).

Although the amplitude initially increases along the body, there is no mode (orthokinetic portion of the body postulated by Breder 1926). That is, no part of the body moves along the axis of progression, but all parts experience some lateral motion (Bainbridge 1963; Webb 1971a).

As with anguilliform motion, segments of the body execute transverse figure eights relative to the fish. In addition, W varies similarly with transverse motion, but the increase in W with position along the body is more marked, because of the increase in amplitude along the body (Fig. 33A). The transverse movements tend to be symmetrical about the axis of progression, but Bainbridge (1963) documented several asymmetries, which can be shown by the changes in W
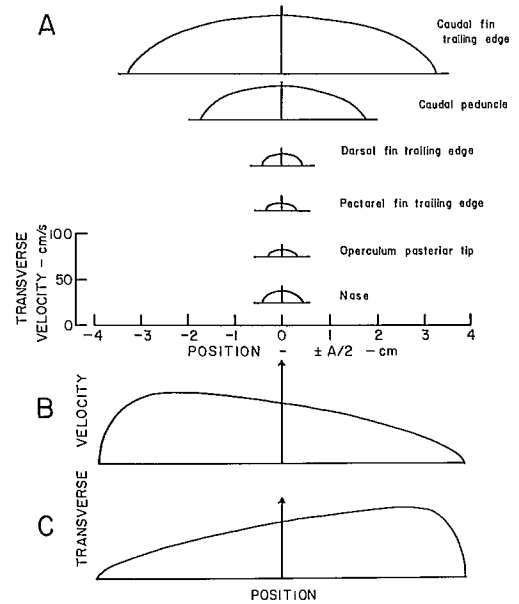
FIG. 33. (A) transverse velocity and amplitude of lateral movements of different segments along body of *Leuciscus leuciscus*. Minimum amplitude occurs at posterior tip of the operculum. U = 48.0 cm/s. (Redrawn from Bainbridge (1963) from the *Journal of Experimental Biology* Vol. 40); (B) diagrammatic representation of asymmetrical motion of a trailing edge segment with W_{max} occurring early in the cycle. This is often associated with acceleration; (C) diagrammatic representation of asymmetrical motion of a trailing edge segment, with W_{max} occurring late in the cycle. This is often associated with deceleration.

during a cycle. Bainbridge (1963) found that for dace, goldfish, and bream the distribution in W was sometimes shifted so that W_{max} occurred early in a cycle (Fig. 33B). In one case the opposite was found, with W_{max} occurring late in a cycle (Fig. 33C). These asymmetries were often associated with accelerations and decelerations, respectively.

In fish swimming in the anguilliform mode, the propulsive wave tends to be transmitted along the whole length of the body by muscular forces. In carangiform modes, the caudal fin is interposed between the body and the trailing edge, and the propulsive wave must be transmitted over a relatively passive portion of the body (Gray 1933c). The caudal fin is extremely flexible in fish swimming in the subcarangiform mode. Under the influence of both hydrodynamic and body muscular forces, coupled with a small amount of intrinsic muscle, the caudal fin has a complex motion of its own. This is shown by anterioposterior bending, dorsoventral bending, and variations in the span of the trailing edge during a cycle (Bainbridge 1963) as indicated in Fig. 34.

The degree of freedom in anterioposterior bending is given by the fin rays. These form
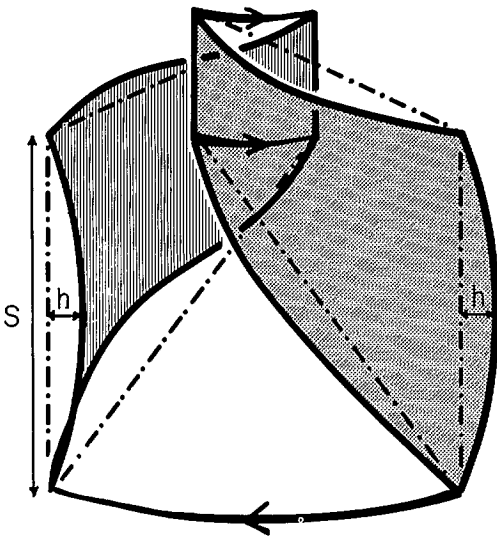
FIG. 34. Diagrammatic representation of caudal fin bending when swimming in subcarangiform mode. For the time shown, the propulsive wave overtakes the tail and motion of anterior and posterior edges is shown by arrows. A rigid tail would take the shape shown by the chain dotted line. Trailing-edge span is shown as S, and dorsoventral bending is measured relative to this, as h.

a girder system of half-rays, each half-ray is free to move relative to the other, up to a limit. This limit defines the maximum anterioposterior bending (McCutcheon 1970). Up to this limit, anterioposterior bending depends almost entirely on hydrodynamic forces (Gray 1933a; Bainbridge 1963). According to McCutcheon (1970) the shape of the tail is defined by these forces and the behavior of the fin rays is such that the shape of the tail ensures a suitable distribution of thrust over its surface. Thus, the shape varies in relation to the instantaneous changes in load that occur during a cycle. McCutcheon (1970) described this behavior as selfcambering.

In contrast to bending along the anterioposterior axis, bending in the dorsoventral plane appears to be only partly because of hydrodynamic forces, although they are still of greatest importance. Curvature of the fin increases as the tail moves away from positions of maximum amplitude, tending to reach a maximum at the end of a transverse cycle. The more flexible fin center then continues to move in the same direction although the return stroke commences with the stiffer portion of the fin moving in the opposite direction. At this point, the curvature of the fin is minimal, but the fin is wrinkled. The degree of dorsoventral bending is not in phase with the transverse motion of the tail (Bainbridge 1963), as shown in Fig. 35, but can largely be attributed to the expected behavior of water on the flexible center of the fin.

If dorsoventral bending was the result of hydrodynamic forces only, then a direct correlation would be expected between changes in span and curvature. This is because the curvature would represent the "bellying" of the fin center between the limits set by the stiffer outer fin rays. Bainbridge (1963) found that span and curvature were not well correlated and were subject to extensive variation (Fig. 35). Bainbridge thought the fish exercised some active control over behavior of the fin, by means of the intrinsic fin muscles observed in several fish (Greene and Greene 1914). Observations of independent movements by individual sections of caudal fins of several fish indicate the activity of an intrinsic caudal fin muscle system (Breder 1926; von Holste and Kuchemann 1942; Harris 1937; Bainbridge 1963; Webb 1971a).

The net effect of dorsoventral bending and changes in span is a rhythmic variation in the projected area of the caudal fin. Variation in the caudal fin area of the fish studied by Bainbridge (1963) was of the order of 10% of the mean area.

41
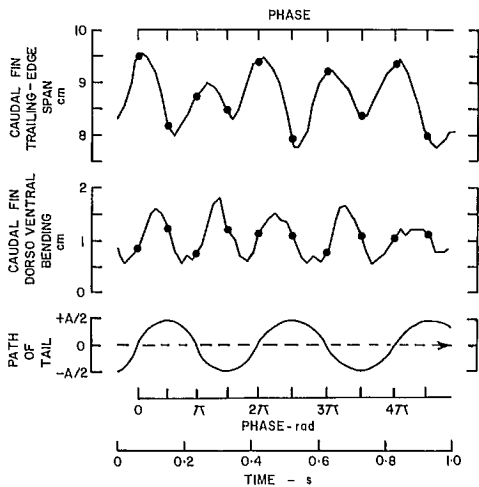
FIG. 35. Relations between caudal fin trailing-edge motion, trailing-edge span, and dorsoventral bending in *Leuciscus leuciscus*. Movements of the trailing edge in space are shown for $\pi/2$ divisions of a cycle by dots on the traces of span and bending. Note the poor correlation between various motions and movement of the tail. (Redrawn from Bainbridge (1963) from the *Journal of Experimental Biology* Vol. 40)

As with span and bending, the area changes were poorly correlated with other kinematic factors, but generally, area was lowest at positions of maximum displacement ($\pm$ A/2), increased rapidly as the tail accelerated away from these positions, and tended to reach maximum area at W_{max}. This maximum area was usually maintained for the remainder of the cycle.

In addition to these rhythmic changes in caudal fin behavior, P. W. Webb (unpublished data) found that depth increased with speed for rainbow trout swimming up to 2 body lengths/s. Depth apparently reaches and remains at maximum values approaching this speed and above. Maximum depth would involve maximum masses of water in propulsive movements and increase thrust and efficiency at these speeds when available energy expenditures would begin to limit further higher performance.

In view of the active control by fish over much of the movement of the caudal fin, it is probable that variations in area during a cycle express control by the fish over thrust produced in response to instantaneous requirements. Other more rhythmic changes were interpreted by Bainbridge (1963 p. 48) in terms of: "a) to allow a rapid initial acceleration of the tail by virtue of its smaller area; b) to maintain a high and uniform thrust when the transverse speed of movement is falling by increasing the area of the tail at that time; c) to facilitate slowing of the tail by this increased area; d) to add a minimum of drag to the moving body by presenting a minimum area to the water when at the extreme lateral positions in the cycle of movement." Although the complex caudal fin movements can be rationalized, it is difficult to measure instantaneous thrust. Consequently, effects of bending and span variations have not been quantitatively measured.

The Carangiform Mode

Apart from the photographs published for mackerel by Gray (1933a), no observations have been made on fish swimming in this mode. Body movements are intermediate between the subcarangiform and carangiform mode with semilunate tail. Otherwise, it is probable that detailed kinematics, particularly in relation to fine tail movements, would be simpler than in the subcarangiform mode and closer to the carangiform mode with lunate tail. This is because the caudal fins of fish swimming in the carangiform mode tend to be scooped out, so that the fin has a swept-back planform (Nursall 1958a; Lighthill 1969). As a result, fin rays become more closely aligned with the span, making the fin stiffer and reducing dorsoventral bending. In addition, the length of the caudal fin becomes smaller, and anterioposterior bending is represented only in the rotational component of motion like that of a body segment in the anguilliform mode. Rotational motion of the tail differs from that of a segment, as it can be more closely controlled by body and caudal fin musculature (Fierstine and Walters 1968).

The Carangiform Mode with Semilunate Tail

The carangiform mode with distinctive semilunate caudal fin has evolved independently in four separate groups of aquatic vertebrates, apparently for two different reasons. Most aquatic animals that swim in this mode are those swimming at high speeds with high efficiency (Lighthill 1969). This includes Lamnid sharks from the elasmobranchs, percomorph fishes from the teleosts, and cetacean mammals. The characteristic body shape is also found in the extinct aquatic reptile *Ichthyosaurus* (Wallace and Srb 1961; Lighthill 1969), so that it, too, probably swam in the carangiform mode with semilunate tail.

The second use of this type of propulsion is apparently associated with slow swimming (Bone 1971). Bone observed two swimming patterns in a deep-sea trichiurid fish, *Aphanopus carbo:* (1) fast swimming in the anguilliform mode using the erected long dorsal fin and body; (2) slow swimming in the carangiform mode using a highly swept-back caudal fin, and the median fin furled. *Aphanopus* probably stalks its prey, detecting it by means of the lateralis system. Effective usage of the lateralis system requires a long stable baseline and minimal local pressure fluctuations. This is achieved by holding the body straight as in carangiform swimming, with anguilliform propulsion used within striking distance of the prey (Bone 1971). Q. Bone (personal communication) considered that such usage of two swimming modes may be a common occurrence, and apply to such fish as *Lophotes* (see Fig. 50). *Gymnarchus* also approaches this carangiform mode, presumably to keep the body straight for efficient electrical reception.

Except for dolphins and porpoises, propulsive movements are apparently the same in the various groups that swim in the carangiform mode with semilunate tail (Fig. 36). Significant lateral propulsive movements are confined to the caudal peduncle and caudal fin. The form of propulsive wave differs somewhat from that of other fish that swim by means of body movements, in that the wave tends to be transmitted across a double-joint system (Parry 1949a, b; Nursall 1956; Slijper 1958; Kramer 1960; Fierstine and Walters 1968; Pershin 1970). The first major axis of bending is the anterior base of the caudal peduncle; motion around this axis results in lateral displacements of the tail. The second major axis is the base of the caudal fin. This permits the rotational motion required to ensure a positive angle of attack. The motion of the caudal fin is similar to that of a segment of the body at the trailing edge in subcarangiform motion. Because of the double-joint system, the wavelength is
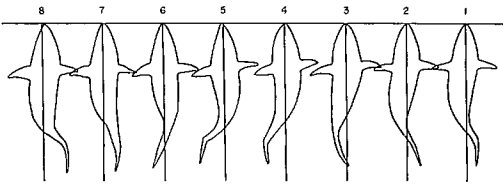
FIG. 36. Body shape during a propulsive cycle in *Euthynnus affinis* swimming in carangiform mode with semilunate tail. Figure drawn from successive photographs taken at 0.06 s intervals. U = 8.2 L/s. (Modified after Fierstine and Walters 1968)

long and the specific wavelength tends to be between 1 and 2.

Compared to the specific amplitudes of lateral movements in the subcarangiform mode, those of the carangiform mode with semilunate tail are lower anteriorly, but can reach higher maximum values posteriorly. In *Euthynnus affinis* A/L is of the order of 0.03 at the leading edge and 0.3 at the trailing edge (Fierstine and Walters 1968). Typically, A/L is of the order of 0.21 at the trailing edge (Hunter and Zweifel 1971).

Measurements of W and α for *E. affinis* have shown asymmetrical caudal fin movements similar to those occasionally found by Bainbridge (1963) in goldfish. W_{max} tended to occur toward the end of a cycle, after the tail had crossed the axis of progression, resulting in a more uniform and longer acceleration phase for the caudal fin (Fierstine and Walters 1968). These authors also found that α tended to be maximum early in the cycle, with lower W, and lowest toward the end of a cycle, with W highest. The inverse relation between W and α, is analogous to that of segments along the body in anguilliform motion, and was interpreted by Fierstine and Walters as a mechanism for smoothing the development of thrust.

As with the carangiform mode, the caudal fin skeleton (fin rays) tends to be oriented along the span of the caudal fin, so that its own motion is relatively simple. There is still some dorso-ventral bending, but in the opposite sections of the fin to that observed in the subcarangiform mode. In *Euthynnus*, the center of the fin leads and the tips follow, because the center of the fin is more rigidly attached to the body than the tips. This contrasts with the subcarangiform mode when dorsal and ventral fin rays are stiffer and consequently more rigidly attached to the body than those at the center. The magnitude of bending of the semilunate tail is much less than that of the caudal fin in the subcarangiform mode (Fierstine and Walters 1968).

The kinematics of cetacean locomotion are generally similar to those of fish swimming in the carangiform mode with semilunate tail (Fig. 37) except movements are in the vertical plane (Gray 1968). Dolphins and porpoises differ somewhat from the general picture, as the body is often thrown into a sharp curve (Slijper 1958, 1961; Lang and Daybell 1963; Pershin 1970). The tail stroke also tends to be asymmetrical in time and space. For example, the stroke tends to be mostly below the axis of the body, rather than symmetrical about that axis (Purves 1963). In
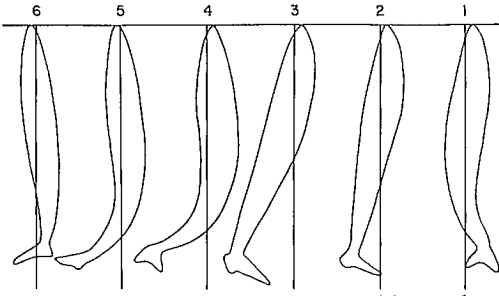
FIG. 37. Body shape during a propulsive cycle of *Lagenorhynchus obliquidens*, to show carangiform motion with semilunate tail in a porpoise. Drawn from photographs taken at 0.2 s intervals. U = 348 cm/s. (Modified after Lang and Daybell 1963)

addition, the upstroke may be shorter, with higher W, than the downstroke. Usually rotation of the tail maintains a favorable relation between W and α (Parry 1949a, b; Lang and Daybell 1963), although in some cases there is division into an active and a recovery phase in each cycle (Purves 1963).

RELATIONS BETWEEN SWIMMING SPEED AND KINEMATICS

For certain species of fish swimming in carangiform modes, quantitative relations have been established between U and the kinematics of the propulsive wave represented by f and A or A/L. This approach was pioneered by Bainbridge (1958) for dace, goldfish, and trout swimming in the subcarangiform mode. Bainbridge concluded that: (1) the distance covered per tail-beat was proportional to A for a given fish; (2) for a given A, U was linearly related to f for a given fish, but this relation did not pass through the origin; (3) for a given f and A, the specific swimming speed, U/L, was the same for fish of different lengths for the three species studied.

These relations have generally been confirmed for fish swimming in the subcarangiform mode (Smit et al. 1971; Webb 1971a) and for several fish swimming in other carangiform modes (Magnuson and Prescott 1966; Yuen 1966; Pyatetskiy 1970a; Hunter and Zweifel 1971).

For fish swimming in the subcarangiform mode, the original equations relating U/L and f found by Bainbridge (1958) appear to apply for swimming speeds greater than about 1 to 2 L/s. Relations between A and the distance moved are only important at speeds lower than these, as then both A and f vary with swimming speed, and U/L is linearly related to the product fA/L

(Webb 1971a, 1973a). A increases as frequency and speed increase to reach a maximum of the order of 0.2 L (Hertel 1966; Hunter and Zweifel 1971). Thus, the linear relation between U/L and f, with A/L fairly constant, includes A/L in the slope (Table 2).

For other carangiform modes, it appears there is less variation in A and f at low speeds, so the whole speed range can be expressed as a function of f only (Hunter and Zweifel 1971).

The various constants found for different species of fish for $U/L = af + b$ or U/L proportional to afA/L are included in Table 2. Complete equations for U/L vs f A/L have not been given. Most measurements were made at high swimming speeds whereas f and A appear to be important only at low speeds. Few measurements have been made in the latter speed range. The slope, a, in the equations varies twofold for the range of species studied, showing that some fish obtain higher specific speeds (in L/s) at a given tail-beat frequency than others. Table 2 shows there is no particular correlation between the value of a and swimming mode. Lowest values are found for *Sardinops* swimming in the carangiform mode, and *Thunnus* and *Euthynnus* swimming in the carangiform mode with semilunate tail. The highest value was found for *Triakis*, a shark that probably swims fairly close to the anguilliform mode (Hunter and Zweifel 1971). Most values tend to cluster around 0.74–0.83.

Values of f and A do not completely characterize the propulsive wave in terms of thrust, so it is not valid to draw too rigorous conclusions based on the slopes for different species. For example, a general interpretation would suggest that those species with low a would tend to be less efficient than those with high a values. Low a, associated with high f at a given U/L, implies the water is accelerated to a greater extent in relation to the incident water velocity than with high a. The greater the acceleration given to the water, the greater the kinetic energy losses, implying that several fish swimming in the carangiform mode with semilunate tail might be relatively inefficient. Although there is no supporting experimental evidence, this is contrary to general biological opinion based on swimming performance and the predictions of hydrodynamic models.

The most probable reason for the apparent discrepancy relates to other kinematic factors. The various relations between U/L and f are for given species, and the relation will apply to a

TABLE 2. Relations between swimming speed (U/L) and propulsion kinematics as A/L and f for fish swimming in carangiform modes. Keys: SC, subcarangiform mode; C, carangiform mode; CSL, carangiform mode with semilunate tail.

Species	Mode	Length (cm)	Speed range (L/s)	$U/L = af + b$ a	b	A/L	$\dfrac{U/L}{afA/L} \cdot \dfrac{\alpha}{a}$	Reference
Leuciscus leuciscus	SC	5.2–24.0						
Salmo(irideus) gairdneri	SC	4.0–29.3	2–15	0.75	−1.00	0.18	4.10	Bainbridge (1958)
Carassius auratus	SC	4.6–22.5						
Carassius auratus	SC	15	1–3.5	0.82	−2.6	0.20[a]	3.20	Smit et al. (1971)
Salmo gairdneri	SC	28.2	0–3	0.74	−1.8	0.19	3.91	Webb (1971a)
Triakis henlei	SC	23.6	0–10	0.93	−0.49	0.21	4.43	Hunter and Zweifel (1971)
Mugil cephalus	SC	26.5–30.0						
Pomatomus saltatrix	C	42	0.5–6	0.82	−0.72	0.20[a]	3.60	Pyatetskiy (1970a)
Sarda (=Pelamys) sarda	CSL	13.8–16.3						
Sarda chiliensis	C	45–59	0–6.5	0.64	+0.49	0.20[a]	3.20	Magnuson and Prescott (1966)
Sardinops sagas	C	13.6	0–10	0.50	+0.21	0.21	2.38	
Scomber japonicus	C	30[b]	0–10	0.82	−0.72	0.21	3.90	Hunter and Zweifel (1971)
Trachurus symmetricus	CSL	15[b]	0–10	0.83	−1.02	0.21	3.95	
Thunnus albacares	CSL	51.9	0.5–14.4	0.57	+2.45	0.20[a]	2.84	Yuen (1966)
Euthynnus pelamis	CSL	57.2	0.5–14.4	0.50	+2.05	0.20[a]	2.50	

[a]Assumed specific amplitude.

[b]Kinematic parameters measured for large size range, and high dependence of those parameters with length. Values shown for center of length range rested.

given form of propulsive wave dictated by morphological considerations. The form of the propulsive wave varies between modes, and in the carangiform mode with semilunate tail in particular, the double joint system will permit high control of such kinematic factors as α. This degree of control is probably far greater than that possible for fish swimming in modes between subcarangiform and carangiform, because of the relatively passive nature with which the shape of the fin varies with load (McCutcheon 1970). According to prediction based on hydromechanical

models (Lighthill 1970), the magnitude of α as well as other kinematic factors will affect propulsive efficiency (and the magnitude of the thrust). It is likely that swimming efficiency of fish that swim in the carangiform mode with semilunate tail with low values of a is markedly affected by greater active control over α than would be expected for more "typical" propulsive waves.

None of the equations relating U with f pass through the origin, and detailed relations for fish of different lengths are not identical. In most cases, the bias introduced by length-dependent factors is small, with the exception of some fish swimming in the carangiform mode with semilunate tail (Hunter and Zweifel 1971). More accurate, unbiased estimates of the relation between U and f have been elaborated by Hunter and Zweifel, and these take the form

$$U - U_o = a[L(f - f_o)] \tag{54}$$

when U_o and f_o are the speeds and frequencies when the general relation between U and f cross the appropriate axis for a fish of a given size. Establishing a model of this type obviously requires much more effort than for those given in Table 2, but Hunter and Zweifel (1971) considered that the unbiased models could be useful in the field for identification of fish in sonar studies.

Ostraciform mode

As far as is known body and caudal fin movements of fish swimming in the ostraciform mode have not been described in detail (Gray 1968). Bodies of such fish are usually enclosed in a rigid nonstreamlined integument, and the tail articulates with the body at a well-defined joint at the base of the fin. The tail tends to be fairly rigid. Ostraciform locomotion does, however, lend itself to the construction of mechanical and hydrodynamic models, because of the relative simplicity of the morphological system. In mechanical models described by Breder (1926), Smith and Stone (1961), and Gray (1968), the tail was represented by an oscillating rigid plate. The authors found that such models generated significant propulsive forces, with positive components throughout the cycle.

The tail probably has some flexibility, in which case the observations made by Gray (1933c) on a whiting with the caudal fin amputated may be applicable to the ostraciform mode in the absence of observations on the mode itself. In the whiting, the tail movements were asymmetrical in space and time in relation to the fish

(Fig. 38). The motion comprised an initial high acceleration from positions of $\pm$ A/2, followed by a fairly uniform phase of constant velocity at W_{max} occupying about three-quarters of the transverse movement and a similar portion of the time for one cycle. The cycle was terminated by a short deceleration phase. α tended to be positive during most of a cycle, but became negative during the deceleration phase. During the period of fairly constant velocity at W_{max}, the tail barely moved forward in relation to the environment, whereas the head moved forward both in relation to the tail and the environment, shown by the body straightening in relation to the tail. Thus with the tail pushing against the water, the fish moved forward because its body resistance was much lower than the tail portion. These movements are similar to initial phases of acceleration (Weihs 1973a) but of smaller amplitude.
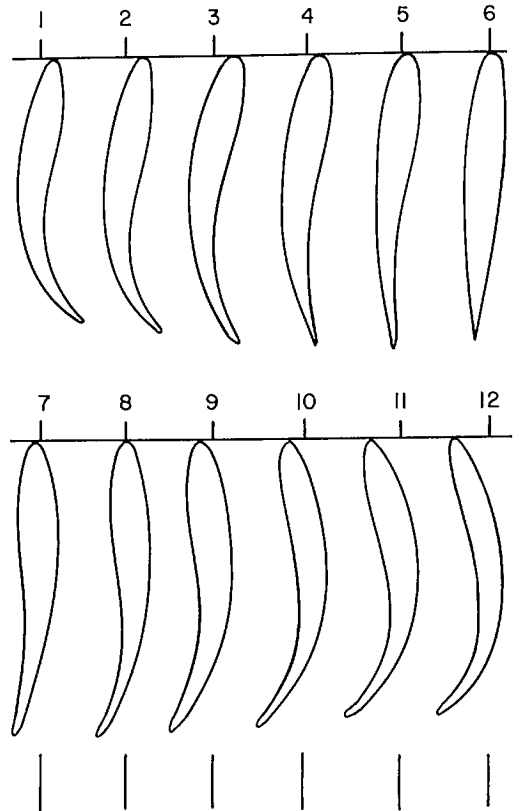
FIG. 38. Body shape during a propulsive cycle for *Gadus merlangus* after amputation of tail. This is probably similar to motion in the ostraciform mode. (Redrawn from Gray (1933c) from the *Journal of Experimental Biology* Vol. 10)

It should be remembered that ostraciform propulsion is not a primary locomotor method (Breder 1926). Fish swimming in this mode have protective mechanisms other than speed, and are often found in situations where free movement is restricted. The primary locomotor method tends to be paired or median fin movements which permit slow, but highly maneuverable movements. The tail serves as a rudder during slow swimming and is otherwise used for high speed acceleration.

Median and Paired Fin Propulsion

Median and paired fins of fish and cetaceans are most commonly used to control stability. Sharks, teleost fish swimming in the carangiform mode with semilunate tail, and cetaceans primarily use their fins in this way. Powered fin locomotion is, consequently, less ubiquitous than body and caudal fin modes, and generally found in association with the anguilliform, subcarangiform, carangiform, and ostraciform variations. Some skates and rays use pectoral fin propulsion exclusively. Otherwise, fin propulsion is employed for low speed, usually high maneuverable locomotion, supplemented or replaced by body and caudal fin propulsion for high speed swimming and fast turns (Breder 1926; Harris 1936, 1937, 1938, 1953; Nursall 1962; Webb 1973b).

Few studies of fin propulsion have been made, the majority confined to teleosts (Breder 1926; Harris 1937, 1953; Breder and Edgerton 1942; Lissman 1961; Nursall 1962; Webb 1973b) with some superficial observations on rays (Breder 1926). Generally, a propulsive wave is propagated anterioposteriorly for forward motion. When pectoral fins are oriented dorso-ventrally, waves pass in this direction as it is the embryological anterioposterior axis (Harris 1937).

Major variations in fin kinematics can be related to the length of the fin and number of wavelengths within that length similar to the classification of body and caudal fin modes. The long fins in amiiform, gymnotiform, balistiform, and rajiform modes contain several half-wavelengths within the fin length — similar to anguilliform propulsion. Diodontiform and tetraodontiform modes involve short fins generally with less than one wavelength, similar to subcarangiform or carangiform propulsion, whereas the short, often relatively stiff, fins in the labriform mode frequently behave in a similar fashion to ostraciform propulsion.

Specific wavelengths, calculated relative to the length of the fin base, range from much less than 1 for the dorsal fin of *Hippocampus*, amiiform mode (Breder and Edgerton 1942); and ventral fin of *Gymnarchus*, amiiform mode (Lissman 1961); through 1.3 for the pectoral fins of *Balistes*, diodontiform mode; to 5.3 for the pectoral fin of *Epinephales*, labriform mode (Harris 1937).

Other differences between the kinematics of major fin and body modes are large. Specific amplitudes (relative to length of fin base) are of the same order as body modes for long fins, between 0.16 and 0.24 in *Hippocampus* (Breder and Edgerton 1942). However, there is no increase in specific amplitude along the length of the fin. In pectoral fin modes, the maximum amplitude is found at the fin leading-edge tip (Harris 1937). In *Cymatogaster*, labriform mode, specific amplitudes reach maximum values of approximately 10 (Webb 1973b).

When fins have a long base and relatively low specific amplitudes, maximum frequencies of lateral movements appear to be higher than for body modes. Breder and Edgerton (1942) reported maximum frequencies of 70/s in *Hippocampus*. When amplitudes are higher, as in the movements of short-based pectoral fins, frequencies are lower and of the same order as caudal fin beat frequencies at similar speeds. Thus, the pectoral fin of *Cymatogaster* beats at frequencies of 4/s at a 45-min critical swimming speed of 3.9 L/s (Webb 1973b).

Detailed movements of other fins are far more complex than those of the body or caudal fins. Propulsive waves can be passed in either direction with facility. Individual segments are capable of fairly extensive independent movement because muscular forces are transmitted to stiff fin rays supporting a thin, highly flexible finweb. Although fin rays are restrained proximally when they articulate with the body, distal portions can move anterioposteriorly to some extent as well as laterally. Variations in wavelength, amplitude, and, to a lesser extent frequency, can occur within the length of the same fin at the same time (Breder and Edgerton 1942).

Short-based pectoral fins are capable of a different form of variation because the axis of the fin motion can be rotated on the fin base. When pectoral fin movements are made about a dorso-ventrally oriented fin base, rotation of the fin motion permits thrust to be generated posteriorly, laterally, or anteriorly. However, this motion requires an action and recovery phase in each stroke to maintain motion in a given direction.

47

Propulsive forces can be generated throughout a pectoral fin beat cycle by rotating ventral segments relative to dorsal segments, so that the fin moves at an angle, or by passing propagated waves along the fin (Harris 1937, 1953).

More common in fish than rotation of the axis of motion of various fin segments is to couple this with rotation of the fin base. For example, the fin base of *Cymatogaster* subtends an angle of about 35° to the long axis of the body, so the fin surface always subtends some angle to the incident flow. During abduction positive thrust and vertical forces are generated, and during adduction a similar thrust force and negative vertical force are generated (Webb 1973b).

When fish using pectoral fin propulsion are forced to swim in a current, regular swimming patterns are adopted in some preferred mode, and the magnitude of variation in movements is reduced. In *Cymatogaster*, swimming speeds between 0.5 and 2 L/s are associated with shorter wavelength pectoral fin movements replaced by more "scull-like" (long wavelength) movements between 2 and 4 L/s. Each type of motion can be characterized in terms of frequency and amplitude of the fin beat, so the product is linearly related to swimming speed (Fig. 39). Pectoral fin movements are supplemented by caudal fin movements between 3 and 4 L/s in *Cymatogaster*. Caudal fin propulsion replaces pectoral fin propulsion at about 1 L/s in *Lepomis* (Brett and Sutherland 1965).

Concluding Comments

When propulsion movements are considered in terms of the motion of individual segments, there is a marked similarity among most modes. Variations among modes can largely be attributed to the number of segments involved in the propulsive wave and the closeness of their coupling.
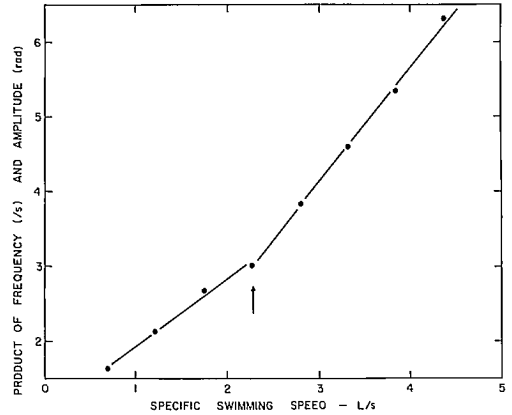
FIG. 39. Relation between the product of pectoral fin beat frequency (/second) and amplitude (radian) with specific swimming speed in *Cymatogaster aggregata*. Arrow indicates speed at which the kinematics changed from labriform propulsion with long wavelength propulsive waves passed along the fins to a more scull-like beat. (Modified after Webb 1973b)

In body modes, segments are closely coupled within the inextensible framework of the body. They are capable of large amplitude lateral movements within the propagated wave. Fin segments of long fins are capable of relatively small amplitude movements because they are constrained proximally by the body, but otherwise coupling is loose. The inability of long fins to achieve high amplitudes may be the reason such fin motions are associated with low swimming speeds. Higher swimming speeds are attained with fin motions of higher amplitude which only appears to be achieved by pectoral fin modes.

It seems probable that a general reduction in the number of segments involved in locomotory movements is associated with increases in propulsive efficiency (see Chapter 5).

48

Chapter 3 — Swimming Speeds

Introduction

Having considered the kinematics of propulsion, levels and magnitudes of swimming performance achieved by fish that swim in various modes may be discussed. Of all facets of vertebrate aquatic locomotion, swimming speeds have been most exhaustively studied. In common with many other aspects of locomotion, these studies have been largely confined to a few groups, mainly animals swimming in carangiform modes.

In view of the magnitude of data on swimming speed, it is not possible, nor desirable, to present a detailed discussion; an excellent review has been published by Blaxter (1969). Instead, various activity levels will be defined as used subsequently in the present work, and orders of magnitude of swimming speeds at these levels will be indicated.

Swimming Levels

Three main swimming activity levels have commonly been distinguished on the basis of the time for which a given speed can be maintained: (1) cruising or sustained, (2) prolonged or steady, (3) sprint or burst levels. Each principal level can be identified from a speed-duration curve (fatigue curve) that shows a wide range of speed and duration. After appropriate transformation of data (often with log time plotted against speed) such a fatigue curve may be resolved into three straight lines corresponding to the principal activity levels (Fig. 40). Between each level is a short transition zone.

These levels are based on locomotion in a primary locomotor mode involving body and caudal fin propulsion. As such, the three levels commonly identified are considered insufficient to adequately describe the diversity of fish activities. It is suggested that the three main categories should be designated principal locomotor levels, subdivided as appropriate to provide a more flexible descriptive framework for fish locomotor behavior. The terms to be used are as follows:

Sustained (Activity level maintained for longer than 200 min.)
Routine. Low levels of routine activity, e.g.,
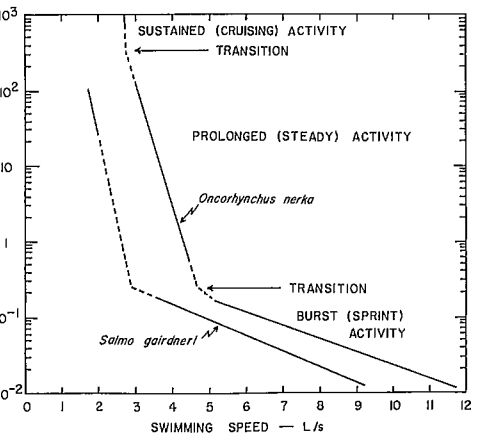
FIG. 40. Fatigue curves for sockeye salmon, *Oncorhynchus nerka*, and rainbow trout, *Salmo gairdneri*, showing three principal activity levels. Broken lines indicate transition zones where variability is expected to be greatest. (Modified after Brett 1964, 1967b)

foraging, station holding, by individual fish or loose schools, exploratory movements, territorial behavior.
Schooling. Low levels of routine activity of fish or cetaceans in organized schools. Includes similar activities to routine activity but also migrations.
Cruising. Higher levels of steady swimming activity, including preferred speeds of negatively buoyant fish, etc.

Prolonged (Activity level maintained between 200 min and 15 s.) Subdivisions possibly based on physiological criteria (Pritchard et al. 1971).

Burst (High activity levels maintained for less than 15 s.)
Sprint. High steady swimming speeds.
Acceleration. High unsteady swimming activity.

Sustained levels

As a principal activity level, sustained swimming speeds have been critically discussed by

49

several authors, particularly Brett (1964, 1965a, b, 1967a). Brett (1967a) recommended standard procedures for measuring activity at sustained levels in experimental situations, and these recommendations may serve as a definition. Sustained swimming would include all speeds and/or locomotor activities maintained for a minimum of 200 min. This definition includes a wide range of locomotor patterns assigned to three groups: routine, schooling, and cruising.

ROUTINE

Routine activity includes all low level activities normally seen in free-swimming fish, whether in primary, secondary, or both, locomotor modes. Routine activity levels will be the mechanical and behavioral equivalents to routine metabolic levels as defined by physiologists (Brett 1972).

SCHOOLING

This activity level includes many characteristics of routine activity except that the activity involves organized groups of fish. Schooling activity frequently includes migration. For some schooling species there is probably a hydromechanical advantage to members of the school that permits more energetically economical swimming performance (Belyayev and Zuyev 1969; Zuyev and Belyayev 1970; Weihs 1973b).

CRUISING

Cruising activity is identified by higher steady swimming speeds than are typical of routine activity, and, in most cases, by schooling. This description embodies the unstated definition of sustained activity in the literature where such levels are based on experimental techniques when fish are forced to adopt a specified relatively high activity level sustained for fairly long periods.

In wider terms cruising will again overlap with other activity levels, in this case with schooling activity in migrations. Preferred swimming speeds of fish that are negatively buoyant and must swim continuously to control vertical stability are included. Preferred speeds are probably minimum speeds for the most efficient generation of required lift forces (Magnuson and Prescott 1966; Magnuson 1970).

Prolonged levels

Prolonged activity levels are defined in relation to sustained activity, and burst activity as speeds that can be maintained for between 15 s and 200 min. Prolonged activity is frequently associated with periods of cruising with occasional bursts.

Most experimental observations on swimming fish have been made for prolonged activity. An important concept in such studies is the accurate measurement of the critical swimming speed, U_{crit} (Brett 1964). The measurement of U_{crit} stems from the convenient increasing velocity test procedure whereby various mechanical or physiological parameters may be measured for a range of speeds up to exhaustion of the fish. In such a test, swimming speed is increased by discrete intervals ΔU every t min. If a fish is exhausted in t_i min following a speed increment from U to U + ΔU, then

$$U_{crit} = U + \left[\frac{\Delta U \, t_i}{t}\right] \qquad (55)$$

and U_{crit} is qualified as the t-min U_{crit}.

Some controversy exists over the requisite value for t. Brett (1964, 1965a, 1967a) recommended 60 min when data for oxygen consumption are required. ΔU and t must consequently be large. Alternatively, Dahlberg et al. (1968) considered t may be as small as 10 min when U_{crit} alone is required, with ΔU being correspondingly smaller.

The U_{crit} results probably tend fairly close to sprint speeds for the 10-min time increment (Fig. 40), whereas the longer 60-min period is known to be about 12% higher than maximum cruising speeds (Brett 1964).

Any speed increment is followed by some period of restlessness by the fish (Webb 1971a, b) and some time is required for the cardiovascular and ventilatory systems to adjust to the changed demands of the tissues (Stevens and Randall 1967a). The latter adjustments take place over approximately 5 min, similar to the maximum period of restlessness observed by Webb. In view of the time required to adjust to a higher speed, any t value of less than about 20 min may be too short. Otherwise the adjustment period occupies a substantial period of time spent at any speed.

In an increasing velocity test ΔU is constant. The power required to swim at any speed is proportional to $U^{2.8}$. It would be expected that the magnitude of required physiological adjustment for successive speed increments would become progressively larger as such a test proceeded, with a possible reduction in the performance of a fish. Preliminary experiments with sockeye salmon in an increasing velocity test with equal $(U_i^{2.8} - U^{2.8})$ increments gave similar U_{crit} values to identical tests with equal ΔU increments (P. W. Webb unpublished data) but the question should be pursued further.

Burst

SPRINTS

Sprint activity includes high steady swimming speeds maintained for less than approximately 15 s. This generalization apparently applies to a wide variety of fish (Blaxter 1969).

The definition includes speeds maintained for less than 1 s, but it is likely these should not be considered as steady speeds but as unsteady peak speeds attained following an acceleration burst.

ACCELERATION

Acceleration activity may be defined as a high level of unsteady activity, probably maintained for less than 1 s. Such phenomena have largely been neglected in research, although acceleration is an integral part of a predator–prey relation and obviously the high sprint speeds attributed to fish can only be reached after an initial acceleration.

From the few measurements made for fish of a wide size range, typical acceleration values appear to be of the order of 40–50 m/s², independent of size (Gero 1952; Gray 1953a; Hertel 1966; Fierstine and Walters 1968; Weihs 1973a).

Included in this level of activity should also be high speed maneuvers, which have mechanical similarities with acceleration (Weihs 1972, 1973a).

There may be some overlap between acceleration at both burst and sustained activity levels. Normal routine activity will include some bursts interposed by glides. Such activity was considered the common form of routine activity among fish, called by Houssay (1912) "nage filée." Weihs (1973d, 1974) has shown that fish swimming at routine levels in such a burst/glide fashion can achieve significant energy savings. The magnitude of accelerations in routine activity may be such that there is no real overlap with burst acceleration activity.

Intermediate levels

Between each principal activity level is a transitional zone, characterized by extensive variance in swimming behavior as fish elect primarily one or another adjacent principal level. Prolonged activity may be interpreted as an intermediate level. Hunter (1971) and Pritchard et al. (1971), for example, have shown that intermediate swimming may be subdivided for *Trachurus*, the subdivisions related to the type of fuel oxidized and the site of usage.

Swimming Speeds and Size Effects

A useful concept in fish and cetacean locomotion studies is expressing swimming speeds in relation to length. Speeds may be expressed as specific swimming speeds in body lengths/s (L/s) after Bainbridge (1958). This normalization method is useful in comparing performance of fish of different sizes under various conditions, although it has recently been shown that size effects can be more accurately defined than in terms of L/s alone (Dahlberg et al. 1968; Hunter and Zweifel 1971). Specific swimming speeds remain the simplest and most useful method of comparison and will be used in the absence of detailed data on performance-size effects for most fish and cetaceans.

Most measurements of swimming speed have been made for fish swimming in various body and caudal fin modes, as with most other aspects of locomotion (Blaxter 1969). Even from these measurements it is clear that few interspecific generalizations can be made (Beamish 1966); the frequently accepted "10 L/s rule of thumb" for maximum sprint performance should certainly be treated with caution. In any propulsion study, it is imperative that performance levels should be determined for the pertinent experimental conditions. For present purposes it is sufficient to summarize briefly the magnitudes of various swimming performance levels reported for fish of different sizes, considered in terms of swimming mode whenever possible.

Anguilliform mode

Few measurements of swimming speed have been reported for fish swimming in this mode. Blaxter (1969) quoted sprint values of 3 L/s for a 10 cm *Pholis* and 1.9 L/s for a 60 cm *Anguilla* (Fig. 41). A size effect on sprint performance is suggested, but clearly the data are insufficient to attempt further conclusions. Pleuronectids also swim in the anguilliform mode, at least at higher performance levels (Breder 1926; Stickney and White 1973), although the body is markedly compressed in comparison with more typical fish swimming in this mode. These fish achieve slightly greater sprint speeds, apparently independent of size up to about 35 cm (Fig. 41).

Subcarangiform and carangiform modes

Pooled data taken from the review by Blaxter (1969) for sprint speeds are plotted against length in Fig. 41. In all groups of fish when speeds have been measured for a large enough size range,

51
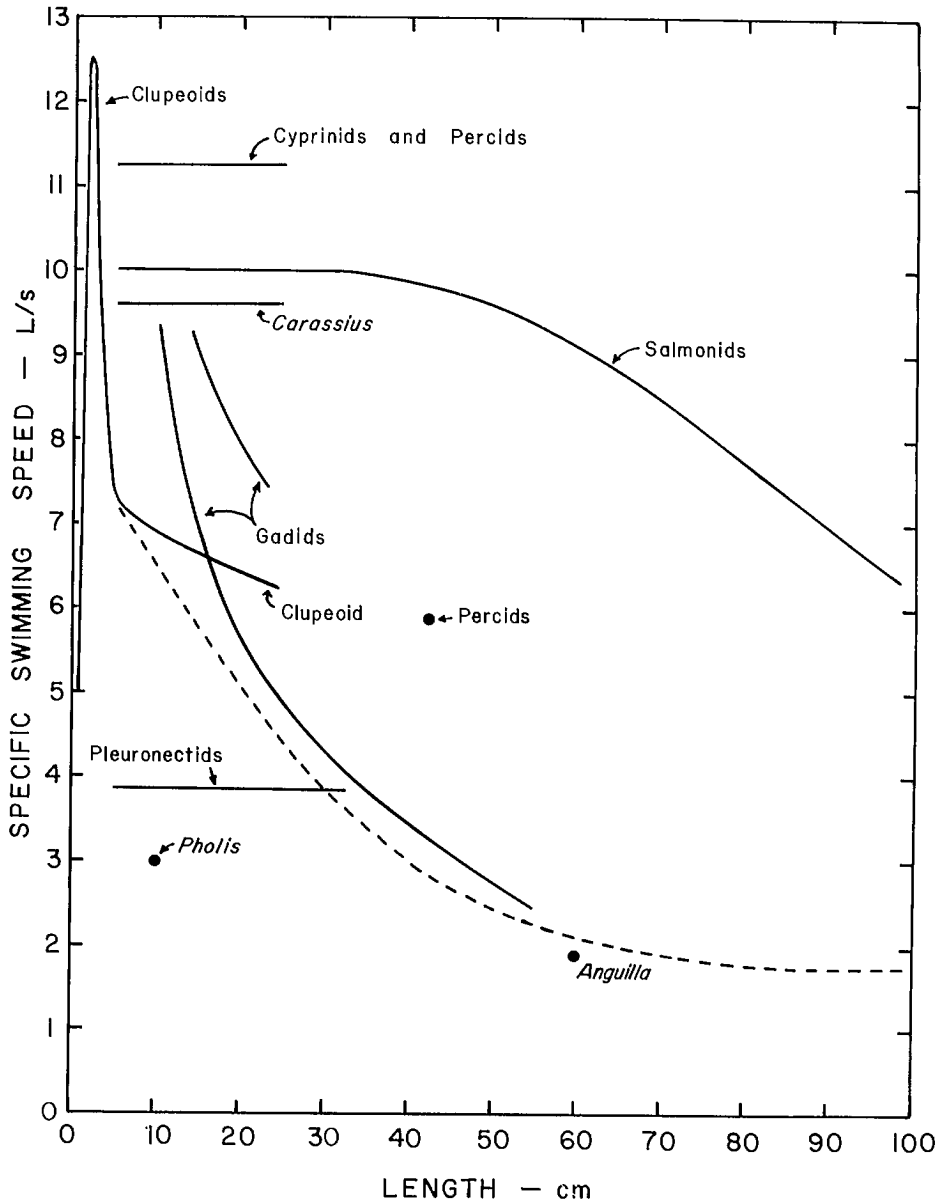
FIG. 41. Relation between maximum specific speeds and length for several groups of fish. Solid lines show maximum sprint levels, broken line highest cruising levels reported for fish. (Data taken from Brett (1964), Brett and Glass (1973), and Blaxter (1969) who may be referred to for further references)

there is a marked dependence of specific speed on size, specific speed decreasing with increasing size. This is particularly well shown for gadids, e.g., *Gadus morhua* (Blaxter and Dickson 1959). For several groups, specific speeds appear almost independent of length to approximately 30 cm, but this is only a superficial result of pooling data.

Measurements on a given species show size dependence (Blaxter 1969; Beamish 1966).

The relation between specific sprint speeds and length for smaller clupeiods is of particular interest. The initial rapid increase in specific speed in young fish occurs with the elaboration of the caudal fin. Increased depth of the caudal

fin produces more efficient propulsion, to which the rapid increase in specific speed might be related. The increase in specific speed to a peak following caudal fin elaboration is followed by a marked size-dependent decrease in specific sprint speed comparable to that observed for gadids (Fig. 41).

The best generalization Blaxter (1969) could reach concerning sprint speeds of fish of different groups, was that small salmonids, cyprinids, and percids could achieve maximum sprint speeds of the order 9–12 L/s, not dissimilar to the 10 L/s speed considered typical of fish by Bainbridge (1958), on the basis of earlier literature and his observations on a relatively small size range of three species. Blaxter (1969) considered that most other fish, including clupeoids and gadids, could normally reach maximum sprint speeds of 4–9 L/s.

In comparison with sprint speeds, cruising and prolonged speeds show much greater variance, not only between species but also to a greater extent as a result of biotic factors (Brett 1962). Figure 41 shows for completion the order of magnitude of maximum cruising speeds measured for salmonids, clupeoids, and percids under optimum conditions (Brett 1965a; Blaxter 1969; Brett and Glass 1973). Other groups can apparently reach cruising speeds of the order of half to three-quarters of these values (Blaxter 1969).

Carangiform mode with semilunate tail

This mode of locomotion is employed by fish and cetaceans reaching the highest swimming speeds, not only in terms of absolute speeds, but in terms of specific swimming speeds. Fish swimming in this mode have commanded substantial research interest probably because of the magnitude of speeds recorded. Because many reach large sizes, the animals are not usually suitable for rigorous experimental observation, with the exception of experiments conducted by Hunter and Zweifel (1971). Most swimming speeds have consequently been measured on large fish and cetaceans swimming in large aquaria (Magnuson and Prescott 1966; Yuen 1966), by timing from boats over some distance (Parry 1949a; Johanessen and Harder 1960; Yuen 1966), or by allowing a fish to run out a line (Gero 1952; Walters and Fierstine 1964). In many cases, speeds may be uncertain, particularly if the animal cannot be seen at all times, and the method of running out a line has obvious disadvantages as discussed by Gero (1952). Additional reliable

data on performance levels and their maxima are required for larger fish and cetaceans.

The various groups of fish and cetaceans will be considered separately.

SCOMBRIDS

Swimming speeds at various activity levels are shown in Fig. 42. Maximum specific sprint speeds to 21 L/s have been reported for *Thunnus albacares* (Walters and Fierstine 1964). These speeds were only maintained for a fraction of a second and were peak unsteady speeds reached after a period of acceleration. Nevertheless, maximum sprint speeds of 10 L/s and above appear to be the rule for scombrids, including those of large size. Little dependence of speed on size has been found, except for *Euthynnus pelamis* (Fig. 42). Schooling speeds have been reported for scombrids between 0.5 and 10 L/s and cruising speeds were reported of the same order (Blaxter 1969; Hunter and Zweifel 1971).

ELASMOBRANCHS

Few data have been reported for elasmobranchs swimming in carangiform modes. Gero (1952) measured what were probably sprint speeds for *Carcharhinus leucas* 153 cm long, and
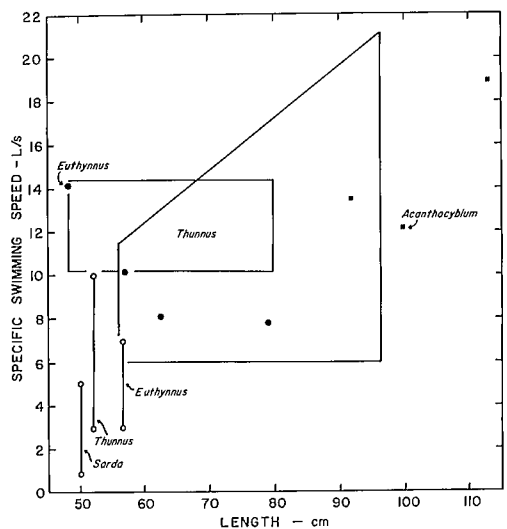
FIG. 42. Relation between specific swimming speeds and length for scombrids. Solid circles and space within quadrilaterals are maximum sprint speeds, open circles are schooling speeds. (Data shown for *Euthynnus pelamis, Acanthocybium solanderi,* Yuen 1966; *Sarda chiliensis,* Magnuson and Prescott 1966; and *Thunnus albacares,* Walters and Fierstine 1964, Yuen 1966)

53

Negaprion brevirostius 184 cm long, of between 3.4 to 3.9 L/s. These speeds are low in comparison with other animals swimming in the same mode and many swimming in other modes. Clearly more data are required.

CETACEANS

Swimming speeds of cetaceans are summarized in Fig. 43. A few of the largest cetaceans attain slightly higher sprint speeds than scombroid fish, dolphins, or porpoises (Gawn 1948), but in general there is little increase in swimming speed for a size range from approximately 100 to 3600 cm. There is a marked dependence of specific swimming speeds on size, and maximum recorded specific swimming speeds are extremely low for large cetaceans. Maximum specific sprint speeds for *Balaenoptera* appear to be of the order 0.5–6.3 L/s (Gray 1936b; Gawn 1948; Norris and Prescott 1961).
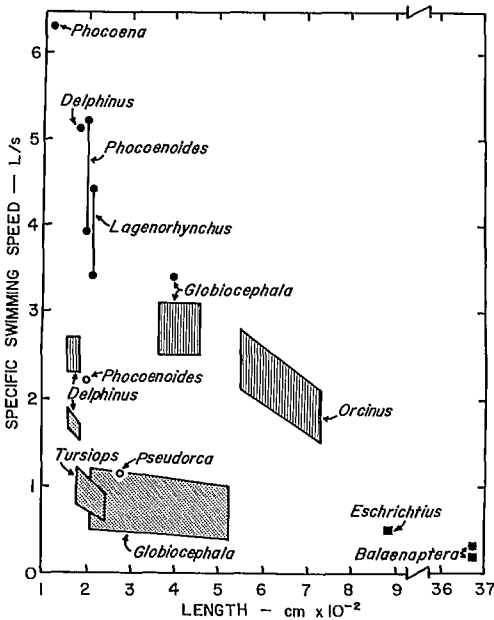
FIG. 43. Relation between specific swimming speeds and length for cetaceans. Solid circles are maximum sprint speeds; solid squares and shaded quadrilaterals, cruising speeds; open circles and stippled quadrilaterals, schooling speeds. (Data shown for *Phocoena communis*, Gray 1936b; *Delphinus delphus* and *D. bairdi*, Gray 1936b, Norris and Prescott 1961; *Phocoenoides dalli*, *Tursiops gilli*, *Eschrichtius glaucus*, and *Pseudorca crassidens*, Norris and Prescott 1961; *Globiocephala melana*, *G. scammoni*, and *Lagenorhyn-chus obliquidens*, Johanessen and Harder 1960, Norris and Prescott 1961; *Balaenoptera borealis*, Gawn 1948; and *Orcinus orca*, Norris and Prescott 1961)

Specific cruising swimming speeds also show marked size dependence from 4.4 to 2.1 L/s for a length of 215–760 cm. For *Balaenoptera* 3672 cm long, sustained speeds fall as low as 0.3 L/s. Schooling speeds range from 2.2 to 0.4 L/s, again showing size dependence (Fig. 43).

Summary — For animals swimming in the carangiform mode with semilunate tail maximum sustained speeds approach maximum burst speeds fairly closely. In general, scombrids cruise between 5 and 10 L/s, with sprint speeds of the order 10–16 L/s. For cetaceans, these values are 2–5 L/s and 3–7 L/s respectively. In comparison, an intermediate-size salmon would cruise at approximately 3 L/s with sprints up to approximately 9.5 L/s, a much greater difference, particularly as propulsive power required increases with $U^{2.8}$. Animals swimming in the carangiform mode, with the semilunate tail modification are apparently designed for high speed sustained activity levels.

Other swimming modes

Measurements at various activity levels have not been made for fish swimming in other modes, with the exception of prolonged swimming for *Cymatogaster aggregata* (Webb 1973b). A 45-min U_{crit} of 3.9 L/s was found for fish 14.3 cm long swimming in the labriform mode. This value compares favorably with many optimum prolonged swimming speeds of other fish swimming in body and caudal fin modes.

Factors Affecting Swimming Speeds

Swimming speeds are affected by numerous factors depending to a large extent on the activity level. This applies particularly to sustained and prolonged activity levels, which have been most extensively studied. Sustained and prolonged activities are dependent on the maintained functioning of supply systems for oxygen and removal of waste metabolic products. Any factor interrupting or affecting supply systems, as well as those affecting the propulsive system itself, affects swimming performance. Burst activity is dependent on immediate energy reserves and appears to be less affected by extraneous factors (Blaxter 1969).

Factors that affect sustained swimming performance will be summarized for completion. More detailed reviews may be found in Brett (1962) and Blaxter (1969) or any standard comparative physiology text.

TEMPERATURE

This is probably of greatest importance. Although it apparently has little effect on sprint performance (Blaxter 1969) temperature markedly affects sustained swimming. An exception is *Clupea harengus* (Blaxter 1969). The response to temperature depends on the temperature to which fish are acclimated and the test temperature. When these are the same, a peaked curve is typical (Fig. 44). A more domed shape appears when acclimation temperatures are constant, and fish are then tested at different temperatures. In terms of overall energetics, at critical swimming speeds, the metabolic cost to travel unit distance appears to be independent of temperature (Brett 1964).
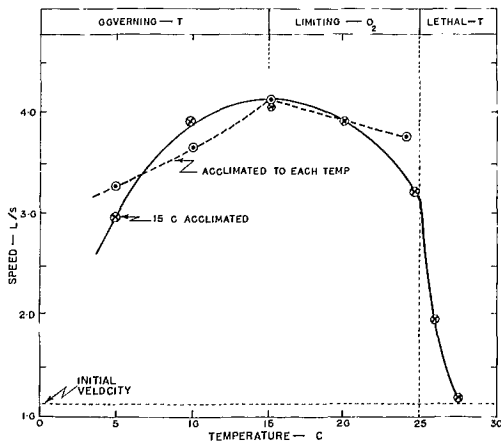
FIG. 44. Relation between swimming speed of sockeye salmon acclimated to 15 C only and tested at various temperatures, and acclimated to each test temperature. (From Brett 1964) Mean lengths were 16.8 and 17.8 cm for the two groups respectively. Effect of environmental factors, temperature (T) and oxygen (O_2) on activity are indicated in the manner of Fry (1947). (From Brett 1967a)

OXYGEN AND CARBON DIOXIDE

Reduction of oxygen between 90 and 60% air saturation reduces performance in salmonids. For fish acclimated to lower levels, oxygen levels of 60% saturation are required before performance is affected (Dahlberg et al. 1968). High oxygen levels above air saturation can increase performance (Brett 1964). At high temperatures, the oxygen content of water is reduced, and this reduces performance, over-riding temperature effects that would be expected to increase performance (Brett 1964). High levels of carbon dioxide apparently have little effect on performance (Dahlberg et al. 1968).

SALINITY

Salinities that differ from normal levels reduce performance, although the reduction is small compared to temperature effects (Blaxter 1969; Griffiths and Alderdice 1972).

PREEXERCISE

Training has mixed effects on performance. In general, training results in higher swimming speeds (Brett et al. 1958; Vincent 1960; Bainbridge 1962; Blaxter 1969).

PREHISTORY

Hatchery-reared fish usually have lower swimming speeds than wild fish (Davies et al. 1963). This may be the result of less training in hatchery fish (Hammond and Hickman 1966). In addition, the conditions under which eggs are hatched, in salmonids at least, affect later swimming performance (Bams 1967). There are also performance differences between stocks (Brett 1964).

HANDLING

Handling is a stress resulting in elevated metabolic rates, probably related to oxygen debt. Recovery from handling may take up to 8 h (Black 1957) or more (Smit 1965). Insufficient recovery times are expected to result in reduced prolonged and burst speeds through reduction of immediate reserves and elevation of catabolite levels.

MATURITY

Fish approaching sexual maturity tend to be less excitable and have reduced performance (Blaxter 1969).

Chapter 4 — Drag

Introduction

Drag is the resistance to motion of a body moving in a fluid. The question of the drag of swimming fish is of fundamental importance to propulsion studies, particularly in considering the energy flow through the "black box" that is the composite propulsion system. Only when oxygen consumption can be related to swimming speed is there any comprehensive information on energy input to this system, but the overall and detailed fate of that energy is largely unknown. Initial characterization of the propulsion system requires information on efficiency, which in turn is contingent on calculation of power expenditure against drag.

There are two approaches to calculating power expenditure; by calculating drag force, or thrust force that must be equal to the drag of the fish.

Measurement of thrust is more difficult than drag (Webb 1971a) and the use of this approach largely depends on the formulation of suitable hydrodynamic models consistent with the kinematics. Until recently, no suitable models were available, and these could not be tested against measurements. The only criteria available for the acceptance of a model was that its predictions should not violate the laws of thermodynamics, and be consistent with the expected behavior of the system interpolated from measurements on other animals.

Because of difficulties in calculating thrust, biologists and mathematicians have tended to calculate swimming power requirements from drag. Two methods have been used. Both assume flow around a swimming fish is mechanically equal to flow around an equivalent rigid body (rigid-body analogy). Then drag may be calculated from standard hydrodynamic equations, i.e. theoretical drag. Alternatively drag may be measured for a (usually dead) fish with the body stretched straight, i.e. dead drag. The use of the rigid-body analogy in calculating drag for swimming fish appears to be based on observations first made by Sir George Cayley (1809, see Gibbs-Smith 1962) that fish and cetaceans with high swimming performance all have streamlined bodies.

The application of drag calculations to energetic studies has produced confusion, as conclusions are conflicting. The most important study was made by Gray (1936b), who calculated there was insufficient muscular power to meet that required to overcome the theoretical drag for a dolphin. This has since been called Gray's paradox, and has stimulated much research to repeat or explain the discrepancy. Similar discrepancies have been found on the basis of theoretical drag for salmon by Osborne (1961), goldfish by Smit et al. (1971), and on the basis of dead-drag measurements by Brett (1963). (See Chapter 7.)

In contrast, Bainbridge (1961) calculated that almost all fish and cetaceans could develop sufficient muscular power to meet their theoretical drag power requirements. Similar results were attained by Smit (1965) for goldfish and by Brown and Muir (1970) for skipjack tuna. Webb (1970) and A. J. Mearns et al. (personal communication) reached similar conclusions from dead-drag measurement of salmon and trout.

Much of the confusion can be attributed to insufficient information on other components of the propulsive system or swimming performance levels. Some discrepancies can be resolved in the light of more complete later data. Nevertheless, it is important to reconsider the question of drag measurements and their application to fish power problems.

Theoretical Drag

Theoretical drag is the hydrodynamic resistance of an equivalent rigid body, with the same dimensions as the fish to which it is compared, moving at the same velocity in the same fluid. In extrapolating theoretical drag calculations to swimming fish, it is implied that swimming drag is equal to that of the body when stretched straight and making no lateral movements. As such, the flow pattern is assumed to be streamline, with boundary-layer flow conditions dictated by R_L, surface conditions, and the intensity of turbulence. The effects of any secondary flow pattern produced by propulsive movements are neglected. For practical purposes, most calculations of

theoretical drag assume the fish is not compressed, and may be compared with a body of revolution, the diameter of which is the mean of the depth and width of the fish. Otherwise, the shape of the body is assumed to be similar to that of the fish in terms of its effects on flow (Chapter 1).

Drag arises from skin frictional forces and longitudinal pressure forces acting on the body, fins, and gills. Drag from gills has been neglected except for calculations made by Brown and Muir (1970) for the skipjack tuna (*Katsuwonis pelamis*) and these will be considered. The fish was 44 cm long, and calculations were made for the preferred swimming speed of 66 cm/s, taken from Magnuson (1970). Other values required for calculation of drag are given in Table 3. R_L was 3×10^5, below $R_{L\ crit}$, so the boundary layer was assumed to be laminar.

For the body, the pressure drag coefficient, C_p, was taken as 0.25 the frictional drag coefficient ($C_{f\ lam}$). For the fins, C_p of 0.5 $C_{f\ lam}$ was taken. This higher value was used because tuna are denser than seawater and lift is generated by the pectoral fins (Magnuson 1970). The value of C_p used was the mean for lifting and nonlifting fins. The total drag for body and fins was calculated as 10,930 dyn.

Gill resistance was calculated using the principles of flow through pipes and engineering experience of energy losses in expansion and contraction sections. Bernoulli's theorem and the laws of the conservation of mass and momentum were used to calculate pressure changes in the expansion section of the system (the buccal cavity), and the contraction section (the opercular cavity). Pressure losses in the two sections were estimated to be 15% of the pressure change in the buccal cavity, and 5% of the pressure change in the opercular cavity. Pressure change across the gills was calculated from Poisseuille's law for the flow through pipes of the measured dimensions of the gill sieve.

Total pressure loss across the gill system was calculated as 1100 dyn/cm² which represented a total drag of 1090 dyn.

From these data, the drag of body and median fins was 77% of the total drag, and that of the pectoral fins 14% (Table 3). This suggests that use of the paired fins as hydrofoils is an expensive method of buoyancy control; the relatively high drag of the pectoral fins was associated with only 3% of the total body and fin area. The gills represented 9% of the total drag (although their area was 30 times that of the body and fins) because the water velocity over the secondary lamellar surface was low, as required for efficient gas exchange (Muir and Kendall 1968; Randall 1970a, b).

Other studies using theoretical drag calculations have been made for dolphins (Gray 1936b), salmon (Osborne 1961), goldfish (Smit 1965; Smit et al. 1971), and for fish and cetaceans in general (Bainbridge 1961). The omission of gill drag for neutrally buoyant fish is likely to have a greater effect on total drag than suggested by Brown and Muir's (1970) calculations because lower energy losses would (theoretically) be associated with the fins, reducing total drag. Based on calculations for skipjack tuna, gill resistance would represent about 12% of the total theoretical drag for neutrally buoyant fish.

Equations normally employed to calculate drag assume that steady-state conditions have been reached. It is improbable that this applies for higher sprint speeds, which can be reached in a short time and are of short duration (Webb 1971a, b; Weihs 1972, 1973a). The resistance of a fish accelerating to these speeds is more likely to be related to its mass and the rate of acceleration, and can be crudely estimated from standard Newtonian mechanics. However, a mass of water is accelerated with the fish, the virtual or added mass, which must be added to the mass of the fish. The added mass is often taken to be 20% of the fish mass (Gero 1952; Webb 1971b).

Dead Drag

Dead drag includes all measurements made on fish with the body stretched straight. Most measurements have been made on freshly killed or pickled fish, but also on anesthetized fish, live fish during a glide, and models. The use of dead-drag measurements in energetics implies that the flow around a swimming fish will be the same as that around the body when stretched straight, hence, the validity of using models. The assumptions concerning the flow pattern are the same as with theoretical drag, and because of this dead drag should be the same as an equivalent rigid vehicle as calculated by standard equations. The only advantages in dead-drag measurements are superficial; assumptions on the effects of surface conditions and effects of body shape on drag are not required. In theory, dead-drag measurements may be used to compare fish with man-made vehicles, and may indicate the presence of passive drag-reducing mechanisms.

TABLE 3. Data and calculation of theoretical drag for a skipjack tuna, *Katsuwonis pelamis* (from Brown and Muir 1970).

Site	Length (cm)	Reynolds Number (R_L)	Frictional drag coefficient ($C_{f\ lam}$)	Pressure drag coefficient (C_p)	Wetted surface area (S_w, cm^2)	Frictional drag (D_p, dyn)	Pressure drag (D_f, dyn)	($D_f + D_p$)	Percent total drag (%)
Body	44.0	2.9×10^5	0.0025	$0.25C_{flam}$	890	5000	1250	6250	52
Caudal fin	2.2	1.5×10^4	0.011		62	1520	760	2280	19
Dorsal and ventral fins	1.3	8.6×10^3	0.015		15	500	250	750	6
Pectoral fin	1.5	9.9×10^3	0.014	$0.50C_{flam}$	35	1100	550	1650	14

	Free stream pressure (dyn/cm^2)	Pressure loss in buccal cavity (dyn/cm^2)	Pressure loss across gills (dyn/cm^2)	Pressure loss in opercular cavity (dyn/cm^2)	Total pressure loss (dyn/cm^2)	Drag (dyn)	Total drag of body, fins, and gills (dyn)	Percent total drag (%)
Gills	2232	240	800	60	1100	1090	— 12,020	9 100

Unfortunately, it has not been possible to obtain sensible dead-drag values for most fish. Most values are much greater than the theoretical drag values expected based on the assumptions involved in dead-drag measurement. The lowest dead-drag measurements are similar to the values expected for equivalent rigid bodies. The following discussion of dead-drag measurements is organized to elucidate reasons for high dead-drag measurements.

Sources of error in dead-drag measurements

The primary reason for measuring high dead-drag values is that fish do not behave like rigid bodies. Instead, the fins, and, to a lesser extent the body, behave more like flags and "flutter" in a stream. Hertel (1966) has shown that this type of behavior is associated with high additional drag forces. The various factors which affect the magnitude of the drag relating to fluttering are most clearly shown by several experiments performed on salmonids by Brett (1963), Webb (1970), and A. J. Mearns et al. (personal communication). All experiments were performed in water tunnels, where the intensity of turbulence would exceed critical values. Therefore, boundary-layer conditions would be turbulent, independent of R_L.

The experiments were as follows: (1) 18.0 cm (47.9 g) sockeye salmon, *Oncorhynchus nerka* (Brett 1963). Fish were supported at the nose on a short flexible connection to a drag balance. The body was partially stiffened by a wire, and the mouth was sewn closed. Air was injected into the abdomen to make the fish neutrally buoyant. The position of the fish in the tunnel was determined by hydrostatic and hydrodynamic forces, and the fish had a fairly high degree of freedom to move relative to the flow. Fins were free to flutter. This will be referred to as Method I, for small fish with low rigidity–high flutter. (2) 30.0 cm (278 g) rainbow trout, *Salmo gairdneri* (Webb 1970). The body was stiffened with wire and the mouth sewn closed. Fish were rigidly held on the tunnel centerline by a drag balance, with the arm embedded in the abdomen. Fins were free to flutter. This will be referred to as Method II, for medium-size fish of medium rigidity–medium body and caudal fin flutter. (3) 29.3 cm (254 g) rainbow trout (Webb 1970). Fish were stiffened as for Method II, and stretched between streamlined bars to further reduce freedom for body and caudal fin flutter. Fish were rigidly held on the tunnel centerline by a drag balance. This will be Method IIIA, for medium fish of high rigidity–low body and caudal fin flutter. Drag was also measured under the same conditions, after amputation of the paired fins, which will be referred to as Method IIIB, low body and caudal fin flutter, and zero fin flutter (Appendix 1). (Methods I to III used freshly killed fish.) (4) 57.3 cm (2217 g) coho salmon, *Oncorhynchus kisutch*, and 48.5 cm (1347 g) rainbow trout, *Salmo gairdneri* (A. J. Mearns et al. personal communication). Lightly anesthetized fish were attached to a strain gauge by an 8-in flexible connector. Hydrostatic and hydrodynamic forces controlled the position of the fish in the tunnel. This will be Method IV, for large fish with low rigidity.

Various results for drag can be compared by calculating drag coefficients and expressing these as a function of R_L (Table 4, Fig. 45); various factors affecting the magnitude of the measured drag can be shown.

In terms of body rigidity, the results from Methods I, II, and IIIA may be compared. Method I gave the highest drag coefficients. There was a large decrease in drag coefficient with Method II, and a small reduction in Method IIIA. Thus, the magnitude of the drag decreased as the body was made progressively more rigid (Fig. 45).

The effect of fin fluttering on drag can be shown by comparing Methods IIIA and IIIB. Drag measured without the paired fins was lower than that for the intact fish, a difference greater than the expected decrease through loss of the small area of the fins.

These results clearly show the effects of body and fin fluttering. As the lowest values remained well above the expected theoretical drag, it is apparent that this source of error was not completely eliminated.

The effect of size on the magnitude of measured drag can be shown by comparing results obtained by Methods I, II, and IV, although the rigidity of the body was not strictly comparable in the three cases. Drag coefficient at a given R_L decreased with increasing body size, the effect being greater between Methods I and II than II and IV because fish in Method II were made more rigid than others. This phenomenon can be interpreted the same as results for body rigidity. Larger fish would have thicker bodies and tend to be more rigid than smaller fish and flutter less in a stream. Consequently, their measured drag is lower than for smaller fish.

Clearly, measured drag is related to the freedom of the fish to flutter and to the size of the fish and the method employed in drag determination. These conclusions may be used to

60

TABLE 4. Drag coefficients and Reynolds numbers calculated from dead-drag measurements on salmonids in water tunnels. Kinematic viscosity of water was taken as 10^{-2} poise.

Species	Weight (g)	Length (cm)	Wetted surface area (cm²)	Velocity (cm/s)	Reynolds Number (1)	Drag (g wt)	Drag coeffi- cient (1)	Reference
				Method I: small fish of low rigidity				
Oncorhynchus nerka	47.9	18.6	138[a]	15.24	2.5×10^4	3.8	0.23	Brett (1963)
				30.48	5.0	12.5	0.19	
				45.72	7.4	22.3	0.15	
				60.96	9.9	35.6	0.14	
				76.20	1.2×10^5	51.1	0.12	
				91.44	1.5	68.7	0.12	
				106.6	1.7	89.6	0.11	
				121.8	2.0	108.0	0.10	
				Method II: medium fish of medium rigidity				
Salmo gairdneri	278	30.0	354	10.3	3.1×10^4	0.82	0.10	Webb (1970)
				13.7	4.1	1.27	0.037	
				17.2	5.1	1.87	0.034	
				20.5	6.2	2.53	0.033	
				24.2	7.3	3.34	0.031	
				27.5	8.3	4.25	0.031	
				31.0	9.3	5.13	0.029	
				37.8	1.13×10^5	7.06	0.027	
				44.7	1.33	9.80	0.027	
				51.5	1.56	13.45	0.026	
				57.9	1.75	17.10	0.027	
				Method IIIA: medium fish of high rigidity				
Salmo gairdneri	254	29.3	342	17.3	5.0×10^4	1.1	0.021	
				24.2	7.1	2.2	0.021	
				31.1	9.2	3.9	0.022	
				38.0	1.12×10^5	5.0	0.019	
				44.7	1.32	7.2	0.020	
				51.8	1.56	9.0	0.019	
				58.7	1.73	11.7	0.019	
				Method IIIB: as method IIIA but with paired fins amputated				
Salmo gairdneri	254	29.3	342	17.3	5.0×10^4	0.89	0.017	
				24.2	7.1	1.51	0.014	
				31.1	9.2	2.52	0.014	
				38.0	1.12×10^5	3.79	0.015	
				44.7	1.32	5.35	0.015	
				51.8	1.53	7.13	0.015	
				58.7	1.73	9.21	0.015	
				Method IV: large fish of low rigidity				
Salmo gairdneri	1347	48.5	–	20	9.7×10^4	–	0.031	A. J. Mearns et al. (personal communication)
				30	1.46×10^5	–	0.021	
				60	2.90	–	0.017	
				90	4.36	–	0.014	
Oncorhynchus kisutch	2217	57.3	–	20	1.15×10^5	–	0.026	
				30	1.72	–	0.025	
				60	3.44	–	0.020	
				90	5.16	–	0.018	

[a]Wetted surface area assumed equal to 0.4 L^2.

61
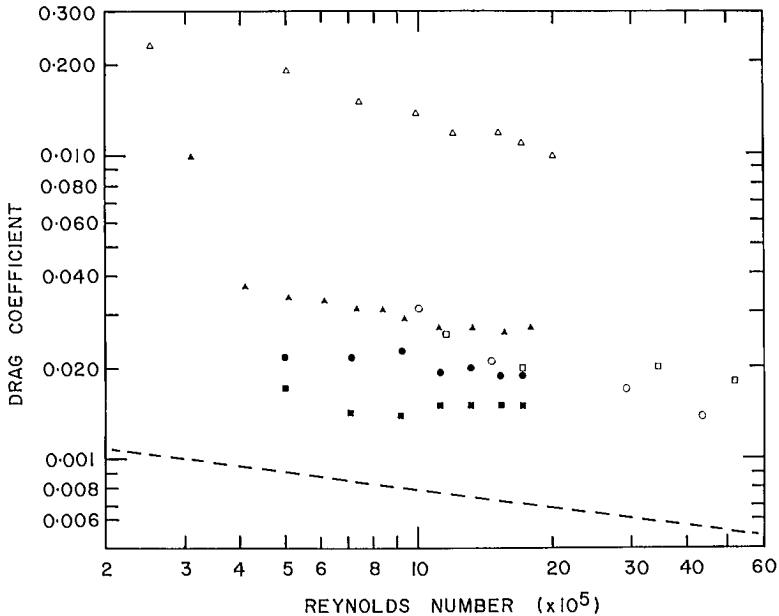
FIG. 45. Relation between dead-drag coefficients for salmonids, and Reynolds Number. Open triangles are for small sockeye salmon with low rigidity — Method I (Brett 1963); solid triangles, medium-sized rainbow trout with medium rigidity — Method II; solid circles, intact medium-sized trout with high rigidity — Method IIIA; solid squares as for Method IIIA but with paired fins amputated — Method IIIB (Webb 1970); open circles, large rainbow trout of low rigidity, and open squares large coho salmon of low rigidity (A. J. Mearns et al. personal communication). Broken line shows theoretical drag coefficients for equivalent rigid bodies with turbulent boundary-layer flow. Gill drag is not included.

discuss other dead-drag values reported in the literature and to compare them with theoretical drag.

Dead drag of fishes

Dead-drag values may be conveniently separated based on method. Data for several drag measurements are given in Table 5, arranged in the order of magnitude of the drag coefficient calculated from that data for each method of measurement. Results will be discussed in terms of drag coefficients, related to R_L (Fig. 46).

Further dead drag values in the Russian literature (Pershin 1970; Pyatetskiy 1970b; Kliashtorin 1973) have recently come to the author's attention. These data follow the same trends shown, and no modification of conclusions is required.

Water Tunnel Measurements

Salmonids have been used in all measurements of dead drag in water tunnels (Brett 1963;

Webb 1970; A. J. Mearns et al. personal communication). The only additional measurement is that of Harris (1936) for a model *Mustelus canis* in a wind tunnel. The drag measured was high in comparison with most other values. The use of the model would be expected to have given values closer to theoretical drag coefficients. The reason for this discrepancy is not known.

Towing Measurements

Dead drag of fish and models has been measured by towing (Houssay 1912; Magnan 1930; Kempf and Neu 1932; Denil 1936; Kent et al. 1961; Sundnes 1963; Q. Bone personal communication). Insufficient data have been given by Houssay (1912) to calculate drag coefficients and R_L. Drag coefficients calculated from the data of Kempf and Neu, Kent et al., and Bone were made in still water below $R_{L\ crit}$ and should be comparable to theoretical drag coefficients for laminar boundary-layer flow. Drag coefficients calculated from Magnan and Sundnes were made above $R_{L\ crit}$ and should be

TABLE 5. Dead-drag coefficients and Reynolds numbers calculated from data in the literature for several fish. Kinematic viscosity of water was taken as 10^{-2} poise. (from Webb 1970)

Species	Weight (g)	Length (cm)	Wetted surface area (cm²)	Velocity (cm/s)	Reynolds Number (1)	Drag (g wt)	Drag coefficient (1)	Reference
Wind Tunnel Measurements								
Mustelus canis (smooth dogfish)	–	87.9	3091[b]	44.7 (water equivalent)	3.9×10^5	69.5	0.022	Harris (1936)
Towing Measurements								
Unspecified	–	–	–	–	4×10^4	–	0.30	Kent et al. (1961)
					6	–	0.29	
					8	–	0.22	
					10	–	0.13	
Esox (pike)	–	40	640[b]	150	6×10^5	225	0.031	Magnan (1930)
Squalus (dogfish)	–	90	3240[b]	180	1.6×10^6	750	0.014	Magnan (1930)
Models of pelagic fish	–	10	40[b]	100	1.0×10^5	3	0.015	Denil (1936–1938)
				150	1.5	6	0.013	
				200	2.0	10	0.012	
				300	3.0	20	0.011	
				400	4.0	50	0.015	
				500	5.0	70	0.014	
				600	6.0	100	0.014	
	–	75	2250[b]	100	7.5×10^5	156	0.014	
				150	1.12×10^6	351	0.014	
				200	1.5	630	0.014	
				300	2.25	1410	0.014	
				400	3.0	2500	0.014	
				500	3.75	3900	0.014	
				600	4.5	5630	0.014	
Esox (pike)	–	73	2132[b]	50	3.6×10^5	47	0.0173	Kempf and Neu (1932)
				100	7.3	112	0.0103	
				150	1.09×10^6	200	0.0082	
				200	1.46	320	0.0074	
				250	1.82	483	0.0071	
				300	2.19	710	0.0073	
				350	2.55	1000	0.0075	
				400	2.95	1350	0.0078	
				450	3.28	1770	0.0080	
Salmo gairdneri (trout)	–	105	4410[b]	100	1.05×10^6	169	0.0075	Sundnes (1963)
				200	2.10	508	0.0056	
				300	3.15	1077	0.0053	
				400	4.20	1892	0.0053	
Scomber scombrus (mackerel)	–	35	455	10	3.5×10^4	0.25	0.106	Q. Bone (personal communication)
				20	7.0	0.40	0.0043	
				30	1.05×10^5	0.90	0.0043	
				40	1.40	1.9	0.0051	
				50	1.75	3.0	0.0052	

63

TABLE 5. Dead-drag coefficients and Reynolds numbers calculated from data in the literature for several fish. Kinematic viscosity of water was taken as 10^{-2} poise. (from Webb 1970)—*Concluded*

Species	Weight (g)	Length (cm)	Wetted surface area (cm^2)	Velocity (cm/s)	Reynolds Number (1)	Drag (g wt)	Drag coefficient (1)	Reference
Free Fall Measurements								
Scomber (mackerel)	100.3	23[a]	212[b]	6.65	1.5×10^4	26.5	5.59	Richardson
				11.00	2.5	40.5	3.10	(1936)
				12.5	2.9	48.0	2.84	
				13.5	3.1	65.0	3.30	
Clupea harengus (herring)	96.4	21[a]	180[b]	5.0	1.1×10^4	13.6	5.94	Richardson (1936)
				10.0	2.1	23.0	2.51	
				12.0	2.5	31.2	2.36	
Amia calva (bowfin)	1250	50[a]	1000[b]	172	8.7×10^5	210	0.0047	Gero (1952)
Glide Measurements								
Ambramis (bream)	–	28.5	325[b]	5	1.42×10^4	0.11	0.027	Magnan (1930)
Salmo	84	21[a]	184[b]	134	2.84×10^5	24	0.015	Gray (1957a)
Lagenorhynchus obliquidens	90,800	216	35,200	420	9.1×10^6	–	0.0034	Lang and Daybell (1963)

[a]Calculated assuming weight = 0.01 (length)^3.

[b]Calculated assuming wetted surface area = 0.4 (length)^2.

comparable to theoretical values for turbulent boundary-layer flow. The same applies to values obtained by Denil (1936) as these were made in a flume of turbulent water.

Kent et al. (1961) reported the highest drag coefficients obtained by towing methods. Other data, such as species, length, and velocity were not given. Drag of the fish was measured by means of a drag balance mounted on a trolly. The fish was attached to the balance by a sting embedded in the caudal peduncle. The position of the sting probably permitted the anterior portion of the body to yaw. This would increase the drag, and explain the high values obtained.

Magnan (1930) measured the drag of a 40-cm pike and a 90-cm dogfish being towed by a line attached to the nose. The fish were freshly killed, body and fins were fairly free to flutter, and drag coefficients were high.

Kempf and Neu (1932) measured drag of freshly killed and pickled pike 73 cm long, using the same methods as Magnan (1930). Drag values for pickled fish are in Table 5. They were about four times lower than the drag obtained for fresh fish. Pickling the fish clearly indicates the effects of body rigidity on the magnitude of measured drag. Results obtained by Kempf and Neu show another aspect of the effects of fluttering on drag; the drag coefficient tended to increase at higher speeds and R_L. At higher speeds, the amount of fluttering of the body and fins tended to increase (Webb 1970), and this was reflected in proportionally higher drag. Effects of this nature are more obvious for relatively stiff fish, as the drag increment with increased fluttering is large in comparison with the increase in body drag. Drag of the pickled pike was still greater than theoretically expected values, showing that fluttering was not completely eliminated, even at low speeds.

Sundnes (1963) measured the drag of several fish, and values for a 105-cm trout are given in
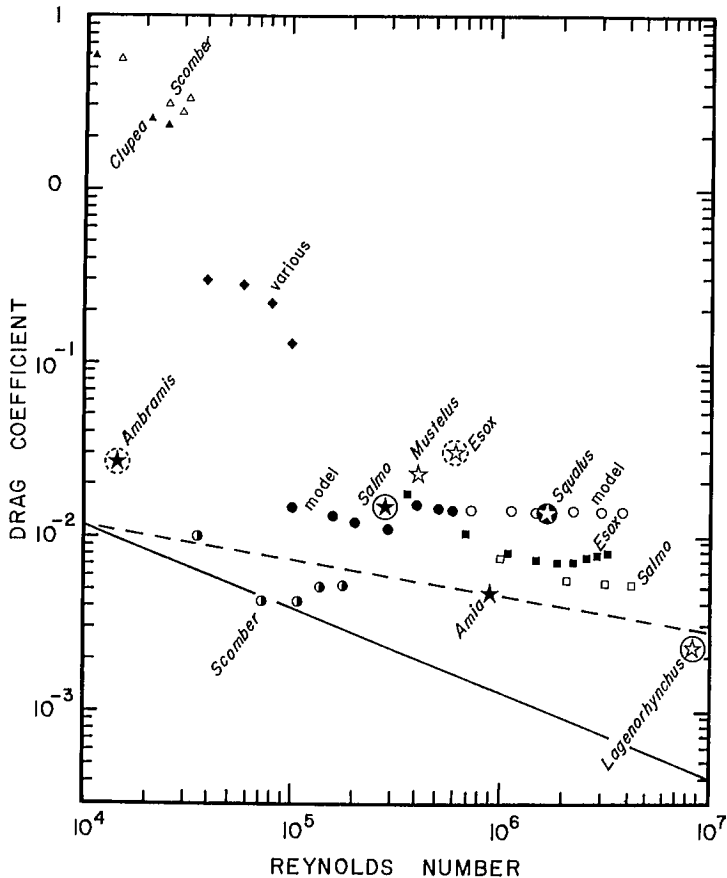
FIG. 46. Relation between calculated dead-drag coefficients from measurements for various fish and cetaceans, and Reynolds Number. Symbols are identified by generic names; references and further details are given in Table 5. Theoretical frictional drag coefficients are shown for laminar boundary-layer flow (broken line) and turbulent boundary-layer flow (solid line).

Table 5. The method used was similar to that of Kent et al. (1961) except that the supporting arm of a drag balance was embedded in quick-setting cement that filled the abdomen, and made the body more rigid. Drag coefficients calculated from Sundnes' data are close to the expected values, and show it is possible to approach equivalent rigid-body conditions with large fish.

Drag values for a 35-cm mackerel obtained by Q. Bone (personal communication) were close to the expected values, in this case laminar boundary-layer flow. The mackerel is a particularly suitable fish to use in drag measurements as the body is fairly rigid. However, the caudal fin is attached to the body by a flexible caudal peduncle, and is expected to flutter to a progres-

sively greater extent as velocity increases. This is reflected by the increasing drag coefficient at higher speeds and R_L similar to those calculated for pike by Kempf and Neu (1932).

The dead drag of most fish tends to be high because of body and fin fluttering. The advantage of models, as used by Denil (1936), is that fluttering could be eliminated. Unfortunately, Denil's measurements were made in a flume of highly turbulent water. As a result, the values obtained were high, and did not reach the lower values obtained for pike (Kempf and Neu 1932) or salmon (Sundnes 1963) at the same R_L. The latter values, in approaching theoretical values, suggest in any case that the apparent advantage of models is nonexistent.

65

Magnan and St. Laque (1929), Magnan (1930), Richardson (1936), and Gero (1952) have used free-fall measurements to measure the drag of fish and models. Magnan and St. Laque and Magnan gave insufficient data to calculate drag coefficients or R_L. Drag coefficients calculated from the data in Richardson should be comparable to theoretical values for laminar boundary-layer flow, as R_L was less than $R_{L\ crit}$. Gero's measurements were made above $R_{L\ crit}$ and should be comparable to theoretical drag coefficients for turbulent boundary-layer flow.

Richardson (1936) measured the drag of 23 cm mackerel and 21 cm herring, and equivalent rigid models of the fish. Drag of the fish and models was similar. Only data for the fish are given in Table 5. Drag coefficients were approximately 2.5 orders of magnitude higher than those expected. As the same values were obtained for the models, and Bone's values for mackerel were similar to theoretical values, it is probable there was some error in Richardson's measurements. The most likely error is that the fish did not reach the terminal velocity as Richardson believed, in which case the drag would have been high for the speeds reported.

The single value obtained by Gero (1952) for *Amia calva* 50 cm in length was the same as the theoretical value. *Amia* is a fairly rigid fish, but has an extensive median fin that would be expected to flutter markedly, with a large drag increment. Gero gave few details of his methods, but his calculations required some estimation of the terminal velocity. The value taken may have been based on experience with rigid bodies, in which case a drag close to the expected value would be obtained.

Glide measurements of drag have been made by Magnan (1930), Gray (1957a), and Lang and Daybell (1963). Those made by Magnan and Gray were made for R_L less than $R_{L\ crit}$ and should be comparable to theoretical values for laminar boundary-layer flow, whereas those made by Lang and Daybell should be comparable to theoretical values for turbulent boundary-layer flow being measured above $R_{L\ crit}$.

Dead-drag values measured for live, gliding fish might be thought more representative of expected values, as fluttering effects should be eliminated through active control of the body and fins by the fish. However, the results for bream 28.5 cm (Magnan 1930) and for trout 21 cm (Gray 1957a) are fairly high compared to values obtained by other methods. This is because fish tend to increase their drag when gliding by using their pectoral fins as brakes (Harris 1937, 1938).

Lang and Daybell (1963) reported drag values for a porpoise, measured during a glide. Although the scatter of their data was high, the mean drag coefficient was just below the value expected for an equivalent rigid body with turbulent boundary-layer flow. The drag coefficient implies that the boundary layer on the porpoise was partly laminar but mainly turbulent, as expected for a solid body under the flow conditions of experiments with R_L of 9.1×10^6.

Validity of Theoretical and Dead-Drag Measurements

The primary object of theoretical and dead-drag measurements is to estimate thrust power requirements of swimming fish, and to compare fish with man-made vehicles. This is possible for dead drag in only a few cases, because practical problems of eliminating flutter prevent the determination of sensible drag values. This implies that only theoretical drag calculations could be used for most fish and cetaceans.

The validity of applying theoretical drag calculations to swimming fish depends on the confidence in assumptions made in employing such calculations. The key assumption is that the flow around a swimming fish is mechanically similar to that around an equivalent streamline body—that streamline flow occurs. The primary source of drag is assumed to be frictional, as the boundary layer would be attached over most of the body. Separation occurs close to the trailing edge, with small pressure drag.

In view of the known kinematics of swimming, it appears unlikely that streamline flow could be maintained around the bodies of most fish, at least those swimming in anguilliform and carangiform modes. These fish swim by means of large amplitude lateral movements made across the axis of motion of the free stream. Cross flows are expected across dorsal and ventral surfaces of laterally moving segments, and the trailing edge of fins. Usually, the body is not streamlined in the direction of lateral motions, and boundary-layer separation is likely, with large energy losses to the wake. The flow pattern in the wake differs markedly from the streamline flow pattern (Chapter 1), containing substantial vorticity (Rosen 1959; Gray 1968). This distortion would certainly

be associated with a higher pressure drag than assumed. Cross flows that lead to separation have been observed using threads or dyes on several fish (Houssay 1912; Rosen 1959). P. W. Webb (unpublished data) observed crossflows at all positions posterior to the dorsal fin in trout.

In addition to higher pressure drags than assumed for a rigid equivalent body, frictional drag will also be higher. Increased frictional drag for laterally moving segments is expected because the boundary layer will be thinner than predicted by R_L. This occurs because the resultant velocity of a segment is greater than the forward velocity of the fish (Bone, in Lighthill 1971; Webb 1973a).

These drag increments are a result of propulsive movements. Frictional drag is probably also increased in many cases when the boundary layer is turbulent at lower R_L. Allan (1961) has shown that the boundary layer of small fish, probably swimming in the subcarangiform mode, becomes turbulent anterior to the shoulder because of roughness of eyes and external nares; on an equivalent rigid body, laminar flow is expected at least up to the shoulder. Allan (1961) and Walters (1962) also observed turbulence resulting from the gill effluent.

In view of the relations between boundary-layer flow and drag (Fig. 17) it might be thought that turbulent boundary-layer flow would offset the effects of cross flows that tend to cause separation. From the few observations made on flow discussed above, it appears that pressure gradients produced by lateral movements are too high for flow to be completely stabilized by a turbulent boundary layer. Allan (1961) found that boundary-layer separation occurred close to the dorsal fin, as expected on the basis of cross flows.

Unless theoretical drag calculations take into account the effect of propulsive movements on flow and drag, they are not likely to give acceptable values for swimming drag. This conclusion applies to anguilliform and subcarangiform modes and probably many fish swimming in the carangiform mode. Fish that use long, median and paired fins in the gymnotiform, amiiform, balistiform, and rajiform modes and hold their bodies rigid when swimming are included, because the fins make movements similar to bodies of fish in the anguilliform mode, and will be associated with large additional drag forces. Fish swimming in the carangiform mode with semilunate tail, in tetraodontiform, diodontiform, and labriform modes all hold their bodies fairly rigid and use a separate "fin propeller" for propulsion. In such cases, theoretical drag may be a good measure of swimming drag at least for the body.

Fish and cetaceans swimming in the carangiform mode with semilunate tail still execute large amplitude lateral movements of the body. These are restricted to the caudal peduncular region, which has a small depth and is often streamlined in the direction of motion (Slijper 1961; Walters 1962; Fierstine and Walters 1968; Magnuson 1970). Often there are finlets to control flow and prevent separation (Walters 1962; Wu 1971c). Streamline flow is probably maintained until close to the trailing edge, and it may be quite legitimate to include these animals among those that approach rigid-body conditions during swimming.

Dead-drag measurements for mackerel, a scombrid swimming in the carangiform mode (Q. Bone personal communication), and for porpoise, a cetacean swimming in the subcarangiform mode with semilunate tail (Lang and Daybell 1963), were similar to theoretical values. If theoretical drag calculations are representative of swimming drag for these animals, then accurately measured dead drag may also be representative when carefully determined.

It is concluded that theoretical and dead-drag calculations and measurements are unsuitable standards to estimate drag of swimming fish, with the possible exception of fish that swim holding their bodies fairly straight and have independent short paired or caudal fin propellers.

Streamlining of the body may appear of little advantage in the majority of fish that use body or long fin propulsion systems. Certainly other explanations may be advanced for the characteristic body shape of all fish with good swimming performance. For example, efficient swimming requires that a propulsive wave be passed back over the body, with the amplitude increasing as rapidly as possible towards the trailing edge (Lighthill 1969, 1970; Wu 1971c). This is obviously facilitated by thinning the body posteriorly, and concentrating the bulk of the muscle anteriorly. Round-bodied fish like the eel can be considered to require more wavelengths within the body before a suitable trailing-edge amplitude is reached because there is no change in flexibility along the body. Similarly the position of the shoulder usually coincides with the gill cavity (Houssay 1912), and may be related to respiratory requirements and gill size.

Because the propulsive wave serves to propel water backward, a streamline shape remains advantageous. Otherwise, discontinuities before the trailing edge would result in high drag as when

pectoral fins are used as brakes. Streamline profiles are advantageous in reducing local surface areas when transverse velocities are higher, and reduce to some extent, frictional drag. In addition, the reduced depth in these regions could lessen the magnitude of separation effects.

Mechanisms to Reduce Drag

Earlier discrepancies between the expected power required for locomotion from drag calculations and the expected power available, led to conclusions that drag of a swimming fish could be less than that of the best equivalent man-made vehicles. This stimulated much research into the possibility that swimming fish possess special mechanisms for reducing drag. On the basis of the hydrodynamic principles outlined in Chapter 1 there are several possible ways in which drag reduction may be achieved.

Drag arises from frictional and pressure forces. Frictional forces for a given body can be reduced by maintaining laminar boundary-layer conditions over as much of the body as possible, and by directly reducing viscosity. Laminar boundary layers are prone to separation, and the pressure drag associated with premature boundary-layer separation tends to be much greater than frictional drag forces. A turbulent boundary layer is less prone to separation, so that it is often profitable to induce turbulent flow. The resultant saving in pressure drag can more than compensate for higher frictional drag (Fig. 17).

A second approach to the problem of reducing energy requirements in swimming is to increase the mechanical efficiency of the propeller system. This could theoretically be achieved by reducing or cancelling vorticity in the wake, and reducing induced drag.

The various postulated drag-reducing mechanisms, most of which involve these principles, are summarized below (after Webb 1970).

METHODS OF MAINTAINING A LAMINAR BOUNDARY LAYER

Passive—(i) Distributed viscous damping of boundary-layer disturbances by the skin (Kramer 1960a, b; Marshall in Bainbridge 1961; Walters 1962; Lang and Daybell 1963). (ii) Distributed dynamic damping of boundary-layer disturbances by the skin (Walters 1962). (iii) Body shape (Walters 1962; Purves 1963; Hertel 1966; Lang 1966).

Active—(i) Properties of propulsive wave (Gray 1936; Richardson 1936; Hertel 1966; Lang 1966). (ii) Periodic oscillation of the skin (Hertel 1966). (iii) Ejection of kinetic energy into the boundary layer (Breder 1926; Walters 1962; Gray 1968).

MECHANISMS TO REDUCE VISCOSITY AND FRICTIONAL DRAG

(i) Mucus (Breder 1926; Kempf and Neu 1932; Lang 1966; Gray 1968; Muir and Kendall 1968; Rosen and Cornford 1971). (ii) Heating the boundary layer (Walters 1962; Lang and Daybell 1963).

MECHANISMS TO DELAY AND PREVENT SEPARATION

(i) Surface roughness (Walters 1962; Ovchinnikov 1966; Bone and Howarth 1966). (ii) Vortex generators (Bone 1972). (iii) Caudal peduncle finlets (Harris 1950; Walters 1962). (iv) Distributed dynamic damping (Lang 1966).

MECHANISMS TO PREVENT ENERGY LOSS AS VORTICITY

(i) Cancellation of vortex street (Kent et al. 1961; Lighthill 1970; Weihs 1973b). (ii) Vortex peg hypothesis (Rosen 1959).

BEHAVIORAL MECHANISMS

(Weihs 1973b, d; 1974)

Several of these mechanisms will be untenable on the basis of the above discussion of flow patterns and drag. Of the mechanisms listed, the most plausible are those postulated to maintain laminar boundary-layer conditions, combined with those designed to delay separation. These mechanisms are usually associated with swimming modes when the body is held fairly straight, particularly in scombroid fish and cetaceans.

Maintenance of a laminar boundary layer

PASSIVE MECHANISMS

Distributed viscous damping — At flow regimes represented by low R_L, viscous forces in the boundary layer suppress and prevent amplification of disturbances that would otherwise lead to turbulence. At flow regimes above $R_{L\ crit}$, viscous forces are insufficient to do this. Kramer (1960a) postulated that the viscosity at a body surface could be artificially increased by a suitable

surface covering. He showed experimentally that such a covering could be constructed from a rubber diaphragm supported by studs, with the spaces between filled with a viscous fluid. Tests of such a covering on a model showed it behaved like a rigid surface at low R_L. At high R_L, the rubber diaphragm tended to reduce the magnitude of a boundary-layer disturbance, and unstable pressure waves caused by a disturbance were transmitted to the viscous layer where they were suppressed.

The skin of dolphins is similar in structure to the covering designed to dampen boundary-layer disturbances and Kramer (1960a, b) suggested the skin would function in the same way. Kramer (1960a) only tested the covering up to R_L of 1.7×10^7, but suggested that disturbances could be damped at any R_L by changing the viscosity of the fluid beneath the rubber diaphragm. On this basis, Lang and Daybell (1963) suggested that distributed viscous damping could be typical of all cetaceans; larger whales swim at speeds with R_L of the order 10^9.

The only evidence for flow conditions in the boundary layer of dolphins is indirect. Lang and Daybell (1963) measured the drag of a dolphin with and without a tripping wire fitted around the head. The tripping wire was designed to cause complete turbulent flow in the boundary layer. The drag was the same with or without the tripping wire, indicating that the boundary layer on the dolphin was normally turbulent. Kramer (1960a) found that his covering was unable to reduce frictional drag for a fully developed, turbulent boundary layer so the skin of the dolphin is not likely to be involved in distributed viscous damping in the proposed manner.

The skin of two scombrid families, Thunnidae (Marshall, in Bainbridge 1961) and Istiophoridae (Walters 1962), has a structure similar to dolphin skin, and the authors suggested that the skin could function the same as the special covering developed by Kramer. These fish, as well as cetaceans, are able to control body temperatures (Barrett and Hester 1964; Carey and Teal 1969b), and likely the particular skin structure is designed to prevent excessive heat loss (Parry 1949b).

Distributed Dynamic Damping — The trachypterid fish, *Desmodema*, is an elongate fish at least 120 cm in length, that swims by means of its elongate dorsal fin, and holds the body straight and rigid (Walters 1963). At speeds as low as 0.4 L/s, R_L is 3.6×10^5, in the critical region for a flat plate. Therefore, transition from laminar to turbulent boundary-layer flow is expected.

The integument of the fish has a subdermal canal system communicating with the body surface by pores. Walters (1963) suggested that high pressure points at a boundary-layer disturbance would cause the thickening boundary layer to sink through the pores into the canal system. This would prevent amplification of the disturbance. As fluid passed into the canal system, fluid would simultaneously reenter the boundary layer at low pressure points. In this way, any disturbance would be damped by spreading its effects over a large area.

Pore canal systems have been reported in a scombrid family, Istiophoridae (Walters 1962). These fish typically swim up to speeds with R_L of the order 7×10^7. It is doubtful that a dynamic damping system could cope with turbulence of the order expected at this R_L, so this pore system probably serves some other function. Ovchinnikov (1966) suggested that Istiophorids will have a completely turbulent boundary layer.

Body shape — Efficiency of a streamlined body in reducing drag depends on two factors, the position of the shoulder and fineness ratio. In most cases, the position of the shoulder is important in defining the portion of the body covered by a laminar boundary layer, because the shoulder determines the portions of the body experiencing favorable and unfavorable pressure gradients.

In most fish, the shoulder is just behind the opercula (Houssay 1912), which means that a small proportion of the body experiences a favorable pressure gradient. Under most conditions, transition probably occurs at the shoulder, and most of the body would be covered by a turbulent boundary layer.

Bodies of scombroid fish have the shoulder situated far back along the body, at a point 0.6 to 0.7 of the length from the nose (Walters 1962; Hertel 1966; Ovchinnikov 1966). This body shape extends the influence of the favorable pressure gradient, encouraging laminar boundary-layer flow over most of the body. In scombrid fishes, the families Scombridae, Thunnidae, and Katsuwonidae have body shapes similar to man-made bodies that can maintain a high proportion of laminar boundary-layer flow to R_L of 2×10^6. This is below the R_L found at maximum sprint swimming speeds, but these fish often have additional drag-reducing mechanisms. The family Cybidae has a different body shape, similar to man-made "laminar" profiles, which can maintain a high proportion of laminar flow up to R_L of the order of 5×10^7 (Walters 1962).

69

Purves (1963) suggested that dolphins could modify their effective body shape by swimming with the long axis of the body at an angle to the axis of progression. This would reduce R_L below $R_{L\ crit}$, but the body would not then be streamlined in the direction of motion. Although a laminar boundary layer might be found on the leading surface, separation would be inevitable on the trailing surface. Evidence for the swimming behavior of the closely related porpoise does not support Purves' hypothesis (Lang and Daybell 1963).

Fineness ratio is related more to pressure than frictional drag, although it will affect the magnitude of the pressure gradients and boundary-layer flow (Chapter 1). For streamlined bodies, optimum fineness ratios are recognized depending on whether minimum surface area or volume is required. For fish, the requirement is probably for maximum volume with minimum surface area for which the optimum fineness ratio is 4.5 (von Mises 1945). Variations in fineness ratio between 3 and 7 are associated with pressure drag changes of the order of 10%. Fish and cetaceans swimming in the carangiform mode with semilunate tail tend to have fineness ratios between 3.5 and 5.0 (Hertel 1966), and fish swimming in the subcarangiform mode obtain values ranging approximately 5.5–7.0 (Hertel 1966; Webb 1971a).

ACTIVE MECHANISMS

Properties of propulsive wave — Gray (1936b) suggested that the propulsive wave could assist in stabilizing a laminar boundary layer in dolphins, and Lang (1966) extended this hypothesis to include all cetaceans. Propulsive movements propel water backward, discharging it into the wake at a velocity slightly higher than that in the free stream. From Bernoulli's theorem, it follows that pressure in the wake will be slightly lower than in the free stream, and would tend to reduce the effects of the unfavorable pressure gradient between the shoulder and trailing edge. This effect must be small, for good propulsive efficiency requires that the velocity increment given to water be as small as possible; otherwise thrust would be associated with high kinetic energy losses.

Richardson (1936) and Hertel (1966) suggested that the harmonic nature of propulsive movements could contribute to laminar boundary-layer stability. Schlichting (1968) described secondary steady flow patterns around oscillating cylinders (Fig. 18), but these require that the amplitude of the motion be small in comparison

with the width of the body. In addition, water at some distance from the surface is mainly affected by such motion. As the amplitude of the lateral movements of the body in fish is large, it is unlikely that the harmonic movements promote laminar flow conditions. In practice, they are likely to cause turbulence and separation.

Periodic oscillation of skin — This method of boundary-layer flow control has been suggested by Hertel (1966) and Lang (1966). The hypothesis is that disturbances could be detected and actively damped out by the skin. Hertel noted that no animal had been found with the requisite sensory and muscular system to implement this method. The response time at which such a mechanism would have to operate suggests it is not feasible.

Ejection of kinetic energy into boundary layer — Breder (1926), Walters (1962), and Gray (1968) suggested that the effluent from the gills could act as a source of kinetic energy and be ejected into the boundary layer to reduce or prevent transition.

Observations made by Allan (1961) showed that, for small fish at least, the gill effluent was a source of turbulence, rather than a turbulence-reducing mechanism. The same observations were reported by Walters (1962) for small fish. Walters considered that kinetic energy in the gill effluent could still be used as a drag-reducing mechanism in fish that used ram ventilation during swimming, when the opercula would function like slots on airfoils. In ram ventilation, injection of the gill effluent into the low momentum, reduced-flow areas of the boundary layer could prevent or delay both transition and separation.

Reducing viscosity and frictional drag

MUCUS

It was originally thought that mucus could reduce drag by virtue of its slippery nature (Breder 1926; Kempf and Neu 1932). Hydrodynamic theory predicts this is not possible, as there is no slip between fluid interfaces, just as there is none between a solid–liquid interface (Richardson 1936; Gero 1952).

It is well known that the addition of small quantities of long chain, high molecular weight polymers to the boundary layer can reduce drag under turbulent boundary-layer conditions (Lumley 1969). For example, Gadd (1966a, b) found that 10 ppm of such a polymer (polyethylene oxide) could reduce frictional drag by 40%.

Lang (1966), Muir and Kendall (1968), and Lighthill (1969, 1971) suggested a similar hydrodynamic function for mucus, which is a long-chain polymer.

Rosen and Cornford (1971) tested dilute solutions of mucus from several species of fish in a rheometer. R_L exceeded critical values. Variable results were obtained; some mucus solutions reduced resistance, but others had no effect. Nor were mucus solutions giving the greatest decreases in resistance necessarily from fish with the highest swimming speeds. In fact, the opposite was also found. From Rosen and Cornford's results it seems probable that mucus does have a drag-reducing function, similar to man-made, long-chain polymers. The variance in results may be related to the amounts of mucus obtained, which were not quantified.

Kowalski (1968) and Dove and Canham (1969) reported results of trials using polyox to reduce the drag of ships. Greatest drag reduction was found when the polymer was introduced into the boundary layer at small angles of incidence, in a pulsatile fashion and at a point near the shoulder. These conditions are often fulfilled by the opercular slits of fish. Gills are typically rich in mucus cells (Hughes and Grimstone 1965; Muir and Kendall 1968; Hughes and Wright 1970). In addition, production over the whole body surface could introduce mucus into the boundary layer, but its effectiveness would possibly be reduced by the rate of diffusion of the large molecules.

A third means by which mucus could reduce drag has been suggested by Breder (1926). He suggested that mucus could fill in irregularities on the surface, and reduce surface roughness or improve streamlining.

HEATING THE BOUNDARY LAYER

Cetaceans, some lamnid sharks, and scombrids maintain body temperatures fairly constant above the ambient water temperature (Barrett and Hester 1964; Carey and Teal 1969a, b; Carey and Lawson 1973). Walters (1962) and Lang (1966) suggested that these animals could heat the boundary-layer water, reducing its viscosity. In practice, such a mechanism is unlikely; cetaceans are covered by an insulation layer (Parry 1949a), and scombrids often have similar oily layers in the skin (Marshall in Bainbridge 1961).

It would also be impractical to warm up the boundary layer. Carey and Teal (1969b) reported a maximum temperature difference of 15 C between the body temperature of skipjack tuna at 30 C

and the ambient water at 15 C. Under these conditions, the maximum decrease in friction drag would be 14%, providing the boundary layer was heated to the body temperature instantaneously. Walters (1962) considered this would not be possible, as the water would only be in contact with a fish for a short period of time. For a 2 kg tuna, Walters calculated that contact would last 0.1 s. It can be shown that the amount of heat required to obtain a 14% reduction in drag for a 2 kg tuna would be about 25 kcal/s, approximately half the thermal capacity of the body.

It can safely be concluded that heating the boundary layer as a method of reducing drag is not used.

Delay and prevention of separation

SURFACE ROUGHNESS

Some fish have roughened body surfaces, apparently to induce transition, delay separation, and reduce pressure drag. Walters (1962) described a corselet of scales and thickened skin near the shoulder of the scombrid families Cybidae, Thunnidae, and Katsuwonidae, which might act the same as a tripping wire. It is more likely that this represents faring of the body to accommodate the pectoral fins.

The scombrid families Xiphiidae (swordfish) and Istiophoridae (sailfish) have poorly streamlined bodies in comparison with other scombrids. Neglecting the rostrum, the shoulder is close to the front of the body and a large proportion of the body will experience an adverse pressure gradient (Ovchinnikov 1966). The presence of the rostrum results in an extended concave surface presented to the incident flow, so that a laminar boundary layer would be difficult to maintain over the remainder of the body (Walters 1962).

Ovchinnikov (1966) calculated that the rostrum of the swordfish, *Xiphias gladius*, is long enough for transition to occur at low swimming speeds. As a result the body would be swept by a more stable turbulent boundary layer. The sailfish, *Histiophorus americanus*, has a shorter rostrum, so transition would only be expected at higher swimming speeds. However, the rostrum has fairly large protuberances, which would penetrate the boundary layer and induce transition at low speeds. Both fish are undoubtedly swept by turbulent boundary layers, tending to offset the apparently poorly streamlined body by reducing the tendency for separation.

Bone and Howarth (1966) suggested that the boundary layer on dogfish would tend to separate

71

during swimming. They considered that the denticles would induce turbulence in the boundary layer, and offset the tendency for separation.

VORTEX GENERATORS

Ruvettus pretiosus, the castor oil-fish, has a special integument which probably functions to generate vortices that not only induce, but maintain, a turbulent boundary layer (Bone 1972). The integument contains an extensive system of subdermal canals communicating with the surface by caudally-directed pores. The integrity of the subdermal canal system is maintained by specialized ctenoid scales, which have projections well beyond the body surface. Bone guessed that the fish would swim at speeds to about 5 L/s, when R_L would be of the order of 1.7×10^7. At this R_L turbulent boundary-layer flow is expected and it is doubtful if the canal system would operate like the distributed viscous damping system of *Desmodema* (Walters 1963).

Bone suggested that vortices generated at the tips of the scales would ensure a turbulent boundary layer, and, because the vortices would be directed backward and toward the surface, they would continually replenish the boundary layer with energy derived from the outer flow assisting the maintenance of an attached boundary layer.

Bone also noted that oscillation of the body of a dead fish, similar to that expected during swimming, caused fluid to be ejected through the pores of the canal system. This might serve as an additional source of kinetic energy for the boundary layer, or to improve turbidity.

CAUDAL PEDUNCLE FINLETS

Finlets are present on the caudal peduncle of all scombrids (Walters 1962) and a fossil shark, *Diademodus hydei* (Harris 1950). The finlets are too small to serve a direct propulsive function. Harris and Walters compared the finlets with multiple wing-tip slots often used on high-lift aerofoils. The finlets probably redirect the flow of water over the caudal peduncle, deflecting it along the body rather than permitting normal flow which could lead to separation (Wu 1971b, c).

DISTRIBUTED DYNAMIC DAMPING

Lang (1966) suggested that the special skin structure of dolphins may not be associated with maintainance of laminar boundary-layer flow. Instead, the skin may be designed to stabilize turbulent boundary-layer flow and prevent separation of this turbulent boundary layer.

There is no evidence for or against such a mechanism. A swimming dolphin is expected to have a turbulent boundary layer, separating at some point beyond the shoulder, but before the trailing edge. This is especially so for dolphins (compared to other vertebrates swimming in the carangiform mode with semilunate tail) because of their high amplitude movements (Slijper 1958, 1961; Lang and Daybell 1963). Observations made by Steven (1950) showed that separation does not occur. Steven observed that the only disturbance caused by dolphins swimming in phosphorescent seas was two diverging lines. These were probably caused by tip vortices around the tail flukes. A separated boundary layer would have been indicated by a broad path of disturbances, as Steven observed for seals.

Prevention of energy loss as vorticity

CANCELLATION OF VORTEX STREET

Kent et al. (1961) suggested that a Karman vortex street would be produced behind the head of a swimming fish. They considered that a second series of vortices would be produced at positions of maximum amplitude of the tail, and the two series could cancel out to prevent energy losses to the wake.

This would only be feasible if the frequency of vortices in each series was the same. The frequency of vortices in a Karman street, f_v, can be calculated from Equation 26, taking the Strouhal Number as 0.2. The frequency of tail vortices will be equal to twice the tail-beat frequency, which can be calculated from equations in Table 2. Consider a 30 cm trout, in which the width of the head would be about 0.1 L. The ratio between the two frequencies will be closest at highest swimming speeds, about 300 cm/s (10 L/s). $2f$ would be 29.3 with f_v 20.0, so under optimum conditions, the maximum drag saving could be of the order of two-thirds.

However, it is unlikely that a vortex street of the type considered by Kent et al. (1961) would be generated behind the head of a fish even when swimming, and the pattern of the vortex street generated by the tail may not be of the nature required. Experiments by Hertel (1966) indicated that a caudal fin will generate stable vortex streets only at some speeds, and often the street will be a single row. Although this has not been confirmed for fish throughout their normal swimming range, it seems unlikely that drag of individual fish would be reduced in the manner proposed by Kent et al. (1961).

Alternatively, drag reductions may be possible by interactions of the wakes of fish swimming in schools (Breder 1926; Belyayev and Zuyev 1969; Zuyev and Belyayev 1970; Weihs 1973b). Typically, schooling fish are of similar size and swim in horizontal diamond patterns (Keenleyside 1955; Nursall 1973). Weihs (1973b) stated, "In this formation, when the lateral distance between adjacent fish is twice the width of the vortex trail, wakes between successive lateral rows are cancelled. The third row will encounter a uniform flow and the total energy saving to the school is half the relative gain to the second row." This drag reduction through school interaction is predicted by idealized hydromechanical modelling, so the actual energy loss would probably be lower (Weihs 1973b).

Weihs also considered the effect of vertical and horizontal interaction among schooling fish on thrust generation. Thrust theoretically could be increased by at least 10% in the horizontal plane and to 30% for an optimum vertical distribution, but without any attendant changes in kinematics.

A different approach to the problem of vortex cancellation for individual fish is included in the hydromechanical models developed by Lighthill (1970) and Wu (1971b, c). A vortex sheet[1] produced downstream by the trailing edge of an anterior median fin or inclined body edge could be resorbed on the leading edge of the next posterior median or caudal fin. The importance of this depends on the distance between the fins.

When the distance between fins is small, as in most fish swimming in the anguilliform and subcarangiform modes, a vortex sheet would fill the gap. The vortex sheet would behave mechanically the same as a fin, and the propulsive mechanics would be equivalent to that for a continuous fin. However, a slight decrease in drag would result because of the reduction in fin area by the gaps.

When gaps between the fins are large, the relative motions of the interacting edges will also be increased because of the nature of the propulsive wave. The vortex sheet could still be resorbed at the leading edge of the posterior fin with no addition to energy loss in the wake. If the phase difference between the motion of interacting edges was large enough, the thrust work done would not be entirely cancelled by resorbtion of the vortex sheet on a downstream posterior fin. This would result in an increase

in total rate of working without an increase in wasted energy, technically an increase in propeller efficiency (Chapter 5).

VORTEX PEG HYPOTHESIS

Rosen (1959) observed the flow pattern found some distance from a fish swimming at sprint speeds. Cross flows around the dorsal and ventral surfaces of the body produced vortices on alternate sides of the body. The vortices were not part of a Karman street, but were associated with thrust rather than drag (Lighthill 1969). Rosen postulated that fish actively induced and energized the vortices so they behaved like quasi-static pegs. These vortices were then used the same as rigid pegs (Gray 1957b); they were also considered to act as rollers between which the fish was pushed, the scales rising from the surface of the body to act as vanes improving the efficiency of the action. The fish left behind a line of free vortices from which all energy had been absorbed; that is, the total energy in a vortex was the same as that in an equivalent mass of the free stream.

Rosen (1959) concluded that the drag on a swimming fish was virtually zero. However, his experiments detected the flow at some distance from the fish, and because high propulsive efficiency requires that velocity increments given to the water be low, the true original movements of the water were undoubtedly obscured (Aleyev and Ovcharov 1969, 1971). In addition, Rosen's conclusion does not take into account the degradation of energy that must occur with each transformation, nor does it fit the observed physiology of swimming fish. Furthermore, it is most unlikely that scales behave like vanes, in which case there would be relative flow between the surface of the fish and the vortices. The velocity of flow adjacent to the fish in the vortex would tend to be higher than that of the free stream, so this motion would be expected to result in a higher drag than otherwise anticipated. In view of these objections, the vortex peg hypothesis is unlikely.

Behavioral mechanisms

Weihs (1973b, d; 1974) described several behavioral mechanisms that can reduce drag or net thrust required to swim at a given mean speed. Energy savings through the cancellation of vortex sheets in some schooling fish is described above. Weihs (1974) has also shown that routine activity interspersing glides with short bursts of activity (burst/glide behavior) can

---

[1]The difference between vortex streets and vortex sheets is discussed in Chapter 1.

decrease the energy required to traverse a given distance in a given time by over 50% compared to swimming at constant speed. Alternatively, under optimum burst/glide conditions range may be increased by a maximum of three times. Negatively buoyant fish could achieve similar energy economies by gradually gliding to a lower depth and then rapidly swimming upwards to the original depth (Weihs 1973d).

Discussion

Only a few of the proposed drag-reducing mechanisms appear plausible, mainly those with analogies in aircraft industrial practices (von Mises 1945; Schlichting 1968). Each mechanism has been considered on its own merits, and none have been rejected because there is no man-made equivalent (e.g., distributed viscous damping for turbulent boundary-layer control). The list of drag-reducing mechanisms reflects current industrial thinking; in all probability there are other novel mechanisms yet to be recognized.

Most of the plausible drag-reducing mechanisms have limited general application to aquatic vertebrates, often being associated with some taxonomic group and its swimming mode. Distributed viscous damping for turbulent boundary-layer control would have a cetacean monopoly with the possible exception of oil-filled canal systems in marlin (Marshall in Bainbridge 1961). Distributed dynamic damping has only been reported in *Desmodema* but is possibly typical of trachipterid fish (Walters 1963). Vortex generators in *Ruvettus* may have wider application (Bone 1972).

Plausible drag-reducing mechanisms for boundary-layer control are commonly found in fish swimming with the body fairly straight. These mechanisms tend to be associated with certain swimming modes. Fish possessing these drag-reducing mechanisms are also those to which theoretical and dead-drag calculations are most likely to give reasonable measures of swimming drag. Drag-reducing mechanisms that follow industrial practices are most easily recognized in these fish.

By contrast, surface roughness (including vortex generators), vortex cancellation in schools, and vortex sheets filling fin gaps are largely related to other swimming modes when the body and/or median fins execute large amplitude movements for much of their length. Problems relating to premature separation are then of paramount importance. Vortex sheets filling fin gaps apply to anguilliform-type propulsion

(including subcarangiform motion). The only exceptions appear to be sailfish and swordfish, when turbulence in the boundary layer is induced in response to special body shapes, rather than swimming mode.

Mucus is potentially the most universal drag-reducing mechanism, with the exception of cetaceans. However, mucus reduces frictional drag in a turbulent boundary layer, and may apply more to anguilliform-type propulsion than other modes. This is because the more advanced carangiform modes and other modes when the body is held more or less straight, are probably associated with a larger proportion of laminar flow over the body.

The probable effectiveness of most drag-reducing mechanisms can readily be appreciated. The advantages of different flow regimes can be shown by calculation (Fig. 17). The potential of mucus (60% reduction in frictional drag) is shown by empirical observations (Rosen and Cornford 1971). Distributed viscous damping for turbulent boundary-layer control is an unknown factor, but its advantages would be immense if separation were avoided. These mechanisms make large reductions in some drag component, which is also a substantial reduction in total drag.

A possible exception is the distributed dynamic damping system of *Desmodema* (Walters 1963). Because this fish swims in the amiiform mode, high drag costs are expected from the anguilliform-type motion of the dorsal fin. In this case, the frictional drag of the fairly straight body would probably represent a small portion of the total drag. Thus, the reduction in drag through the maintenance of laminar boundary-layer flow over the body would be small in relation to total drag, with consequent small energetic saving.

The various drag-reducing mechanisms are not likely to apply at all swimming speeds. The special body shapes of scombroid fish and cetaceans only maintain a high proportion of laminar flow at regimes with R_L between 2 and 5×10^7, whereas maximum speeds occur with R_L of the order 7×10^7. Similarly, *Desmodema*'s distributed dynamic damping system would be ineffective with intensity of turbulence at high speeds. In contrast, surface roughness could be effective at all speeds, but at higher speeds early transition would be expected in any case. Mucus could be more effective at higher speeds in large fish when transition occurred at progressively more anterior positions, but in most fish transition is likely through other causes at lower speeds, in which

case mucus would apply equally here. Vortex sheets filling fin gaps are part of the thrust mechanism, and would operate at all speeds. In general, it appears that drag-reducing mechanisms apply mainly to cruising speeds and lower sprint speeds. Most fish activity will be in this area, simply because the metabolic machinery cannot cope with continual high speeds. Thus, drag savings apply to those activity levels when energetic expenditure will be highest in the long term.

A further reason for the operation of drag-reducing mechanisms at lower speeds would be applicable if high-speed sprints were associated more with the work required to overcome the inertia of the body and added mass rather than drag caused by boundary-layer effects. In this case, it is possible that a series of further drag-reducing mechanisms could be identified in relation to reducing the total mass that must be accelerated. Perhaps the more cylindrical bodies of fish like pike, which attack prey by sudden darts, is associated with lower added mass than the more elliptical bodies of fish like carp, browsing on the bottom. This is in the realm of speculation with no evidence for support.

Chapter 5 — Thrust and Power

Introduction

The preceding discussion on the use of drag measurements to calculate swimming power reveals several disadvantages, both in theory and practical measurement techniques. Consequently, it is advantageous to measure thrust, because, being equal to total drag, it will include any gross flow effects, interactions, and drag-reducing mechanisms (without identifying them) that drag calculations or measurements do not include.

A few attempts have been made to measure thrust power directly (Houssay 1912; Gero 1952; Lang and Daybell 1963; Gray 1968). Most were concerned with peak power levels for sprints or fish jumping from the water and often only a portion of the total power was measured. It is difficult to relate such measurements to any particular swimming speed, and it is not possible to construct any relation between thrust power and speed.

The most satisfactory means of direct calculation of thrust and power output would be from a complete description of the flow around a swimming fish at different speeds. This would require an exorbitant amount of work. At the present time, flow has only been described qualitatively for the boundary layer (Allen 1961) and outer flow some distance from the fish (Houssay 1912; Gray 1936b; Rosen 1959; Aleyev and Ovcharov 1969, 1971) at a few swimming speeds.

Indirect approaches to calculate thrust and power are, therefore, likely to be of greater value in fish propulsion energetics studies at the present time. Of indirect approaches, the development of suitable hydrodynamic models is of greatest importance. Other approaches using mechanical models (Breder 1926; Gray 1936b; Kramer 1960; Kelly 1961; Smith and Stone 1961; Hertel 1966; Pyatetskiy 1970b; Siekmann 1963) or relations between added drag loads and kinematics (Webb 1971a) are by comparison of limited application and mainly important in testing, or giving additional input to models of wider application.

Hydrodynamic models have always been important in the study of fish locomotion. They were initially used qualitatively to show that the observed movements executed by swimming fish would generate large thrust forces, and to evaluate the kinematic requisites for the generation of thrust (Gray 1933a, b, c, 1953b, 1968; Harris 1937; Breder and Edgerton 1942; and others) or to elucidate the distribution of thrust (Bainbridge 1963).

Further expansion of these qualitative models into a quantitative form has generally proved difficult, not only because of the detailed measurements required in their application (Taylor 1952; Gray 1953b) but because they are based on too great an oversimplification of the propulsive system, particularly in neglecting interaction between segments.

Many of these problems also apply to models originally developed in quantitative form (Webb 1971a). Recent models have been proposed that can either be reduced to simple terms related to easily measurable key kinematic parameters, or predict some form of thrust coefficient similarly based on measurable kinematic parameters (Lighthill 1960, 1969, 1970, 1971; Wu 1961, 1971a, b, c; Weihs 1972, 1973a). These models hold the greatest potential for application to a wide range of fish energetics problems.

Direct Measurements of Power Output

The most comprehensive series of power output measurements were made by Houssay (1912), for fish of various sizes from 18 species. Each fish was attached to a balance so that as it swam it was forced to lift weights of various sizes. The power developed by the fish was calculated from the product of the mass lifted and the distance it was raised. Only part of the work done by the fish was measured. Work to overcome: (1) drag of the fish, (2) drag of the balance, (3) inertia of the balance, and weights a distance from the fulcrum, (4) friction in the balance was unaccounted for. In addition, fish were forced to swim in a tight arc, which undoubtedly reduced their performance (Bainbridge 1963).

Gero (1952) calculated the power required during acceleration of a perch from a standing start, and for a porpoise jumping from water. It

is not known if these animals were then developing maximum power. The power developed by a porpoise during acceleration was also measured by Lang and Daybell (1963).

Gero (1952) also measured the thrust and power output of several fish attached to a fishing line. The strain was measured on the line as the fish swam away from a boat. Gero pointed out that only power in excess of the drag power for the fish and line was measured. He also noted that measurements were subject to error if the fish swam at an angle to the line and boat, and that the line must have interfered with the fish.

Despite their recognized inaccuracies, the above measurements of thrust and power are the only ones available. They are given in Table 6. The measured power output is compared to estimated values based on information for vertebrate muscle systems and expected caudal propeller efficiency. Thus, a muscle power output of 8×10^5 erg/s per g was taken for cold water fish, and 40×10^5 erg/s per g for mammals (Bainbridge 1961). The latter figure applies to cetaceans, and possibly Gero's (1952) sharks, grouper, and barracuda if they can control their body temperatures. It was assumed that half the body mass was propulsive muscle, half of which works at any instant, and that caudal propeller efficiency was 0.75.

Estimated power outputs are up to an order of magnitude greater than measured values, with a greater difference for smaller than larger animals (Fig. 47). The difference may largely be attributed to unmeasured power output in the experiments. For example, in Houssay's experiments, some portion of the unmeasured work depended on the design of the balance, and consequently this portion would have represented a relatively greater proportion of the potential maximum power output of smaller fish than larger fish. In general, there is agreement between measure and calculated propulsive power output values.

Hydromechanical Models and Indirect Measurements

The basis for descriptions of kinematics in fish propulsion is the identification of arbitrary segments, regarded by Gray (1968) as "the fundamental unit of aquatic undulatory propulsion." This concept applies also to models relating the kinematics to thrust production, the application of various models differing to a large extent in the emphasis given to different segments. Models that assume segments may be compared to

hydrofoils tend to consider all segments (Taylor 1952). Others who consider reaction forces associated with virtual mass effects also consider all segments, but can relate bulk energy changes to a single segment at the trailing edge, with consequent emphasis there (Lighthill 1969, 1970, 1971, 1972; Wu 1971a, b, c).

Apart from this basic similarity, hydromechanical models can be divided into two main groups, depending on certain assumptions made in their formulation. These are summarized in Table 7 for various quantitative models. The two assumptions consider either resistance forces or reaction forces to be dominant. In the former, instantaneous forces acting on a segment are regarded as resistive forces depending only on the segment's resultant velocity at some angle of attack to the incident flow. This approach is sometimes called quasi-static, as it also assumes that the forces acting on a segment at any instant are the same as those acting under equivalent steady-state conditions of velocity and angle of attack. The net effect of the motion of any segment during a cycle is the sum of the steady-state forces for all instances in that cycle (Gray 1953b).

The reactive force approach considers the inertial forces acting on a segment. These forces
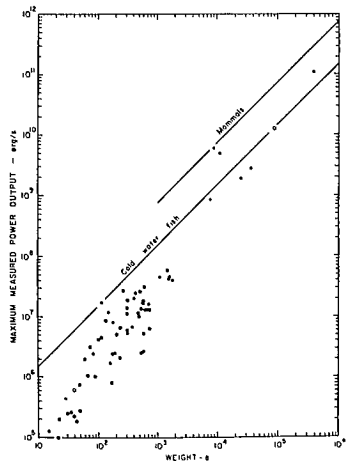
Fig. 47. Maximum measured power output of fish and cetaceans as a function of weight. Solid circles show values calculated for 17 species of fish from data in Houssay (1912), solid squares for three species of fish from data in Gero (1952), open squares and open circles for cetaceans from data in Gero (1952) and Lang and Daybell (1963) respectively. Solid lines represent estimates of muscle power output expected for fish and mammals. Further explanation is given in text and Table 6.

TABLE 6. Values for highest power outputs of fish and cetaceans, from direct measurements. For reasons discussed in text these are probably not maximum power outputs of the various species.

Species	Weight (g)	Power output (erg/s)	Reference	Species	Weight (g)	Power output (erg/s)	Reference
Merlangus				*Alburnus*	40	6.04×10^5	Houssay
pollachius	530	2.63×10^7	Houssay	*lucidus*	32	2.50×10^5	(1912)
(? whiting)	405	2.02×10^7	(1912)		15	1.24×10^5	
	150	1.20×10^7					
	135	8.53×10^6		*Barbus*	548	1.33×10^7	
	75	3.18×10^6		*fluviatilis*	240	6.61×10^6	
Labrus	322	1.87×10^7		*Scardinius*	205	5.03×10^6	
bergylta	180	8.20×10^6		*erythroph-*	180	2.40×10^6	
	100	4.27×10^6		*thalmus*			
Pagellus	312	1.12×10^7		*Cyprinus*	1,628	4.34×10^7	
centrodentus				*carpio*	498	9.94×10^6	
					320	5.37×10^6	
					235	2.10×10^6	
Cottus	68	1.04×10^6			171	7.92×10^5	
bulbalis	28	4.44×10^5					
				Tinca	732	1.61×10^7	
Platessa	710	1.29×10^7		*vulgaris*	376	6.80×10^6	
vulgaris	80	2.41×10^6			23	2.00×10^5	
	50	7.32×10^5					
				Gobio	35	2.56×10^5	
Crenilabrus	40	2.25×10^5		*fluviatilis*	21	1.00×10^5	
melops							
				Leuciscus	159	1.71×10^6	
Raja punctata	1,863	4.02×10^7		*rutilus*	90	1.02×10^6	
and *R.*	1,570	4.13×10^7			44	2.86×10^5	
clavata	1,132	4.49×10^7					
	730	1.30×10^7		*Perca*	109	3.44×10^7	Gero
	490	1.15×10^7		*flavescens*			(1952)
	272	2.70×10^7					
	195	2.49×10^6		*Charcharhinus*	26,332	1.93×10^9	
	50	2.67×10^5		*leucas*	9,534	9.30×10^8	
Scyliorhinus	760	6.38×10^6		*Negaprion*	36,774	2.83×10^9	
canicula	590	5.29×10^6		*brevirostius*			
	590	2.58×10^6					
	540	2.47×10^6		*Promicrops*	7,718	8.60×10^8	
				itaiara			
Esox lucius	1,525	5.62×10^7					
	620	3.03×10^7		*Sphyraena*	11,350	3.92×10^9	
	440	2.42×10^7		*barracuda*	9,080	6.04×10^9	
	59	2.02×10^6					
				Tursiops	431,300	1.13×10^{11}	
Salmo irideus	633	1.30×10^7		*truncatus*			
	590	1.86×10^7					
	585	1.71×10^7		*Lagenorhyn-*	90,800	1.27×10^{10}	Lang and
	317	1.40×10^7		*chus*			Daybell
	125	4.27×10^6		*obliquidens*			(1963)

TABLE 7. Models of propulsion for fish and cetaceans. Key to swimming modes: A = anguilliform; C = carangiform; CST = carangiform with semilunate tail; O = ostraciform; R = rajiform.

Swimming mode	Amplitude of lateral movements	Flow restrictions		Notes	Reference
		Dimensions	Separation		

Hydromechanical

Resistive (quasi-static)

	lifting wing theory				
O,CST	small	2	yes	–	von Holste and Kuchemann (1942)
CST	large	2	yes	–	Parry (1949a)
CST	large	2	yes	–	Gero (1952)
	lifting cylinder theory				
A	large	3	yes	amplitude constant along body length.	Taylor (1952)
A	large	2	no	„	Gray (1953b)

Reactive (inviscid)

	slender body theory				
A	small	2	no	amplitude increases along body length.	Gadd (1952, 1963)
A,C	small	2	no	amplitude increases along body length; separation discussed.	Lighthill (1960, 1969, 1970)
C	large	2	no (discussed)	amplitude increases along body length.	Lighthill (1971)
C	large	2	no (discussed)	acceleration.	Weihs (1972, 1973a)
	lifting wing theory				
A	small	2	no	amplitude increases along body length.	Smith and Stone (1961)
A,R	small	2	no	„	Siekman (1962, 1963)
C	small	2	no	„	Bonthron and Fejer (1963)
A	small	2	no	„	Pao and Siekman (1964)
A,C	small	2	no	as above; body thickness effect considered.	Uldrick and Siekman (1964)
R	small	2	no	amplitude increases along body length; high RL.	Wu (1961, 1971a,b) Kelly (1961)
CST	large	2	no	–	Lighthill (1969, 1970)
C, CST	small	2	no	–	Wu (1971b,c)
C	small	2	no	amplitude increases along body length; body thickness effects considered.	Wu and Newman (1972) Newman and Wu (1973) Newman (1973)

Mechanical

A	large	–	–	amplitude constant.	Gray (1936b)
Various	–	–	–	–	Kramer (1960)
O	large	–	–	–	Breder (1926) Hertel (1966)
A,R	large	–	–	amplitude constant.	Kelly (1961) Siekman (1963)
A	large	–	–	amplitude increases along length.	Smith and Stone (1961)

80

are proportional to the rate of change of resultant velocity, and the virtual mass associated with a segment's motion (see particularly Lighthill 1970).

Each main group can be subdivided depending on the type of hydromechanical theory, whether for slender bodies or lifting wings.

In his survey of aquatic animal propulsion, Lighthill (1969, 1970) showed that the two hydromechanical approaches have different areas of application. For small animals with $R_L < 1$, resistive theory is applicable, and this probably applies to $R_L = 10^3$ when there is no particular lateral flattening of the animals, as in many invertebrates. For vertebrate propulsion, lateral flattening is normal. This substantial increase in depth is associated with large virtual mass effects during swimming, so that resistance forces tend to be small in comparison with reaction forces (Lighthill 1970). This also applies in any case when $R_L > 10^3$.

There will, of course, be intermediate forms expected to use a combination of resistive and reactive forces. Lighthill (1970) considered this to be the case for eellike fish, where lateral compression has not progressed to the same extent as fish swimming in other body modes.

A further difference between resistive and reaction approaches is the "fluid" to which the models apply. The use of quasi-static resistive theory permits analysis of locomotion in a real fluid. In fact, segments may be compared to hydrofoils so that the various forces acting at any instant may be computed from empirical observations of mechanically similar systems. Motion in a real fluid includes boundary-layer growth and separation effects but neglects interaction between segments. In contrast, reaction forces have been analyzed for inviscid fluids that do not initially take into account forces of viscous origin. Lighthill (1960, 1970) set out a preliminary consideration of the effects of such forces, which are likely to be most relevant in anguilliform propulsion.

A common difficulty with most models is expressing kinematics in suitable mathematical terms. The usual assumption is that segments move with simple harmonic motion, and as seen in Chapter 2, this is not strictly so. Differences between simple harmonic motion and observed motion are small (Gray 1933a). In addition, the practical difficulties encountered in measuring any kinematic parameter mitigate against too rigorous an application of this objection.

Kinematic variation occurs at all levels with different species, individuals, and time (Nursall

1958b) and has effects on thrust that are difficult to determine. The most sensible method of overcoming this problem is to use a quasi-static approach to consider detailed movements of segments. When used in most resistive models this tends to ignore segmental interactions (Gray 1933a, 1953b), but can be used successfully with reaction models considering a trailing-edge segment (Lighthill 1971). Another practical difficulty is encountered, for involvment in a comprehensive analysis of this nature requires an immense amount of work (Taylor 1952; Gray 1953b). Taylor considered that the inherent variation in propulsive movements would probably prevent the measurement of "sufficiently realistic values" for kinematic parameters.

The problem faced by the biologist who wants to use hydromechanical models to calculate thrust and power in swimming fish is "which one to use." This will depend on several factors, such as swimming mode, his primary area of interest (mechanics or energetics, etc.). In general, a reaction model is likely to be most important, and then one that considers energy changes in terms of key kinematic parameters, measurable with some accuracy and repeatability. In this respect, key parameters may be identified as the wavelength of the propulsive wave, λ_B, tail-beat frequency, f, and amplitude, A (Webb 1971a, 1973a). Key kinematic parameters dictate fixed relations between body movements and resultant velocity, angle of attack, etc., during propulsive cycles. They will also reflect the mean propulsive effort of a fish, with results similar to a more detailed analysis of the quasi-static type (Lighthill 1970, 1971; Wu 1971a, b, c).

Qualitative quasi-static models

With the exception of body swimming modes, most swimming movements have only been considered in qualitative form at the present time. This approach to the motion and forces for various segments was used in all earlier work on fish locomotion, beginning with Borrelli (1680), Pettigrew (1873), Marey (1874, 1895), Breder (1926), and particularly Gray (1933–1968). Bainbridge (1963) extended quasi-static approaches for hydrofoils to estimate the importance of various segments along the body in generating thrust for *Ambramis*, *Carassius*, and *Leuciscus* (subcarangiform mode). Bainbridge assumed thrust proportional to the square of the local transverse velocity (W^2) and local area. Angle of attack was assumed positive at all times, and variations along the length of the body were

neglected. Bainbridge's estimates suggested that the caudal fin would generate 45, 65, and 84% of total thrust in *Ambramis*, *Carassius*, and *Leuciscus*, respectively. This follows a trend toward concentration of significant lateral movements to the posterior of the fish, so that *Ambramis* kinematics tended more to anguilliform propulsion, and *Leuciscus* more to carangiform propulsion.

Paired and median fin propulsion and ostraciform propulsion have only been discussed qualitatively, with the exception of the rajiform mode (Wu 1961, 1971a; Kelly 1961; Siekmann 1962, 1963). Movements of the caudal fin in ostraciform propulsion, and pectoral fins in labriform propulsion have been envisaged generating thrust the same as a fan (Harris 1937; Gray 1968). Positive thrust appears to be generated throughout a cycle from a combination of resistive and reactive forces (Gray 1968).

For other fin modes, when the base of the fin is relatively large and specific wavelengths small, longitudinal forces in the direction of the fin base are generated the same as anguilliform propulsion. Because the fins are attached at their bases to the body, forces are also generated normally to the fin base (Harris 1937; Breder and Edgerton 1942). Similar forces are generated to those of the fins used in ostraciform and labriform modes. In the case of pectoral fin movements, such forces will be associated with yawing couples, cancelling out for symmetrical movements of both fins. Asymmetrical movements between pairs of fins contribute significantly to maneuverability.

Forces generated normally to the long axis of median fins contribute to thrust when the fins are set backward at an angle to the body axis as in *Monocanthus* (Harris 1937). The kinematics of these fins will be associated with pitching couples, again cancelling out for symmetrical movements when the fins occur in pairs, as in balistiform propulsion. The situation in gymnotiform and amiiform propulsion is uncertain, as the median fins are not found in functional pairs. Forces generated normal to the fin's long axis would be expected to cause the animals to rise or fall in the water as they move forward. The effect of such forces could be counteracted by appropriate buoyance mechanisms, or a large number of wavelengths along the fin.

The long pectoral fins of skates probably function the same as long median fins in similar modes. Yawing forces generated by these fins would be cancelled out during normal forward propulsion because the structures are paired.

Quantitative models

Quantitative models are presently restricted to anguilliform and carangiform propulsion. Wu's (1961, 1971a) model is an exception, applicable to rajiform propulsion, but there are no data. The kinematic data available for input to body swimming mode models are also limited to steady[2] swimming at speeds maintained for at least a second. Higher speeds undoubtedly involve predominantly acceleration phenomena and this may be treated by a modification of a basic model (Weihs 1972, 1973a).

In the following discussion of quantitative models, steady swimming for each of the main body swimming modes will be considered. Subsequently the available information on acceleration and steady-state models will be combined in an attempt to predict acceleration energy expenditure.

A resistance and a reaction model is considered for each mode, with numerical solutions calculated for each. However, only one example of each is considered, selected from those summarized in Table 7. Selection was based on a model's value in biological situations. For most body swimming modes, the resistance model proposed by Taylor (1952) is discussed. This model has the advantage over others because it considers three-dimensional flow, and is consequently most realistic. It is also in a form that can be easily applied to real fish-type motions. Of reactive models, that proposed by Lighthill (1969, 1970, 1971) is considered most appropriate. In detailed form, it is descriptive of real fish motions, and can be simplified to a form relating to key kinematic parameters without substantial loss in accuracy. It discusses forces of viscous origin, and furnishes hydromechanical explanations for much of the morphological variability observed among fish. The conclusions given by Lighthill's models have almost simultaneously been obtained by Wu (1971b, c). However, these latter models require the use of thrust-related coefficients making them of less immediate biological use.

A special lifting-wing model is required to describe carangiform propulsion with semilunate tail. All relevant models proposed to date require the use of thrust-related coefficients. The models proposed by Parry (1949a) and Lighthill (1969, 1970) are discussed. Additional relevant calculations were set out by Wu (1971b, d).

---

[2]Time independent.

Steady Swimming

Anguilliform propulsion

RESISTIVE (QUASI-STATIC) MODEL

Taylor (1952) considered resistance forces acting on a long narrow smooth cylindrical body, each segment of which executed simple harmonic motion of constant large amplitude. Flow was assumed to be laminar. The motion of a segment was considered quasi-statically. Its instantaneous motion was compared with steady flow around inclined cylinders under equivalent conditions for each segment. Empirical data for lift (thrust) and drag forces on such cylinders, at different flow velocities and angles of attack, were combined with the equations of motion of a segment in order to calculate "thrust coefficients" per unit length of the hypothetical fish.

Then, the power output per unit length, E_s, was

$$E_s = 2.7 \, \rho \, U^3 \, G_{(n,a)} \, R_d^{-\frac{1}{2}} \qquad (56)$$

when

d = diameter of cylindrical body,
R_d = Reynolds Number based on d,
$G_{(n,a)}$ = thrust coefficient.

$G_{(n,a)}$ was based on metameters n and a for propulsion kinematics, when

$$n = U/V \qquad (57)$$

$$a = A/2 \, \lambda_B \qquad (58)$$

These then dictate the magnitude of a segment's resultant velocity, W_R, and angle of attack, α, and assume correlation between the two. Values for $G_{(n,a)}$ are shown as isopleths in relation n and a in Fig. 48, after Taylor (1952 figure 8).

The total power output of the propulsive wave, E, is given by

$$E = E_s \, l \qquad (59)$$

when

l = body length generating thrust.

The model differs from real fish propulsion in several ways: (1) the body is not usually cylindrical, (2) amplitude increases along the body, (3) interactions between segments are neglected.

Body shape — Taylor's model correctly applies to round-bodied animals, such as snakes, etc., rather than fish which are usually laterally flattened to some extent. Fish cross sections are further laterally flattened by the presence of median fins. In this case, it is expected that the model would give low values for thrust power, because separation would inevitably occur at the dorsal and ventral edges of the body with higher pressure forces, whereas on a cylinder separation could occur later (von Mises 1945). In turbulent flow, this difference would be amplified, as flow would be relatively more stable for the cylinder.

Amplitude — Amplitude of the propulsive wave of fish typically increases with position, x, along the body, so that mean values for $W_R(x)$ and $\alpha(x)$ will vary with A(x). Figures by Gray (1933a) showed that A tends to be fairly high, close to maximum values over much of the length, and it was shown in Chapter 2 that $W_R(x)$ tends to be inversely correlated with $\alpha(x)$. These two factors may offset to some extent the assumption that amplitude is constant in Taylor's model.

The model also assumes W_R and α directly correlated. This appears to be the case for segments bounded by segments on both sides, which includes the whole body except for segments at leading and trailing edges. Of these, the trailing edge is most important, having a high amplitude and generating thrust, whereas the leading-edge segment has low amplitude, and, according to Alexander (1967), this motion is probably associated with drag as negative thrust. A segment at the trailing edge usually follows the motion of immediately anterior segments so that W_R and α are correlated, but exceptions have been reported (Nursall 1958b).

Interaction between segments — Gray (1933a, 1953b) pointed out with reference to his own qualitative approach to thrust production, that interaction between segments is neglected, whereby the motion of an anterior segment will modify the incident flow to a posterior segment. This also applies to Taylor's model. The flow downstream of moving segments is likely to be turbulent, based mainly on limited observation of the subcarangiform mode. Turbulence is also expected in comparing a fish segment with a cylinder, for the boundary layer would certainly separate, with turbulence in the downstream flow. With separation occurring on the trailing surfaces of segments representing the first (anterior) half wavelength, subsequent flow would be turbulent. Any surface roughness would further encourage turbulence in the boundary layer and this could result in greater flow stability on circular sections rather than fish-type sections. Taylor (1952) developed alternative treatments to consider roughness and resulting turbulence, but the magnitude of this is far greater than would be expected in fish. The latter modification of the model applies to polychaete worms.

Neglect of interaction effects is expected to give higher thrust power values, more than offsetting the opposite effect of body shape assumptions.

Example — To show the magnitude of thrust power predicted from calculations for Taylor's model, data from photographs published by Gray (1933a) for *Anguilla, Pholis* (= *Centronotus*), and *Ammodytes* swimming in the anguilliform mode may be used. Amplitude increased to reach maximum values over about half the body, and were close to the trailing edge amplitude, A_T. To take in effects of $A(x)$ on $W_R^2(x)$ to which thrust will be related, a weighted mean amplitude can be calculated, A_W. Calculations of W_R^2 for different positions and amplitudes along the body show A_W to be approximately 0.9 A_T. This value of A was used to determine A, with λ_B calculated from Gray's data. Values of V and U for the calculation of n were also taken directly from Gray (Table 8). Appropriate values for $G_{n,a}$ were taken from Fig. 48.

For the three fish, typical values of d were taken from various published sources (e.g. Nikolskii 1961). Using these data, E_s was calculated (Table 8). The length, l, was assumed to be equal to L for the fish, from which E was 196, 2926, and 4034 erg/s for *Anguilla, Pholis*, and *Ammodytes*, respectively.

TABLE 8. Examples of calculations of swimming power output of three fish swimming in the anguilliform mode. Calculations for resistance forces from the model proposed by Taylor (1952). Data for kinematics are from Gray (1933a).

Species	L	U	V	$n=U/V$	λ_B	A_T	Mean A_w weighted	$A_w/2\lambda_B$	$G_{(n,a)}$	d	R_d	Swimming power per unit length	total power
	(cm)	(cm)	(cm/s)	(l)	(cm)	(cm)	(cm)	(l)	(l)	(cm)	(l)	(erg/s)	(erg/s)
Anguilla vulgaris	7.0	4.0	6.2	0.65	4.0	2.1	1.9	0.24	3.4	0.91	364	28	196
Pholis gunnellus	12.2	11.7	17.5	0.67	8.8	3.7	2.7	0.15	1.5	1.59	1860	239	2926
Ammodytes lanceolatus	17.8	8.0	16.0	0.50	8.0	3.1	2.8	0.18	3.5	1.78	1424	227	4034
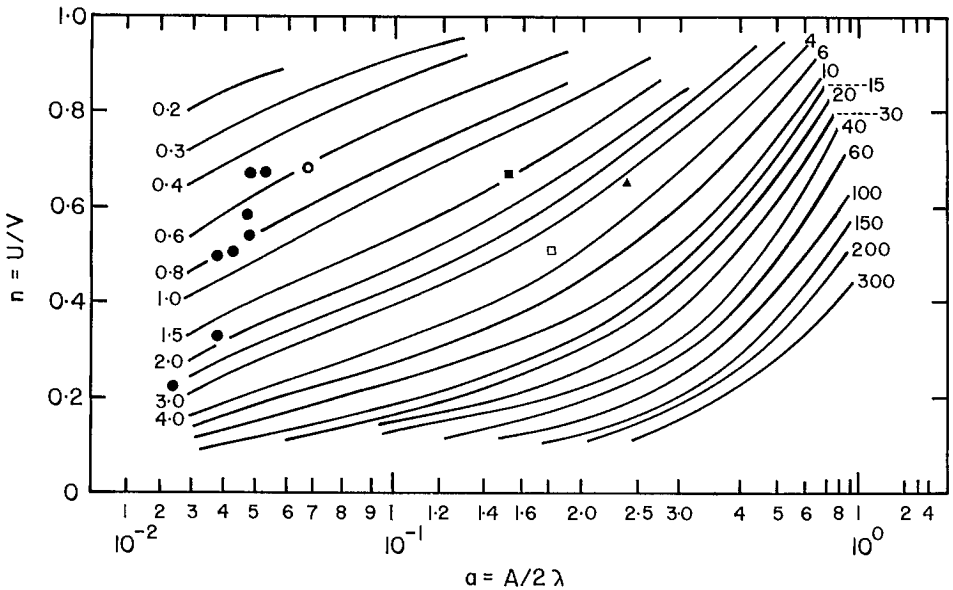
FIG. 48. Isopleths for constant $G_{(n,a)}$ (thrust coefficients for Equation 56) for various values of n and a. (Redrawn from G. Taylor; 1952 Proceedings of the Royal Society of London Biological Sciences A 214, p. 158; used with permission of the Royal Society of London) ●, *Salmo gairdneri;* ○, *Gadus merlangus;* ■, *Pholis gunnellus;* □, *Ammodytes lanceolatus;* ▲, *Anguilla vulgaris* (see Table 8, 12)

These power outputs may be compared to the theoretical frictional drag power, calculated from standard hydrodynamic equations. The body was assumed to be straight and rigid.

The theoretical frictional drag power is *only* a convenient reference to compare different calculations. It does *not* assume that this is the expected drag for the swimming fish. In fact, the drag is that for a flat plate of equivalent wetted surface area, and is an absolute minimum value for the frictional drag component only, a minimum not expected to be obtained in fish.

The theoretical frictional drag power was 16, 529, and 292 erg/s, respectively, for *Anguilla*, *Pholis*, and *Ammodytes*; that is, the calculated thrust power was 12, 6, and 14 times greater than this for the three fish, respectively (Table 9).

In comparing the calculations from the model with theoretical frictional drag power values, the comments made above should be borne in mind concerning variability in propulsive cycles. In view of the known variation in kinematics, it cannot be certain that photographs of a single cycle given by Gray (1933a) are truly representative of "typical" movements at the observed speeds. Slight, but undetected, acceleration during the course of the cycle shown could result in calculation of high values. Nevertheless, the large differences between the two sets of values suggest that real fish would experience drag much higher than expected from theoretical drag calculations, as defined in Chapter 4. Of the thrust power values for the three fish, that for *Pholis* is most similar to the values expected for swimming fish (Lighthill 1971; Webb 1971a).

REACTION MODEL

Lighthill (1960, 1969, 1970, 1971) discussed several developments in the formulation of reaction models (see also Wu 1971a, b, c, d). Many models require for the biologist a rigorous and complex hydromechanical analysis. The detailed form of the basic models can be simplified by a consideration of bulk momentum and energy changes around the trailing edge to calculate thrust and swimming power. Similar results are given by the basic approaches of both Lighthill and Wu, and the bulk momentum simplification gives similar results to a more detailed approach (Lighthill 1970; Wu 1971d). The simplified latter approach is most suitable for practical application and will be emphasized.

Lighthill (1960, 1969, 1970) considered a hypothetical fish swimming in the anguilliform mode with increasing small amplitude lateral movements. As soon as any segment of the body starts moving, a reaction force is generated proportional to the velocity of the segment and the virtual mass of water affected by the segment. For fish of constant depth along body length, the mass of water affected by all segments will be the same, but the momentum associated with that mass will slowly be increased as the velocity of segments increases with amplitude along the body. Water is shed into the wake, with momentum defined by the kinematics of a trailing-edge segment. Thrust is proportional to the rate at which this momentum is shed into the wake (at a rate U). The gross rate of working of the propulsive wave is equal to the rate at which the trailing edge does work against this momentum. Thus gross power output can be expressed in terms of momentum and energy changes for a single segment at the trailing edge.

To understand how the motion of the trailing edge gives estimates of thrust power, consider the effect of such a segment on a water slice just left behind by that edge at time $t = t$ as shown in Fig. 49 (after Lighthill 1969, figure 4). The length of the segment, Vt, is defined in

TABLE 9. Frictional drag for fish listed in Table 8 and 10, calculated from standard hydrodynamic equation (theoretical drag for body stretched straight).

Species	L (cm)	U (cm/s)	R_L (1)	S_w^a (cm²)	$C_{f\,lam}$ (1)	Frictional drag power (erg/s)
Anguilla vulgaris	7.0	4.0	2,800	20	0.025	16
Pholis gunnellus	12.2	11.7	14,274	60	0.011	529
Ammodytes lanceolatus	17.8	8.0	21,716	127	0.009	292

[a]Assumes $S_w = 0.4.L^2$, which is more likely to be a high, rather than a low, estimate.
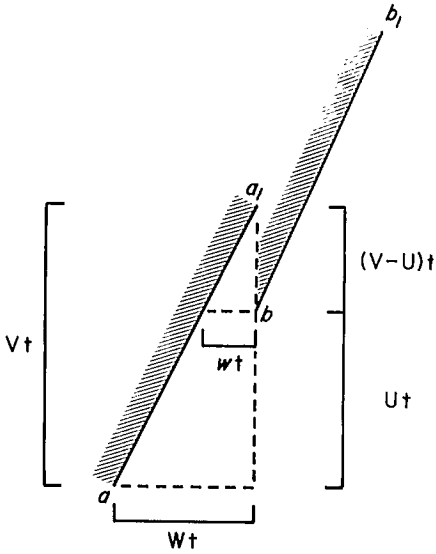
FIG. 49. A highly simplified diagrammatic representation of movements of a trailing-edge segment at two instances in a cycle of transverse motion. For explanation, see text. (Based on Lighthill 1969)

relation to the speed V at which the propulsive wave is propagated, overtaking the water slice at that speed. In time t, this segment moves from positions aa_1 to bb_1, with the trailing edge moving laterally a distance Wt, and forward a distance Ut. The water is pushed laterally a smaller distance wt, and the momentum gain is $m_T w$, when m_T is the virtual mass, and w the velocity at which it is pushed by the motion of the segment.

Lighthill showed that w is given by the kinematic parameters U, V, and W from similar triangles in Fig. 49. Thus

$$\frac{w\,t}{W\,t} = \frac{(V-U)t}{V\,t}$$

or

$$w = W[(V - U)/V] \qquad (60)$$

Momentum, $m_T w$ is shed into the wake at U, and the trailing edge does work against this at W. Thus, the total rate of working, E_T, is given by

$$E_T = m_T w\,U\,W \qquad (61)$$

E_T contains two components, the energy required to overcome the total drag (thrust power) and wasted energy shed into the wake. The latter is kinetic energy, E_K, associated with acceleration of water to w. This kinetic energy

associated with w is thus

$$E_K = \tfrac{1}{2}\,m_T\,w^2\,U \qquad (62)$$

and the thrust power, E, is given by subtraction

$$E = E_T - E_K = m_T(w\,W\,U - \tfrac{1}{2}\,w^2\,U) \qquad (63)$$

The virtual mass associated with the lateral motion of a segment is

$$m_T = \frac{k\,\rho\pi\,d^2}{4} \qquad (64)$$

when

d = depth of segment, or trailing-edge depth.

k is a constant close to 1 for a variety of fish sections, including various combinations of dorsal and /or ventral median fins. For practical purposes Equation 64 can then be written;

$$m_T = \rho\pi\,d^2/4 \qquad (65)$$

An important effect of forces produced by any lateral motion is the resulting yawing couple. These yawing forces, termed recoil forces (Lighthill 1960) are associated with recoil movements of anterior portions of the body, which could be associated with large energy losses (Lighthill 1960, 1969, 1970). All segments executing lateral movements are, of course, doing work associated with recoil forces. The mean time average of these forces in anguilliform propulsion is zero for symmetrical movements, except at the trailing edge (Lighthill 1970). In anguilliform propulsion when there tends to be a complete propulsive wavelength, the integral of recoil forces along the body length tends toward zero. Recoil forces cannot completely cancel out when the amplitude increases along the body, as they will similarly increase. This is reflected by the movement of the nose in anguilliform fish, which has an amplitude slightly higher than the minimum amplitude observed a short distance along the body (Fig. 27).

The model discussed above differs from real fish as follows: (1) amplitudes are assumed to be small, (2) forces of viscous origin are neglected, except in terms of thrust having to overcome a drag component of viscous origin, (3) efficiency of the caudal propeller is always greater than 0.5. *Amplitude* — The amplitude of real fish movements is large, rather than small. Lighthill (1971) considered the effects of large amplitude motion for the subcarangiform mode, and found it had little effect on total power values in comparison with those expected for the small amplitude model.

86

The rate of energy loss to the wake was increased by a factor $1/\cos\theta$, when θ was the angle subtended by the trailing edge normal to the axis of forward progression of the fish. (Gray (1933a, b,c) and others usually measured angles subtended by the body of the path of a segment relative to the axis of transverse motion. In Chapter 2, the angle subtended by the body and this transverse axis was given as θ_B, related to θ as $\theta = 90 - \theta_B$ degrees.)

For normal propulsion in the subcarangiform mode, with θ about $60°$, the mean value of $\cos\theta$ for a cycle of trailing-edge movement is about 0.85, making $1/\cos\theta$ about 1.18 (Lighthill 1971). For anguilliform propulsion, Gray (1933a) noted values of θ to $70°$, in which case $1/\cos\theta$ would take mean values of about 1.20. In terms of the overall energetics of the propeller system, the factor $1/\cos\theta$ will only be important at low propulsive (propeller) efficiencies. With efficiencies of the order 0.75–0.90, the error involved in using the small amplitude model would be about 5%.

Thrust forces of viscous origin (resistive forces) — Resistive thrust forces, as vorticity shed by a segment, increase with time, and the momentum of the water increases gradually above $m_T w$ (Lighthill 1970). Vortex forces add to both the momentum of the water and the wasted kinetic energy. For this added momentum to be useful in generating thrust, it must be correlated with the trailing-edge motion, as is $m_T w$ with W for reaction forces. Lighthill (1970) showed this was not the case, but rather the momentum resulting from viscous forces would be so correlated that negligible addition to thrust would accrue. The kinetic energy involved would still add to energy loss, with concomitant reduction in propeller efficiency. Therefore, neglect of these forces is likely to include a relatively small error in the model's estimation of thrust power, but a larger uncertain error in terms of propeller efficiency.

Propeller efficiency — The small amplitude model assumes that caudal propeller mechanical efficiency will always be greater than 0.5. This follows from Equation 61, 62, 63, for if mechanical propeller efficiency, η_p, is

$$\eta_p = \frac{E}{E_T} = \frac{E_T - E_K}{E_T} \qquad (66)$$

then

$$\eta_p = 1 - 0.5[(V - U)/V], \qquad (67)$$

neglecting forces of viscous origin.

Then, as $V \to U$, $\eta_p \to 1$, whereas when $V > > U$, $\eta_p \to 0.5$. Generally, the model applies for values of U/V between 0.7 and 0.9, when η_p will be high. According to Webb (1971b) this is only likely to occur at speeds approaching maximum cruising speeds and sprint speeds, at least in the subcarangiform mode. In that mode, low cruising speeds are associated with U/V as low as 0.23. A consideration of probable muscle behavior suggested that η_p would then be of the order 0.2–0.25. η_p increases with swimming speed and increasing U/V, so that optimum conditions for Lighthill's model are approached at higher speeds. Most measurements in the anguilliform, as well as the subcarangiform mode, have been made for U/V below 0.7 (see values for n in Table 8 and Webb 1971b), in which case the reaction model will tend to overestimate efficiency and thrust power.

In summary, the reaction model is expected to give fair estimates of thrust power, if not total power output, for anguilliform propulsion. The small amplitude model has important advantages in the ease with which key kinematic parameters can be measured without resort to thrust coefficients.

Example — Data from Gray (1933a) for fish swimming in the anguilliform mode, can again be used with the reaction model (Table 10). The trailing-edge lateral velocity can be calculated assuming its motion is simple harmonic, the root mean square value being appropriate for mean power output.

The thrust power output of *Anguilla, Pholis,* and *Ammodytes* for reaction forces was 42, 1714, and 1423 erg/s, respectively, or 2.6, 3.2, and 4.9 times the theoretical frictional drag power in each case. These values are likely to be slightly high, but show that swimming drag will be higher than theoretical drag.

Of the two approaches, resistive or reactive, that proposed by Lighthill is preferred. As set out by Lighthill (1969, 1970) it gives a closer representation of swimming kinematics, and considers those forces likely to be of greatest importance. It also makes no critical assumptions concerning body sectional shape (see Wu 1971b, c), and in fact includes variations in morphology as a factor affecting hydromechanical efficiency (see next section).

MODIFICATIONS IN THE ANGUILLIFORM MODE

An important part of Lighthill's (1969, 1970) and Wu's (1971c) analyses of fish propulsion is the hydromechanical interpretation

TABLE 10. Examples of swimming power output of three fish swimming in anguilliform mode, calculated for reaction forces from the model proposed by Lighthill (1969, 1970). Data for kinematics are from Gray (1933a).

Species	L	U	V	f	A_T	W(rms)	w	d	m_T	Total power generated	Kinetic energy lost to wake	Thrust power
	(cm)	(cm/s)	(cm/s)	(s)	(cm)	(cm/s)	(cm/s)	(cm)	(g/cm)	(erg/s)	(erg/s)	(erg/s)
Anguilla vulgaris	7.0	4.0	6.2	1.6	2.1	7.5	2.6	0.91	0.65	51	9	42
Pholis gunnellus	12.2	11.7	17.5	2.0	3.7	16.4	5.4	1.59	1.98	2052	338	1714
Ammodytes lanceolatus	17.8	8.0	16.0	2.0	3.1	13.8	6.9	1.78	2.49	1897	474	1423

of some aspects of morphological variation among fish. These are summarized in Fig. 50 and Table 11 based on Lighthill (1969, 1970). Modifications of fish morphology relations to anguilliform motion will be discussed, with some modifications applicable more to the subcarangiform mode when this tends towards the anguilliform mode.

Lighthill (1969, 1970) noted several morphological types in the anguilliform mode, associated with tapering posterior body portions, and the subdivision of median fins into discrete fins. Tapering of the posterior of the body reduces mechanical efficiency. Work is done proportional to a segments virtual mass (with d^2) and its lateral velocity. When depth decreases, the virtual mass is progressively decreased, and, as with the eel, is associated with only small increases in W. Most work is done by more anterior segments, whereas posterior segments contribute little to thrust but may make substantial contributions to frictional drag and wasted energy in the wake. Two grades of body taper are shown in Fig. 50, *Lophotes* when this is relatively small, and *Gastrostomus* when it is large. Some tapering occurs in any case in *Clamydoselachus*, *Anguilla*, and *Lampetra* (Fig. 50). However, this is of smaller magnitude compared to the length of the body, and is not likely to alter thrust estimates made with the reaction model.

In contrast, discrete median fins can improve hydromechanical efficiency in comparison with continuous median fins. Two types of morphology are involved, when gaps between the fins are small and when they are large. The former appears more characteristic of such fish as gadids in the subcarangiform mode.

The trailing edge of any fin does work the same as the trailing edge of the caudal fin, and a wake is formed downstream. The wake carries that momentum and energy dictated by the trailing-edge motion in the form of a vortex sheet. When the vortex sheet is shed at the trailing edge of an anterior median fin, it may be resorbed at the leading edge of the next posterior fin, providing its depth is at least as great as that of the anterior fin trailing edge. The wake shed by the posterior fin's trailing edge is dictated by that edge's motion, so that no part of the upstream wake anterior to the posterior fin remains. Thus, the kinetic energy of the upstream motion makes negligible contributions to the total energy wastage (Lighthill 1970; Wu 1971c). A similar interaction would be expected for vortex sheets shed by tapering body shapes anterior to a large caudal fin.

When the gaps between median fins are small, as in *Gadus*, the motion of the leading edge of a posterior fin is similar to that of the wake shed by the trailing edge of an immediately anterior fin, as the phase difference in their motions is small. As such, the leading edge of the posterior fin does no net positive work against the incident wake momentum and the wake momentum is cancelled out over a cycle the same as segments of a continuous fin. The flow is mechanically similar to that of a continuous fin, and thrust and efficiency as calculated for the caudal fin trailing edge will be the same. A slight reduction in drag occurs because the gaps in the fins reduce the total surface area.

A different situation applies when gaps are large. The vortex sheet may be resorbed the same as small gaps without a large addition to

TABLE 11. Variations in body and median fin morphology that relate to hydromechanical swimming efficiency and variations in kinematics for fish swimming in different body modes. Arrows indicate morphological changes associated with higher hydromechanical efficiency. Body forms are illustrated in Fig. 50.

Body movements carangiform, with lunate caudal fin, but whole body involved in high amplitude movements. High aspect ratio lunate tail, with low spanwise flexibility. Extreme narrow necking. Streamline caudal peduncle. Dolphins and porpoises

Body movements carangiform with lunate caudal fin. High aspect ratio lunate tail, with low spanwise flexibility. Extreme narrow necking, and streamline caudal peduncle. Scombroid fish and cetaceans

↑

Body movements anguilliform. Intermediate aspect ratio heterocercal tail. Moderate narrow necking. Depth augmented at other anterior positions by median fins. Small sharks

Body movements carangiform. High aspect ratio swept-back tail with low spanwise flexibility. Extreme narrow necking. Caudal peduncle sometimes streamlined. *Caranx, Scomber, Pneumatophorus*

↑

↑

Body movements anguilliform. Low aspect ratio tail with high spanwise flexibility. Narrow necking offset by discrete median fins, gaps filled by vortex sheets. *Heterodontus, Rabidus*

Body movements carangiform. High aspect ratio tail scooped out centrally. Moderate spanwise flexibility. Moderate narrow necking. *Clupea*

↑

↑

Body movements "pure" anguilliform. Negligible aspect ratio tail. High flexibility. Body span virtually constant for whole body length. *Lampetra, Anguilla, Clamydoselachus*

Body movements subcarangiform, tend towards anguilliform. Low aspect ratio tail, with high spanwise flexibility. Narrow necking offset by discrete median fins, gaps filled by vortex sheets. *Gadus, Merlangus*

Body movements subcarangiform, tend towards carangiform. Low aspect ratio tail, with high spanwise flexibility. Narrow necking only partly offset by median fins. *Salmo, Oncorhynchus, Carassius, Leuciscus*

↑

Body movements anguilliform. Body span tapers posteriorly over short portion of body length. *Lophotes*[a]

↑

Body movements anguilliform. Body span tapers slowly over most of body length. *Gastrostomus*

Body movements ostraciform. Low aspect ratio tail, with high rigidity. Body form highly variable.

[a]May have alternate carangiform propulsion for slow swimming as *Aphanopus* (see Bone 1971).

89

FIG. 50. Diagram illustrating morphological variations that affect mechanical swimming efficiency of fish and cetaceans swimming in various body modes. The important morphological characteristics are given in Table 11.

energy losses. There will now be a large phase difference between the motions of an anterior fin's trailing-edge motion and that of the next posterior fin's leading edge. Lighthill (1970) showed that if the phase difference was greater than 0.5π, the momentum in the upstream wake would not be completely resorbed at the posterior fin's leading edge. Then, there would be a net increase in thrust, without a similar increase in energy losses.

The phase difference between the motion of an anterior fin's trailing edge at a position x_1 on the body, and the next posterior fin's leading-edge motion at position x_2 is given by

$$\text{Phase difference} = \frac{2\,\pi\,(x_2 - x_1)}{\lambda_B}\left[\frac{V}{U} - 1\right] \quad (68)$$

when

$$\frac{2\,\pi\,(x_2 - x_1)}{\lambda_B}$$

gives the phase difference between lateral movements at x_1 and x_2, and $\frac{V}{U} - 1$ modifies this as the vortex street moves downstream at U with the propulsive wave travelling at V.

This situation probably applies to most sharks, such as *Heterodontus* and *Squalus*, and fish like *Rabidus* when the caudal fin is fully expanded (Fig. 50). For example, Gray (1933a) showed figures of *Acanthias vulgaris* swimming with U = 17.8 cm/s, V = 25.6 cm/s. Length was 46.0 cm, λ_B 30.0 cm. The trailing edge of the

first dorsal fin was about 19.4 cm from the nose, the second dorsal fin was small, so the vortex sheet shed by the first anterior fin would be absorbed at the caudal fin leading edge, at about 37.1 cm. The phase difference between these two is thus, 2π (37.1 − 19.4) (0.44)/30.0 or 0.52π.

In many small sharks there is also a trend to reduction of the body depth posteriorly, with an increase to a high trailing-edge depth at the caudal fin. This is similar to the trend observed in carangiform modes (Fig. 50), except that many elasmobranch body movements are anguilliform. The median fins probably contribute mostly to thrust, rather than to stability as is the case for anterior median fins in the carangiform mode (Lighthill 1970).

Carangiform modes

The hydromechanical theory discussed for anguilliform modes applies to most carangiform modes. An exception is the mode with semilunate tail, and other conditions in the carangiform mode when the caudal fin is highly swept-back, approaching the semilunate condition, (e.g., *Pneumatophorus*, Fig. 50). Carangiform modes differ from anguilliform modes in the concentration of significant propulsive movements to the posterior portion of the body (Breder 1926). This applies equally when less than a half wavelength of the propulsive wave is present, as in the carangiform mode proper, and when more than that is present in the subcarangiform variant.

The amplitude of lateral movements increases rapidly over a relatively small portion of the body, compared with a slow rate of increase in the anguilliform mode. According to Lighthill (1970) this is an important hydromechanical improvement, related to the magnitude of resistance thrust forces of viscous origin. In carangiform modes, the time over which these can develop is greatly reduced, and acceleration of water occurs over a short period. The lessening in resistance forces reduces the amount of energy lost to the wake in comparison with the anguilliform mode.

In the anguilliform mode, a trend was noted to greater lateral compression and emphasis on the caudal fin, as in small sharks. This is a dominant trend in carangiform modes, when increased thrust comes through increased virtual mass effects at the trailing edge of the body, with increase in that edge's depth.

Although the bulk of thrust will be generated by a caudal fin trailing-edge segment, segments anterior to this trailing edge will also contribute (Wu 1971a, b, c, d). Wu considered in some

detail the effects on thrust of body span (depth) variations between the shoulder and the caudal peduncle particularly as modified by different median fin shapes. Such anterior body section and fin trailing edges will generate a vortex sheet as described above. In the case of anterior fins with sharp trailing edges and a gradually tapering body, thrust enhancement from the motion of segments anterior to the trailing edge is apparently small (Lighthill 1970; Wu 1971c, d). The data discussed below concerns this type of morphology.

When long median fins occur (ribbon-type fins as in the dolphin fish *Corphaena hippurus*) thrust may be greatly enhanced by the momentum shed by anterior segments (Wu 1971a, b, c, d). Such effects are difficult to include in any analysis, in part because of the complexity of the mathematical format and adequacy and feasibility of collecting the necessary data. Problems of incorporating effects of morphological variation are discussed in Chapter 7.

With the concentration of thrust forces towards the caudal fin, large recoil forces are also generated, no longer balanced by similar lateral forces as with a complete wavelength in the anguilliform mode. Efficient propulsion requires that these forces be minimized, and this is achieved by the characteristic body shape in the carangiform mode. This shape appears from a trend to narrow necking, with body depth progressively reduced in the caudal peduncular region where amplitude increases to its trailing-edge maximum (Lighthill 1969, 1970). It is a trend to the separation of two mass centers; virtual mass effects at the caudal fin as caudal propeller, and the body anterior to the caudal peduncle. Recoil forces generated by the caudal propeller do work against the mass and virtual mass of the body. Where recoil forces act, the body virtual mass is often augmented by a dorsal median fin. Median fins contribute to yawing stability, rather than the generation of thrust. Recoil forces do work against a comparatively greater inertia, effectively minimizing recoil movements. This is clearly shown by the small amplitude movements of the nose of *Euthynnus* (Fig. 36).

In fish swimming in the subcarangiform mode, narrow necking is poorly developed compared to other carangiform modes. It is often offset by median fins as in *Gadus*, or anal fins as in salmonids (Fig. 50). In these cases, recoil movements will be less effectively minimized by body shape per se, but it is in these fish that vestiges of anguilliform motion are retained. The presence of a complete propulsive wave,

admittedly with rapidly increasing amplitude with length, probably contributes to the reduction of recoil movements as in anguilliform propulsion.

Application of Lighthill's (1969, 1970) models to carangiform propulsion is subject to the same comments made for the anguilliform mode. The small amplitude model will probably slightly underestimate kinetic energy losses by a factor $1/\cos\theta$, and thrust and efficiency similarly. Propeller efficiency is still assumed greater than 0.5, but some improvement is seen in terms of neglect of vortex forces of viscous origin. The rapid increase in amplitude reduces these, and, because of narrow necking, they will be further reduced in the caudal peduncular region. Reaction models are likely to give a far better estimate of thrust power for carangiform modes than for anguilliform motion. Resistive models are likely to greatly underestimate thrust power as resistance forces become much smaller in relation to reaction forces (Lighthill 1970, 1971; Wu 1971b).

For completion, calculations will be considered for both resistive and reaction models as for anguilliform propulsion. Comparison of the various results will be deferred until both have been considered. Most complete data are available for subcarangiform propulsion, so that calculations will unfortunately be confined to this mode.

RESISTIVE MODEL EXAMPLE

Taylor's (1952) model is the most appropriate. Data can be found for *Gadus merlangus*, whiting (Gray 1933a), and *Salmo gairdneri*, rainbow trout (Webb 1971a and unpublished data). Measurements of amplitude distribution with length, and expected values of W_R^2 for assumed simple harmonic motion of segments, give $A_w = 0.5A_T$. This weighting is preferred to that used by Webb (1971a) which emphasized trailing-edge values with W only. The relation is lower than for anguilliform propulsion because the amplitude is only large for a small portion of the body.

Values for U given by Webb (1971a) are mean values for all segments of a fish, including a mean correction for local solid blocking velocity increments. Depth, d, was taken as the mean value for the posterior of trout included in a propulsive wave, and was assumed to be in the same ratio with length for whiting. This assumed that only one wavelength contributes to thrust and $l = \lambda_B$. This seems likely, as the remainder of the body executes small amplitude recoil-type movements and is probably associated with drag, not thrust (Alexander 1967).

Otherwise various data are given in Table 12, with values for $G_{(n,a)}$ taken from Fig. 48.

REACTION MODEL EXAMPLE

Data and calculations for the same fish are in Table 13 for Lighthill's (1970, 1971) reaction models. Values for $\cos\theta$ were measured for trout (P. W. Webb unpublished data) but assumed to be 0.85 for whiting. The latter is a mean value measured by Lighthill (1971) for

TABLE 12. Examples of calculations of swimming power output using Taylor's (1952) resistance model for two fish swimming in subcarangiform variant of carangiform mode. Data from Gray (1933a) and Webb (1971a and unpublished).

Species	L	U	V	n	λ_B	A_T	A_w	$A_w/2\lambda_B$	$G_{(n,a)}$	d	R_d	Swimming power per unit length	total power
	(cm)	(cm/s)	(cm/s)	(l)	(cm)	(cm)	(cm)	(l)	(l)	(cm)	(l)	(erg/s)	(erg/s)
Gadus merlangus	24.0	16.8	25.0	0.67	18.2	5.0	2.5	0.068	0.60	4.0	8,400	334	0.061×10^5
Salmo gairdneri	28.2	10.1	44.1	0.23	21.4	2.1	1.1	0.026	2.5	5.0	5,050	489	0.10×10^5
		17.2	50.5	0.34		3.2	1.6	0.038	1.8		8,600	1329	0.28×10^5
		23.9	48.8	0.49		3.9	1.5	0.035	0.8		11,950	1353	0.28×10^5
		30.7	60.6	0.51		3.6	1.8	0.042	0.8		15,350	2520	0.53×10^5
		37.5	69.3	0.54		3.8	1.9	0.045	0.8		18,750	4157	0.87×10^5
		44.3	76.0	0.58		3.8	1.9	0.045	0.7		22,150	5514	1.16×10^5
		51.6	76.8	0.67		4.3	2.2	0.052	0.5		25,600	5760	1.21×10^5
		58.1	86.5	0.67		4.2	2.1	0.049	0.5		29,050	7787	1.64×10^5

TABLE 13. Examples of calculations of swimming power output using Lighthill's (1969, 1970, 1971) reaction models for three fish swimming in subcarangiform variant of carangiform mode. Data from Gray (1933a), Webb (1971a) and Lighthill (1971). Figures in brackets are approximations.

Species	L (cm)	U_T (cm/s)	V (cm/s)	f (s)	A_T (cm)	W(rms) (cm/s)	w (cm/s)	d (cm)	m_T (g/cm)	Cosθ (1)	Total power generated (E_T) (erg/s)	Kinetic energy lost to wake (E_K) (erg/s)	Thrust power (E) (erg/s)
Gadus merlangus	24.0	16.8	26.4	2.0	5.0	22.2	11.3	(4.8)	18.1	0.85	0.76×10^5	0.23×10^5	0.53×10^5
Salmo gairdneri	28.2	10.1	44.9	2.1	2.1	9.8	7.8	4.2	13.9	0.88	0.097×10^5	0.044×10^5	0.063×10^5
		15.2	51.4	2.4	3.2	17.1	12.0	4.4	15.2	0.88	0.47×10^5	0.19×10^5	0.28×10^5
		21.3	49.2	2.3	3.9	19.9	11.3	4.8	18.1	0.89	0.87×10^5	0.28×10^5	0.59×10^5
		27.4	59.9	2.8	3.6	22.4	12.1	5.5	23.8	0.93	1.77×10^5	0.51×10^5	1.26×10^5
		33.5	68.5	3.2	3.8	27.0	13.8	5.6	24.6	0.93	3.07×10^5	0.84×10^5	2.23×10^5
		39.6	77.0	3.6	3.8	30.4	14.9	6.0	28.3	0.94	5.08×10^5	1.32×10^5	3.76×10^5
		45.7	77.0	3.6	4.3	34.4	14.1	6.1	29.2	0.94	6.47×10^5	1.41×10^5	5.06×10^5
		51.8	85.6	4.0	4.2	37.3	14.5	6.1	29.2	0.93	8.18×10^5	1.71×10^5	6.47×10^5
Leuciscus leuciscus	30	48	62	(2.5)	(6.7)	37	9	8.7	59	0.85	9.60×10^5	0.96×10^5	8.64×10^5

Leuciscus from Bainbridge (1963). Trailing-edge depth, *d*, was measured for trout (P. W. Webb unpublished data) but assumed to be 0.2 L for whiting.

For trout, two values of U are appropriate, one for drag and one for thrust. The value applicable to drag, U_d, is the corrected velocity for interference with the flow in the water tunnel where the fish swam. Interference resulted mainly in local drag increments when the body had substantial local sectional area. U_d was the same as U used with Taylor's (1952) model. The caudal fin trailing-edge segment was of negligible cross-sectional area, so the incident velocity for thrust calculations, U_T, will be equal to the free stream velocity, lower than U_d.

In addition to calculations relating to bulk momentum and energy, the model proposed by Lighthill (1971) can be used quasi-statically when the net thrust force is the mean value of instantaneous forces through a cycle. These give the same results as the bulk momentum approach (Lighthill 1970). The required calculations for the latter analysis have been made by Lighthill (1971) for data on *Leuciscus* from Bainbridge (1963). Mean values of the calculations are in Table 13. Webb made similar calculations at several low cruising speeds for a single trout (see below).

COMPARISON OF RESULTS FROM MODELS

Results of calculations of thrust power may be compared with theoretical frictional drag as a reference the same as for the anguilliform mode. A turbulent boundary layer is assumed, as measurements on trout were made in water with an intensity of turbulence greater than 0.03. Outer flow conditions are uncertain for *Gadus*, but a turbulent boundary layer would be expected with the locomotory movements, roughness at eyes and nares, etc. *Leuciscus*, swimming in a fish wheel (Bainbridge and Brown 1958), was probably swimming in its own wake to some extent. Results of calculations for theoretical frictional drag power are given in Table 14, and various results for this and thrust power from models compared in Table 15.

Of the results, those for *Salmo* are of greatest interest, based on means of many observations at different swimming speeds. For these fish the measurements of thrust power calculated from the effects of extra drag loads on the kinematics are also available (Webb 1971a) (Table 15). Compared to theoretical frictional drag power, values from both models are relatively higher for lower swimming speeds, although measured values tend to be a constant multiple of approximately 2.8. Thrust power from the resistive force model decreased from 6.7 to 0.8 times the theoretical frictional drag power from low to higher speeds. Values less than 1 must be considered impossible. High thrust power is associated with relatively high values of *f* and V with low U, when $G_{(n,a)}$ is low. The thrust power for *Gadus* is of the same order as *Salmo* at similar R_L.

Thrust power values calculated from reaction forces for *Salmo* decreased with speed from

TABLE 14. Frictional drag for fish listed in Table 12 and 13 calculated from standard hydrodynamic equations.

Species	L (cm)	U (cm/s)	R_L (1)	S_w (cm)^2	$C_{f\,turb}$ (1)	Frictional drag power (erg/s)
Gadus merlangus	24.0	16.8	4.03×10^4	230.4[a]	0.0086	0.047×10^5
Salmo gairdneri	28.2	10.1	2.45×10^4	311.3	0.0095	0.015×10^5
		17.2	4.85×10^4		0.0083	0.066×10^5
		23.9	6.74×10^4		0.0078	0.17×10^5
		30.7	8.66×10^4		0.0074	0.33×10^5
		37.5	1.06×10^5		0.0071	0.58×10^5
		44.3	1.25×10^5		0.0069	0.93×10^5
		51.6	1.46×10^5		0.0067	1.43×10^5
		58.1	1.64×10^5		0.0065	1.98×10^5
Leuciscus leuciscus	30.0	48.0	1.31×10^5	360.0[a]	0.0067	1.33×10^5

[a]Assumed $S_w = 0.4 \cdot L^2$.

94

TABLE 15. Summary of swimming power output and requirements from Table 12, 13, 14. Power outputs calculated from models by Taylor (1952) and Lighthill (1969, 1970, 1971) and Webb (1971a) are shown as multiples of the theoretical frictional drag.

Swimming speed (cm/s)	Theoretical frictional drag power (erg/s)	Thrust power from Taylor's (resistance) model (erg/s)	Resistance frictional thrust power	Thrust power from Lighthill's (reaction) model (erg/s)	Reaction frictional thrust power	Thrust power measured (erg/s)	Measured frictional thrust power
				Gadus merlangus			
16.8	0.047×10^5	0.061×10^5	1.33	0.53×10^5	11.5	–	–
				Salmo gairdneri			
10.1	0.015×10^5	0.10×10^5	6.7	0.063×10^5	4.2	0.04	2.7
17.2	0.066×10^5	0.28×10^5	4.2	0.28×10^5	4.2	0.30	4.5
23.9	0.17×10^5	0.28×10^5	1.6	0.59×10^5	3.5	0.58	3.4
30.7	0.33×10^5	0.53×10^5	1.6	1.26×10^5	3.8	1.14	3.5
37.5	0.58×10^5	0.87×10^5	1.5	2.23×10^5	3.8	2.02	3.5
44.3	0.93×10^5	1.16×10^5	1.2	3.76×10^5	4.0	3.06	3.3
51.6	1.43×10^5	1.21×10^5	0.8	5.06×10^5	3.5	4.51	3.2
58.1	1.98×10^5	1.64×10^5	0.8	6.47×10^5	3.3	6.33	3.2
				Leuciscus leuciscus			
48.0	1.33×10^5	–	–	1.01×10^6	7.6	–	–

4.2 to 3.3 times the theoretical frictional drag power. This modest decrease can be attributed to changes in U/V which approach conditions more appropriate for the model as U increases. At higher speeds, thrust power from reactive forces is about 20% higher than that measured by Webb (1971a). This too may be attributed to relatively low U/V, when η_p is likely to be overestimated. The maximum value for U/V was 0.67 for *Salmo*, but higher values are expected at higher speeds (Webb 1971b). These higher speeds will be those more typical of higher cruising speeds of most fish, and of sprint speeds.

Differences between the thrust power from reaction forces and theoretical frictional drag for *Gadus* and *Leuciscus* were 11.5 and 7.6, respectively, much higher than for trout. This could partly be the effects of nonrepresentative sampling in the sequences used in the analysis as for data in the anguilliform mode. A series of calculations for a single trout swimming over the same speed range as those above was made for the detailed quasi-static approach described by Lighthill (1971) (P. W. Webb unpublished data). This was subject to the same reservations, and gave a mean thrust power 1.3 times the theo-

retical frictional drag power. This indicates a possible range in results based on observations of single cycles of propulsive activity.

It appears that Lighthill's (1969, 1970, 1971) models will give a reasonable estimate of swimming thrust power requirements. This conclusion must be qualified by two conditions. First, the obvious condition that calculations must be based on a large number of observations. This practically limits general usage to the small amplitude model, with cos θ taken into account as its mean value. Second, the model is most acceptable at higher cruising speeds and sprint speeds, speeds greater than 2 L/s.

Carangiform mode with semilunate tail

The carangiform mode with semilunate tail is characteristic of fast swimming fish and cetaceans, and probably fish requiring a stable base line for the lateralis or electrical detection systems at low speeds. As details of the locomotion of the latter group are not known, discussion will be restricted to the former.

The fastest swimming fish and cetaceans have developed to the greatest extent the various

trends seen in carangiform propulsion. They have a well-defined 'caudal propeller,' the shape of which gives this variant of the carangiform mode its name. The 'propeller' is linked to the body by a narrow caudal peduncle. The caudal peduncle is often streamlined to further reduce flow disturbances anterior to the caudal fin (Slijper 1961; Fierstine and Walters 1968; Magnuson 1970). The body itself tends to be more circular than elliptical (see sections in Carey and Teal 1969a, b). This will be associated with concentration of body mass forward to reduce recoil movements, but with a relative reduction in wetted surface area in comparison with elliptical sections. Body mass is further augmented by virtual mass effects associated with the added depth of median fins.

The restriction of significant propulsion to a caudal propeller of short chord (length) in relation to body length means that the slender body theory discussed for long fish will not apply (Lighthill 1970; Wu 1971b). Instead, a different model must be formulated, based on lifting-wing theory for oscillating aero/hydrofoils. Approaches to thrust power may be resistive and quasi-static (von Holste and Kuchemann 1942; Parry 1949a; Gero 1952) or reactive (Lighthill 1969, 1970). The hydromechanical theory demanded by propulsion with semilunate tail is far more complex than that for elongate fish. Models are generally in preliminary form, and rigorous development is required. This is hampered by the paucity of data for animals swimming in this mode.

The application of models of carangiform propulsion with semilunate tail is otherwise simplified at the present time, for most predict thrust or thrust coefficients based on key kinematic factors. This short circuits the complex hydromechanics for biological application, and these will be considered. Details of the mechanics can be found in the references in Table 7.

Resistance (Quasi-Static) Model

The most suitable model is that developed by Parry (1949a) based on the theory of quasi-static flow around oscillating simple aerofoils, from von Holste and Kuchemann (1942). Parry formulated a general equation for dolphins and porpoises, whereby thrust power, E, was

$$E = 0.0175 \, L^2 \, U^3 \left[\left(\frac{0.38 \, L \, f}{U} \right) - 0.047 \right] \quad (69)$$

This considered thrust power proportional to f for a dolphin of given size and speed, assuming fixed relations between α, A, and f. Insufficient data is available to confirm these assumptions.

Data for L, U, and f can be found in Norris and Prescott (1961) for Pacific common dolphin, *Delphinus bairdi*, and Dall porpoise, *Phocoenoides dalli*, and in Lang and Daybell (1963), for Pacific striped porpoise, *Lagenorhynchus obliquidens*. These data are given in Table 16 with thrust power calculated from Equation 69. Comparing this with theoretical frictional drag power (Table 16) thrust power was 6.3, 9.4, and 16.0 times higher

Table 16. Calculations of swimming power output of three cetaceans from the quasi-static model proposed by Parry (1949a), and a comparison with theoretical frictional drag power. Data from Norris and Prescott (1961) and Lang and Daybell (1963).

Species	L (cm)	U (cm/s)	f (s)	Model thrust power (erg/s)	R_L (1)	$C_{f\;turb}$ (1)	S_w^a (cm²)	Theoretical frictional drag power (erg/s)	Model thrust power as multiple of frictional drag power (1)
Delphinus bairdi	170	430	1.8	8.96×10^9	7.31×10^6	0.0031	11,560	1.42×10^9	6.3
Phocoenoides dalli	200	430	2.1	1.80×10^{10}	8.60×10^6	0.0030	16,000	1.91×10^9	9.4
Lagenorhynchus obliquidens	204	554	3.9	6.18×10^{10}	1.13×10^7	0.0028	16,646	3.96×10^9	16.0

[a]Assumes $S_w = 0.4 \cdot L^2$.

for *Delphinus, Phocoenoides,* and *Lagenorhynchus,* respectively. These thrust power values would not be unreasonable for dolphins swimming near the surface, when drag power could be increased up to 5 times (Hertel 1966 and Fig. 7). Data used were recorded at or near the surface. Two conflicting pieces of information must also be considered. In Chapter 2 it was noted that porpoise locomotion is often associated with high amplitude movements involving much of the body. This would be expected to cause premature separation and increase drag. On the other hand, the observation made by Stevens (1950) on the relatively undisturbed flow in the wake of a swimming dolphin suggests this does not occur. Obviously more information is required on dolphin and porpoise propulsion.

REACTION MODEL

Thrust values from Lighthill's (1970) preliminary two dimensional model will be discussed for flow in a perfect fluid (see calculations in Wu 1971b). Lighthill's model predicts values for a thrust coefficient, C_T, related to thrust, E_T, by

$$E_T = \tfrac{1}{2} \rho \, S_h \, W^2 \, C_T \qquad (70)$$

when

S_h = projected area of caudal fin hydrofoil.

Total power developed, E_T is then

$$E_T = \tfrac{1}{2} \rho \, S_h \, W^2 \, C_T \, U \qquad (71)$$

whereas thrust power E, is given in relation to η_p as

$$E = E_T \, \eta_p, \qquad (72)$$

C_T is related to two metameters of the kinematics, frequency parameter and proportional feathering, and to the axis about which the plane of the fin rotates (yawing axis).

The frequency parameter is given by

$$\text{frequency parameter} = \omega \, c \, / U \qquad (73)$$

when

$\omega = 2 \, \pi \, f$, the angular velocity for assumed simple harmonic motion,
c = chord length

and

$$\text{proportional feathering} = \frac{\alpha_{max}}{W_{max}} \qquad (74)$$

when

α_{max} = maximum angle of attack, in radians
W_{max} = maximum trailing-edge lateral velocity

This assumes that α_{max} and W_{max} will be correlated.

The yawing axis appears to be toward the center of the caudal fin on the basis of osteology of scombrid fish (Fierstine and Walters 1968). This will be assumed for fish and cetaceans. Details of the effects of the position of yawing axis on C_T and η_p are given by Lighthill (1970) and Wu (1971b).

Lighthill (1970) produced diagrams relating C_T to frequency parameter, for isopleths of equal proportional feathering. An example is in Fig. 51 for the yawing axis at the half-chord position.

Few data are available for use with the model. Most complete data for kinematics have been published by Fierstine and Walters (1968) for *Euthynnus affinis,* but length was not given, and by Lang and Daybell (1963) for *Lagenorhynchus obliquidens.* C_T will be nondimensional, and if

Thrust power = $\tfrac{1}{2} \rho \, S_h^2 \, W^2 \, U \, C_T$
                     = drag power = $\tfrac{1}{2} \rho \, S_w^2 \, U^3 \, C_D$

dimensional similarity will be maintained, for S_h and S_w are proportional to L^2, whereas W (with f and A) and U are related to length (Hunter and
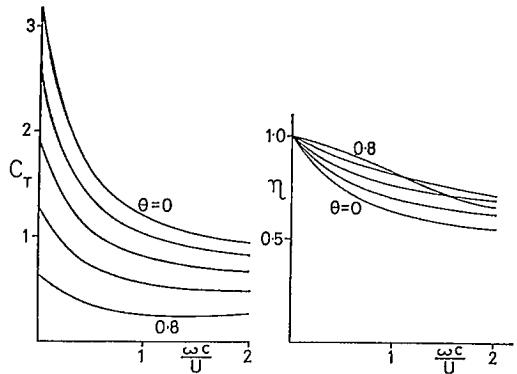
FIG. 51. Relation between thrust coefficient, C_T, and frequency parameter for isopleths of equal proportional feathering, θ, for caudal fin in carangiform swimming with semilunate tail. The yawing axis is assumed to be at half chord position. (From Lighthill 1969) (Reproduced with permission from *Hydromechanics of Aquatic Animal Propulsion* in Annual Review of Fluid Mechanics, Vol. 1, p. 433; © Annual Review Inc. 1968. All rights reserved)

97

TABLE 17. Calculations of swimming power output for two species swimming in carangiform mode with semilunate tail from Lighthill's (1970) preliminary two-dimensional model for motion in a perfect fluid. Data for kinematics are from Lang and Daybell (1963) and Fierstine and Walters (1968).

Species	L (cm)	U (cm/s)	f (s)	A (cm)	W_{max} (cm/s)	α_{max} (rad)	Proportional feathering (1)	Frequency parameter (1)	C_T (1)	W(rms) (cm/s)	S_h (cm²)	p (1)	Total swimming power (erg/s)	Thrust power (erg/s)	Thrust power as multiple of theoretical frictional drag power
Euthynnus affinis	50	155	7.7	10	242	0.52	0.33	0.62	1.1	171	26.8	0.77	0.67×10^8	0.51×10^8	5.7
		190	9.1		286	0.87	0.58	0.60	0.7	202		0.85	0.73×10^8	0.62×10^8	3.9
		200	10.1		317	0.52	0.33	0.64	1.1	225		0.77	1.49×10^8	1.15×10^8	6.4
		235	12.5		393	0.87	0.52	0.67	0.8	278		0.86	1.95×10^8	1.68×10^8	5.9
		410	14.5		456	1.05	0.94	0.44	0.3	322		0.92	1.71×10^8	1.57×10^8	1.2
Lagenorhynchus obliquidens	204	554	3.9	60	735	0.28	0.21	0.40	1.5	520	466	0.77	5.24×10^{10}	4.03×10^{10}	10.2

Zweifel 1971). Therefore, a typical value for L will be assumed for *Euthynnus* of 50 cm.

Measurements of other factors, particularly S_h, have not been made, but can be estimated from aspect ratio. The aspect ratio of the caudal fin of scombrids like *Euthynnus* was found to be 6.8 by Fierstine and Walters (1968) (see Nursall 1958a). Span takes values of about 0.27 L (here 13.5 cm), giving a mean chord of 2.0 cm and area of 26.8 cm² from Equation 37. Similarly, the span and mean chord are shown as 52.1 and 9.0 cm (Lang 1966) for the *Lagenorhynchus* used by Lang and Daybell (1963). This gives an aspect ratio of 5.8, and area of 466 cm².

Amplitudes of caudal fin lateral movements for scombrids are 0.2 L, and independent of size (Hunter and Zweifel 1971). This will be taken here for *Euthynnus*.

Various measured and estimated values for kinematics, etc., for the two species are shown in Table 17, with η_p and thrust power values based on C_T from Fig. 51. Theoretical frictional drag power data and calculations are given in Table 18. Comparing these two sets, the thrust power from Lighthill's model was on average 4.6 times higher than the theoretical frictional drag power for *Euthynnus* and 10.2 times higher for *Lagenorhynchus*. In the former, a large proportion of the difference may be explained on the basis of drag calculations made by Brown and Muir (1970) for this species. The frictional drag at a speed of 1.5 L/s was 41% of the total theoretical drag, and taking this into account would decrease the difference between thrust power for the reaction model and theoretical drag to 1.8 times. Further

reduction in this difference would accrue if gill drag as a percentage of the total drag increased at higher speeds as suggested by Brown and Muir (1970).

The high value obtained for *Lagenorhynchus* can be partly explained in terms of extra drag when swimming near the surface. The most important point is that the models are still preliminary in form.

Discussion

Results of all calculations can be compared by calculating a nondimensional drag coefficient, related to the thrust power, which must equal total drag power. This drag coefficient, C_D, is given by

$$C_D = \frac{\text{thrust power}}{\frac{1}{2} \rho \, S_w \, U^3} \qquad (75)$$

and is dimensionally similar to the frictional and dead drag coefficients. C_D is higher than theoretical frictional-drag coefficients, except for two low values for resistive forces in Taylor's (1952) model (Fig. 52). Also, resistive forces give high C_D for the anguilliform mode compared to reactive forces, but the opposite is the case for subcarangiform propulsion. For carangiform with lunate tail propulsion, both models give similar results, but these are in preliminary form.

A second approach to the results of calculations is to compare thrust power values from models with possible power output from muscle systems (Fig. 53). Values for muscle power output for fish and cetaceans at various activity levels were taken from Bainbridge (1963) (Chapter 6

TABLE 18. Calculations for theoretical frictional drag for *Euthynnus affinis* and *Lagenorhynchus obliquidens* in Table 17.

Species	L (cm)	U (cm/s)	R_L (1)	$C_{f \, turb}$ (1)	S_w^a (cm²)	Theoretical frictional drag power (erg/s)
Euthynnus affinis	50	155	7.75×10^5	0.0048	1,000	0.89×10^7
		190	9.50×10^5	0.0046		1.58×10^7
		200	1.00×10^6	0.0045		1.80×10^7
		235	1.18×10^6	0.0044		2.86×10^7
		410	2.05×10^6	0.0039		13.4×10^7
Lagenorhynchus obliquidens	204	554	1.13×10^7	0.0028	16,646	3.96×10^9

[a]Assumes $S_w = 0.4 \cdot L^2$.
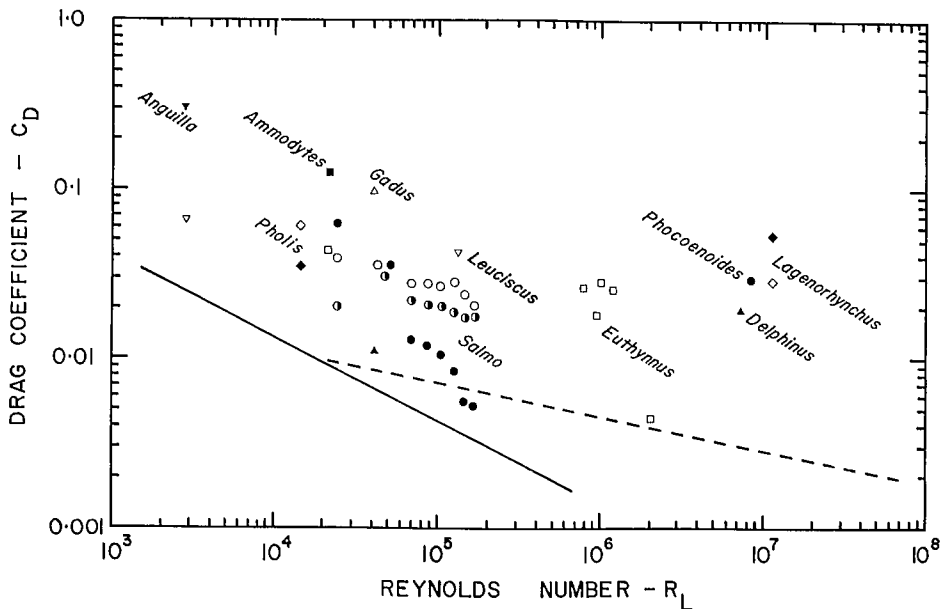
FIG. 52. Relation between drag coefficient, C_D, and Reynolds Number, R_L. Drag coefficient was calculated for thrust power values given by hydromechanical models. Open symbols are resistive models, closed symbols reaction models, and half closed symbols measured values. Symbols are identified by generic names. References and further data are given in text, and Table 8, 10, 12, 13, 15, 16, and 17. Theoretical frictional drag coefficients are shown as functions of Reynolds Number for laminar (solid line) and turbulent (broken line) boundary-layer flow.

and Table 19). Making general assumptions that mass = 0.01 L^3 and 0.001 L^3 for fusiform and eellike fish, respectively (Bainbridge 1961; Gray 1936a), that cruising muscle represents 0.025 body mass and sprint muscle 0.5 body mass, and η_p is 0.75, the thrust power output of the muscles can, be estimated. Only half the available muscle works at any instant.

Most estimates are probably conservative. For example, dogfish myotomes contain 18% red (cruising) muscle (Bone 1966), rainbow trout 17% (Webb 1970, 1971a), and haddock up to 8% (Fraser et al. 1961). Many fish contain more than 50% total muscle (Bainbridge 1962). η_p will probably be greater than 0.75. No direct data are available for fish muscle power outputs, but from Fig. 47 those selected are of the right order.

Thrust power calculated from the various models was within the capacity of estimated muscle power output (Fig. 53). It is not certain in most cases if recorded speeds were sprint or cruising speeds. For most carangiform swimmers, including those with semilunate tail, thrust power was of the order of estimated cruising muscle power output. For the anguilliform mode, speeds would probably require sprint and cruise muscle, as would *Delphinus* and *Lagenorhynchus*, swimming in the carangiform mode with lunate tail. In general, the only difficulty expected in finding sufficient muscle power to meet thrust requirements would be for *Lagenorhynchus*, should it try to swim much faster than the observed 2.5 L/s. This calculation was based on a single tail-beat cycle of a porpoise accelerating slightly.

The acceptance of any model from comparisons like those in Fig. 53 involves a tautology, because both thrust power and muscle power are estimates and each has been used to estimate the other. Nevertheless, it indicates that the models are "reasonable" and encourages wider use. Much of the discussion of results from the models emphasized inadequacies in the biological data rather than in the models themselves.

It is necessary to summarize recommendations for use of various models. Following

100
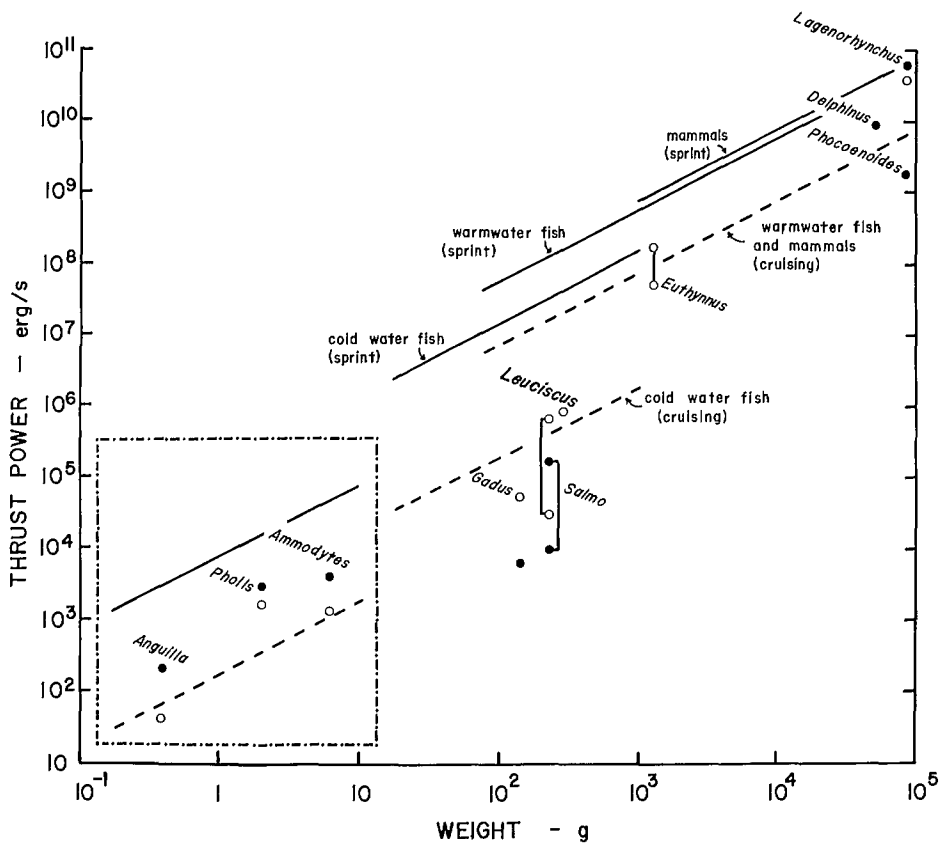
FIG. 53. A comparison between thrust power given by various models of fish locomotion, and estimated propulsive muscle power output. Further explanation is given in text. Open symbols are resistive models; closed symbols reaction models, and half-closed symbols measured values.

Lighthill (1970), no truly applicable model for anguilliform propulsion is available. A model combining resistive and reactive approaches is required, which would be difficult to formulate. Otherwise, of the models available, the most suitable is probably that of Lighthill (1960, 1969, 1970) as it makes fewer assumptions than other models and is easiest to apply to real fish data. For carangiform propulsion, excluding the lunate tail variant, the reactive model proposed by Lighthill (1969, 1970) appears most suitable, modified for large amplitude motions after Lighthill (1971). Carangiform propulsion with lunate tail, in preliminary form at present, obviously requires further refinement. Otherwise, Lighthill's (1970) is most suitable for general application (see also Newman 1973; Newman and Wu 1973; Wu 1973a, b, c; Wu and Newman 1972).

Acceleration

Introduction

Acceleration, and closely related high-speed maneuver, have been virtually neglected by experimental biologists and hydrodynamicists. Research effort has concentrated on cruising swimming, with the exception of Bainbridge's studies on sprint speeds (1958, 1960, 1962) and occasional reports of acceleration rates (Gero 1952; Gray 1953a; Fierstine and Walters 1968; Hertel 1966; Weihs 1973a). The latter suggested a fairly constant acceleration of the order of 40–50 m/s² for fish ranging from trout to tuna.

Most fish include acceleration phenomena as an integral part of their normal locomotor activity. This is reflected by the muscular system when twitch (fast) muscle typically takes up the larger portion of the axial body-muscle mass

101

(Bone 1966; Love 1970). Acceleration and fast maneuver are essential components of predator approach and/or avoidance behavior, including fishing nets. Clearly this is an area requiring much research.

Kinematics

Weihs (1973a) analyzed qualitatively and quantitatively the mechanics of rapid starting (high speed acceleration) in trout and pike, as an extension of his analysis of high speed maneuver (Weihs 1972). Three stages are identified in acceleration.

Preparatory phase — The fish changes its configuration from stretched straight to L-shaped by moving the tail laterally so it becomes approximately perpendicular to the body. This takes approximately 0.075 s. Yawing forces are obviously set up by movement of the tail so that the anterior portion of the fish is also rotated about the center of mass.

Propulsive stroke — The caudal fin moves laterally at high speed, subtending a small angle of attack to its direction of motion, and reaching a final position similar to, but the mirror-image of, the original position. The trailing edge moves perpendicularly to the original axis of the fish. The fish initially accelerates at some angle to the original axis because of the rotation of the anterior of the body in the preparatory stage. This takes approximately 0.125 s.

Weihs observed that trout used pectoral fins to return the direction of acceleration to the original axis of the fish. Control of this form will probably be general among fish, as rapid starting is presumably used to reach some objective in minimum time. The propulsive stroke may be repeated several times.

Final phase — Fish behavior is variable in this phase. Fish may continue in a glide with the body stretched straight as in the "nage filée" considered by Houssay (1912) to be the characteristic form of fish swimming. Alternatively, the final stage may be continued swimming in some other propulsion pattern. Unless control movements have been made, the axis of motion in the final phase will continue to subtend some angle to the original axis of the fish.

Weihs also set out a hydromechanical model consistent with the observed kinematics. Numerical solutions gave accelerations in reasonable agreement with observed rates.

Power requirements

An attempt is made to estimate the costs of acceleration for fish of various sizes accelerating at various rates to various final speeds. A simplified model will be used, based on thrust/drag predictions for hydromechanical models extrapolated to accelerating fish on the basis of certain assumptions.

The principal assumptions are that acceleration, a, is constant, and that frictional drag at any instant can be calculated from standard hydrodynamic equations

$$D = \tfrac{1}{2} \rho \, S_w \, U^2 \, C_D \tag{76}$$

The value C_D can be modified to take into account the drag expected for a swimming fish, as predicted by the models discussed above. The ratio between calculated thrust (predicted by application of Lighthill's models to fish) and the frictional drag for an equivalent flat plate was 4.94 for fish swimming in subcarangiform modes. Most data is available for this mode, and acceleration will be considered for a hypothetical fish, like the trout, swimming in this mode.

Equation 76 can then be rewritten for a swimming fish

$$D = \tfrac{1}{2} \rho \, S_w \, U^2 \, (4.94 \, C_D) \tag{77}$$

The boundary layer is most likely to be turbulent so that

$$D = \tfrac{1}{2} \rho \, S_w \, U^2 \left[0.35 \left(\frac{L \, U}{v} \right)^{-0.2} \right] \tag{78}$$

and grouping constants for a given fish

$$D = K_1 \, U^{1.8} \tag{79}$$

The work done against drag, W_D, for uniform acceleration from a speed $U_O = 0$ to $U = U$ is given by

$$W_D = K_1 \int_o^x U^{1.8} \, dx \tag{80}$$

102

when x is the distance covered in acceleration, given by standard Newtonian mechanics from

$$U^2 = U_o^2 + 2\,a\,x \qquad (81)$$

Then

$$W_D = K_1 \int_o^x \left[U_o^2 + (2\,a\,x)^{0.9} \right] dx \qquad (82)$$

Equation 82 gives the work done against hydrodynamic drag. This is only part of the drag as work is also done in accelerating the fish mass

plus added mass. This is the kinetic energy W_K, given by

$$W_K = 1.2\,M\,\tfrac{1}{2}\,(U^2 - U_o^2) \qquad (83)$$

when added mass is taken as 0.2 body mass, M.

Then the total work done, W, in accelerating the fish is given by

$$W = K_1 \int_o^x \left[U_o^2 + (2\,a\,x)^{0.9} \right] dx + $$

$$0.6\,M\,(U^2 - U_o^2) \qquad (84)$$
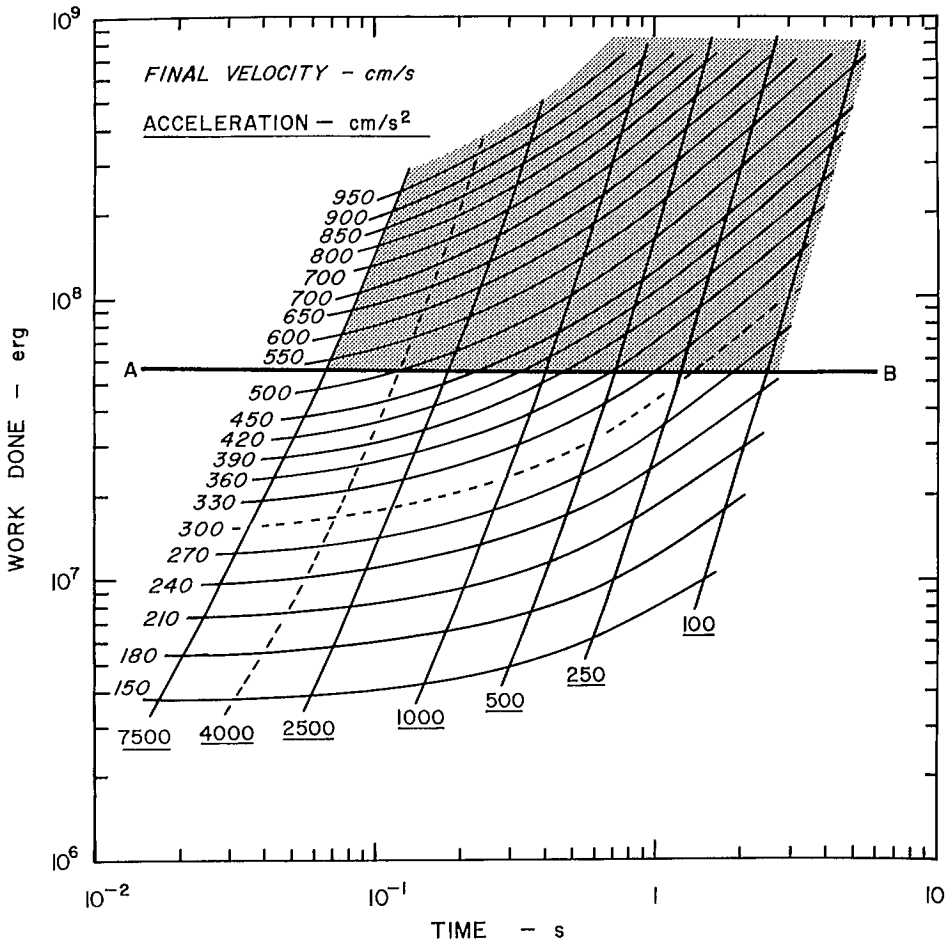
Fig. 54. Work done in accelerating from rest at various constant rates to various final speeds shown as a function of time to reach final speed. Isopleths are shown for acceleration rates and final speeds. Line AB indicates the limit of expected muscle energy expenditure, the shaded area above this line delimiting speeds and acceleration combinations outside the capabilities of the hypothetical fish.

103

The work done in accelerating at various a to various U is shown in Fig. 54 for a hypothetical fish with L = 30 cm, S_w = 360 cm², m = 270 g, and v = 10^{-2} poise.

Calculations indicate that the faster a fish accelerates the lower the total energy expended to reach a given speed. This is because the distance covered in reaching a given speed is relatively greater at lower rates of acceleration. Furthermore, the greater the acceleration the shorter the time required to reach a given speed. These two points are of obvious selective advantage.

The isopleths for an acceleration rate of 40 m/s² and final speed of 300 cm/s are shown by a broken line. These are typical values for a trout of the dimensions used here (Bainbridge 1958; Weihs 1973b), and intersect in the area of the figure when energy expenditure for this acceleration rate approaches minimal values, and the speed is reached in a short time. The time is about 0.1 s, and reasonably similar to that found by Weihs (1973b) for the acceleration propulsion stroke of a trout 33 cm long.

Included in Fig. 54 is an estimate of muscle power expenditure for the fish, calculated similarly to values shown in Fig. 53. It assumes an exponential decrease in work done per unit time for the muscle. Fish could reach much higher speeds at the end of acceleration than are generally accepted. Obviously, they could only be maintained for short periods of time. The performance of fish for periods of less than a second have not been studied. According to Fig. 54, high speeds would be difficult to attain at low acceleration rates.

The effect of size on work done in accelerating at 40 m/s² to various specific swimming speeds is shown in Fig. 55. Dimensions are assumed isometric, so that S_w = 0.4 L² and m = 0.01 L³. The broken line shows the limit of expected muscle energy available. As with other performance levels, smaller fish are capable of higher specific swimming speeds, although absolute speeds reached would increase with increasing size. Maximum speeds suggested by the calcula-

tions greatly exceed the generally accepted values (10 L/s "rule of thumb"). The cost of reaching a given specific swimming speed also increases with size.

The above model is of course greatly simplified. Absolute values for work or time, etc., as shown in Fig. 54, 55 cannot be used without validation. The shape of figures is probably of greatest importance for this will be relatively unchanged by gross errors in any of the assumptions. The general trend for low costs at high acceleration rates, reaching high speeds in short times, would still be found and the scanty data for fish suggest this is realistic. Ideally, the above figures should be used as the framework in which research may be oriented.
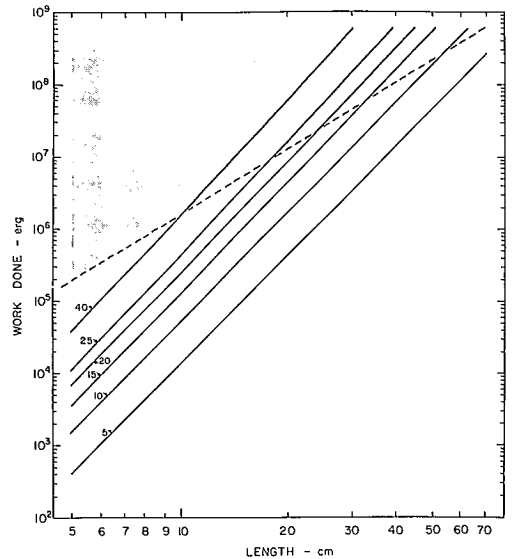
FIG. 55. Work done in accelerating at 40 m/s² to various final specific swimming speeds shown as a function of length. Broken line indicates limit of expected muscle power output, the shaded area delimiting specific speeds outside the capabilities of hypothetical fish.

Summary

The main points from Part 1 pertinent to energetics studies are in Chapter 4 and 5, following the discussion of hydrodynamics principles and reviews of kinematics and performance. It is concluded (in Chapter 4) that theoretical drag calculations and dead-drag measurements are not valid for the calculation of power requirements of swimming fish and cetaceans, with a few exceptions. The validity of the rigid-body analogy is denied because movements of swimming fish will greatly modify flow with consequent substantial drag increments relative to an equivalent rigid body.

Alternative methods of calculating thrust (equal to drag) and power required are explored in Chapter 5. These require the application of hydromechanical models which predict thrust developed by propulsive movements. It is concluded that the inviscid models formulated by Lighthill (1960, 1969, 1970, 1971), hereafter referred to as Lighthill's model, are most suitable for application to biological situations at the present time. Predictions of power required in swimming from Lighthill's model agree with the expected muscle power available. These values exceed those for equivalent rigid bodies by 3 to 5 times.

PART 2

Chapter 6 — Metabolism and Energy Distribution

Introduction

The propulsive power system of fish can be considered as a "black box" with various energy inputs and outputs. Propulsive power output is the rate of expenditure of only one energy output. In practice, the propulsive system is comprised of several components (Fig. 56). Some may be shown
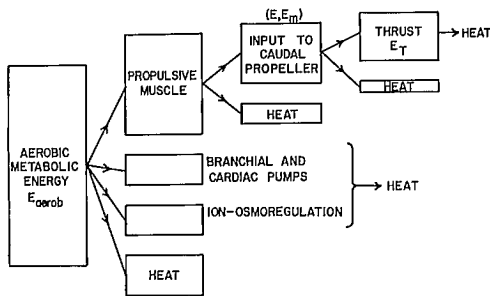
FIG. 56. Diagrammatic representation of energy distribution to various components involved in the propulsion energy system, or "black box," at sustained swimming speeds. Size of the rectangles represents approximate distribution proportions of an initial 100 units of energy input to the system.

as serial components within which various energy transformations are accomplished in generating thrust. Other components may be visualized as arranged in parallel (e.g., support systems) and are required for, or are consequences of, continuous operation of propulsive muscles. The "black box" analogy puts the various components in perspective, and at the same time shows distribution and energy flow through the system.

Characterization of the propulsive system requires quantification of the various energy inputs and outputs, with the object of relating these in terms of conversion efficiencies. Such efficiencies must be known before locomotory energetics may be usefully applied outside laboratory situations. This chapter considers the metabolic input to the propulsive system and the distribution of metabolic energy within that system, preparatory to a discussion of energetic efficiency in the subsequent chapter.

The question of metabolism is an immense subject in its own right. Certain aspects have been extensively studied (e.g., oxygen consumption rates), others have only recently become amenable to research (e.g., energy required in circulating blood), whereas such areas as the precise nature of energy distribution remains largely speculative.

This chapter is orientated primarily to non-biologists. Metabolism and energy distribution are not considered in full detail, as discussed in the introduction to this work.

Production of Biological Energy

Metabolic pathways

Energy is released by a series of chemical reactions, often referred to as intermediary or cellular metabolism, from one or more basic body fuels (fat, carbohydrate, and protein). Details of these chemical reactions and energy changes are given in standard texts on biochemistry (e.g., Conn and Stumpf 1963), and have been reviewed by Hochachka (1969) for fish. Only the major energetic pathways will be considered.

Two principal energetic pathways may be identified: (1) aerobic metabolism and (2) anaerobic metabolism. The former requires oxygen for complete oxidation of the fuel, whereas the latter can progress in the absence of oxygen, involving incomplete oxidation. Anaerobic metabolism is often referred to as glycolysis, as the carbohydrates glucose or glycogen are the most common sources of energy.

Both pathways generate adenosine triphosphate (ATP) directly or by coupled reactions. ATP is the immediate cellular source of energy for most biological functions. Hydrolysis of ATP releases approximately 12 kcal/mol (5×10^{12} erg/mol). Fraser et al. (1966) found that cod muscle contained approximately 20 μmol ATP/g, equivalent to 10^8 erg/g if completely hydrolyzed.

Aerobic and anaerobic pathways generate different amounts of ATP from the same unit potential energy source. For example, 1 mol of glycogen could generate 38 mol ATP/mol glycogen in aerobic metabolism, with carbon

109

dioxide and water as the end products. Glycolysis would generate 3 mol ATP/mol glycogen, with lactic acid as the main end product.

Aerobic metabolism is dependent on the continuous function of cardiovascular and ventilatory support systems for the uptake of oxygen and removal of waste products. The various reactants have high diffusion coefficients in the tissues, and are generated in small amounts in proportion to the energy released. They do not accumulate in the tissues. Aerobic metabolism is the most important metabolic pathway; in normal activity it is generally limited to long-term energy requirements.

Anaerobic metabolism does not depend immediately on physiological support systems, although ultimately aerobic metabolism is responsible for metabolizing lactic acid, either reconstituting it to glycogen or further metabolizing it to carbon dioxide or water. Anaerobic metabolism can generate large amounts of energy rapidly, to supply demands of short-term bursts of activity. Lactic acid has a relatively low diffusion coefficient in tissues compared to the products of aerobic metabolism, and tends to be accumulated. Tissues in the fish propulsion system that function mainly anaerobically (white muscle) require large amounts of energy. As the products of glycolysis tend to be toxic in high enough concentrations, these factors in combination may set a limit to the duration for which glycolysis can operate.

Measurement of Biological Energy

Basic considerations in the measurement of biological energy released by metabolism have been extensively discussed, particularly for domestic animals (Brody 1945; Kleiber 1961); application of these principles to fish have been summarized by Brett (1962, 1973; Krueger et al. 1968; Phillips 1969).

Metabolic energy expenditure of fish is measured by one of two methods: bomb calorimetry or indirect calorimetry.

Bomb calorimetry

Metabolic rate of terrestial animals can be measured from rates of heat production and loss. The most similar method for fish is to measure net caloric (heat) content changes over a given period of time from control samples (at zero time) and exercised experimental samples, each completely combusted in a calorimeter. This method has not been used in locomotion studies.

Indirect calorimetry

Indirect calorimetry is based on calorific determinations of the heats of combustion of various fuels. Energy released by metabolism is calculated indirectly from the rates at which fuels are used or the rate of oxygen consumed in their combustion. Alternatively energy expenditure may be calculated from the rate of production of such components as carbon dioxide, ammonia, and lactic acid. Indirect calorimetry has been widely applied to locomotion studies and will be considered in some detail.

ENERGY EXPENDITURE FROM BODY FUEL USE

Energy expenditure at any level of activity can be computed from the rate of depletion of body fuels. The three body fuels take heat of combustion values of the order of 9.45 kcal/mol (4.0×10^{11} erg/mol) for a typical fat, 5.65 kcal/mol (2.4×10^{11} erg/mol) for a typical protein, and 4.1 kcal/mol (1.7×10^{11} erg/mol) for a typical carbohydrate. Actual values vary to a small extent depending on the particular chemical compounds of fuel used. For fats and carbohydrates, the heats of combustion are equal to the total energy liberated by aerobic metabolism, that is, the physiological equivalents are equal to the total physical heats of combustion as the fuels are biologically oxidized to carbon dioxide and water. Proteins contain nitrogen which is transformed and excreted mainly as ammonia (60–70%) and other nitrogenous compounds such as urea and trimethylamine oxide. Proteins are incompletely oxidized in vivo, and the physiological equivalent is lower than the heat of combustion, taking values of the order of 4.8 kcal/g (2.0×10^{11} erg/g) or 85% of the potential energy (Brody 1945; Kleiber 1961; Brett 1973).

Energy expenditure of sockeye salmon has been computed from fuel depletion at known sustained and prolonged activity levels by Kreuger et al. (1968) and Brett (1973). Total fuel usage of several species of salmon during upstream migration has also been measured (Idler and Clemens 1959; Osborne 1961), but details of performance levels are unknown. Maximum glycogen usage after strenuous activity has been measured, mainly for salmonids (e.g., Black et al. 1966; Stevens and Black 1966; Wendt 1965, 1967) although not in relation to any defined activity level. Glycogen depletion has been measured at sustained and prolonged speeds for *Gadus morhua*

by Beamish (1968), and for *Carassius carassius* by Johnston and Goldspink (1973a, b, c). Variance in glycogen values for control and experimental groups was too high for these data to be used in calculating energy expenditure (Johnston and Goldspink 1973a).

In theory, accurate calculation of energy expenditure from depletion of body fuels requires additional information on particular metabolic pathways. This applies especially to glycogen which is used as the principal fuel for glycolysis (MacLeod et al. 1963; Black et al. 1960; Black et al. 1961; Stevens and Black 1966), as well as being a fuel for aerobic metabolism (Beamish 1968). In practice the relation between metabolic pathways and activity levels is probably sufficiently accurate at sustained and burst activity levels that energy contributions from one of the paths may be neglected. For example, at burst activity levels metabolism is mainly anaerobic and contributions from other sources may be neglected as insignificant (Miller et al. 1959; Black et al. 1960; Black et al. 1962; Connor et al. 1964; Beamish 1968).

At intermediate and prolonged activity levels the contribution of various metabolic pathways to the total energy budget is more complex. *Gadus morhua* and *Carassius carassius* apparently use glycogen for both aerobic and anaerobic metabolism (Beamish 1968; Johnston and Goldspink 1973a, b, c). Salmonids apparently use glycogen almost exclusively for anaerobic metabolism, and fat and protein for aerobic metabolism (Idler and Clemens 1959; Miller et al. 1959; Black et al. 1960, 1962). The situation for mackerel, *Trachurus symmetricus*, is also complex (Pritchard et al. 1971). Clearly complete energy budgeting using indirect calorimetry for prolonged speeds would require more complete information on various aspects of metabolic pathways employed and their relative contributions to energy expenditure. It seems probable that such an analysis would lack accuracy, and be sufficiently time-consuming to be of uncertain value. As experimental studies would require sacrificing the fish in any case, it is considered that energy expenditure at these levels could be more profitably explored by bomb calorimetry.

OXYGEN CONSUMPTION AND CARBON DIOXIDE PRODUCTION

Oxygen consumption is the most commonly used indirect method of estimating energy expenditure mainly for sustained and prolonged activity levels (Fry 1971). Calorific equivalents for energy expended when a measured amount of oxygen is respired (oxycalorific equivalents) depend on the fuel being oxidized; equivalents take values of the order of 3.5 cal/mg O_2 (1.47×10^8 erg/mg O_2) for a typical fat, 3.22 cal/mg O_2 (1.35×10^8 erg/mg O_2) for a typical carbohydrate, and 3.2 cal/mg O_2 (1.35×10^8 erg/mg O_2) for a typical protein.

These oxycalorific equivalents were initially applied to fish on the basis of comparative physiological equivalents for mammals. Kreuger et al. (1968), in discussing their application to fish, found that the energy expenditure computed from oxygen consumption data was much lower than that computed from fuel consumption based on fat metabolism. This work cast doubt on the application of mammalian derived oxycalorific equivalents to fish. Brett (1973), in a more detailed study of the question, has shown acceptable agreement between the energy expenditure computed from oxygen consumption and that for fuel depletion, allowing for a small amount of error from slight anaerobic metabolism. Brett was able to show that the conclusion of large differences made by Kreuger et al. (1968) was based on several false premises.

Measurement of oxygen consumption alone is insufficient to precisely characterize metabolic rate in terms of energy expenditure. Different fuels require differing amounts of oxygen for complete combustion and produce different amounts of carbon dioxide per unit mass metabolized. As a result the ratio of carbon dioxide produced to oxygen consumed, or the respiratory quotient, RQ, varies with the three fuels and aids in identifying the fuel used. The RQ takes values of 1.0 for carbohydrate, 0.8 for fats, and 0.7 for proteins. In practice, RQ varies fairly extensively with the chemical species of fuel used, particularly fats when the amount of oxygen consumed depends on the degree of saturation of the molecule. In addition, as all fuels may be used synchronously, RQ values less than 1.0 or greater than 0.7 cannot fully identify the proportions of fuel used. An improvement in the accuracy of using RQ may be achieved if the rate of excretion of nitrogenous materials is also measured. Then the amount of protein metabolized can be estimated separately (Winberg 1956; Brett 1962, 1973; Kutty 1972).

These complicating factors suggest that extremely comprehensive data are required to calculate energy expenditure by means of indirect calorimetry from the proportions of respiratory

111

gases used and excreted. Consequently, in practice a mean oxycalorific equivalent is frequently taken; Brett (1973) used 3.36 cal/mg O_2 (1.41 erg/mg O_2) for sockeye salmon, with an assumed RQ of 0.8. The error in using such a mean value for the oxycalorific equivalent of oxygen would be approximately 4% if all protein were used. Measurements of RQ for *Salmo gairdneri* and *Tilapia mossambica* (Kutty 1968, 1972) at average sustained swimming speeds, and *Carassius auratus* at low sustained speeds (Kutty 1968) gave values between 0.8 and 0.9. Proximate analysis of the body constituents of migrating salmon show that mainly fat was used by the fish (Idler and Clemens 1959). These observations indicate that the error in assuming a mean oxycalorific equivalent would be substantially lower than the 4% maximum. Winberg (1956) considered the use of indirect oxygen calorimetry alone gave an accuracy of $\pm$ 1.5% for a normal body fuel usage.

Use of oxygen consumption measurements is also subject to a further possible source of error if some part of the energy budget is made up by anaerobic metabolism. Anaerobic metabolic activity can be detected when the RQ exceeds 1.0, i.e., when more carbon dioxide is produced than oxygen consumed.

Anaerobic energy contributions are usually most important at high activity levels (prolonged and burst swimming) and stress conditions (Brett 1962, 1973; Fry 1971; Kutty 1968). There are certain exceptions, notably the goldfish (Hochachka and Somero 1971; Smit et al. 1971). This fish can sustain RQ values of between 2 and 3 for long periods of time, and operate anaerobically under sustained activity conditions (Kutty 1968). Lactic acid measurements in the muscle used for sustained activity in the tunalike fish *Trachurus symmetricus* have also shown elevated levels in comparison with those in other fish (Pritchard et al. 1971). This may be a consequence of the circulatory heat-exchanger in these fish which is designed to conserve heat in the muscles (Barrett and Hester 1964; Carey and Teal 1969a; Carey and Lawson 1973). The commonly used increasing velocity test for studying power-performance relations for fish usually also neglects anaerobic energy contributions to the total budget. These are expected at each speed increment and at prolonged speeds. In practice it is likely that the energy from this source is small enough to neglect (Webb 1971b).

Oxygen consumption data have been used to estimate the amount of anaerobic metabolism that has occurred. Lactic acid metabolism ultimately depends on oxygen, so that a period of strenuous activity is followed by elevated oxygen consumption levels. As a result an animal accrues an oxygen debt during that strenuous activity, which is subsequently paid back.

The use of oxygen debt repayment to measure the amount of anaerobic metabolism that has occurred is not particularly satisfactory. Elevated oxygen consumption persists for approximately 5 h after exhaustion of sockeye salmon (Brett 1964) and elevated lactic acid levels persist for approximately 8 h (Black et al. 1960, 1962), implying poor agreement between the oxygen consumption and magnitude of the real debt. In addition, some lactic acid may be excreted, although this amount is undoubtedly small (A. J. Mearns personal communication). Of greater importance may be lactic acid produced during recovery, for example as a result of hyperventilation required to obtain the additional oxygen to repay the initial oxygen debt. Factors such as these represent sources of substantial error in estimating anaerobic energy contributions from oxygen debt measurements.

LACTIC ACID PRODUCTION

The amount of lactic acid produced during burst activity levels represents a possible factor for an indirect estimate of the energy released by glycolysis. Extensive studies of lactic acid production have been made mainly by Black and his collaborators for salmonids and by Beamish (1968) for cod. These studies have been concerned with the time course of lactate metabolism rather than the relations between specific amounts of lactic acid produced during periods of activity at known levels, and these data are of little use for energetics analysis.

Lactic acid production alone is insufficient to calculate energy released by glycolysis, because lactic acid is in equilibrium with a second acid, pyruvic acid, at a junction in the metabolic pathways of glycolysis and aerobic metabolism. Pyruvic acid feeds into the aerobic metabolic pathway, and both increased aerobic and anaerobic metabolism are expected to elevate lactic and pyruvic acid levels. Aerobic metabolism is expected to elevate pyruvic acid levels by an amount similar to lactic acid, whereas anaerobic metabolism would elevate lactic acid levels far in excess of pyruvic acid levels. Therefore, it would be necessary to estimate anaerobic energy expenditure from the amount of lactic acid

112

produced in excess of pyruvic acid (Huckabee 1958). Measurements in sufficient detail, and at specified activity levels, have not been made for fish.

Measurement of energy released by anaerobic metabolism from lactic acid production usually entails sacrificing the fish. Cannulation of the vascular system and serial measurement of blood lactic acid may be a suitable substitute, but lactic acid appears in the blood over long periods of time following strenuous activity, so estimates of total production would be difficult. Also, metabolism of lactic acid in situ, excretion, production by hyperventilation, etc., may be sufficient to further confound such measurements.

SUMMARY

Indirect calorimetry using oxygen consumption data remains the most valuable method of measuring energy expenditure for most fish at sustained and lower prolonged activity levels. Insufficient data are available to make useful generalizations concerning other methods, applying largely to higher activity levels. Because of the usual necessity to sacrifice the fish, and complexities of analysis, bomb calorimetry is probably a more acceptable method of measuring energy expenditure than indirect methods at higher activity levels.

Metabolic Rates

Aerobic metabolism

OXYGEN CONSUMPTION AND SWIMMING SPEED

Aerobic metabolic rates are measured in terms of oxygen consumption, sometimes supplemented by RQ data. Brett (1964) indicated that the relation between oxygen consumption, Q_{O_2}, and swimming speed typically took the form

$$Q_{O_2} = a\, e^{bU} \qquad (85)$$

when a and b are constants. Q_{O_2} is commonly measured in mg O_2/kg per h.

This general relation has been confirmed for all species studied swimming in body and caudal fin modes (e.g. Brett and Sutherland 1965; Muir et al. 1965; Smit 1965; Hart 1968; Rao 1968; and others; see Fry 1971), and for *Cymatogaster aggregata* swimming in the labriform mode (P. W. Webb unpublished data).

METABOLIC LEVELS

Various levels of metabolic rates are commonly defined from the relation between oxygen consumption and swimming speed. The two principal levels are identified as standard and active rates, at zero and maximum sustained swimming speeds respectively. Standard metabolic rate is defined as the rate when the fish is at complete rest; it is calculated by extrapolating the Q_{O_2}–U relation (semilog transformation) to "zero swimming speed." Active metabolic rate is defined as the metabolic rate for maximum sustained activity, although more commonly it is calculated as the metabolic rate at U_{crit}. As such, the active rate represents maximum oxygen consumption at some specified prolonged activity level (see Chapter 3). The anaerobic contribution to metabolic rate under these circumstances is neglected, but since Q_{O_2} and U_{crit} values are measured from swimming periods of the order of 60 min at each test speed, that is probably not a serious omission (Webb 1971b).

The determined difference between active and standard rates is the scope for activity (Fry 1947). It represents the amount of oxygen (and indirectly the power) available for propulsion, in excess of that expended in maintaining the system.

Metabolic levels between active and standard metabolism are variously referred to as routine or intermediate rates. The former will be employed. Routine metabolic rates apply to "normal activity without stress" (Brett 1972).

METABOLIC RATES

Magnitudes of metabolic rates are extremely variable, depending on environmental factors and interspecific differences. Effects of environmental factors on metabolic rates have recently been reviewed by Fry (1971). In general, factors that reduce swimming performance (Chapter 3) also affect metabolic rates by elevating standard metabolism, and/or reducing active metabolism, or by elevating anaerobic metabolism (Dickson and Kramer 1971). In each case, scope for activity and swimming performance are invariably reduced. It is imperative that experimental work should take these various metabolic responses into account so that spurious data are avoided (Brett 1962, 1970).

Interspecific differences in metabolic rates also represent a substantial source of variation. Generalizations are difficult to formulate as too few species have been studied in sufficient detail. Variations in standard and active rates of four

113
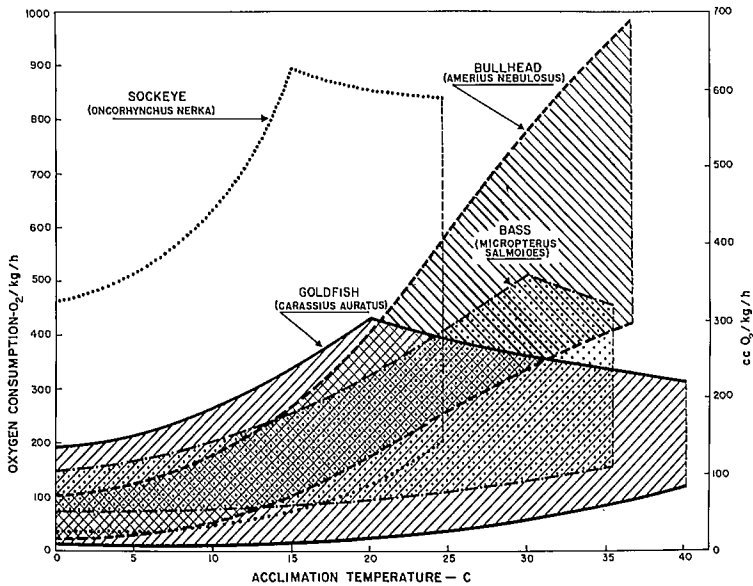
FIG. 57. Rates of oxygen consumption as a function of temperature for four active fish. Active and standard metabolic rates are upper and lower lines for each species respectively. Lethal temperature for each species is the vertical broken lines. (From Brett 1972) (Reproduced with permission of North Holland Publishing Co., Amsterdam, Holland)

common species are shown in Fig. 57 as a function of temperature, probably the most important factor affecting metabolic rates in the presence of adequate oxygen. At a given temperature, active and standard rates may vary between species by a factor of up to 5 times.

All fish in Fig. 57 are active fish. Sluggish fish have not been widely studied, but appear capable of substantially lower metabolic rates (Brett 1972).

It is clear that in using oxygen consumption data to calculate energy expenditure, consumption rates should be measured directly for the particular experimental conditions. Furthermore, in energetics studies, oxygen consumption data and hydrodynamic data from different sources should be used with caution (Chapter 7).

Anaerobic metabolism — energy released

Anaerobic metabolic rates have not been measured for fish at specific activity levels. Most studies have measured the total glycolytic activity of fish arbitrarily exercised to exhaustion. Mainly salmonids have been used. By pooling the salmonid data (Miller et al. 1959; Black et al. 1960; Black et al. 1962; Miller and Miller 1962; Wendt

1965, 1967) it was found that when fish were exercised to exhaustion approximately 0.19 g glycogen/100 g muscle was used, equivalent to 1.59×10^{11} erg/100 g muscle.

The Muscle System

Red and white muscle

Functional characteristics rather than structural characteristics of muscle components of the propulsive system are of greater importance in considering energetics. Axial (myotomal) muscle structures have been discussed by Nursall (1956) and Alexander (1967, 1968, 1969).

The muscle system of fish is mainly comprised of two functional groups. These are designated red and white muscle because of their characteristic coloration in many fish. The two types are usually found in discrete blocks, as shown for *Scyliorhinus* in Fig. 58. Red muscle is usually superficial, and forms a relatively small portion of the myotome (Boddeke et al. 1959). Some fish have an intermediate muscle system, either as a thin sheet separating red and white muscle blocks as in *Scyliorhinus* (Bone 1966) or as scattered fibers among the white muscle as in

114
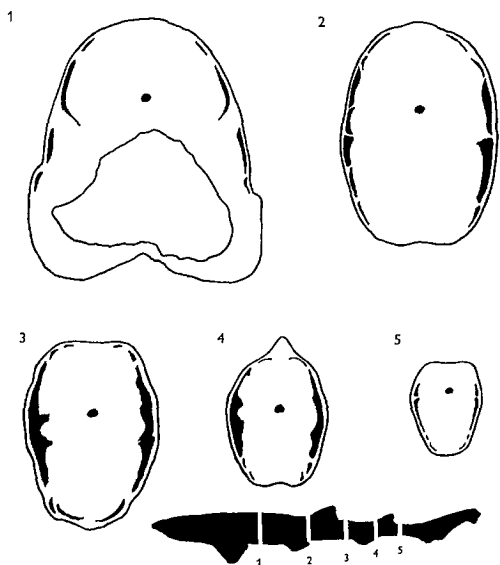
FIG. 58. Distribution of red and white muscle at several positions along the body of *Scyliorhinus canicula*. Red muscle is the black areas. Central black circle is the vertebral column. (From Bone 1966) (Reproduced with permission of the Marine Biological Association of the United Kingdom.)

Salmo gairdneri (Hudson 1973), *Carassius carassius* (Johnston and Goldspink 1973a, b, c), and *Oncorhynchus nerka* (P. W. Webb unpublished data). The latter fiber organization has been called mosaic muscle (Boddeke et al. 1959).

Red muscle is usually slow or phasic, with a low contractile power output compared to that of white muscle, and is used at sustained and prolonged activity levels. Energy is supplied mainly by aerobic metabolic pathways. White muscle is fast or twitch muscle with a relatively high power output for use mainly at burst activity levels at which energy is derived mainly anaerobically (Hess 1970). Intermediate muscle, as the name implies, apparently possesses characteristics of both systems. In the salmonids studied, this system operates to support the red muscle at prolonged speeds (Hudson 1973; P. W. Webb unpublished data), and in *Carassius*, at both sustained and prolonged speeds (Smit et al. 1971; Johnston and Goldspink 1973a, b, c).

Evidence for the functional differences among muscle systems in fish is largely indirect, based to a large extent on the comparative physiology of better known vertebrate systems. Red and white systems have been most thoroughly studied.

Histological observations of the fine structure of the fibers that make up the types of muscle show that red muscle usually has narrow fibers (10–80 μ diam), contains numerous mitochondria (the sites of aerobic metabolic pathways), little ATP, and is well supplied with capillaries. White muscle fibers are larger (of the order of 50–200 μ diam), contain few mitochondria, large amounts of ATP, and are usually poorly vascularized (Boddeke et al. 1959; George 1962; Bone 1966; Engel and Irwin 1967; Roberts 1969b; Webb 1970).

Differential activity levels of aerobic and anaerobic metabolism in red and white muscle respectively have been demonstrated by biochemical studies (George 1962; Beatty et al. 1963; Bilinski 1963; Wittenberger and Diatuic 1965; Bone 1966; Fraser et al. 1966; Wittenberger 1968; Wittenberger et al. 1969).

Mechanical properties of various muscle types in fish have received little study. Hidoka and Toida (1969) and Roberts (1969) demonstrated electrical properties in fish red muscle similar to those in red muscles in other vertebrate systems. Electrical recordings from muscle bundles at various activity levels have shown that red muscle operates at sustained speeds. At burst speeds, white muscle is the principal or only operating system (Bone 1966; Rayner and Keenam 1967; Roberts 1969a, b; Webb 1970; Hudson 1973). At prolonged speeds, red muscle may be supported by intermediate and/or white muscle. There is also a general correlation between the amount of muscle and normal activity patterns of fish. Fish that normally swim at high levels of sustained activity have greater proportions of red muscle than more sluggish fish. Ranking fish by characteristic activity level, red muscle in the caudal peduncle has been measured at 27% in mackerel (Mannan et al. 1961b), 24% in rainbow trout (Webb 1970), 18% in dogfish, *Scyliorhinus* (Bone 1966), 7.5% in halibut (Mannan et al. 1961a), and from approximately 1 to 0% in benthic fish (Braekkan 1956; Blaxter et al. 1961).

All evidence available on muscle function may be interpreted (though circumstantially for most data) as supporting a hypothesis that various muscle systems are designed for specific activity levels. The biochemical data has been interpreted differently by some authors. They suggest that red muscle could function in a similar fashion to liver-type cells, metabolizing products of white muscle metabolism for reuse by that muscle. Arguments for the two hypotheses are summarized by Love (1970). Pritchard et al. (1971)

115

suggested that the red muscle of *Trachurus* could function in an analogous fashion to the liver at high swimming speeds in addition to its normal muscular activities at lower speeds. In general, it appears that the "liver" hypothesis is supported by few data, whereas that for mechanically different functional systems is comparatively well supported by all data, and is least open to speculation.

Although most fish show well-demarcated red and white muscle blocks, this is not always the case. For example, the myotomal muscle of *Anguilla* appears to be superficially white, but must function as red muscle to complete the long migrations made by these fish (Boddeke et al. 1959). Structural and functional variations also occur. Red fin muscle in *Hippocampus* is functionally a twitch muscle (Bergman 1964), comparable to the red, fast, flight muscle in hummingbirds (Aulie and Enger 1969; Grinyer and George 1969). Details of intermediate muscle function remain vague. The extent of such diverse functions contributes to the difficulties of interpreting swimming energetics data (Smit et al. 1971).

Muscle power output

At present, no measurements of fish muscle power output have been made. For practical purposes it is assumed that fish muscle is typical of most vertebrate muscle, and that muscle power outputs are comparable on the basis of comparative physiology. Assumed fish muscle power values are usually taken from Bainbridge (1961). Power outputs currently used for fish and cetacean muscle are summarized in Table 19.

TABLE 19. Values for maximum muscle power output assumed for various fish and cetacean muscles (based on Bainbridge 1961).

	Muscle power output (erg/s/g)	
	Red muscle (slow, nontwitch)	White muscle (fast, twitch)
Cold-water fish	2×10^5	8×10^5
Warmwater fish	8×10^5	30×10^5
Thermo-conserving fish	8×10^5	40×10^5
Mammals	8×10^5	40×10^5

Many problems introduced by "Grays' Paradox" and the use of rigid body analogies to estimate swimming drag are probably related to the use of muscle power values not appropriate for the activity level in question. For example, Gray (1936b) computed muscle power output values for a swimming dolphin on the basis of the unit rate estimated for an Olympic rowing crew working for a 20-min period, that is, probably prolonged activity. The dolphin was undoubtedly swimming at a burst activity level (probably sprint level) when a different muscle system would operate, capable of developing substantially higher power outputs. The rowing crew was certainly using mainly "slow" muscle whereas the dolphin was probably using "fast" muscle.

Power output and muscle shortening speed

Power output of a muscle is not constant but depends on the load and speed of contraction or shortening speed, U_m. Studies by Hill (1950) (see Alexander 1968; Gray 1968) have shown that maximum power is developed when a muscle contracts against a maximum load at a shortening speed of approximately 33% of the maximum shortening speed $U_{m\ max}$, (attained with zero load, Fig. 59). Power outputs remain
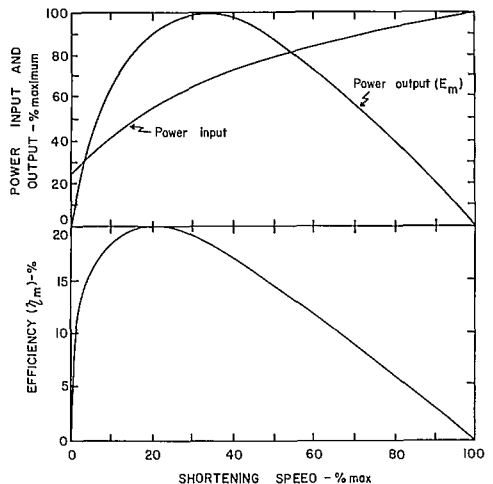
FIG. 59. Relations between muscle power input, output, and efficiency as functions of muscle shortening speed, expressed in relation to maximum power, efficiency, and shortening speeds. (Redrawn from Hill (1950) from Science Progress, Vol. 38; used with permission of Blackwell Scientific Publications.)

close to this maximum over a speed range from approximately 20 to 40% $U_{m\,max}$, decreasing rapidly outside that range. Generally, muscle contracts at a specific speed against a particular load, developing a fixed power.

Maximum efficiency is obtained at approximately 20% $U_{m\,max}$, and the relation between efficiency and shortening speed is such that efficiency remains fairly close to this maximum over a range of approximately 15–25% $U_{m\,max}$. Efficiency decreases rapidly outside this range of shortening speeds. Maximum power and efficiency show reasonable correspondence.

Alexander (1969) suggested that different muscles are designed to operate either at maximum efficiency or maximum power output under normal operational conditions. Red muscle would be expected to operate normally at optimum efficiency, as its most likely function is continual working at minimal energetic costs. White muscle is required for burst activity, frequently elicited in response to some threat or attack stimulus. The requirement for this muscle would be to develop maximum power output.

Energy Distribution in the Propulsive System

Anaerobic metabolic energy

Studies on anaerobic metabolism in fish indicate that any energy release will be distributed solely to the propulsive muscles. Strenuous activity results in a rapid decrease in muscle glycogen and a concomitant rise in lactic acid levels, followed later by an increase in blood lactic and pyruvic acid levels. It is logical that all available energy should be so distributed to the muscles at high activity levels, with other organ systems being involved after that activity, during recovery.

Aerobic metabolic energy

The amount of energy available for locomotion is commonly calculated from the difference between oxygen consumption at a given speed and the standard rate, equal to the metabolic scope at the critical swimming speed when the active rate is reached. Not all energy so calculated is available to the propulsive muscles for locomotion, as is implicit in many analyses of propulsion energetics (Brett 1963; Smit 1965; Webb 1971a, b; Smit et al. 1971). This limitation is usually recognized in such studies, for Brett (1963) emphasized that standard rate is the minimum deductable from the total oxygen at any speed.

In practice, part of the energy available is required by other systems as illustrated by the flow diagram in Fig. 56. Branchial muscle requires energy for ventilation and the heart for circulation (Brett 1971). Some energy will also be required in the adjustment of the ion-osmoregulatory system which is perturbed as a result of increased oxygen demand. This occurs because increased oxygen consumption via the gills cannot be achieved without increased exchange of ions and water (Steen 1971; Wood and Randall 1973a, b, c). Essentially the energy expenditure by such systems may be considered an increase in maintenance energy costs, proportional to the increase in metabolic rate.

The three principal systems recognized as requiring some portion of the aerobic energy developed to provide for locomotion will be considered separately.

ION-OSMOREGULATION

Energetic costs of ion and water regulation are not well known. Rao (1968) measured differences in oxygen consumption of rainbow trout at various salinities and at different swimming speeds. He assumed that ion-osmoregulatory costs were minimal at a salinity of 7.5 ‰. Using this as a reference point the additional ion-osmoregulation oxygen costs resulting from swimming activity may be calculated (Fig. 60). Accord-
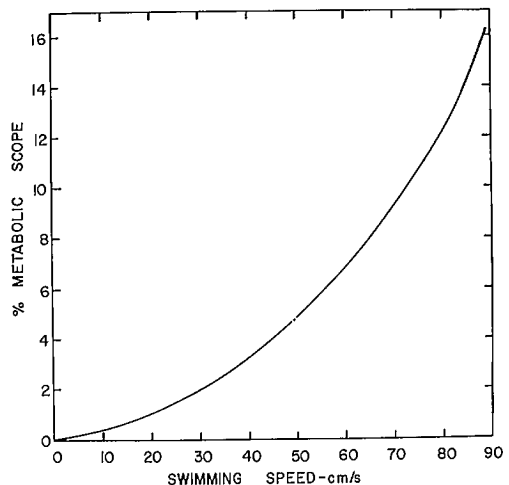
FIG. 60. Relation between ion-osmoregulatory costs, expressed as a percentage of metabolic scope, and swimming speed for a 100 g rainbow trout at 15 C in fresh water. Reference salinity was 7.5‰. (Data from Rao 1968)

ing to these data, ion-osmoregulatory costs increase exponentially with speed to reach approximately 16.7% of the metabolic scope close to U_{crit}. A similar maximum value at a swimming speed of 60 cm/s for 80 g *Tilapia nilotica* may be calculated from data in Farmer and Beamish (1969.)

Branchial Pump and Ventilation

Energetic costs of ventilation have been reviewed by Randall (1970b) and Jones (1971). Energy expenditure by the branchial pumps has most commonly been estimated from mean pressure-flow relations across the gills. Energetic costs, as oxygen consumption, have been calculated either by assuming some efficiency value for the system, or by measuring oxygen consumption after flow and pressures have been increased, by reducing the oxygen content of the water or increasing the water carbon dioxide content. A critique of these methods has been given by Alexander (1967) and Cameron and Cech (1970) who generally concluded that the methods were unsatisfactory. The latter authors attempted to estimate oxygen consumption by the branchial pump from the amount of muscle involved. Estimates of the oxygen cost of the ventilation system vary between approximately 2 and 43% of total oxygen consumption measured (all estimates for restrained fish).

The work of ventilation in swimming fish is even less certain than that for restrained fish, particularly as some part of that work is undoubtedly performed by the locomotory musculature, fluid pressure at the mouth assisting the flow of water across the gills (ram ventilation). Three ventilation patterns may be identified among fish based on the operation of the branchial pump during swimming and the dependence on the branchial muscles. A classification of ventilatory systems of free-swimming (pelagic) fish follows (Webb 1970):

Obligatory ram ventilation — Fish swim continuously with mouth open. Branchial apparatus not used in ventilation. Scombrids. (Hall 1930; Walters 1962; Muir and Kendall 1968; Brown and Muir 1970).

Facultative ram ventilation — Fish swim with mouth open and only use branchial apparatus at rest and low swimming speeds. *Triakis semifasciata* (Hughes 1960a), *Remora remora* (Muir and Buckley 1967), *Oncorhynchus nerka* (Smith et al. 1967).

Other pelagic fish — Branchial apparatus operates at all swimming speeds and at rest. *Clupea harengus*, *Gadus merlangus*, *Onus mustela*, *Crenilabrus melops* (Hughes 1960a, b); *Salmo gairdneri* (Stevens and Randall 1967; Webb 1971a); *Salmo trutta* (Sutterlin 1969); *Cymatogaster aggregata* (P. W. Webb unpublished data).

Many scombrids rely exclusively on ram ventilation and must swim continuously to obtain oxygen. Ram ventilation is obligatory and the work of ventilation is consequently performed by the propulsive muscles of the body. The same applies to "facultative" ram ventilation when ram ventilation is used mainly or exclusively when swimming, and normal branchial ventilation employed at rest.

The situation is uncertain for fish that continue to operate the branchial pump during locomotion. It is likely that, although the branchial muscles operate continuously, positive pressure at the mouth and negative (venturi) pressure at the opercular slit will greatly assist water flow through the ventilatory system. Observations on *Salmo gairdneri* and *Cymatogaster aggregata* (Webb 1971a, unpublished data) suggested that this is often the case. Amplitude and frequency of ventilatory movements showed no significant increases with increased swimming speed in *Salmo*, although oxygen consumption increased approximately 8–10 times. In *Cymatogaster*, ventilation and locomotory movements (labriform mode) are correlated so the mouth opens as the fish surges forward during pectoral fin adduction.

It seems likely that gill ventilation is largely a function of the propulsive muscles during swimming, at least in pelagic fish. The additional resistance to water flow becomes an integral part of drag, and ventilatory work is performed by the locomotory muscles rather than a second (branchial) muscle system. If this were generally applicable to fish, then almost negligible amounts of energy would be distributed to the branchial muscle system in excess of that included in the energy of standard metabolism.

Brown and Muir (1970) calculated that obligatory ram ventilation in *Katsuwonis pelamis* would represent 9% of theoretical drag, which is probably close to gill drag for fish swimming in the carangiform mode with semilunate tail (Chapter 4). It was suggested, on the basis of these calculations, that in neutrally buoyant fish ventilation could represent approximately 12% of theoretical drag (approximately 4% of total

118

drag). Fish that continue to use the branchial pump during swimming fall into this group. Jones (1971) in a theoretical study computed that ventilation of a salmonid-type fish would require a maximum of 9% of the active rate at the associated level of activity.

In summary, the distribution of energy and the exact requirements of the branchial pump remain somewhat uncertain. A maximum requirement of the order of 10% of the active rate appears reasonable, distributed to the branchial muscles when they continue to do the bulk of the ventilatory work. Otherwise, the energy distributed to these muscles may differ little from that at rest. Additional research on this problem is clearly required.

CARDIAC PUMP

The oxygen consumption costs of the heart may be calculated the same as those of the branchial muscles — from pressure-flow relations for blood circulation (Davis 1968; Randall 1970a; Jones 1971), but few data are available. A most useful study by Jones (1971) combines various data available in the formulation of a theoretical model of cardiac oxygen costs at various total oxygen demand levels for a 1000 g salmonid-type fish. Jones estimated that the maximum cardiac oxygen requirements amounted to 11% of the active rate at that level of activity.

PROPULSIVE MUSCULATURE

The balance of gross aerobic metabolic energy is directed to the propulsive musculature. This proportion can be obtained by subtracting energy distributed to other systems from the total energy made available. Jones' (1971 figure 2) analysis of branchial and cardiac muscle requirements may be replotted to show the percentage of metabolic scope for activity distributed to these systems at different swimming speeds (Fig. 61). In converting Jones' figure to swimming speeds, a direct relation was assumed between the logarithm of oxygen consumption and swimming speed shown as % U_{crit} in Fig. 61. Jones' model was based on fish similar to *Salmo gairdneri*, a fish that continues to operate the branchial pump during swimming. In the absence of conclusive data to the contrary, it was assumed that the branchial pump performed a major portion of the ventilatory work during swimming. Ion-osmoregulatory work was assumed equal to that shown in Fig. 60 for a 100 g rainbow trout. These costs are undoubtedly overestimated for
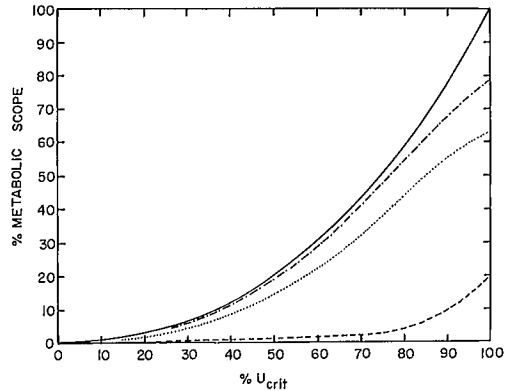
FIG. 61. A tentative representation of distribution of oxygen made available for propulsion to various parts of the propulsive and support systems. Oxygen made available is shown as a percentage of the metabolic scope for activity as a function of swimming speed, shown as % U_{crit}. Total oxygen made available (solid line), and that required by branchial and cardiac systems (broken line), are based on Jones (1971). The difference between these, oxygen made available to the tissues in the absence of ion-osmoregulatory work, is shown by the chain-dashed line. Ion-osmoregulatory costs were taken from Fig. 60 (on a tentative basis) and were subtracted from the total to estimate net oxygen available for the locomotory muscles (dotted line).

the 1000 g fish on which Jones' analysis was based, as Rao (1968) found substantial dependence of ion-osmoregulatory work on weight, but unfortunately the data are insufficient to extrapolate to the higher weight with confidence.

Figure 61 summarizes the distribution of aerobic energy, in terms of metabolic scope, to four systems as swimming speed increases. When the branchial and cardiac energy requirements are subtracted from the total aerobic energy available most energy is directed to the propulsive muscles to a swimming speed of approximately 80% U_{crit}. The proportion of energy so directed is substantilly reduced above this swimming speed. Proportional increase in ion-osmoregulatory energetic costs with swimming speed reduces the proportion of energy directed to propulsive muscles at all speeds. The sum of ion-osmoregulatory, branchial, and cardiac costs may reduce the proportion of aerobic energy for the propulsive muscles by a maximum of 37% of the metabolic scope. At high activity levels, aerobic metabolic energy is augmented by anaerobic metabolism.

119

Chapter 7 — Propulsion Efficiency

Introduction

To understand propulsion problems, evaluation of propulsive system efficiency is fundamental. In bringing together the hydrodynamics and metabolic energetics discussed in preceding chapters, efficiency studies serve to evaluate various inputs and outputs of the propulsion system. Like an equation these must balance and efficiencies must be biologically sensible as deduced on the basis of the comparative physiology of similar systems. As such, efficiency studies are an important, although indirect, method of evaluating models used to calculate thrust power. Efficiency studies serve to identify or emphasize key areas requiring further research. Efficiency is probably of greatest importance if models are to be used to calculate propulsive metabolic power requirements in field situations.

Many studies have been made on the efficiency of various components of the system, but few consider the behavior of the overall propulsion system. For example, hydromechanical models are concerned only with caudal propeller efficiency (Lighthill 1970; Wu 1971a, b, c). The extensive review of energetics of Bainbridge (1961) discussed only muscle power to thrust power conversions at all activity levels considered.

At present the overall efficiency of fish propulsion systems is most important. Characteristics of system components are often a matter of speculation, at least of uncertainty. Study of the overall efficiency is the first step in characterizing the behavior of these components, or indicating the degree of likelihood that current assumptions are valid.

Only overall efficiency will be considered, as deficient areas requiring research are immediately obvious. These have been frequently mentioned in preceding chapters and include anaerobic metabolic situations, most nonbody/caudal fin modes and, of course, the behavior of system components. The discussion will be limited to studies of aerobic efficiency, and treated on the basis of the method used to determine drag or thrust power: the theoretical drag, dead drag, measured power, or hydro-mechanical models. Optimum swimming speeds will be discussed as a special case of efficiency.

Results from efficiency studies concerning the ability of fish to develop metabolic power commensurate with thrust power requirements have caused some controversy. "Gray's Paradox" is an excellent example. Much of this controversy depends on the method used to determine the power required to overcome drag, and also on availability and quality of data. In some cases confounding factors such as the activity of the dual muscle system also make interpretation difficult.

Definitions

Efficiencies may be defined in relation to a flow diagram as shown in Fig. 56. Considering first the propulsive power system alone, the rate of aerobic energy made available (metabolic power) may be written E_{aerob}. The rate of energy expenditure by the propulsive wave in developing thrust to overcome drag (thrust power) may similarly be written as E_T. Then the overall aerobic efficiency, η_{aerob}, is given by

$$\eta_{aerob} = E_T/E_{aerob} \qquad (86)$$

The locomotory muscles develop power at E_m. The efficiency of conversion of metabolic to muscle power, η_m, is therefore

$$\eta_m = E_m/E_{aerob} \qquad (87)$$

The muscle power output is also the power input to the "caudal propeller," equal to the total rate of working, E, of the propulsive wave. The mechanical efficiency of the caudal propeller, η_p, will be given by

$$\eta_p = E_T/E_m = E_T/E \qquad (88)$$

If the various efficiencies are written as decimals rather than percentages, it follows from the above equations that

$$\eta_{aerob} = \eta_m \times \eta_p \qquad (89)$$

121

These equations neglect the metabolic power dissipated by support systems. If the metabolic power required by support systems is E_{sup}, then this portion may be included in equations 86 to 89 by making the energy directed to the propulsive system alone equal to $E_{aerob} - E_{sup}$. Then modified efficiencies taking into account energy distribution to all nonpropulsive components may be calculated, written as η'_{aerob}, η'_m, and η'_p.

Efficiency Studies

Efficiency and theoretical drag

Calculations of efficiency from metabolic power and power required to overcome theoretical drag made by Osborne (1961), Smit (1965), and Smit et al. (1971) for fish swimming in carangiform modes, and for *Cynatogaster aggregata* (P. W. Webb unpublished data), swimming in the labriform mode are discussed.

SALMON MIGRATION

Osborne (1961) compared the power required to overcome the theoretical drag of several species of salmon with the power available from their consumption of fuel, during upstream migration along the Columbia River system. The latter was computed from published data on body constituents measured at the beginning and end of migration. Theoretical drag power was calculated for a mean migration speed and conditions of turbulent boundary-layer flow. Osborne assumed efficiencies of 30% for muscle, η_m, and and 80% for propeller efficiencies, η_p, to compare supply and demand, rather than calculate efficiencies themselves. Calculations of metabolic power from fuels and power required to overcome drag, E_T, were expected to show reasonable agreement. Such agreement was found for only two of six salmon runs for three species, the remainder showed E_T in excess of metabolic power available. The discrepancy reported was relatively small, but as E_T would undoubtedly exceed the theoretical drag power, the discrepancy would in fact be greater.

Osborne pointed out that actual swimming speeds of fish during migration are not known, nor is the behavior. Swimming behavior is undoubtedly significant during migration whereby fish can take advantage of low water velocity areas and eddies. Weihs (1974) has shown that burst/glide behavior could decrease energy required by 50%. Fish were assumed to rest for two-thirds of the time for the completion

of migration. A shorter resting period would reduce the required migration speed of the fish, and could materially affect calculated power requirements. A more comprehensive study of fuel usage for Fraser River migrants using improved analytical methods has shown that salmon are capable of consuming more fuel than estimated in the early literature (Idler and Clemens 1959). Such factors would probably give values for power requirements and metabolic power available of the same order of magnitude.

GOLDFISH AT SUSTAINED AND PROLONGED SPEEDS

Smit (1965) and Smit et al. (1971) considered the efficiency of propulsion at sustained and prolonged activity levels of goldfish. Initially, Smit (1965) analyzed oxygen consumption data and power required to overcome theoretical drag the same as Osborne. Overall efficiency, η_{aerob}, was assumed to be 28%. He found that the metabolic power available exceeded that required by up to 3.5 times, implying either a higher drag or very low swimming efficiency.

Smit et al. (1971) explored efficiency relations using a variety of experimental designs at several temperatures. Their interpretation led to a relation between η_{aerob} and swimming speed such that η_{aerob} was proportional to $U^{1.6}$. The latter conclusion was based on several assumptions that probably did not strictly apply to their experiments. Power required to overcome drag was assumed to increase with $U^{2.6}$, the mean of that expected for laminar or turbulent boundary-flow conditions. The experiments were performed in a Blazka respirometer where the intensity of turbulence undoubtedly exceeded critical values resulting in a fully turbulent boundary-layer flow. It is expected that power required would increase with $U^{2.8}$.

The conclusion that η_{aerob} was related to $U^{1.6}$ led to the deduction that metabolic rate increased with $U^{1.0}$. Smit et al. discussed at some length the relation between metabolic rate and U, and concluded that metabolic rate was related to e^{Ub} for their fish, as is typical for all other species studied in sufficient detail so far (Chapter 6). It appears that efficiency relations are not related to U in any simple fashion (see also Kliashtorin 1973).

In addition to these general relations for efficiency and swimming speed, efficiencies calculated reached values up to 100% at higher sustained speeds (to 8.5 L/s). Smit et al. (1971) considered a η_{aerob} of 20% to be the maximum

consistent with purely aerobic metabolism, and values above this would imply a substantial anaerobic contribution to the total energy budget. No oxygen debt was accrued (Kutty 1968). It was concluded from the data that both red and white muscles were used for sustained swimming, which leads to the conclusion that white muscle in goldfish is almost inexhaustible. This part of Smit et al.'s (1971) work leads to several questions concerning the comparative physiology of fish muscle, and the behavior of goldfish muscle in particular, and suggests some desirable lines of research.

Cymatogaster AT 45-MIN U_{crit}

Discussion of swimming efficiency and theoretical drag will be restricted to the critical swimming speed for simplicity. Theoretical drag was calculated from equations 29, 31, and 33 for a 45-min U_{crit} of 56.5 cm/s for fish with a mean length of 14.3 cm and measured wetted surface area of 90.91 cm². Power required was 7.52×10^4 erg/s.

Metabolic power was calculated from the difference between the standard and active rate, equal to 76 mg O_2/kg h and 663 mg O_2/kg h respectively. The mean weight of the fish was 35.55 g. The oxycalorific equivalent was assumed to be 1.4×10^8 erg/s. Metabolic power expended was 8.13×10^5 erg/s.

From these values for theoretical drag power and metabolic power, η_{aerob} is 9.2%. This value is low compared to caudal fin propulsion at U_{crit}. It is likely that the muscles would be working at optimum efficiency at U_{crit} (Alexander 1969) when muscle efficiency would be approximately 20%. Then the low overall efficiency must result from a low pectoral fin propeller efficiency or, alternatively, the drag of the fish is underestimated.

Observing movements by *Cymatogaster* during swimming, Webb (1973b) showed that drag would be augmented as a result of recoil movements, fluttering of inactive fins and gill drag (P. W. Webb unpublished data). Such factors could increase total drag to 1.53 times the theoretical drag. This would then give a value of η_{aerob} of 14%, with a propeller efficiency of 70%. The latter value for maximum propeller efficiency is only a little lower than values measured for caudal fin propulsion, although it is substantially lower than optimum (maximum) values determined from models (Lighthill 1970; Wu 1971d).

Drag of swimming fish is likely to exceed theoretical drag with the possible exception of fish that swim holding the body fairly straight

and use independent short paired or caudal fin propulsion (Chapter 4). This does not apparently apply to *Cymatogaster* swimming under these conditions, using an independent pectoral fin propulsion system.

Efficiency and dead drag

Brett (1963), Webb (1970), and A. J. Mearns et al. (personal communication) compared power requirements to overcome dead drag with metabolic power for several species of salmonids. Data from the latter authors, analyzed by the same method as used by Osborne, show reasonable agreement between power required and that available at normal efficiencies.

Brett (1963) measured the drag of yearling sockeye salmon and found that power required exceeded aerobic metabolic power available by a factor up to 2.2 times. Various differences between these data and that of Mearns et al. and Webb can be attributed to difficulties in measuring dead drag as described in Chapter 4 (Webb 1974).

Brett (1963) also computed trends in efficiency changes with swimming speed by means of a power ratio;

Power ratio =

$$\frac{\text{Power required to overcome dead drag}}{\text{Aerobic metabolic power available}}$$

Power ratio is shown as a function of swimming speed in Fig. 62. Brett found that power
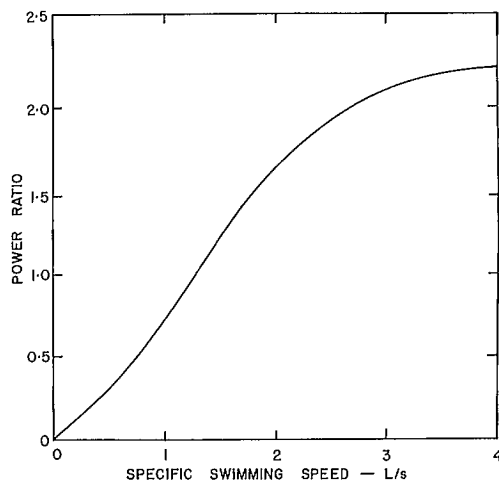
FIG. 62. Relation between power ratio and specific swimming speed for yearling sockeye salmon tested at 15 C. (Simplified after Brett 1963, 1965b)

123

ratio and efficiency increased with swimming speed, reaching a plateau of maximum efficiency at 60-min U_{crit} values.

Efficiency and measured power

Webb (1971a, b) measured both the swimming drag and oxygen consumption of rainbow trout at sustained and prolonged activity levels from which power required and aerobic metabolic power were calculated. Values for muscle efficiency, η_p, were computed on the basis of comparative physiology. From these, overall aerobic efficiency, η_{aerob}, and caudal fin propeller efficiency, η_p, were calculated (Fig. 63).

Efficiencies were of the same order as those for *Cymatogaster*, η_{aerob}, reaching 15.8% at U_{crit}, following trends similar to goldfish (Smit et al. 1971) and sockeye salmon (Brett 1963). η_p reached values of the order of 75% at U_{crit}. Energetics and efficiencies were thermodynamically acceptable and similar to those expected on the basis of comparative physiology for other vertebrate systems.

Efficiency and hydromechanical models

Lighthill's model has been applied to salmonids to calculate swimming thrust power, (Webb 1971a,b, 1973a). Webb (1971a) found that this model in the bulk momentum form gave good estimates of propulsive power requirements compared with measured values for rainbow trout. Calculations of overall aerobic efficiency would follow those shown in Fig. 63 with similar maximum efficiencies. Webb (1973a), using the same model, calculated a maximum overall efficiency of 22% for yearling sockeye salmon, a value still within the range of values reported for other vertebrate systems.

Predictions of propeller efficiency, η_p, were higher than values calculated from overall efficiencies and expected muscle efficiencies, particularly at lower swimming speeds (Fig. 63). At a swimming speed of 20% U_{crit}, the model would predict a η_p of approximately 62% compared to the calculated value of 15%. At higher speeds, η_p approaches values only slightly lower than those predicted by the model. Power dissipated by support systems is not accounted for in the calculations by Webb. Inclusion of some estimate for this energy expenditure would give agreement between the two sets of efficiencies at higher swimming speeds.

The difference between predicted efficiencies and those calculated for low swimming speeds was attributed to the nature of the model, which considered a perfect fluid and neglected viscous forces. The latter forces were considered small enough to neglect by Lighthill (1960, 1970) but this applies particularly to conditions when the ratio of swimming speed to the speed of the propulsive wave, U/V, is of the order of 0.8. For trout, it was found that U/V increased with speed and was substantially lower than 0.8 at low swimming speeds.

Viscous forces are likely to be of greater importance at speeds where U/V is low. Viscous forces are out of phase with momentum changes
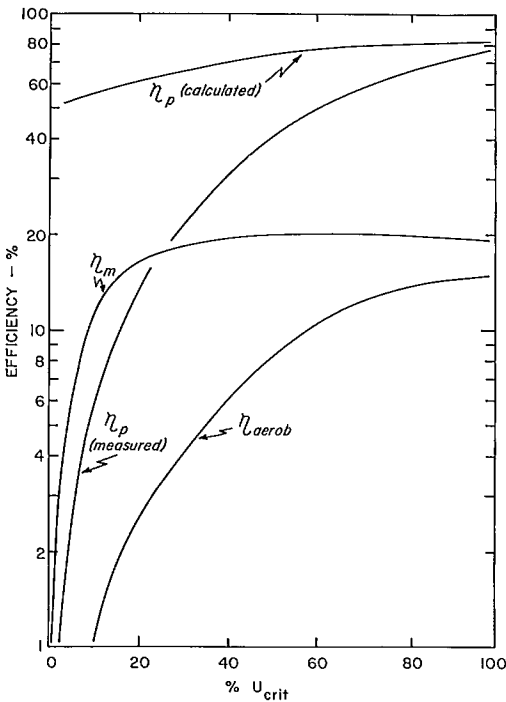
FIG. 63. Relations between overall aerobic efficiency, η_{aerob}, muscle efficiency, η_m, and caudal fin propeller efficiency, η_p, as a function of swimming speed expressed as a percentage of the critical swimming speed, for *Salmo gairdneri*. Values for η_p (measured) were calculated from measured oxygen consumption and swimming drag, and expected muscle efficiencies. Values for η_p (calculated) were calculated from Lighthill's model. (Based on data in Webb 1971a, b)

124

and with body movements which do most propulsive work against the inertial forces. As a result, viscous forces add to energy lost in the wake without making significant contributions to thrust (Lighthill 1970). When U/V is small, the time for nonthrust viscous force interactions would be increased, whereas viscous forces developing in magnitude with time (Lighthill 1970) would remain out of phase with body movements and still not contribute to thrust. Webb (1971b) has shown indirectly that η_{aerob} is related to U/V in the expected fashion.

In general, at low speeds with low U/V, η_p appears to be overestimated by the currently most applicable hydromechanical model. As swimming speed increases so does U/V to reach maximum values of the order of 0.8 as U_{crit} is approached, and probably remaining of that order at higher speeds (Webb 1971b). Then Lighthill's model predicts η_p with good accuracy. Lighthill (1969, 1970) indicated the necessity of formulating a model that would sufficiently describe both viscous and inertial forces.

Optimum speed

Another approach to the question of efficiency is optimum speed, defined as the speed at which total energy expenditure per unit distance travelled is minimal.

Brett (1965b) has shown that the relation between cost per unit distance and swimming speed has a U-shape (Fig. 64). The initial shape
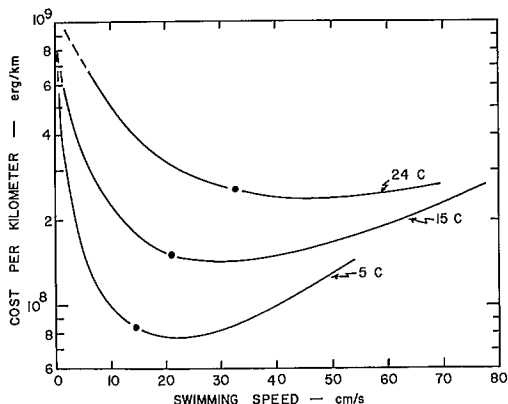
FIG. 64. Relation between energetic costs (erg/km) and swimming speed of yearling sockeye salmon at three temperatures. Optimum swimming speeds occur at the lowest point of the curve. Predicted optimum speeds (Weihs 1973c) are solid circles. (Based on data in Brett 1964, after Brett 1965b)

of the curve arises because of the inclusion of standard metabolism in total costs; otherwise curves would take a form similar to those shown in Fig. 62, 63. When swimming speed is low, standard metabolic energy costs are high relative to locomotion costs, and the time required to cover unit distance is high. Total costs per unit distance are also high. The situation is further compounded at low speeds as both muscle and propeller efficiencies are low at low speeds. In practice, costs per unit distance are probably overestimated for low swimming speeds as fish are apt to shift to some alternative (more efficient) propulsive mode (e.g., paired fin modes typical of station holding). Such a shift has been observed (Brett and Sutherland 1965; Webb 1971a; Hudson 1973) but has not been rigorously studied, probably because energetics studies become confounded by excitement and restless behavior at low speeds.

Figure 64 shows that the optimum speed shifts and increases with temperature. Energy costs per kilometer also increase with temperature, influenced by the increase in standard or maintenance metabolism, so that it becomes more costly to travel unit distance.

Above the optimum speed, energetic costs per kilometer increase as locomotory costs increase with $U^{2.8}$ and progressively exceed standard metabolic rate.

Weihs (1973c) derived an expression for optimum speed which predicts that optimum speed would occur when oxygen consumption equals twice the standard rate. These predicted values are included in Fig. 64; they occur somewhat lower than the determined optimum speeds. The difference between predicted and determined optimum speeds probably derives from the assumption made by Weihs that η_{aerob} increases proportionally with U. η_{aerob} is more likely to increase with U raised to some power. Taking this into account would increase the optimum speed predicted by the model, probably approaching the observed values as noted by Weihs.

Analysis of Overall Efficiencies

At present Lighthill's model is most suitable for application to bioenergetic studies of fish propulsion. The input parameters may be measured with relative ease for swimming fish. Model predictions of thrust power are within the expected scope of the muscle system. More important than this rather tautological support are the efficiency calculations which show that

125

when sufficient data are available for the calculation of both metabolic and mechanical power expenditures, predictions of thrust power are similar to expected values; in the case of rainbow trout, thrust power calculations show reasonable agreement with measured values. In general, hydromechanical predictions of thrust power are thermodynamically and biologically logical.

The prediction of total power and η_p by the model apparently differs from expected values. This part of the model is of less importance to its full application, as overall efficiencies and indirect calculation of total energy expenditure would likely be of greatest importance in applied situations. The question of η_p does require better evaluation.

Hydrodynamic models differ from alternative methods of calculating thrust-drag power (theoretical and dead drag) as calculations are based on the movements actually made by swimming fish rather than assumptions concerning the effects of such movements on drag, which can be shown to be poorly founded in most cases (Chapter 4). Because of the dubious applicability of rigid-body drag calculations, those of hydromechanical models take on a special importance as the only possible alternate method for calculating thrust power with sufficient breadth to be of general predictive value to aquatic vertebrate propulsion problems.

Taking these factors together — the predictive potential of models and their agreement to date with the known physiology and bioenergetics of propulsion system — a more extensive analysis of efficiency based on Lighthill's model is desired.

Such a treatment must be tentative in nature. Agreement between biologically expected and hydromechanically predicted values of thrust power have only been obtained when sufficient data have been available. In contrast, when data from different sources have been equated, discrepancies commonly result as with other methods of estimating thrust-drag power.

The major constraint of data availability limits the analysis to salmonids and effects of size. Only one level of activity will be considered, a 60-min U_{crit} for sockeye salmon (close to maximum cruising speeds; Brett 1967a). Data are available mainly for metabolic rates of sockeye salmon at 60-min U_{crit} and, to a lesser extent, the appropriate kinematics (Brett 1964, 1965a, 1967a, and personal communication; Brett and Glass 1973; Webb 1973a, unpublished data). Data are available for kinematics of

rainbow trout in Bainbridge (1958, 1960, 1962, 1963) and Webb (1971a,b).

The model is likely to be most applicable at the activity level selected, when U/V is expected to be high and close to the optimum values.

Lighthill's bulk momentum model, modified for large amplitude motions, will be used. To recapitulate

$$E_T = (m_T\, U\, w\, W) - (\tfrac{1}{2}\, m_T\, w^2\, U / \cos\theta) \quad (90)$$

for which the basic input data required are f, A, λ_B, d_T, ρ, β, and $\cos\theta$ for any value of U_{crit} because

$$W \simeq \pi f A / \sqrt{2} \quad (91)$$

$$w = (f\,\lambda_B - U)/f\,\lambda_B \quad (92)$$

$$m_T = \pi\,\rho\,\beta\,d_T^2 \quad (93)$$

β will be equal to 1 for the caudal fin trailing edge (Lighthill 1970). $\cos\theta$ will be assumed equal to 0.85 as measured by Lighthill (1971) for dace, as there are no other measurements.

Kinematics

Data for tail-beat frequency, f, are given by Brett and Glass (1973) and Webb (1973a and unpublished data) for three lengths approximately 5–50 cm. Following the analysis of relations between f, L, and U of Hunter and Zweifel (1971), it was found that

$$(f - f_o) = 0.339 + 0.540\, U/L \quad (94)$$
$$(R = 0.963)$$

when f_o is the tail-beat frequency at which the regression between f and U/L crosses the U/L axis. f_o was found to be related to L by

$$\log f_o = 0.799 - 0.474 .\, \log L \quad (95)$$
$$(R = 0.999)$$

Values for U_{crit} are obtained from Brett and Glass (1973) for acclimation and test temperatures of 15 C according to the equation

$$\log U_{crit} = 1.129 + 0.634 \log L \quad (96)$$

when U_{crit} is given in cm/s. Numerical values for f and U_{crit} from these equations are in Table 20.

Various values of tail-beat amplitude, A, have been measured for salmonids, mainly for

TABLE 20. Basic data for kinematic parameters used to calculate mechanical energy expenditure for sockeye salmon at the 60-min U_{crit}.

Length	U_{crit}	f	A	λ_B	λ_B/L	d_T
(cm)	(cm/s)	(s)	(cm)	(cm)		(cm)
5	37.4	7.31	1.06	7.31	1.46	1.0
10	58.0	5.58	2.01	14.85	1.49	2.0
15	75.1	4.78	3.00	22.44	1.49	3.0
20	90.1	4.39	4.02	30.00	1.50	4.0
25	104	3.95	4.91	37.50	1.50	5.0
30	116	3.70	5.64	44.94	1.50	6.0
40	140	3.32	6.78	60.11	1.50	8.0
50	161	3.07	7.67	74.92	1.50	10.0
60	181	2.87	8.40	90.00	1.50	12.0

rainbow trout (Table 21). They suggest that A is size dependant, with A/L decreasing with increasing L (Hunter and Zweifel 1971). As there are insufficient data for sockeye salmon alone, salmonid values were pooled with the exception of an extremely low value of A/L obtained by Bainbridge (1958) for a trout 29.3 cm long. This value for A/L differs markedly from the remainder of the data, and it is not certain if it is in fact representative for trout. A curve was fitted by eye to the relation between A and L. Values of A were then obtained by inspection. No satisfactory linear transformation was found between

TABLE 21. Values for A measured for salmonids.

Species	Length (cm)	A (cm)	A/L	Source
Salmo gairdneri	13.5	2.66	0.197	Bainbridge (1963)
	23.2	4.57	0.197	
	29.3	5.13	0.175	Webb (1971a)
Oncorhynchus nerka	20.4	4.08	0.20	Webb (1973a)
	51.0	8.00	0.158	J. R. Brett (unpublished data)
Salmo gairdneri	29.3	4.01[a]	0.137[a]	Bainbridge (1963)

[a]See text.

A and L. Values for A used in calculating E_T are included in Table 20.

Estimation of propulsive wavelength, λ_B, is more difficult. Initially the general relation for λ_B/L noted by Webb (1971b) and Wu (1971d) was used, but this gave values of E_T that decreased with increasing size, which would obviously be unacceptable as inconsistent with both mechanical and physiological considerations. In addition, Webb (1973a) found λ_B to be 1.0 for sockeye salmon 20.4 cm long. It appears that the mean λ_B/L obtained by pooling data from several species swimming in similar modes (Webb 1971b) is not generally applicable, as differences between species are of sufficient importance to negate that relation. Sample calculations using a constant λ_B/L suggest this ratio will be size dependent, at least for sockeye salmon.

An alternative method was sought for estimating λ_B. On the basis of observations for rainbow trout and several other species swimming in the same mode, Webb (1971b) noted that $U/f\lambda_B$ (= U/V) increased with swimming speed to reach values of the order of 0.7 when close to the 60-min U_{crit}. This relation was assumed to apply to sockeye salmon, and λ_B calculated accordingly (Table 20). Some size dependance of λ_B/L is indicated, and all values are greater than the value found for one length by Webb (1973a).

No data are available for trailing-edge depth, d_T. d_T reaches maximum values at speeds approaching U_{crit} (P. W. Webb unpublished data). This is probably general among fish optimizing swimming efficiency the same as screw propellers tend to be more efficient with large

TABLE 22. Calculated values for mechanical power outputs E, E_K, and E_T for sockeye salmon of various sizes at the 60-min U_{crit}.

Length	E	E_K	E_T
cm	(erg/s)	(erg/s)	(erg/s)
5	2.61×10^3	4.60×10^2	2.15×10^3
10	3.39×10^4	5.98×10^3	2.79×10^4
15	1.62×10^5	2.85×10^4	1.33×10^5
20	5.22×10^5	9.21×10^5	4.30×10^5
25	1.14×10^6	2.01×10^5	9.37×10^5
30	2.12×10^6	3.73×10^5	1.74×10^6
40	5.28×10^6	9.31×10^5	4.35×10^6
50	1.04×10^7	1.83×10^6	8.55×10^6
60	1.76×10^7	3.11×10^6	1.45×10^7

disc diameters (Chapter 1). Anatomically, d_T could reach 0.2 L for salmon. Values of this order have been measured for swimming salmon and trout, but only for restricted size range (Bainbridge 1963; P. W. Webb un; :blished data). Therefore, d_T will be assumed equal to 0.2 L.

Values for total power, E, power lost in the wake, E_K, and thrust power, E_T, calculated from these data are given in Table 22.

Oxygen consumption

At prolonged swimming speeds, which include the 60-min U_{crit}, most energy is assumed made available by aerobic pathways and any anaerobic contribution will be neglected (Chapter 6).

Energy made available for propulsion may be calculated from the difference between active and standard rates of oxygen consumption, using oxycalorific equivalents. From Brett and Glass (1973) metabolic rates at 15 C are given by

$$\text{Standard rate} = 0.150 \, M^{0.846} \quad (97)$$
$$(\text{mg } O_2/\text{h})$$

$$\text{Active rate} = 0.951 \, M^{0.963} \quad (98)$$
$$(\text{mg } O_2/\text{h})$$

These equations require conversion factors for weight and length. Weight–length data for 32 fish from 5.5 to 18.8 cm, and from 41.8 to 61.4 cm in length were given by Brett and Glass (1973). These were supplemented with weight–length data for 20 fish from 19 to 35 cm long to calculate a more complete weight–length relationship

$$\log M = -2.180 + 3.089 \log L \quad (99)$$
$$(R = 0.987)$$

Values for weight calculated from Equation 99 are included in Table 23, with active and standard metabolic rates.

The mechanical equivalent of oxygen was taken as 1.4×10^8 erg/mgO$_2$. Computed values for metabolic power, E_{aerob} are given in Table 24.

Efficiency

Overall efficiency, η_{aerob}, was calculated (Table 24) and is shown as a function of size in Fig. 65. The relation is curved, with efficiency increasing almost logistically with length to reach

TABLE 23. Calculations for weight, standard, and active metabolic rates for sockeye salmon at the 60-min U_{crit}.

Length (cm)	Weight (g)	Standard metabolic rate (mg O_2/h)	Active metabolic rate (mg O_2/h)
5	0.95	0.10	0.75
10	8.11	0.88	7.14
15	23.33	2.54	23.8
20	68.98	5.39	56.1
25	137.4	9.66	108.9
30	241.6	15.6	187.4
40	587.2	33.0	441.2
50	1170	59.1	856.7
60	2055	95.0	1473

TABLE 24. Summary of calculations for E_T, E_{aerob}, η_{aerob}, for sockeye salmon at the 60-min U_{crit}.

Length	E_T	E_{aerob}	η_{aerob}
cm	(erg/s)	(erg/s)	(%)
5	2.15×10^3	26.7×10^3	8.1
10	2.79×10^4	25.6×10^4	10.9
15	1.33×10^5	8.69×10^5	15.3
20	4.30×10^5	20.7×10^5	20.8
25	9.73×10^5	40.5×10^5	24.0
30	1.74×10^6	7.02×10^6	24.8
40	4.35×10^6	16.7×10^6	26.0
50	8.55×10^6	32.6×10^6	26.2
60	1.45×10^7	5.63×10^7	25.8

an asymptote at about 50 cm length. All efficiencies are within the range of values anticipated on a comparative physiological basis, but the shape of the curve itself is highly improbable; all efficiencies would be expected to fall within the range of 20–30%.

The shape of the curve, with low efficiencies obtained for small fish, may be explained in one of two ways — either the data or the model are insufficient for the description of the propulsive system. Data for E_{aerob} are based on extremely comprehensive measurements obtained over many years for large numbers of fish. There is no reason to assume a size dependent variable anaerobic contribution. In contrast, kinematic data are far from complete and solutions to the model can be no better than the input data.

A critical gap exists with respect to kinematic data. Superficially it appears that the assumptions involved are adequate in obtaining numerical solutions for E_T for larger fish (but see below) to which most available data are applicable, although assumptions require validation and, in all probability, correction. Extrapolation of the data for larger fish to smaller fish is clearly not valid — that is, the assumptions made do not apply throughout the size range considered. This implies that kinematic factors during swimming for sockeye salmon are size-dependent and require further research. Of particular interest is the possibility that λ_B/L (and d_T) varies with size so there could be a change in swimming mode with increasing length. If small fish tended to swim toward the mechanically less efficient anguilliform fashion of the subcarangiform mode, and large fish in a more efficient carangiform fashion, then a change in

kinematics with size would be found. In addition, an efficiency-length curve of the form shown in Fig. 65 could be obtained but in a less extreme form.
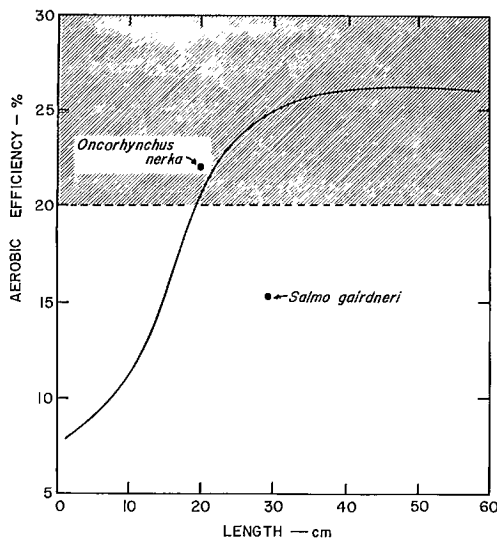
FIG. 65. Tentative estimates of overall efficiency η_{aerob}, as a function of length for sockeye salmon at 15 C. Further explanation is given in the text. Measured values for *Oncorhynchus nerka* (Webb 1973a) and *Salmo gairdneri* (Webb 1971b). Shaded area indicates range of maximum expected efficiencies.

Another factor that could influence the shape of the curve obtained would be neglect of viscous force effects by the model. At a

length of 5 cm, R_L at U_{crit} is 1.9×10^4 compared with 1.1×10^6 at 60 cm. Although both values are high, the difference may be sufficient to slightly reduce efficiency estimates for small fish.

Thrust and drag

A consideration of thrust and drag reveals further physiological and/or mechanical problems not apparent in the analysis of efficiency alone. The values for E_T may be converted to thrust (= drag) coefficients as described in Chapter 5, and compared to theoretical drag coefficients for an equivalent rigid body with turbulent boundary-layer flow. The latter flow conditions are dictated by the microturbulent nature of flow in the water tunnels used in the experiments. In addition, an expected value for E_T may be estimated from data for E_{aerob} based on the assumption that overall efficiency is 25%. These values for E_T can then be expressed as drag coefficients in the same way (Table 25).

The calculations suggest that drag coefficients decrease with size, as expected. Such a phenomenon could be partially rationalized if swimming mode changes with increasing size.

Comparison between theoretical drag coefficients and those calculated from E_T suggest that swimming drag is reduced. Alternatively, if drag were several times theoretical drag as seems more likely, then insufficient aerobic power would be available for fish greater than 30 cm in length as calculation of drag coefficients from E_{aerob} also gives values less than theoretical drag coefficients. This implies that Gray's

Paradox may apply, but it cannot be assumed that the fish are achieving a much reduced drag; other explanations are possible.

In view of the flow conditions in the water tunnels, and the discussion of drag in Chapter 4, the only likely drag-reducing mechanism applicable is mucus, reducing frictional drag in a turbulent boundary layer. Substantial reductions in drag are feasible under time-independent steady flow, but it is not known to what extent drag may be reduced by agents such as mucus in unsteady flow. In general, it seems unlikely that the drag of the swimming fish would be reduced below theoretical drag.

If drag is not reduced, or is reduced by only a small amount, then it must be assumed that more energy is made available to the propulsive system than computed from oxygen consumption; that is, the anaerobic energy contribution cannot be neglected for this fish. The problem is analogous to that found by Smit et al. (1971) for goldfish, and they suggested that additional power was made available by the white muscles at higher speeds to supplement the red muscle. The difference between goldfish and salmon problems is one of degree — goldfish can sustain a large anaerobic energy expenditure whereas salmonids cannot (Kutty 1968). Calculation of the possible glycolytic contribution, based on observed maxima discussed in Chapter 6, indicates that adequate energy could be made available to the salmon propulsion system by this means. It may be significant to the solutions of this problem that both cyprinids and salmonids are unusual in having relatively large amounts of intermediate muscle which are electrically active

TABLE 25. A comparison between thrust and drag, expressed as drag coefficients. C_T is calculated from data for E_T as $E_T/\frac{1}{2}\rho \, S_W U^3$. C_{aerob} is calculated from data for E_{aerob} assuming $E_T = 0.25 \, E_{aerob}$ $C_D = (1.2) \, 0.072 \, R_L^{-\frac{1}{5}}$.

Length (cm)	S_W^a (cm²)	R_L	C_T	C_{aerob}	C_D
5	7.19	1.70×10^4	0.0114	0.0355	0.0123
10	31.7	5.27×10^4	0.0090	0.0207	0.0098
15	75.5	1.02×10^5	0.0083	0.0136	0.0086
20	139.8	1.64×10^5	0.0084	0.0101	0.0078
25	225.3	2.36×10^5	0.0074	0.0080	0.0073
30	332.8	3.16×10^5	0.0067	0.0068	0.0069
40	616.0	5.09×10^5	0.0051	0.0049	0.0062
50	993.1	7.32×10^5	0.0041	0.0039	0.0058
60	1467.0	9.87×10^5	0.0033	0.0032	0.0055

[a]S_W determined from empirical relationship $S_W = 0.43.L^{2.14}$ (R = 0.9973; n = 29).

130

at the required speeds (Chapter 6). According to Webb's (1970) measurements, intermediate muscle could comprise approximately 13% of the myotome. If this muscle is truly intermediate, it would be necessary to substantially revise efficiency criteria at prolonged speeds, such as the 60-min U_{crit} used here. Questions on energetics of the intermediate components of the propulsive system and division of labor between various muscle systems require substantial research, including comparative studies.

Discussion

Studies of efficiency support the conclusion made in Chapter 4 that rigid-body analogy is unsuitable for estimating the drag of swimming fish. Previously, this conclusion was based on hydrodynamic reasons. Here it is based on biological energetic reasons in that balanced energy equations are not usually obtained when the power required to overcome drag is calculated from theoretical equations or measured for dead fish. In contrast, it was concluded in Chapter 5 that Lighthill's model was most suitable for calculating thrust power, again mainly for hydrodynamic reasons. Comparison between muscle power output and thrust power (Chapter 5) and efficiency calculations provide general biological support.

Efficiency calculations also support the statements of several authors of hydromechanical models that present models are not complete. For example, caudal fin propeller efficiency appears to be overestimated by Lighthill's model. This probably stems from the treatment of perfect fluid forces, neglecting viscous thrust and drag forces. Lighthill (1969) clearly pointed to the need for a composite model, especially for anguilliform propulsion, to which may be added propulsion of small fish. Lighthill also pointed out that formulation of such a model is mathematically problematic. Unfortunately it is still not certain that such a "reaction-resistance" model would be of additional biological value. Undoubtedly a greater number of parameters and metameters would be required which may not be amenable to accurate or actual measurement. It is possible that such a development would return to the situation described by Taylor (1952) when the measurement of comprehensive input data would be so tedious and time-consuming, possibly with only marginal improvements in quality, as to make such a model essentially useless for application. It might be of heuristic hydromechanical value only.

Practical application of models does not necessarily require accurate prediction of propeller efficiency, providing thrust power and overall efficiency are correctly predicted. This introduces a philosophical difficulty, in that thrust power is derived from total power and wake power and η_p which contains formulation uncertainties. In these terms, it is obvious that no truly satisfactory conclusion can be made. Conceptually the principal problem of viscous forces is recognized — that is, the mechanical system may be described but the problem remains of formulating these concepts in an adequate mathematical–hydromechanical framework. Inclusion of viscous forces will tend to lead to increases in total power and wake power, reducing propeller efficiency but apparently not substantially affecting thrust power (Lighthill 1969, 1970). The probable exceptions for the anguilliform mode and small fish have been mentioned.

Although these points do not resolve the philosophical questions of applying current models, they at least question the biological need or value of more complex, perhaps too complex, models for application, assuming that currently applied models in simpler form are not grossly fallacious. Questions of this nature must be resolved by the continued development of models by hydrodynamicists in working partnership with biologists. The point concerning input data was brought out in the discussion of overall efficiencies of sockeye salmon. In contrast to the conceptual climate of understanding of the mechanics of propulsion by the caudal propeller system, clear deficiencies are demonstrable in kinematic input data. Such data are few, and this is particularly unfortunate as models cannot be better than input data, nor can they be improved and remain accurate in terms of real fish movements, as pointed out by Breder (1926).

It is legitimate to ask what potential the models have in applied biology. The principal answer to this question revolves around estimation of locomotory energy requirements of swimming fish, an expenditure that can represent a large proportion of a fish's total energy budget (Brett 1960; Fry 1957, 1971; Kerr 1971a, b, c; Weatherley 1972). Brett (1972) stated: "As yet no one has devised a means for determining metabolic rates of fish in nature." Typically, attempts to measure metabolic energy expenditure involve the assumption of some relation between metabolic rate and weight for some assumed mean routine activity level, a method with obvious drawbacks. Brett (1970, 1972) favored the method of measuring time spent at various activity levels and applying laboratory

determinations of energy requirements to each level, summated for all daily activities to provide a total energy expenditure. This is the method successfully used with higher vertebrates. Brett (1970) discussed this point in greater detail and concluded that extensive research is required in the power-performance area, dividing this into two main areas concerning locomotory mechanics. Brett called for research in: "1) levels of performance which characterize type activities or behaviour in nature, recorded in such a way that accompanying metabolic costs can be determined by experimentation e.g., tail-beat frequencies, distance, and frequency of darts, etc. 2) the development of a means for determining the drag force on swimming fish and hence to evaluate the efficiency of propulsion."

By the use of models in energetics studies it seems likely that a large measure of these objectives should be possible. Modern sonar and tagging methods permit measurement of not only speeds and distances covered by fish during their normal activities, but are becoming capable of measuring and transmitting other parameters, for example tail-beat frequencies (Weatherley 1972; Young et al. 1972). Brett (1972) noted that additional parameters such as tail-beat frequency, observable in nature, are desirable, and are "amenable to ascertaining the associated energy demands."

Use of models in estimation of metabolic costs of locomotion is, then, a step further in the direction pointed out by Brett, a method capable of accurate evaluation of mechanical energy expenditure. Parameters such as propulsive wave length may be readily measured in laboratory and (perhaps directly) from field situations. Similarly, relations between trailing-edge depth and speed may be measured in laboratory studies. Tail-beat frequency and amplitude, the principal variants relating speed with thrust power, are observable in the field, as is swimming speed. Variations in cos θ appear to be small enough that a mean value is acceptable with little loss in accuracy, although this too may be measured in the laboratory. Basic parameters for the measurement of thrust for body and caudal fin propulsion should, therefore, present little problem.

Once good measures of thrust power are possible, metabolic costs may be estimated indirectly. For example, it appears that mechanical efficiencies of the propeller system could be empirically related to U/V and/or other specific morphological variations. It also seems likely that muscle efficiencies will not vary signfiicantly from other vertebrate systems, nor between species of fish, although interspecific differences in the use of various muscle systems may present some problems. Efficiencies of the muscle and propeller system are likely to be related to the same kinematic parameters that provide input data for calculation of thrust power and could facilitate indirect calculation of metabolic energy expenditure.

Such a procedure has a possible advantage with respect to estimating energy expenditure from correlation between swimming speed duration and metabolic rate. Interspecific differences could be accommodated within a semiempirical model, without recourse to detailed measurements of metabolic rates for all species of interest. This does not imply that all fish would have the same locomotory costs (for this is patently untrue), but rather that such variations may be related to specific differences in the efficiencies of the components making up the propulsive system. Changes in efficiency of these components at different swimming speeds (and between species) could be quantitatively related to kinematic parameters. Such a semiempirical model for fish energetics might be based on simple equations describing swimming kinematics, appropriately "weighted" by suitable coefficients to take into account the effects of morphological and kinematic–energetic variations on thrust and metabolic power. A particularly good example of a semiempirical model to evaluate hovering mechanisms in flying animals was developed by Weis-Fogh (1973).

As a semiempirical model for fish would logically take as its reference point the mechanics of the propulsion system and estimates of thrust power, the nature of the mechanical part should be explored.

The elegant simplicity of the basic bulk-momentum form of Lighthill's model cannot be denied; in fact this is a principal reason the model is suitable for practical application and the reason for emphasis on that model. But this model is neither complete nor definitive. As such, some may argue that the emphasis on one particular model is excessive and this may prove correct. Nevertheless, at present no other model combines the applicability and predictive scope. A positive approach dictates that Lighthill's model should be pursued, but other models, extensions of the same model, and experimental data should be employed to improve its application. In particular the discussion points to changes that would improve a model's prediction of thrust power, and at present this leads to the possibility of a semiempirical model.

A positive approach to improving any basic model leads to semiempirical forms at present, because factors neglected in inviscid models are not amenable to simple description in terms of reasonably measurable parameters on swimming fish. Neglect of viscosity is obvious, but D. Weihs (personal communication) developed a mathematical expression to explain the effects of viscosity on the inviscid model. Although the resultant expression is not readily amenable to reduction into measurable terms for swimming fish, Weihs was able to indicate the magnitude of the effect of viscosity on virtual mass in terms of modes. Swimming modes themselves are merely verbal descriptions of swimming patterns that may now be expressed in a relatively concise mathematical form, and perhaps ultimately in terms of fish geometry alone. Therefore, the requisite corrections might be numerically approximated in coefficient form as functions of mathematically defined key modal kinematic parameters, and these coefficients in turn could be used to improve the basic model. Also related to mode are the effects on thrust of the rate of increase in amplitude of propulsive movements along the length of the body for which Lighthill (1970) developed a mathematical expression. It seems likely that these effects would also be most readily incorporated by suitable coefficients. Similarly, the majority of fish propulsion models are for slender bodies, neglecting or underestimating the interaction of that vorticity carrying thrust-related momentum with body thickness. This aspect, and the interaction of upstream trailing vortex sheets with downstream leading edges executing propulsive movements, has been the subject of extensive mathematical research (Lighthill 1970; Wu and Newman 1972; Newman and Wu 1973; Newman 1973). Newman (1973) concluded that such effects would modify Lighthill's (1970) conclusions on forces acting on a swimming fish, but by not more than a maximum of 10%; most fish shapes would involve a negligible correction. Newman pointed out that these effects cannot easily be estimated quantitatively for fish-type motions, a situation analogous to that for viscosity, but vortex interaction could be expressed in coefficient form related to fish geometry and kinematics and so applied to the basic model.

Use of the suggested coefficients is not novel to fish propulsion. Lighthill (1970) used such factors to take into account effects of fin and body geometry on virtual mass. Wu (1961, 1971a, b, c), Wu and Newman (1972), Newman and Wu (1973), and Newman (1973) used a coefficient approach to simplify equations for lift and drag of swimming fishes. All models for carangiform propulsion with semilunate tail involve coefficients. In both cases these coefficients are related to fish body geometry and kinematics, computed from solutions to hydrodynamic equations.

The use of a semiempirical model is an extension of this trend to quantitatively describe factors which cannot be precisely measured. With increased understanding of the propulsive system, the number and variety of coefficients could probably be reduced to a relatively simple multifactorial equation, or perhaps a simple factor table similar to that obtained by Weis-Fogh (1973) to describe wing geometry of hovering animals. With the probability that a concise and comprehensive hydrodynamic model may be an unreasonable objective, a semiempirical model becomes an attractive alternative, based when possible on good approximations from the more complex aspects of present and future hydromechanical models.

The objective of a general semiempirical model to describe fish propulsion is still a continuation of lines of thought already contained in the biological literature discussed (see Brett 1970, 1972; Fry 1971); the development of these lines of thought is largely speculative, but it must be concluded that such a model, coupled with energetics studies, would provide a suitable and more accurate method to determine locomotory costs under natural conditions.

Summary

Part 2 discussed metabolic aspects of fish propulsion, and brought them together with hydrodynamics to calculate propulsive efficiencies. These calculations lead to conclusions similar to those from Part 1, principally that Lighthill's model provides a suitable system for calculating thrust power requirements for a swimming fish. The provisor is made that adequate kinematic data must be obtained. Efficiency calculations also indicate the magnitude of current restrictions of inviscid models.

The object of formulating a model to predict metabolic power expended at given swimming speeds from kinematic and morphological input data is discussed. It is suggested Lighthill's model would form a suitable framework and the depth of the model could be increased by means of semiempirical coefficients. These could take into account (in coefficient form) factors that present measurement or mathematical problems.

Closing Remarks

The most fundamental and difficult problem in fish propulsion studies is the calculation of mechanical thrust (drag) power output. The evolution of the conceptual basis for locomotion studies has largely revolved around this question, a common denominator throughout this work. The question of the drag of swimming fish has been examined from hydrodynamic and metabolic points of view, and it has been found that many approaches to the problem lead to dead ends. It is possible to summarize the main conclusions pertinent to ongoing energetics studies in a few sentences, as in the summaries of Parts 1 and 2. But what has been gained by this dissection of the subject?

The principal conclusion is that hydro-dynamic models provide the best solutions to calculations of thrust power, as the models take as their starting point movements made by swimming fish. Efficiency calculations based on Lighthill's model show that thrust power predictions are within a few percent of values that would be predicted from the comparative physiology of propulsion systems, providing complete data are given. This is a marked quantitative improvement over early methods of calculating thrust power from theoretical or dead drag, when discrepancies between hydrodynamic and metabolic estimates of power required differed by up to 5 times for the former, and to several orders of magnitude for dead drag.

The crux of the thrust-power question is not this quantitative improvement. The vital point is the different conceptual basis for calculating thrust power, starting from movements made by swimming fish, rather than on too arbitrary, unsubstantiated assumptions that flow is not seriously disturbed by these movements (rigid-body analogy). This qualitative difference is considered to make such studies as that leading to "Gray's Paradox" irrelevant because the basic premise on which calculations of hydrodynamic power were made is questioned. The assumptions concerning flow in using the rigid-body analogy are qualitatively different from that on which workable hydrodymanic models are based, because the latter can show that neglect of vis-cosity is likely to have small effect on the flow and mechanics for most fish. Nevertheless, the ques-tion is recognized and is the subject of ongoing research.

In considering the current position of fish en-ergetics studies, problems, pitfalls, and omissions have been continually pointed out, in addition to questions of model application. The major omis-sions must again be emphasized, because under-standing of the gamut of propulsive systems in fish is far from complete. Biological and physical propulsion studies are largely restricted to cruising activity levels for body/caudal fin modes; nonbody/caudal fin modes and low and high (burst, acceleration) activity are identified as the main deficiency areas. It must be emphasized that problems associated with these and other areas are not truly soluble without permanent exchange between physical and biological scien-tists. Discussions in different chapters clearly show why this is necessary.

Finally it will not be amiss to briefly reiterate the objectives of this work. Primarily the intention was to summarize and bring together two ap-proaches to the question of aquatic vertebrate (mainly fish) propulsion energetics with intended mutual benefit. These objectives, with the necessary speculative nature of much of Chapter 7, mean that no attempt has been made to write a definitive treatise; such would be contrary to its intentions, contrary to the definition of research, and would automatically imply stagnation. Given the stated intentions, it is hoped this work will contribute to active, ongoing research by simpli-fying interdisciplinary exchange of ideas. As a result, the only acceptable measure of success will be the rapidity with which this work is outdated.

Acknowledgments

References

ALEXANDER, R. M. 1967. Functional design in fishes. Hutchinson University Library, London, Eng. 160 p.

1968. Animal mechanics. Biology Series. Sidgewick and Jackson, London, Eng. 346 p.

1969. The orientation of muscle fibres in the myotome of fishes. J. Mar. Biol. Assoc. U.K. 49: 263–290.

ALEYEV, Y. C., AND O. P. OVCHAROV. 1969. Development of vortex forming processes and nature of the boundary-layer with movements of fish. Zool. Zh. 48: 781–790.

1971. The role of vortex formation on locomotion of fish, and the influence of the boundary between two media on the flow pattern. Zool. Zh. 50: 228–234.

ALLAN, W. H. 1961. Underwater flow visualization techniques. U.S. Nav. Ord. Test Sta. Tech. Publ. 2759: 28 p.

AULIE, A., AND P. S. ENGER. 1969. The flight muscles in a bird with high wing-stroke frequency, the zebra finch. Physiol. Zool. 42: 303–310.

BAINBRIDGE, R. 1958. The speed of swimming of fish as related to size and to the frequency and the amplitude of the tail beat. J. Exp. Biol. 35: 109–133.

1960. Speed and stamina in three fish. J. Exp. Biol. 37: 129–153.

1961. Problems of fish locomotion. Symp. Zool. Soc. Lond. 5: 13–32.

1962. Training, speed and stamina in trout. J. Exp. Biol. 39: 537–555.

1963. Caudal fin and body movements in the propulsion of some fish. J. Exp. Biol. 40: 23–56.

BAINBRIDGE, R., AND R. H. J. BROWN. 1958. An apparatus for the study of the locomotion of fish. J. Exp. Biol. 35: 134–137.

BAMS, R. A. 1967. Differences in performance of naturally and artificially propagated sockeye salmon migrant fry as measured with swimming and predation tests. J. Fish. Res. Board Can. 24: 1117–1153.

BARRETT, I., AND F. J. HESTER. 1964. Body temperature of yellowfin and skipjack tuna in relation to sea surface temperature. Nature 203: 96–97.

BEAMISH, F. W. H. 1966. Swimming endurance of some northwest Atlantic fishes. J. Fish. Res. Board Can. 23: 341–347.

1968. Glycogen and lactic acid concentrations in Atlantic cod (Gadus morhua) in relation to exercise. J. Fish. Res. Board Can. 25: 837–851.

BEATTY, C. H., R. D. PETERSON, AND R. M. BOCEK. 1963. Metabolism of red and white muscle fibre groups. Am. J. Physiol. 204: 939–942.

BELAYEV, V. V., AND G. V. ZUYEV. 1969. Hydrodynamic hypothesis of school formation in fishes. J. Ichthyol. 9: 578–584.

BELL, W. H., AND L. D. B. TERHUNE. 1970. Water tunnel design for fisheries research. Fish. Res. Board Can. Tech. Rep. 195: 69 p.

BERGMAN, R. A. 1964. The structure of the dorsal fin musculature of the marine teleost Hippocampus hudsonius. Bull. John Hopkins Hosp. 114: 344–353.

BILINSKI, E. 1963. Utilization of lipids by fish. (1) Fatty acid oxidation by tissue slices from dark and white muscle of rainbow trout, Salmo gairdneri. Can. J. Biochem. Physiol. 41: 107–112.

BLACK, E. C. 1957. Alterations in the blood level of lactic acid in certain salmonid fishes following muscular activity. 1) Kamloops trout, Salmo gairdneri. J. Fish. Res. Board Can. 14: 117–134.

BLACK, E. C., A. R. CONNOR, K. C. LAM, AND W. G. CHIU. 1962. Changes in glycogen, pyruvate and lactate in rainbow trout (Salmo gairdneri) during and following muscular activity. J. Fish. Res. Board Can. 19: 409–436.

BLACK, E. C., G. T. MANNING, AND K. HAYASHI. 1966. Changes in levels of hemoglobin, oxygen, carbon dioxide and lactate in venous blood of rainbow trout (Salmo gairdneri) during and following severe muscular activity. J. Fish. Res. Board Can. 23: 783–795.

BLACK, E. C., A. C. ROBERTSON, A. R. HANSLIP, AND W. G. CHIU. 1960. Alterations in glycogen, glucose and lactate in rainbow and kamloops trout (Salmo gairdneri) following muscula. activity. J. Fish. Res. Board Can. 17: 487–500r

BLACK, E. C., A. C. ROBERTSON, AND R. R. PARKER. 1961. Some aspects of carbohydrate metabolism in fish, p. 89–124. In A. W. Martins [ed.] Comparative physiology of carbohydrate metabliosm in heterothermic animals. Univ. of Washington Press, Seattle, Wash.

137

BLAXTER, J. H. S. 1969. Swimming speeds of fish. FAO Fish. Rep. 62, Vol. 2; 69–100.

BLAXTER, J. H. S., AND W. DICKSON. 1959. Observations on the swimming speeds of fish. J. Cons. Int. Explor. Mer 24; 472–479.

BLAXTER, J. H. S., C. S. WARDLE, AND B. L. ROBERTS. 1971. Aspects of the circulatory physiology and muscle systems of deep-sea fish. J. Mar. Biol. Assoc. U.K. 51: 991–1006.

BLAZKA, P., M. VOLF, AND M. CEPELA. 1960. A new type of respirometer for the determination of metabolism of fish in an active state. Physiol. Bohemoslov. 9: 553–558.

BODDEKE, R., E. J. SLIJPER, AND A. VAN DER STELT. 1959. Histological characteristics of the body musculature of fishes in connection with their mode of life. Proc. K. Ned. Akad. Wet. Ser. C. Biol. Med. Sci. 62: 576–588.

BONE, Q. 1966. On the function of the two types of myotomal muscle fibre in elasmobranch fish. J. Mar. Biol. Assoc. U.K. 46: 321–349.

1971. On the scabbard fish, *Aphanopus carbo*. J. Mar. Biol. Assoc. U.K. 51: 219–225.

1972. Buoyancy and hydrodynamic functions of the integument in the castor-oil fish, *Ruvettus pretiosus* (Pisces: Gempylidae). Copeia 1972: 78–87.

BONE, Q., AND J. V. HOWARTH. 1966. Page 19 *in* Report to Council 1966–67. Marine Biol. Assoc. U.K.

BONTHRON, R. J., AND A. A. FEJER. 1963. A hydrodynamic study of fish locomotion. Proc. 4th. Natl. Congr. Appl. Mech. WHOI Coll. Reprint 1300: 1249–1255.

BORRELLI, G. A. 1680. De motu animalium ex principio mechanico statico. Rome.

BRAEKKEN, O. R. 1956. Function of the red muscle of fish. Nature (Lond.) 178: 747–748.

BREDER, C. M. 1926. The locomotion of fishes. Zoologica (N.Y.) 4: 159–256.

BREDER, C. M., AND H. E. EDGERTON. 1943. An analysis of the locomotion of the seahorse, *Hippocampus*, by means of high speed cinematography. Ann. N.Y. Acad. Sci. 43: 145–172.

BRETT, J. R. 1962. Some considerations in the study of respiratory metabolism in fish, particularly salmon. J. Fish. Res. Board Can 19: 1025–1038.

1963. The energy required for swimming by young sockeye salmon with a comparison of the drag force on a dead fish. Trans. R. Soc. Can. 1, Ser. IV: 441–457.

1964. The respiratory metabolism and swimming performance of young sockeye salmon. J. Fish. Res. Board Can. 21: 1183–1226.

1965a. The relation of size to the rate of oxygen consumption and sustained swimming speeds of sockeye salmon (*Oncorhynchus nerka*). J. Fish. Res. Board Can. 22: 1491–1501.

1965b. The swimming energetics of salmon. Sci. Am. 213: 80–85.

1967a. Swimming performance of sockeye salmon in relation to fatigue time and temperature. J. Fish. Res. Board Can. 24: 1731–1741.

1967b. Salmon. McGraw-Hill Encycl. Sci. Technol. Yearb. 1967: 348–349.

1970. Fish—the energy cost of living, p. 37–52. *In* W. J. McNeil [ed.] Marine aquaculture. Oregon State Univ. Press, Corvallis, Ore.

1971. Energetic responses of salmon to temperature. A study of some thermal relations in the physiology and freshwater ecology of sockeye salmon (*Oncorhynchus nerka*). Am. Zool. 11: 99–113.

1972. The metabolic demand for oxygen in fish, particularly salmonids, and a comparison with other vertebrates. Respir. Physiol. 14: 151–170.

1973. Energy expenditure of sockeye salmon (*Oncorhynchus nerka*) during sustained performance. J. Fish. Res. Board Can. 30: 1799–1809.

BRETT, J. R., AND N. R. GLASS. 1973. Metabolic rates and critical swimming speeds of sockeye salmon (*Oncorhynchus nerka*) in relation to size and temperature. J. Fish. Res. Board Can. 30: 379–387.

BRETT, J. R., M. HOLLAND, AND D. F. ALDERDICE. 1958. The effect of temperature on the cruising speed of young sockeye and coho salmon. J. Fish. Res. Board Can. 15: 587–605.

BRETT, J. R., AND D. B. SUTHERLAND. 1965. Respiratory metabolism of pumpkinseed, *Lepomis gibbosus*, in relation to swimming speed. J. Fish. Res. Board Can. 22: 405–409.

BRODY, S. 1945. Bioenergetics and growth. Reinhold Publishing Corporation, New York, N.Y. 1023 p.

BROWN, C. E., AND B. S. MUIR. 1970. Analysis of ram ventilation of fish gills with application to skipjack tuna. J. Fish. Res. Board Can. 27: 1637–1652.

CAMERON, J. N., AND J. J. CECH. 1970. Notes on the energy cost of gill ventilation. Comp. Biochem. Physiol. 34: 447–455.

CAREY, F. G., AND K. D. LAWSON. 1973. Temperature regulation in free-swimming bluefin tuna. Comp. Biochem. Physiol. 44A: 375–392.

CAREY, F. G., AND J. M. TEAL. 1969a. Mako and porbeagle: warm bodied sharks. Comp. Biochem. Physiol. 28: 199–204.

1969b. Regulation of body temperature by the bluefin tuna. Comp. Biochem. Physiol. 28: 205–213.

CONN, E. E., AND P. K. STUMPF. 1963. Outlines of biochemistry. International edition. John Wiley and Sons Inc., London. p. 396.

CONNOR, A. R., C. H. ELLING, E. C. BLACK, G. B. Collins, J. R. GAULEY, AND E. TREVOR-SMITH. 1964. Changes in glycogen and lactate levels in migrating salmonid fish ascending experimental "endless" fishways. J. Fish. Res. Board Can. 21: 255–290.

DAHLBERG, M. L., D. L. SHUMWAY, AND P. DOUDOROFF. 1968. Influence of dissolved oxygen and carbon dioxide on the swimming performance of large-mouthed bass and coho salmon. J. Fish. Res. Board Can. 25: 49–70.

DAVIES, G. E., J. FOSTER, C. E. WARREN, AND P. DOUDOROFF. 1963. The influence of oxygen concentrations on the sustained swimming performance of juvenile Pacific salmon at various temperatures. Trans. Am. Fish. Soc. 82: 111–124.

DAVIS, J. C. 1968. The influence of temperature and activity on certain cardiovascular and respiratory parameters in adult sockeye salmon. M.Sc. Thesis. Univ. British Columbia, Vancouver, B.C. 114 p.

DENIL, G. 1936–1938. La mécanique du poisson de rivière; qualité nautique du poisson; ses méthodes locomotrices; ses capacités; ses limites; résistance du fluide; effet de la vitesse, de la pente; résistance du seuil. Bruxelles. 395 p.

DICKSON, I. W., AND R. H. KRAMER. 1971. Factors influencing scope for activity and standard metabolism of rainbow trout (*Salmo gairdneri*). J. Fish. Res. Board Can. 28: 587–596.

DOUDOROFF, P., AND D. L. SHUMWAY. 1970. Dissolved oxygen requirements of freshwater fishes. FAO Fish. Tech. Pap. 86: 1–291.

DOVE, H. L., AND H. J. S. CANHAM. 1969. Trials of H.M.S. Highburton: effect of the ejection of polyox into the boundary-layer. Admir. Exp. Works (Haslar, Gosport) Rep. 11/69: 1–18.

DUBOIS, A. B., G. A. CAVAGNA, AND R. S. FOX. 1974. Pressure distribution on the body surface of a swimming fish. J. Exp. Biol. 60: 581–591.

ELDER, J. W. 1960. The flow past a plate of finite width. J. Fluid Mech. 9: 133–153.

ENGEL, W. K., AND R. L. IRWIN. 1967. A histochemical–physiological correlation of frog skeletal muscle fibres. Am. J. Physiol. 213: 511–518.

FARMER, G. J., AND F. W. H. BEAMISH. 1969. Oxygen consumption of *Tilapia nilotica* in relation to swimming speed and salinity. J. Fish. Res. Board Can. 26: 2807–2821.

FIERSTINE, H. L., AND V. WALTERS. 1968. Studies of locomotion and anatomy of scombroid fishes. Mem. S. Calif. Acad. Sci. 6: 1–31.

FRASER, D. I., W. J. DYER, H. M. WEINSTEIN, J. R. DINGLE, AND J. A. HINES. 1966. Glycolytic metabolites and their distribution at death in white and red muscle of cod following various degrees of antemortem muscular activity. Can. J. Biochem. 44: 1015–1033.

FRASER, D. I., A. MANNAN, AND W. J. DYER. 1961. Proximate composition of Canadian Atlantic fish. III) Sectional differences in the flesh of a species of Chondrostei, one of Chimaerae and of some miscellaneous teleosts. J. Fish. Res. Board Can. 18: 893–905.

FRY, F. E. J. 1947. Effects of the environment on animal activity. Publ. Ont. Fish. Res. Lab. No. 68. Univ. Toronto Stud. Biol. Ser. No. 55. 62 p.
1957. The aquatic respiration of fish, p. 1–63. *In* M. E. Brown [ed.] Physiology of fishes. Vol. I. Academic Press, New York, N.Y.
1971. The effect of environmental factors on the physiology of fish, p. 1–98. *In* W. S. Hoar and D. J. Randall [ed.] Fish physiology. Vol. 6. Academic Press, New York, N.Y.

GADD, G. E. 1952. Some hydrodynamic aspects of swimming in snakes and eels. Philos. Mag. 48 7th. Ser. 663–670.
1963. Some hydrodynamic aspects of swimming. Natl. Phys. Lab. U.K. Ship. Div. Rep. 45: 1–22.
1966a. Reduction of turbulent friction in liquids by dissolved additives. Nature 212: 874–877.
1966b. Differences in normal stress in aqueous solutions of turbulent drag reducing additives. Nature 212: 1348–1350.

GAWN, R. W. L. 1948. Aspects of the locomotion of whales. Nature 161: 44–46.

GEORGE, J. C. 1962. A histophysiological study of the red and white muscles of the mackerel. Am. Midl. Nat. 68: 487–494.

GERO, D. R. 1952. The hydrodynamic aspects of fish propulsion. Am. Mus. Novit. 1601: 1–32.

GIBBS-SMITH, C. H. 1962. Sir George Cayley's aeronautics 1796–1855. H. M. Stationery Off. Sci. Mus. London. p 41–42.

GOSLINE, W. A. 1971. Functional morphology and classification of teleostean fishes. Univ. of Hawaii Press, Honolulu, Hawaii. 208 p.

GRAY, J. 1933a. Studies in animal locomotion. I. The movement of fish with special reference to the eel. J. Exp. Biol. 10: 88–104.
1933b. Studies in animal locomotion. II. The relationship between the waves of muscular contraction and the propulsive mechanism of the eel. J. Exp. Biol. 10: 386–390.
1933c. Studies in animal locomotion. III. The propulsive mechanism of the whiting. J. Exp. Biol. 10: 391–400.

1936a. Studies in animal locomotion. V. Resistance reflexes in the eel. J. Exp. Biol. 13: 181–191.

1936b. Studies in animal locomotion. VI. The propulsive powers of the dolphin. J. Exp. Biol. 13: 192–199.

1953a. The locomotion of fishes, p. 1–16. *In* S. M. Marshal and P. Orr [ed.] Essays in marine biology. Elmhirst Memorial Lectures. Oliver and Boyd, Edinburgh.

1953b. Undulatory propulsion. J. Microsc. Sci. (Oxf.) 94: 551–578.

1955. The movements of sea-urchin spermatozoa. J. Exp. Biol. 32: 775–801.

1957a. How fish swim. Sci. Am. 197: 48–54.

1957b. How animals move. Penguin Books, London. 144 p.

1968. Animal locomotion. World Nat. Ser. Weidenfeld and Nicolson, London, 479 p.

GREENE, C. W., AND C. H. GREENE. 1914. The skeletal musculature of the king salmon. U.S. Bur. Sport Fish. Wildl. 32: 25–59.

GRIFFITHS, J. S., AND D. F. ALDERDICE. 1972. Effects of acclimation and acute temperature experience on the swimming speed of juvenile coho salmon. J. Fish. Res. Board Can. 29: 251–264.

GRINYER, I., AND J. C. GEORGE. 1969. Some observations on the ultra-structure of the hummingbird pectoral muscles. Can. J. Zool. 47: 771–774.

HALL, F. G. 1930. The ability of the common mackerel and certain other marine fish to remove dissolved oxygen from sea water. Am. J. Physiol. 93: 417–421.

HAMMOND, B. R., AND C. P. HICKMAN. 1966. The effect of physical conditioning on the metabolism of lactate, phosphate and glucose in rainbow trout, *Salmo gairdneri*. J. Fish. Res. Board Can. 23: 65–83.

HARRIS, J. E. 1936. The role of fins in the equilibrium of swimming fish. 1) Wind-tunnel tests on a model of *Mustelus canis* (Mitchell). J. Exp. Biol. 13: 476–493.

1937. The mechanical significance of the position and movements of the paired fins in the teleostei. Tortugas Lab. Pap. 31: 173–189.

1938. The role of the fins in the equilibrium of the swimming fish. II). The role of the pelvic fins. J. Exp. Biol. 15: 32–47.

1950. *Diademodus hydei*, a new fossil shark from Cleveland shale. Proc. Zool. Soc. Lond. 120: 683–697.

1953. Fin patterns and mode of life in fishes, p. 17–28. *In* S. M. Marshal and P. Orr [ed.] Essays in marine biology. Elmhirst Memorial Lectures. Oliver and Boyd, Edinburgh.

HART, J. S. 1968. Respiration of the Winnipeg goldeye (*Hiodon alosoides*). J. Fish. Res. Board Can. 25: 2603–2608.

HERTEL, H. 1966. Structure, form and movement, Reinhold Publishing Corporation, New York. N.Y. 251 p.

HESS A. 1970. Vertebrate slow muscle fibres. Physiol. Rev. 50: 40–62.

HIDOKA, T., AND N. TOIDA. 1969. Biophysical and mechanical properties of red and white muscle fibres in fish. J. Physiol (Lond.) 201: 49–59.

HILL A. V. 1938. The heat of shortening and the dynamic constants of muscle. Proc. R. Soc. Lond. Ser. B Biol. Sci. 126: 136–195.

1939. The transformation of energy and mechanical work of muscles. Proc. Phys. Soc. 51: 1–18.

1950. The dimensions of animals and their muscular dynamics. Sci. Prog. 38: 209–230.

HILLS, B. A., AND G. M. HUGHES. 1970. A dimensional analysis of oxygen transfer in the fish gill. Respir. Physiol. 9: 126–140.

HOBBS, A. 1952. Tables for seawater density. U.S. Navy H.Q. Publ. 615. 62 p.

HOCHACHKA, P. W. 1969. Intermediary metabolism in fishes, p. 351–390. *In* W. S. Hoar and D. J. Randall [ed.] Fish Physiology. Vol. 1. Academic Press, New York, N.Y.

HOCHACHKA, P. W., AND G. N. SOMERO. 1971. Biochemical adaption to the environment, p. 100–156. *In* W. S. Hoar and D. J. Randall [ed.] Fish Physiology, Vol. 6. Academic Press, New York, N.Y.

HOERNER, S. F. 1958. Fluid-dynamic drag. Chapter 13. Published by author. Midland Park, N.J.

VON HOLSTE, E., AND D. KUCHEMANN. 1942. Biological and aerodynamic problems of animal flight. J. R. Aero. Soc. 46: 44–54.

HORA, S. L. 1935. Ancient Hindu conceptions of correlation between form and locomotion of fishes. J. Asiatic Soc. Bengal Sci. 1: 1–7.

HOUSSAY, S. F. 1912. Forme, puissance et stabilité des poissons. Herman, Paris. 372 p.

HUCKABEE, W. E. 1958. Relationship of pyruvate and lactate during anaerobic metabolism. II. Exercise and the formation of oxygen debt. J. Clin. Invest. 37: 255–263.

HUDSON, R. C. L. 1973. On the function of the white muscles in teleosts at intermediate swimming speeds. J. Exp. Biol. 58: 509–522.

HUGHES, G. M. 1960a. Mechanism of gill ventilation in the dogfish and skate. J. Exp. Biol. 37: 11–27.

1960b. A comparative study of gill ventilation in marine teleosts. J. Exp. Biol. 37: 28–45.

1966. The dimensions of fish gills in relation to their function. J. Exp. Biol. 45: 177–197.

1970. A comparative approach to fish respiration. Experientia 26: 113–122.

HUGHES, G. M., AND A. V. GRIMSTONE. 1965. The fine structure of the secondary lamellae of the gills of *Gadus pollochius*. Q. J. Microsc. Sci. 106: 343–353.

HUGHES, G. M., AND D. E. WRIGHT. 1970. A comparative study of the ultra-structure of the water–blood pathway in the secondary lamellae of teleost and elasmobranch fishes. Benthic forms. Z. Zellforsch Mikrosk. Anat. Abt. Histochem. 104: 478–493.

HUNTER, J. R. 1971. Sustained speed of jack mackerel, *Trachurus symmetricus*. Fish. Bull. 69: 267–271.

HUNTER, J. R., AND J. R. ZWEIFEL. 1971. Swimming speed, tail beat frequency, tail beat amplitude and size in jack mackerel, *Trachurus symmetricus*, and other fishes. Fish. Bull. 69: 253–266.

IDLER, D. R., AND W. A. CLEMENS. 1959. The energy expenditure of Fraser River sockeye salmon during spawning migration to Chiko and Stuart Lakes. Int. Pac. Salmon Fish. Comm. Prog. Rep. 80 p.

JOHANESSEN, C. L., AND J. A. HARDER. 1960. Sustained swimming speeds of dolphins. Science 132: 1550–1551.

JOHNSON, W., P. D. SODEN, AND E. R. TRUEMAN. 1972. A study in jet propulsion: An analysis of the motion of the squid, *Loligo vulgaris*. J. Exp. Biol. 56: 155–165.

JOHNSTON, I. A., AND G. GOLDSPINK. 1973a Quantitative studies of muscle glycogen utilization during sustained swimming in crucian carp (*Carassius carassius*). J. Exp. Biol. 59: 607–615.

　　1973b. A study of glycogen and lactate in the myotomal muscles and liver of the coalfish (*Gadus virens*) during sustained swimming. J. Mar. Biol. Assoc. U.K. 53: 17–26.

　　1973c. A study of the swimming performance of the crucian carp (*Carassius carassius*) in relation to the effects of exercise and recovery on biochemical changes in the myotomal muscles and liver. J. Fish. Biol. 5: 249–260.

JONES, D. J. 1971. Theoretical analysis of factors which may limit the maximum oxygen uptake of fish: The oxygen cost of the cardiac and branchial pumps. J. Theor. Biol. 32: 341–349.

KEENLEYSIDE, M. H. S. 1955. Some aspects of the schooling behavior of fish. Behaviour 8: 183–248.

KELLY, H. R. 1961. Fish propulsion hydrodynamics. Dev. Mech. 1: 442–450.

KEMPF, G., AND W. NEU. 1932. Schleppversuche mit Hechten sur Messung des Wasserwiderstandes. Z. Wiss. Biol. C. 17: 353–364.

KENT, J. C., A. DeLACY, T. HIROTA, AND B. BATES. 1961. Flow visualization and drag about a swimming fish. Fish. Res. Inst. Coll. Fish., Univ. Wash. Tech. Rep. 23 p.

KERR, S. R. 1971a. Analysis of laboratory experiments on growth efficiency of fishes. J. Fish. Res. Board Can. 28: 801–808.

　　1971b. Prediction of fish growth efficiency in nature. J. Fish. Res. Board Can. 28: 809–814.

　　1971c. A simulation model of lake trout growth. J. Fish. Res. Board Can. 28: 815–819.

KLEIBER, M. 1961. The fire of life. J. Wiley and Sons Inc., New York, N.Y. 454 p.

KLIASHTORIN, L. B. 1973. The swimming energetics and hydrodynamic characteristics of actively swimming fish. Express Information: 1–19. (In Russian)

KOWALSKI, T. 1968. Turbulence suppression and viscous drag reduction by non-Newtonian fluids. R. Inst. Nav. Arch. Rep. 110. 207 p.

KRAMER, E. 1960. Zur form and funktion des locomotion apparatus der fische. Z. Wiss. Zool. 163: 1–36.

KRAMER, M. O. 1960a. Boundary-layer stabilization by distributed damping. J. Am. Soc. Nav. Engin. 72: 25–33.

　　1960b. The dolphin's secret. New Sci. 7: 118–120.

KREUGER, M. H., J. B. SADDLER, J. J. TINSLEY, AND R. R. LOWRY. 1968. Bioenergetics, exercise and fatty acids of fish. Am. Zool. 8: 119–129.

KUTTY, M. N. 1968. Respiratory quotients in goldfish and rainbow trout. J. Fish. Res. Board Can. 25: 1689–1728.

　　1972. Respiratory quotient and ammonia excretion in *Tilapia mossambica*. Mar. Biol. (N.Y.) 16: 126–133.

LANG, T. G. 1966. Hydrodynamic analysis of cetacean performance. p. 410–432. *In* K. S. Norris [ed.] Whales, dolphins and porpoises. Univ. of California Press, Berkley, Calif.

LANG, T. G., AND D. A. DAYBELL. 1963. Porpoise performance tests in a seawater tank. Nav. Ord. Test Stat. Tech. Rep. 3063: 1–50.

LIGHTHILL, M. J. 1960. Note on the swimming of slender fish. J. Fluid Mech. 9: 305–317.

　　1969. Hydromechanics of aquatic animal propulsion. Annu. Rev. Fluid Mech. 1: 413–446.

　　1970. Aquatic animal propulsion of high hydromechanical efficiency. J. Fluid Mech. 44: 265–301.

　　1971. Large-amplitude elongated-body theory of fish locomotion. Proc. R. Soc. Lond. Ser. B Biol. Sci. 179: 125–138.

　　1972. Aquatic animal propulsion. 13th Int. Congr. Theor. Appl. Mech. Moscow.

LISSMAN, H. W. 1961. Zoology, locomotory adaptions and the problem of electric fish, p. 301–307. *In* J. A. Ramsay and V. B. Wigglesworth [ed.] The cell and the organism. Cambridge Univ. Press, Cambridge.

LOVE, R. M. 1970. The chemical biology of fish. Academic Press, New York, N.Y. 547 p.

LUMLEY, J. L. 1969. Drag reduction by additives. Annu. Rev. Fluid Mech. 3: 367–384.

MAGNAN, A. 1930. Les caractéristiques géométriques et physiques des poissons. Ann. Sci. Nat. 10ᵉ sér. 13: 1971–1981.

MAGNAN, A., AND A. StLAQUE. 1929. Essai de théorie du poisson. Bull. Tech. Serv. Aérotech. Paris 50: 1–180.

MAGNUSON, J. J. 1970. Hydrostatic equilibrium of *Euthynnus affinis*, a pelagic teleost without a gas bladder. Copeia 1970: 56–85.

MAGNUSON, J. J., AND J. H. PRESCOTT. 1966. Courtship, feeding and miscellaneous behaviour of Pacific bonito (*Sarda chiliensis*). Anim. Behav. 14: 54–67.

MANNAN, A., D. I. FRASER, AND W. J. DYER. 1961a. Proximate composition of Canadian Atlantic fish. I) Variation in composition of different sections of the flesh of Atlantic halibut (*Hippoglossus hippoglossus*). J. Fish. Res. Board Can. 18: 483–493.
    1961b. Proximate composition of Canadian Atlantic fish. II) Mackerel, tuna and swordfish. J. Fish. Res. Board Can. 18: 495–499.

MAREY, E. J. 1874. Animal mechanism. London. 283 p.
    1895. Movement. London. 323 p.

MARR, J. 1959. A proposed tunnel design for a fish respirometer. Pac. Nav. Lab. Esquimalt, B.C. Tech. Memo. 59–3: 1–13.

MEARNS, A. J., P. B. SWIERKOWSKI, AND L. S. SMITH. 1970. New estimates of drag-force on salmonid fishes. Univ. Washington, Seattle, Wash. 20 p.

MILLER, R. B., AND F. MILLER. 1962. Diet, glycogen reserves and resistance to fatigue in hatchery-reared rainbow trout. Part II. J. Fish. Res. Board Can. 19: 365–375.

MILLER, R. B., A. C. SINCLAIR, AND P. W. HOCHACHKA. 1959. Diet, glycogen reserves and resistance to fatigue in hatchery rainbow trout. J. Fish. Res. Board Can. 16: 321–328.

VON MISES, R. 1945. Theory of flight. Dover Books, New York, N.Y. New ed. 1959. 629 p.

MUIR, B. S., AND R. M. BUCKLEY. 1967. Gill ventilation in *Remora remora*. Copeia 1967: 581–586.

MUIR, B. S., AND J. I. KENDALL. 1968. Structural modifications in the gills of tunas and other oceanic pelagic fishes. Copeia 1968: 388–398.

MUIR, B. S., G. J. NELSON, AND K. W. BRIDGES. 1965. A method for measuring swimming speed in oxygen consumption studies on the aholehole, *Kuhlia sanddvicensis*. Trans. Am. Fish. Soc. 94: 378–382.

MACLEOD, R. A., R. E. E. JONAS, AND E. ROBERTS. 1963. Glycolytic enzymes in the tissues of a salmonid fish (*Salmo gairdneri gairdneri*). Can. J. Biochem. Physiol. 41: 1971–1981.

MCCUTCHEON, C. W. 1970. The trout tail fin: A self-cambering hydrofoil. J. Biomech. 3: 271–281.

NEWMAN, J. N. 1973. The force on a slender fish-like body. J. Fluid Mech. 58: 689–702.

NEWMAN, J. N., AND T. Y. WU. 1973. A generalized slender-body theory for fish-like forms. J. Fluid Mech. 57: 673–693.

NIKOLSKII, G. V. 1954. Special ichthyology. (Transl. from Russian by Israel Program for Sci. Transl., Jerusalem, and National Science Foundation, Washington 1961)

NORRIS, K. S., AND J. H. PRESCOTT. 1961. Observations on Pacific cetaceans of California and Mexican waters. Univ. Calif. Publ. Zool. 63: 291–402.

NURSALL, J. R. 1956. The lateral musculature and swimming of fish. Proc. Zool. Soc. Lond. (B) 126: 127–143.
    1958a. The caudal fin as a hydrofoil. Evolution 12: 116–120.
    1958b. A method of analysis of the swimming of fish. Copeia: 1958: 136–141.
    1962. Swimming and the origin of paired fins. Am. Zool. 2: 127–141.

OSBORNE, M. F. M. 1961. Hydrodynamic performance of migratory salmon. J. Exp. Biol. 38: 365–390.

OVCHINNIKOV, V. V. 1966. Turbulence in the boundary-layer as a method for reducing the resistance of certain fish on movement. Biophysics 11: 186–188.

PAO, S. K., AND J. SIEKMAN. 1964. Note on the Smith–Stone theory of fish propulsion. Proc. R. Soc. Lond. Ser. A Phys. Sci. 280: 398–408.

PARRY, D. A. 1949a. The swimming of whales and a discussion of Gray's Paradox. J. Exp. Biol. 26: 24–34.
    1949b. The structure of whale blubber, and a discussion of its thermal properties. Q. J. Microsc. Sci. (Oxf.) 90: 13–25.

PAULICK, G. J., AND A. C. DeLACY. 1957. Swimming abilities of upstream migrant silver salmon, sockeye salmon and steelhead at several water velocities. Univ. Wash. Coll. Fish. Tech. Rep. 44: 40 p.

PERSHIN, C. V. 1970. Kinematics of dolphin propulsion, Bionika 1970: 31–36. (In Russian)

PETTIGREW, J. B. 1873. Animal locomotion. London. 264 p.

PHILLIPS, A. M. 1969. Nutrition, digestion and energy utilization, p. 391–432. *In* W. S. Hoar and D. J. Randall [ed.] Fish physiology. Vol. 1. Academic Press, New York, N.Y.

POPE, A., AND J. J. HARPER. 1966. Low speed wind tunnel testing. John Wiley and Sons Inc., New York, N.Y. 474 p.

PRANDTL, L., AND O. G. TIETJENS. 1934a. Fundamentals of hydro and aeromechanics. New ed. 1957. Dover Books, New York, N. Y. 270 p.

    1934b. Applied hydro and aeromechanics. New ed. 1957. Dover Books, New York, N.Y. 311 p.

PRITCHARD, A. W., J. R. HUNTER, AND R. LASKER. 1971. The relation between exercise and biochemical changes in red and white muscle and liver in the jack mackerel, *Trachurus symmetricus*. Fish. Bull. 69: 379–386.

PURVES, P. E. 1963. Locomotion in whales. Nature (Lond.) 197: 334–337.

PYATETSKIY, V. E. 1970a. Kinematic characteristics of some fast marine fish. Bionika 1970: 11–20. (In Russian)

    1970b. Hydrodynamic characteristics of swimming of some fast marine fish. Bionika 1970: 20–27. (In Russian)

RANDALL, D. J. 1970a. The circulatory system, p. 133–172. *In* W. S. Hoar and D. J. Randall [ed.] Fish physiology. Vol. 4. Academic Press, New York, N.Y.

    1970b. Gas exchange in fish, p. 253–292. *In* W. S. Hoar and D. J. Randall [ed.] Fish physiology. Vol. 4. Academic Press, New York, N.Y.

RAO, R. M. M. 1968. Oxygen consumption of rainbow trout (*Salmo gairdneri*) in relation to activity and salinity. Can. J. Zool. 46: 781–786.

RAYNER, M. D., AND M. J. KEENAM. 1967. Role of red and white muscles in the swimming of skipjack tuna. Nature (Lond.) 214: 392–393.

RICHARDSON, E. G. 1936. The physical aspects of fish locomotion. J. Exp. Biol. 13: 63–74.

ROBERTS, B. L. 1969a. Spontaneous rhythms in the motoneurons of spinal dogfish (*Scyliorhinus canicula*). J. Mar. Biol. Assoc. U.K. 49: 33–49.

    1969b. The co-ordination of the rhythmical fin movements of the dogfish. J. Mar. Biol. Assoc. U.K. 49: 357–425.

ROSEN, M. W. 1959. Water flow about a swimming fish. U.S. Nav. Ord. Test Stat. Tech. Publ. 2298: 1–96.

ROSEN, M. W., AND N. E. CORNFORD. 1971. Fluid friction of fish slimes. Nature (Lond.) 234: 49–51.

SCHLICHTING, H. 1968. Boundary-layer theory. 6th ed. McGraw-Hill, New York, N.Y. 747 p.

SHAPIRO, A. H. 1961. Shape and flow. Science Study Series, Heinmann Educational Books. 186 p.

SIEKMANN, J. 1962. Theoretical studies of sea animal locomotion. Part 1. Ing. Arch. 31: 214–228.

    1963. Theoretical studies of sea animal locomotion. Part 2. Ing. Arch. 32: 40–50.

SLIJPER, E. J. 1958. Walvissen. D. B. Centens Vitgevers-Maatschappij, Amsterdam. 524 p.

    1961. Locomotion and locomotory organs in whales and dolphins (Cetacea). Symp. Zool. Soc. Lond. 5: 77–94.

SMIT, H. 1965. Some experiments on the oxygen consumption of goldfish (*Carassius auratus* L) in relation to swimming speed. Can. J. Zool. 43: 623–633.

SMIT, H., J. M. AMELINK-KOUTSTAAL, J. VIJVERBERG, AND J. C. VON VAUPEL-KLEIN. 1971. Oxygen consumption and efficiency of swimming goldfish. Comp. Biochem. Physiol. 39A: 1–28.

SMITH, E. H., AND D. E. STONE. 1961. Perfect fluid forces in fish propulsion. Proc. R. Soc. Lond. Ser. A Phys. Sci. 261: 316–328.

SMITH, L. S., J. R. BRETT, AND J. C. DAVIS. 1967. Cardiovascular dynamics in swimming adult sockeye salmon. J. Fish. Res. Board Can. 24: 1775–1790.

STASBURG, D. W., AND H. S. H. YUEN. 1960. Progress in observing tuna underwater at sea. J. Cons. Int. Explor. Mer 26: 80–83.

STEEN, J. B. 1971. Comparative physiology of respiratory mechanisms. Academic Press, London and New York. 182 p.

STEVENS, E. D., AND E. C. BLACK. 1966. The effect of intermittent exercise on carbohydrate metabolism in rainbow trout (*Salmo gairdneri*). J. Fish. Res. Board Can. 23: 471–485.

STEVENS, E. D., AND D. J. RANDALL. 1967. Changes in blood pressure, heart rate and breathing rate during moderate swimming activity in rainbow trout. J. Exp. Biol. 46: 307–315.

STEVENS, G. A. 1950. Swimming of dolphins. Sci. Prog. 38: 524–525.

STICKNEY, R. R., AND D. B. WHITE. 1973. Observations on fin use in relation to feeding and resting behaviour in flat fishes (Pleuronectiformes). Copeia 1973: 154–157.

SUNDNES, G. 1963. Energy metabolism and migration of fish. ICNAF Environ. Symp. Spec. Publ. 6: 743–746.

SUTTERLIN, A. M. 1969. Effects of exercise on cardiac and ventilatory frequency in three species of freshwater teleosts. Physiol. Zool. 42: 36–52.

SVERDRUP, H. V., M. W. JOHNSON, AND R. H. FLEMING. 1963. The oceans. Prentice–Hall Inc. 1087 p.

TAYLOR, G. 1952. Analysis of the swimming of long narrow animals. Proc. R. Soc. Lond. Ser. A Biol. Sci. 214: 158–183.

ULDRICK, J. P., AND J. SIEKMAN. 1964. On the swimming of a flexible plate of arbitrary thickness. J. Fluid Mech. 20: 1–33.

VINCENT, R. E. 1960. Some influences of domestication upon three stocks of brook trout (*Salvelinus fontinalis* Mitchell). Trans. Am. Fish. Soc. 89: 35–52.

143

WALLACE, B., AND A. M. SRB. 1961. Adaption. Foundations of Modern Biology Series, Prentice–Hall, New York, N.Y. 113 p.

WALTERS, V. 1962. Body form and swimming performance in scombroid fishes. Am. Zool. 2: 143–149.

1963. The trachypterid integument and an hypothesis on its hydrodynamic function. Copeia 1963: 260–270.

1966. The 'problematic' hydrodynamic performance of Gero's great barracuda, *Sphyraena barracuda* (Walbaum). Nature 212: 215–216.

WALTERS, V., AND H. L. FIERSTINE. 1964. Measurements of swimming speeds of yellowfin tuna and wahoo. Nature (Lond.) 202: 208–209.

WEATHERLEY, A. H. 1972. Growth and ecology of fish populations. Academic Press, London and New York. 293 p.

WEBB, P. W. 1970. Some aspects of the energetics of swimming of fish with special reference to the cruising performance of rainbow trout. Ph.D. Thesis. Univ. Bristol. Bristol, England. 189 p.

1971a. The swimming energetics of trout. I) Thrust and power output at cruising speeds. J. Exp. Biol. 55: 489–520.

1971b. The swimming energetics of trout. II) Oxygen consumption and swimming efficiency. J. Exp. Biol. 55: 521–540.

1973a. Effects of partial caudal-fin amputation on the kinematics and metabolic rate of underyearling sockeye salmon (*Oncorhynchus nerka*) at steady swimming speeds. J. Exp. Biol. 59: 565–581.

1973b. Kinematics of pectoral fin propulsion in *Cymatogaster aggregata*. J. Exp. Biol. 59: 697–710.

1974. Pisces (Zoology). Bionergetics. McGraw-Hill Encycl. Sci. Technol. Yearb. 1973. 333–336.

WEIHS, D. 1972. A hydrodynamical analysis of fish turning manoeuvres. Proc. R. Soc. Lond. Ser. B Biol. Sci. 182: 59–72.

1973a. The mechanism of rapid starting of slender fish. Biorheology 10: 343–350.

1973b. Hydromechanics of fish schooling. Nature 241: 290–291.

1973c. Optimal cruising speed for migrating fish. Nature 245: 48–50.

1973d. Mechanically efficient swimming techniques for fish with negative buoyancy. J. Mar. Res. 31: 194–209.

1974. Energetic advantages of burst swimming of fish. J. Theor. Biol. (In press)

WEIS-FOGH, T. 1973. Quick estimates of flight fitness in hovering animals, including novel mechanisms for lift production. J. Exp. Biol. 59: 169–230.

WENDT, C. 1965. Liver and muscle glycogen and blood lactate in hatchery reared *Salmo salar* following exercise in winter and summer. Rep. Inst. Freshwater Res. Drottningholm 46: 167–184.

1967. Mortality in hatchery-reared *Salmo salar* after exercise. Rep. Inst. Freshwater Res. Drottningholm 47: 98–112.

WINBERG, G. G. 1956. Rate of metabolism and food requirements of fishes. Belorussian State Univ. Minsk. (Transl. from Russian by Fish. Res. Board Can. Transl. Ser. No. 194, 1960)

WITTENBERGER, C. 1968. Biologie du chinchard de la mer Noire (*Trachurus mediterraneus ponticus*). Mar. Biol. 2: 1–4.

WITTENBERGER, C., A. CARO, G. SUAREZ, AND N. PORTILLA. 1969. Composition and bioelectrical activity of the lateral muscles in *Harengula humeralis*. Mar. Biol. 3: 24–27.

WITTENBERGER, C., AND I. V. DIACUIC. 1965. Effort metabolism in lateral muscles in carp. J. Fish. Res. Board Can. 22: 1397–1406.

WOOD, C. M., AND D. J. RANDALL. 1973a. The influence of swimming activity on sodium balance in the rainbow trout (*Salmo gairdneri*). J. Comp. Physiol. 32: 207–233.

1973b. Sodium balance in the rainbow trout (*Salmo gairdneri*) during extended exercise. J. Comp. Physiol. 82: 235–256.

1973c. The influence of swimming activity on water balance in the rainbow trout (*Salmo gairdneri*). J. Comp. Physiol. 32: 257–276.

WU, T. Y. 1961. Swimming of a waving plate. J. Fluid Mech. 10: 321–344.

1971a. Hydromechanics of swimming propulsion. Part 1. Swimming of a two-dimensional flexible plate at variable forward speeds in an inviscid fluid. J. Fluid Mech. 46: 337–355.

1971b. Hydromechanics of swimming propulsion. Part 2. Some optimum shape problems. J. Fluid Mech. 46: 521–544.

1971c. Hydromechanics of swimming propulsion. Part 3. Swimming and optimum movements of slender fish with side fins. J. Fluid Mech. 46: 545–568.

1971d. Hydromechanics of swimming fishes and cetaceans. Adv. Appl. Math. 11: 1–63.

WU, T. Y., AND J. N. NEWMAN. 1972. Unsteady flow around a slender fish-like body, p. 33–42. *In* Proc. Int. Symp. on Directional Stability and Control of Bodies Moving in Water, London, 1972. Paper 7. Inst. Mech. Eng. Publ.

YOUNG, A. H., P. TYTLER, F. G. T. HOLLIDAY, AND A. MACFARLANE. 1972. A small sonic tag for measurement of locomotor behaviour in fish. J. Fish. Biol. 4: 57–65.

YUEN, H. S. H. 1966. Swimming speeds of yellowfin and skipjack tuna. Trans. Am. Fish. Soc. 95: 203–209.

ZUYEV, G. V., AND V. V. BELYAYEV. 1970. An experimental study of the swimming of fish in groups as exemplified by the horse mackerel (*Trachurus mediterraneus ponticus* Aleev). J. Ichthyol. 10: 545–549.

144

Appendix I — Methods

Flow Visualization

The most direct approach to the mechanics of fish locomotion would be to measure pressure distribution around a swimming fish, but the methods available rarely give quantitative results. Pressure distribution is difficult to measure directly, although the static pressure distribution can be found from tubes inserted through the body musculature, opening to the surface (P. W. Webb unpublished data). Dubois et al. (1974) described a method for obtaining the pressure distribution along the body of a swimming fish. Pressure distribution would be most easily calculated from the flow pattern, made visible by some means. In practice, this has proved difficult, and flow visualization methods reported in the literature have either unsuccessfully shown the details of flow, or are subject to other mechanical reservations. As a result, these observations are at present only of qualitative value; as a tool for studying mechanics they should be further explored.

Outer flow

Threads (Houssay 1912), dyes (Rosen 1959; Walters 1962; McCutcheon 1970), and suspended solids (Gray 1936b, 1953a; Gero 1952; Rosen 1959; Kent et al. 1961) have been used. Threads are limited to visualization of gross flow patterns in the immediate vicinity of the fish, particularly the position of cross flows. Short threads (approximately 0.02 L) are more effective than the long threads used by Houssay (1912). It is imperative that threads have negligible rigidity, and be attached below the skin at the upstream end. Any protuberance in this area of the flow must be avoided, as these would encourage separation (P. W. Webb unpublished data).

Dyes and suspended particles can show the flow pattern outside the boundary layer. However, dyes are rapidly dissipated which limits their use in conventional water tunnels available to biologists. In still water, dyes are apparently also of limited value (McCutcheon 1970) and the behavior of the fish is difficult to control.

Suspended particles, approaching neutral buoyancy, are potentially the most useful flow visualization method. Large particles are avoided by fish (Kent et al. 1961) whereas denser particles such as milk only detect flow effects at some distance from the fish (Rosen 1959; Aleyev and Ovcharov 1969). Small particles of appropriate size, not interfering with the fish or the flow, require special detection methods; Gray (1953a) and Gero (1952) used the effects of tobacco mosaic virus and bentonite respectively on polarized light, but details of their techniques have not been published. A method that has not been used is electrolytic generation of extremely small bubbles. These could be detected by means of the reflection and refraction effects of the gas/water interfaces and could be generated in arbitrary shapes by various electrode configurations. These methods are ideally suited for use in water tunnels.

Boundary-layer flow

The only successful method to visualize the boundary layer has been the Schlieren technique used by Allan (1961) and Kent et al. (1961). This requires that the fish be cooled approximately 5.5 C below water temperature in the test flume. Transfer of heat from the boundary layer then results in changes in the refractive index of the water. The detection system is complex, and is described by the above authors. The disadvantage of the method is that boundary layer cooling could markedly affect the flow in comparison with normal conditions, and fish performance levels cannot be controlled.

Drag Measurements

Several factors confounding drag measurements were discussed in Chapter 4, and control of these is required in all drag measurement methods. Most methods assume that the long axis of the fish moves along, and does not subtend any angle to its direction of motion. This should always be confirmed, otherwise drag (error) increments will arise from rolling, pitching, and yawing. Of greater magnitude are fluttering effects. When using anesthetized fish, it is probably impossible to eliminate such effects; they can be reduced by selecting a suitable species and/or large individuals.

145

For dead fish, body fluttering has been commonly reduced by inserting stiffening wires (Richardson 1936; Brett 1963; Webb 1970) or a quick drying cement (Sundnes 1963) into the body. Webb (1970) improved these methods by including the caudal fin, with the fish stretched on a rack (Fig. 66). These stiffening methods are
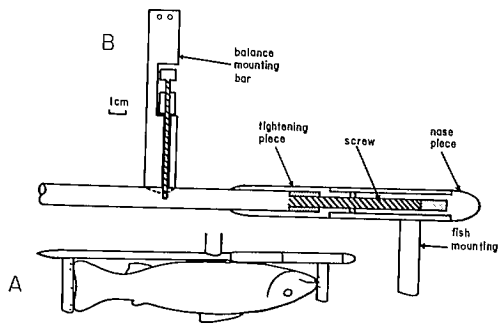
FIG. 66. (A) rack for mounting and stretching fish to reduce body and fin fluttering and improve accuracy of drag measurement; (B) details of stretching mechanism. (From Webb 1970)

never entirely successful because of fluttering of other fins. The surface area of these fins is small, as will be their contribution to frictional drag, and most of the additional drag (error) arises from pressure forces. Improved drag values, involving only a small error, can be obtained by amputating such fins (Webb 1970).

Another method to reduce fluttering of fish themselves is pickling (Kempf and Neu 1932). Passive drag-reducing mechanisms, such as mucus or the elasticity of the integument, will obviously be destroyed. Shrinkage of the body can change the surface roughness characteristics.

Models that completely eliminate fluttering have been widely used (Houssay 1912; Kempf and Neu 1932; Denil 1936; Harris 1936; Richardson 1936; Gero 1952). Their use is quite legitimate in view of the basic assumptions made in any dead-drag measurement (Chapter 4). Models exclude passive drag-reducing mechanisms the same as pickling.

Methods

Four methods have been employed in measuring drag: fish in free fall, during a glide, towing and water or wind tunnels.

FREE FALL

Use of this method is discussed in detail by Gero (1952). The equation of motion for a body in free fall, accelerating from rest through a fluid at rest, is

$$Dg = M_w g - M_w a \qquad (100)$$

when

D = drag
M_w = weight of fish in water
g = acceleration due to gravity
a = acceleration of the fish in free fall

At the terminal velocity, $a = 0$, and drag is equal to the weight of the fish in water. Acceleration rates and terminal velocity can be varied by loading the fish internally with weights.

GLIDING FISH

Details of methods are given by Lang and Daybell (1963) and Johnson et al. (1972). The equation of motion for a gliding fish is similar to that of free fall, except that the fish is decelerating as a result of the drag force, not accelerating under gravity. Thus

$$Dg = Ma \qquad (101)$$

M is the mass of the fish, and must be increased for the added mass of water entrained by the body.

TOWING

This method, in common with tunnel measurements, requires some constraint on the fish to attach a drag balance or other recording device. Such constraint can be used to advantage to ensure that pitching, rolling, and yawing are eliminated. Any drag measurement requires some movement of the fish relative to its axis of progression. Effects of such motions on drag can be minimized by using strain gauges, and designing balances on the basis of a parallelogram. In this case, the long axis of the fish never subtends an angle to its axis of progression. These features are included in the towing trolly/balance used by Kent et al. (1961) or designed for conventional wind and water tunnels (Pope and Harper 1966).

It is obviously important that a towing tank be sufficiently long to ensure that a steady state is reached after the initial acceleration. Fish should be submerged to a depth equal to at least three times its own maximum depth to avoid additional drag from gravitational (wave) forces (see Fig. 7).

146

Water tunnel measurements have the advantage over other methods because the fish can be observed at all times, and is stationary relative to the flow. The most accurate method would be to use properly designed aeronautical (wind) and water tunnels, and balances (Pope and Harper 1966).

Several types of balance have been used with water tunnels designed for respiration studies. Of these, the balance used by Webb (1970) is probably the most suitable (Fig. 67).
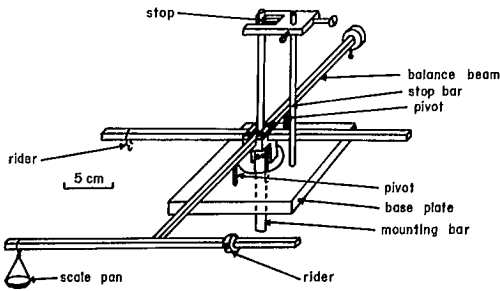
FIG. 67. Beam-type drag balance. (From Webb 1970)

FIG. 68. Drag balance described by Brett (1963).

The fish is held rigidly on the tunnel centerline by a streamline mounting bar. This is attached to a supporting beam mounted on needlepoint bearings. An additional vertical bar rests against a stop. The entire balance can be rotated around vertical and horizontal axes to ensure that the fish is on the centerline, in the minimum drag position. To measure drag at any speed, weights are placed on a scale pan until the vertical bar is just lifted off the stop. As the fish subtends some angle to the flow as soon as this equilibrium point is reached, there is a sudden drag increment at that point. This assists the vertical bar to lift off the stop, improving sensitivity.

A different type of balance (Fig. 68) was used by Brett (1963). The equilibrium point in this case was found by returning the fish to the centerline by means of a calibrated spring. A balance working on the same principle gave the same drag values as the balance illustrated in Fig. 67 (Webb 1970).

The accuracy of balances for towing and tunnels must be tested, usually using bodies of known drag. Kent et al. (1961) used spheres and fuselage shapes. Webb (1970) used a flat plate, and found that the balances designed like those in Fig. 68 and 69 could be accurate to within

$\pm$ 0.02 g wt. Use of a flat plate requires that edge corrections be taken into account, as described by Elder (1960) (see Fig. 16). In addition, the residual drag of the submerged portions must be measured, and be kept as small as possible. The latter requires that submerged portions of a balance be streamlined. Accuracy can further
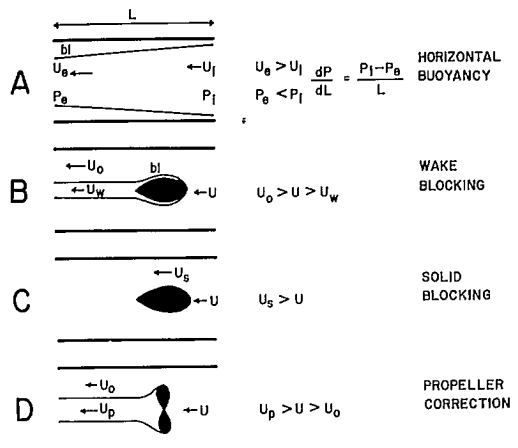
FIG. 69. Summary of speed corrections. Further explanation is given in text.

147

be improved by fixing objects to the balance as rigidly as possible. Flexible connections result in problems with buoyancy (Brett 1963), and fish are free to roll, yaw, and pitch.

Speed corrections for water tunnels

All water tunnel measurements of drag or any other physiological parameter, require corrections to take into account the effects of walls restricting flow. Flow restrictions result in various pressure changes that affect drag. Such drag changes mean that a fish may do more or less work than is expected from the measured free stream velocity (see reviews by Pope and Harper 1966; Bell and Terhune 1970).

The most satisfactory correction for free swimming fish is to compare some kinematic parameter for fish swimming in flumes and in tunnels (Brett and Glass 1973). This is not always possible, and the correction must be computed for the shape of the fish and tunnel characteristics (Pope and Harper 1966; Bell and Terhune 1970). The relevant corrections are then horizontal buoyancy, wake blocking, solid blocking, and propeller correction as shown in Fig. 69.

Horizontal Buoyancy

There is an increase in static pressure along the axis of any parallel-sided tunnel. This results from increase in boundary-layer thickness with increasing distance along the length of a test section. The increasing thickness of the boundary layer effectively reduces the cross-sectional area available for flow. As the volume of water passing through any cross section is constant (law of continuity, Chapter 1), the velocity increases along the test section length. Upstream velocity, U_i, is lower than the downstream velocity, U_e (Fig. 69A). Bernoulli's theorem predicts that the increase in velocity is associated with a pressure change, so that the upstream pressure, P_i, will be greater than the downstream pressure, P_e. The resultant pressure gradient along the chamber length tends to suck any object toward the test section exit. The force experienced by an object in the pressure gradient is called horizontal buoyancy and must be subtracted from the measured drag.

The horizontal buoyancy drag increment, ΔD_B, is given by

$$\Delta D_B = \frac{\pi}{4} \lambda_3 \overline{d}^3 \frac{dP}{dl} \qquad (102)$$

when

$\lambda_3 =$ nondimensional shape factor, approximately 3.5 for fish shapes (see tables in Pope and Harper 1966).

$\dfrac{dP}{dl} =$ pressure gradient $(P_i - P_e)/\ell$

$\overline{d} =$ mean depth and width of fish

$\ell =$ test section length

Measurements of ΔD_B for the respirometer described by Brett (1963, 1964) gave a maximum of about 1% for drag values obtained for 30 cm trout, as measured by Webb (1970).

The phenomenon of horizontal buoyancy was discussed by Denil (1936) who suggested it could reduce the effectiveness of underwater enclosed fish passes. In practice, the size of such passes is large compared to the size of the fish, so this is unlikely.

Wake Blocking

Any body in a test section will have a wake formed from its boundary layer. The velocity in the wake, U_w, is less than the free-stream velocity, U (Fig. 69B). Because a constant volume of water must pass through a given section, the velocity outside the wake, U_o, must be greater than U. As pressure changes resulting from velocity changes are inversely related to the square of the velocity (Bernoulli's theorem), there is a low pressure in the fluid downstream of the body. This is transmitted to the body, and results in a drag increment.

The correction for wake blocking is usually taken into account by a speed correction, ΔU_{wb} (Fig. 69B). This is the increment that must be added to U to give the velocity at which the measured drag would be found under unrestricted conditions. Thus

$$\Delta U_{wb} = \frac{S_w}{4\,S_t}\, C_D U \qquad (103)$$

when

$S_w =$ surface area of the body

$S_t =$ tunnel sectional area

$C_D =$ measured drag coefficient.

This error is likely to be small in most cases. Maximum values of ΔS_{wb} calculated for large fish in a relatively small tunnel by Webb (1970) were 2.2% of U.

148

Solid Blocking

Solid blocking is probably the most important speed correction. It arises from the increased velocity around any solid body in a tunnel, so that the velocity at the surface of the body, U_s, exceeds U (Fig. 69C). For a body of uniform sectional area, U_s is given by

$$U_s = \frac{S_t}{S_t - S_b} U \qquad (104)$$

when

$$S_b = \text{cross-sectional area of the body.}$$

This correction has also been applied to fish swimming in tunnels taking S_b as the maximum sectional area (Paulick and DeLacy 1957; Smit 1965; Smit et al. 1971). For fusiform bodies the correction gives a high value for U_s, because the mean correction depends on the shape of the body and distribution of blocking along its length.

The general blocking correction for fish-shape bodies can be expressed as a speed increment, ΔU_{sb}, given by

$$\Delta U_{sb} = \frac{K_3 \tau (\text{body volume})}{S_t^{\frac{2}{3}}} \qquad (105)$$

when

K_3 = shape factor, related to the thickness (see tables in Pope and Harper 1966).

τ is a coefficient dependant on the tunnel test section shape, and dimensions of the body. For fish-shaped bodies and bodies of revolution in circular tunnels, this is given by

$$\tau = 2\bar{d}/d_t \qquad (106)$$

when

d_t = tunnel section diameter.

The correction calculated from Equation 105, 106 is small enough to be neglected for fish with maximum cross-sectional areas up to about 10% of the tunnel sectional area (Brett 1964). For large fish in relatively small chambers, the equations tend to give high ΔU_{sb} values. In this case, the correction can be calculated from the blocking distribution and its effects on local frictional drag.

To calculate the correction for larger fish, consider a fish swimming in a test section as shown in Fig. 70. Consider a small section of the
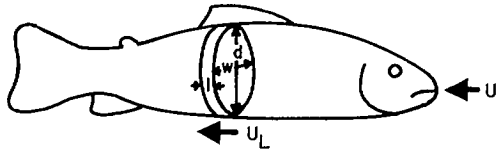
FIG. 70. For explanation, see text.

body, length, l, depth, d, and width, w, and assume the section is elliptical, with circumference, c, and area, S_h, given by $c \times l$. The local water velocity, U_L, will be given by Equation 104. The local frictional drag, D_L, is then given by

$$D_L = \tfrac{1}{2} \rho S_L U_L^2 C_d \qquad (107)$$

Turbulent flow conditions are likely in tunnels designed for biological use, in which case the turbulent drag coefficient, $C_{D\,turb}$ would be required. As this is proportional to $U_L^{-\frac{1}{5}}$, and will not vary much with different sections along the body, Equation 108 can be simplified to

$$D_L \; \alpha \; S_L \, U_L^2 \qquad (108)$$

Total drag of the fish is the sum of D_L for all sections

$$\text{Total drag} = \Sigma D_L \propto \Sigma (S_L \, U_L^2) \qquad (109)$$

However, total drag will also be given by

$$\text{Total drag} \propto S_w \, (U + \Delta U_{sb})^2 \qquad (110)$$

where the wetted surface area, $S_w = \Sigma S_L \qquad (111)$

Therefore

$$\text{Total drag} \propto \Sigma S_L \, (U + \Delta U_{sb})^2 = \Sigma (S_L \, U_L^2) \qquad (112)$$

from which

$$U + \Delta U_{sb} = \sqrt{\frac{\Sigma (S_L \, U_L^2)}{\Sigma S_L}} \qquad (113)$$

The parameters required for calculation of the speed correction can readily be measured. An example of results of such calculations for

149
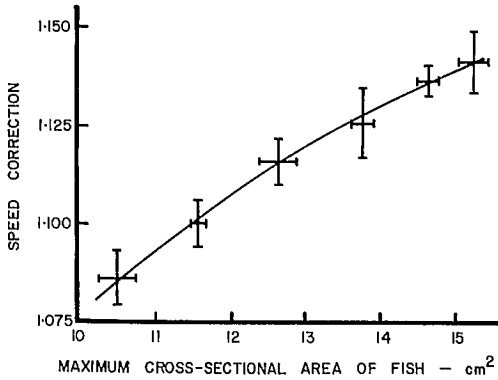
FIG. 71. Relation between the solid blocking speed correction and maximum body cross-sectional area for rainbow trout swimming in an 11.5 cm diameter water tunnel. (From Webb 1970)

30 cm rainbow trout is shown in Fig. 71, with the speed correction $(U + \Delta U_{sb})/U$, shown as a function of the maximum cross-sectional area of the fish. These calculations were based on a tunnel section diameter of 11.5 cm. The speed correction can be assumed independent of the value of U.

PROPELLER CORRECTION

The caudal propulsion system behaves as a propeller. Water in the propeller wake has a velocity U_p, greater than that of the free stream (Fig. 69D). This results in a pressure impressed on the wake greater than the freestream pressure, as the velocity outside the propeller wake must be lower than U. This is the opposite to wake blocking, and adds to thrust. The correction is calculated as a speed correction ΔU_{pb}:

$$\Delta U_{pb} = \frac{\tau\,\alpha}{2\sqrt{(1 + 2\,\tau)}} \qquad (114)$$

when

τ = thrust coefficient, $\dfrac{\text{Thrust}}{\frac{1}{2}\,\rho\,S_p\,U^2}$

$\alpha = S_p/S_l$

S_p = propeller cross-sectional area, equal to the product of amplitude and tail depth for fish.

Equation 114 requires some measurement of thrust, which is not usually available. For the trout used by Webb (1971a) for which measurements of thrust were made, the maximum correction was about 0.7% of U (Webb 1970). These fish were relatively restricted, so normally this error is expected to be negligible.

USE OF TUNNEL CORRECTIONS

Corrections should be applied for drag measurements, horizontal buoyancy, wake blocking, and solid blocking. In most cases, the sum of these errors is likely to be small enough to ignore, providing fish do not occupy more than about 10% of the chamber area at their maximum thickness.

For swimming fish, horizontal buoyancy, solid blocking, and propeller corrections are required. Horizontal buoyancy adds to drag, whereas the propeller correction is opposite in effect; these tend to cancel out, so solid blocking remains the only important correction.

Appendix II — Symbols

Arabic Symbols

A	amplitude	cm
A_T	trailing-edge amplitude (e.g., caudal fin)	cm
A_w	weighted mean amplitude (with quasi-static hydrodynamic models)	cm
AR	aspect ratio	–
a	acceleration	cm/s^2
C	chord length (hydrofoil)	cm
C_D	drag coefficient	–
C_f	frictional drag coefficient (with subscripts *lam, turb, tran*)	–
C_I	induced drag coefficient	–
C_L	lift coefficient	–
C_P	pressure drag coefficient	–
C_p^i	pressure drag coefficient dependant on relative camber	–
C_T	total drag coefficient	–
D	drag	dyn
D_I	induced drag	dyn
D_f	frictional drag	dyn
D_P	pressure (form) drag	dyn
D_T	total drag	dyn
d	diameter or depth of a solid body	cm
d_T	trailing-edge depth	cm
E	total power	erg/s
E_{aerob}	power released by aerobic metabolism	erg/s
E_{glyc}	power released by anaerobic metabolism	erg/s
E_K	power associated with kinetic energy lost in wake	erg/s
E_m	power developed by muscles	erg/s
E_p	propeller power output	erg/s
E_{sup}	power required by supporting systems (aerobic metabolism)	–
E_T	thrust power	erg/s
F	force	dyn
F_g	gravitational force	dyn
F_i	inertial force	dyn
F	viscous force	dyn
F^L	Froudes Number	–
FR	fineness ratio	–
f	frequency	/s
f_v	vortex frequency	/s
$G_{(n,a)}$	thrust coefficient (used in quasi-static hydrodynamic models)	–
g	acceleration due to gravity	cm/s^2
h	depth of water	cm
h_s	Karman vortex street row interval	cm
I	intensity of turbulence	–
J	advance ratio of propeller	–
k_{crit}	critical thickness for roughness elements	cm
L	length	cm
lam	laminar flow	–
l_s	Karman street vortex interval	cm
M	mass	gm
m_T	trailing-edge virtual mass	g/cm
$u u^v$	virtual mass	

P	pressure	dyn/cm^2
R	Reynolds Number	–
R_C	Reynolds Number based on chord, C	–
R_d	Reynolds Number based on diameter, d	–
R_L	Reynolds Number based on length, L	–
S	span of hydrofoil	cm
S_b	cross-sectional area of a solid body	cm^2
S_h	maximum projected surface area of a hydrofoil	cm^2
S_p	propeller cross-sectional area	cm^2
S_t	cross-sectional area of water or air tunnel	cm^2
S_w	wetted surface area	cm^2
T	thickness of hydrofoil	cm
T_p	propeller thrust	dyn
t	time	s
$tran$	transitional flow	–
$turb$	turbulent flow	–
U	water velocity, swimming speed	cm/s
U_m	muscle shortening speed	cm/s
$U_{m\ max}$	maximum shortening speed of muscle	cm/s
U/L	specific swimming speed (body lengths/s)	–
V	backward velocity of propulsive wave	cm/s
W	transverse velocity of a body segment or fin; total works done in acceleration	cm/s
W_D	(acceleration) work done against hydrodynamic drag	erg
W_K	(acceleration) work appearing as kinetic energy	erg
W_{max}	maximum transverse velocity	–
W_R	resultant velocity for incident flow to segment of body of fin	cm/s
w	resultant velocity at which water is displaced laterally by fins in hydromechanical models;	cm/s erg
	width	cm
x	distance	cm

Greek Symbols

α	angle of attack	degree
β	dihedral angle	degree
δ	boundary-layer velocity thickness	cm
δ^*	boundary-layer displacement thickness	cm
δ_{lam}	laminar boundary-layer velocity thickness	cm
δ_{turb}	turbulent boundary-layer velocity thickness	cm
δ_{tran}	transitional boundary-layer velocity thickness	cm
δ_{crit}	velocity thickness of boundary layer at critical Reynolds Number	cm
η	efficiency	cm
η_{aerob}	overall aerobic efficiency (neglects sub)	%
η_m	muscle efficiency	–
η_p	"propeller" efficiencies	%
θ_s	angle subtended by path of a segment in space and transverse axis of motion	degree
θ_b	angle subtended by a segment of body or fin with mean transverse axis of motion	degree
θ	angle subtended by trailing edge and axis of motion of fish	degree
λ_B	wavelength of the propulsive wave	cm
λ_S	wavelength of the path of a segment or fin traced in space	cm
μ	viscosity	poise
v	kinematic viscosity	stoke
ρ	density	g/cm^3
ω	angular velocity	rad/s
ω_s	Strouhal Number	–

152

Systematic Index

155

Subject Index

1960–63	New respirometers developed by P. Blazka et al. and J. R. Brett permitted accurate measurement of power available to a swimming fish using methods of indirect calorimetry.
1963	J. R. Brett compared power available to a cruising salmon (calculated by indirect calorimetry) with drag measured on a dead fish, and found insufficient power available to meet the drag.
1960–71	Sir James Lighthill developed hydromechanical models of fish propulsion, covering full range of caudal fin propulsion types. These were the first models of practical biological use having deductive and inductive values.

Recent Bulletins/Récents Bulletins

BULLETIN OF THE FISHERIES
RESEARCH BOARD OF CANADA.